# Highly Accelerated Myocardial Perfusion Magnetic Resonance Imaging

Jogiya, Roy Ramesh

*Awarding institution:*
King's College London

# Highly Accelerated Myocardial Perfusion Magnetic Resonance Imaging

**Roy Jogiya**
BSc (Hons), MBBS, PGDip, MRCP

A dissertation submitted for the degree of

**Doctor of Philosophy**
of the
**University of London**

Division of Imaging Sciences and Biomedical Engineering

School of Medicine, King's College London

January 2016

## Dedication

In loving memory of Bhanumati Jogiya (1944-2014) a kind, gentle and wonderful mummy who is greatly missed and thought about every day.

## Abstract

## Introduction

First-pass myocardial perfusion cardiovascular magnetic resonance imaging (CMR) has become an established method for the non-invasive diagnosis of ischaemic heart disease (IHD). As complete datasets are acquired every heart beat, first-pass perfusion CMR is challenging, and compromises have to be made between competing demands for spatial resolution, cardiac coverage, and temporal resolution. Accelerating data acquisition with *k-t* undersampling techniques is a strategy that could overcome some of the remaining limitations of first-pass perfusion CMR, and influence the management of patients with IHD.

The use of a *k-t* Principle Component Analysis (PCA) acceleration method will be investigated for its technical feasibility and clinical merit for acquisition with improved spatial resolution, greater myocardial coverage, and higher heart rates. Supplemented by three additional chapters as appendices, this thesis presents the use of spatio-temporal undersampling for advanced perfusion CMR. The research has the following aims.

## Aims and Methods

1. To establish the clinical feasibility of 3D perfusion CMR technique in relation to fractional flow reserve (FFR) and the Duke Jeopardy Score. Accuracy in diagnosis and comparison of ischaemic burden with invasive indices of myocardial ischaemia, will be determined.

2. To compare the estimation of ischaemic burden using 3D perfusion CMR against the estimation using the clinical standard single-photon emission computed tomography (SPECT).

3. Optimization and design of a 3D perfusion CMR sequence based on *k-t* acceleration and PCA reconstruction using a turbo field-echo (TFE) pulse sequence, and development of balanced steady-state free precession (bSSFP) perfusion imaging at 3 Tesla (3T).

4. To use *k-t* acceleration schemes to establish the feasibility of first-pass stress perfusion CMR in a rodent model, and to validate this against the microspheres method.

5. Multicentre evaluation of 3D perfusion CMR imaging for the detection of IHD defined by fractional flow reserve (FFR)(appendix).

6. To use *k-t* acceleration schemes for high-resolution quantitative first-pass perfusion imaging, and to determine reproducibility (appendix).

7. To compare advanced perfusion CMR imaging techniques: high-spatial resolution versus 3D whole-heart coverage (appendix).

## Results

This research provides novel experimental evidence and technical advancements on the clinical utility of *k-t* PCA acceleration methods, and demonstrates the following:

1. That 3D whole-heart myocardial perfusion CMR imaging at 3T accurately detects functionally significant CAD;

2. That 3D whole-heart myocardial perfusion CMR imaging can determine ischaemic burden with accuracy comparable to current imaging techniques that rely on ionising radiation;

3. That the development of a 3D bSSFP myocardial perfusion CMR sequence is feasible using radio frequency (RF) shimming with dual-source parallel RF transmission at 3T.

4. That first-pass myocardial stress perfusion CMR imaging is feasible in a murine model using a 3T clinical scanner.

The use of *k-t* spatio-temporal undersampling also yielded the following findings:

5. 3D whole-heart myocardial perfusion CMR imaging was highly efficient in the detection of functionally significant CAD in a multicentre study (appendix).

6. Quantitative high-resolution myocardial perfusion CMR showed inter-study reproducibility with no significant diurnal variation (appendix).

## Conclusion

These findings have important implications, lending support to the clinical use of 3D whole-heart perfusion imaging for the detection of coronary disease. The use of *k-t* acceleration schemes is feasible for both clinical and pre-clinical models. When combined with CMR assessment of function and viability, the technique holds promise as a completely non-invasive and radiation-free diagnostic and risk-stratification tool for patients with known or suspected CAD.

## Declaration

The work presented in this thesis is my own. I produced the study paperwork, amended existing study protocols, ethics committee and research and development department approval. Throughout the thesis I performed the necessary and appropriate study administration. In line with the college guidelines for PhD incorporating publications, the research chapters were published with myself as the lead author. I was responsible for the study design, patient recruitment, imaging, data collection, analysis and reporting. All aspects were conducted under the direct guidance of my primary supervisor Professor Sven Plein. The works included in the appendix, are an extension of the thesis, for which I significantly contributed and was a leading author in the subsequent publications.

## Publications

1. **Jogiya R**, Kozerke S, Morton G, De Silva K, Redwood S, Perera D, Nagel E, Plein S.
Validation of dynamic 3-dimensional whole heart magnetic resonance myocardial perfusion imaging against fractional flow reserve for the detection of significant coronary artery disease.
J Am Coll Cardiol. 2012 Aug 21;60(8):756-65.

2. **Jogiya R**, Morton G, De Silva K, Reyes E, Hachamovitch R, Kozerke S, Nagel E, Underwood SR, Plein S.
Ischemic burden by 3-dimensional myocardial perfusion cardiovascular magnetic resonance: comparison with myocardial perfusion scintigraphy.
Circ Cardiovasc Imaging. 2014 Jul;7(4):647-54

3. **Jogiya R**, Schuster A, Zaman A, Motwani M, Kouwenhoven M, Nagel E, Kozerke S, Plein S.
Three-dimensional balanced steady state free precession myocardial perfusion cardiovascular magnetic resonance at 3T using dual-source parallel RF transmission: initial experience.
J Cardiovasc Magn Reson. 2014 Nov 28;16:90.

4. **Jogiya R**, Makowski M, Phinikaridou A, Patel AS, Jansen C, Zarinabad N, Chiribiri A, Botnar R, Nagel E, Kozerke S, Plein S.
Hyperemic stress myocardial perfusion cardiovascular magnetic resonance in mice at 3 Tesla: initial experience and validation against microspheres.

J Cardiovasc Magn Reson. 2013 Jul 21;15:62

5. Manka R, Wissmann L, Gebker R, **Jogiya R**, Motwani M, Frick M, Reinartz S, Schnackenburg B, Niemann M, Gotschy A, Kuhl C, Nagel E, Fleck E, Marx N, Luescher TF, Plein S, Kozerke S.
Multicenter evaluation of dynamic three-dimensional magnetic resonance myocardial perfusion imaging for the detection of coronary artery disease defined by fractional flow reserve.
Circ Cardiovasc Imaging. 2015 May;8(5) e003061

6. Morton G, **Jogiya R**, Plein S, Schuster A, Chiribiri A, Nagel E.
Quantitative cardiovascular magnetic resonance perfusion imaging: inter-study reproducibility.
Eur Heart J Cardiovasc Imaging. 2012 Nov;13(11):954-60

7. Motwani M, **Jogiya R**, Kozerke S, Greenwood JP, Plein S.
Advanced cardiovascular magnetic resonance myocardial perfusion imaging: high-spatial resolution versus 3-dimensional whole-heart coverage.
Circ Cardiovasc Imaging. 2013 Mar 1;6(2):339-48

## Presentations

1. 3D myocardial perfusion-CMR using a multi-transmit coil and k-t PCA reconstruction to detect flow limiting coronary stenosis

**Roy Jogiya**, Amedeo Chiribiri, Andreas Schuster, Christian Jansen, Kalpa De Silva, Divaka Perera, Simon Redwood, Eike Nagel, Sebastian Kozerke, Sven Plein

J Cardiovasc Magn Reson. 2011; 13(Suppl 1): P12.

2. Whole heart myocardial perfusion imaging: Validation of CAD detection

**Roy Jogiya**, Geraint Morton, Kalpa De Silva, Sebastian Kozerke, Divaka Perrera, Simon Redwood, Eike Nagel, Sven Plein

Circulation. 2011; 124: A10847

3. Ischaemic burden by whole heart perfusion: a comparison against conventional slice coverage.

**Roy Jogiya**, Geraint Morton, Kalpa De Silva, Sebastian Kozerke, Eike Nagel, Richard Underwood, Sven Plein

Eur Heart J (2012) 33 (suppl 1): 941-1105

4. Quantitative cardiovascular magnetic resonance myocardial perfusion imaging: inter-study reproducibility

G Morton, **R Jogiya**, A Schuster, A Chiribiri, E Nagel

Heart 2012;98:Suppl 1 A56-A57

5. Dynamic three-dimensional whole heart magnetic resonance myocardial perfusion imaging: validation against pressure wire derived fractional flow reserve for the detection of flow-limiting coronary heart disease

**R Jogiya**, G Morton, K De Silva, D Perera, S Redwood, S Kozerke, E Nagel, S Plein Heart 2012;98:Suppl 1 A14-A15

6. First pass vasodilator-stress myocardial perfusion CMR in mice on a clinical whole-body 3 Tesla scanner: validation against microspheres

**R Jogiya**, M Makowski, A Phinikaridou, A Chiribiri, N Zarinabad, S Kozerke, R Botnar, E Nagel, S Plein

Heart 2012;98:Suppl 1 A66-A67

7. Dynamic three-dimensional whole heart magnetic resonance myocardial perfusion imaging: validation against the Duke Jeopardy Score to assess myocardium at risk

**R Jogiya**, G Morton, K De Silva, D Perera, S Redwood, S Kozerke, E Nagel, S Plein

Heart 2012;98:Suppl 1 A57-A58

8. Validation of dynamic three-dimensional whole heart magnetic resonance myocardial perfusion imaging at 3.0 Tesla against fractional flow reserve for the detection of flow-limiting coronary heart disease

**Roy Jogiya**, Geraint Morton, Kalpa De Silva, Simon Redwood, Sebastian Kozerke, Divaka Perera, Eike Nagel, Sven Plein

J Cardiovasc Magn Reson. 2012; 14(Suppl 1): O92

9. Multicenter evaluation of dynamic three-dimensional whole-heart myocardial

perfusion imaging for the detection of coronary artery disease defined by fractional flow reserve

Robert Manka, Rolf Gebker, Lukas Wissmann, **Roy Jogiya**, Manish Motwani, Michael Frick, Sebastian D Reinartz, Bernhard Schnackenburg, Eike Nagel, Sven Plein, Sebastian Kozerke

J Cardiovasc Magn Reson. 2013; 15(Suppl 1): O103

10. Myocardial ischaemic burden assessed by three-dimensional perfusion CMR - comparison with Myocardial Perfusion Scintigraphy

**Roy Jogiya**, Geraint Morton, Mark Peterzan, Kalpa De Silva, Sebastian Kozerke, Eike Nagel, Stephen R Underwood, Sven Plein

J Cardiovasc Magn Reson. 2013; 15(Suppl 1): P175

11. Validation of dynamic three-dimensional whole heart magnetic resonance myocardial perfusion imaging at 3.0 Tesla against the duke jeopardy score to assess myocardium at risk

**Roy Jogiya**, Kalpa De Silva, Geraint Morton, Simon Redwood, Sebastian Kozerke, Divaka Perera, Eike Nagel, Sven Plein

J Cardiovasc Magn Reson. 2012; 14(Suppl 1): O91

12. Validation of dynamic three-dimensional whole heart magnetic resonance myocardial perfusion imaging against single photon emission computed tomography for the detection of functionally significant coronary heart disease

**Roy Jogiya**, Geraint Morton, Yasmine Samaroo, James Otton, Eike Nagel, Sebastian Kozerke, Stephen R Underwood, Sven Plein

J Cardiovasc Magn Reson. 2012; 14(Suppl 1): O47

13. First pass vasodilator-stress myocardial perfusion CMR in mice on a whole-body 3Tesla scanner: validation against microspheres

**Roy Jogiya**, Marcus R Makowski, Alkystis Phinikaridou, Christian Jansen, Niloufar Zarinabad, Amedeo Chiribiri, Rene M Botnar, Eike Nagel, Sebastian Kozerke, Sven Plein

J Cardiovasc Magn Reson. 2012; 14(Suppl 1): P61

14. Feasibility of three-dimensional (3D) balanced steady-state-free-precession (bSSFP) myocardial perfusion MRI at 3 Tesla using local RF Shimming with dual-source RF transmission

**Roy Jogiya**, Andreas Schuster, Arshad Zaman, Yasmine Samaroo, Eike Nagel, Sebastian Kozerke, Sven Plein

J Cardiovasc Magn Reson. 2013; 15(Suppl 1): P23

## Table of contents

## Keywords

- Cardiovascular magnetic resonance imaging
- *k-t* principle component analysis
- Three-dimensional perfusion imaging
- Myocardial ischaemic burden
- Coronary angiography
- Fractional flow reserve
- Myocardial perfusion scintigraphy
- Single photon emission computed tomography
- Murine perfusion imaging
- Balanced steady state free precession
- Artefact
- High resolution imaging
- Inter-study reproducibility

## Abbreviations

CMR = Cardiovascular magnetic resonance

IHD = Ischaemic heart disease

CAD = Coronary artery disease

*k-t* PCA = k space – time principle component analysis

LV = Left ventricle

FFR = Fractional flow reserve

DJS = Duke Jeopardy Score

QCA = Quantitative coronary angiography

2D = Two-dimensional

3D = Three-dimensional

LGE = Late gadolinium enhancement

MPS = Myocardial perfusion scintigraphy

SPECT = Single photo emission computed tomography

MBF = Myocardial blood flow

MPR = Myocardial perfusion reserve

3T = 3 Telsa

BSSFP = Balanced steady state free precession

TGRE = Turbo gradient echo

SNR = Signal to noise ratio

SAR = Specific absorption rate

CABG = Coronary artery bypass grafting

CV = Cardiovascular

## Acknowledgements

I am grateful to a number of people without whom this thesis would not have been possible. Firstly, I would like to thank my supervisor Professor Sven Plein, who gave me the opportunity to work under his guidance. I will always be grateful for his teaching, advice, support and encouragement throughout all stages of this work. His meticulous approach helped me keep my focus throughout all the important steps needed to successfully finish the project. His flexibility and support at times of need will never be forgotten.

I would also like to express my gratitude to my second supervisor, Professor Eike Nagel, for his support, advice and pearls of wisdom. Furthermore, I thank Professor Richard Underwood who first inspired and developed my interest in cardiovascular science and myocardial perfusion over 15 years ago. I am indebted to Professor Sebastian Kozerke for providing invaluable help and technical expertise throughout the work for this thesis. Thanks also go to Professor Rene Botnar for practical help and Professor Reza Rezavi, who always showed an interest and readiness to offer expertise and guidance.

The participation of all the patients and study volunteers, which made the research possible, has been very much appreciated. I would also like to thank all my colleagues in the Division of Imaging Sciences. My time in research will always be associated with fond memories of the people I have had the pleasure to work with. Particular thanks go to Geraint Morton, Kalpa De Silva, Shazia Hussain, Andreas Schuster, Zhong Chen and Alkystis Phinikaridou for their help and friendship.

This work would not have been possible without generous support from the British Heart Foundation and the help and collaborations of Manish Motwani, Professor Simon Redwood, Ian Webb, Lorna Smith, Stephen Sinclair, James Clark and Ash Patel.

I am grateful to my parents and siblings, who provided me with unconditional love and support throughout. I am grateful to Victoria for giving me the motivation and support to push through and complete the final stages of the thesis. Finally, I am forever grateful to my children Jevan and Olive for providing me with such welcome distraction. Although last in my acknowledgements, they are always foremost in my thoughts. Thank you, thank you.

# List of Figures



# List of Tables

# Chapter 1 Introduction

## 1.1 Ischaemic Heart Disease

### Epidemiology

Ischaemic heart disease (IHD) is the leading cause of death worldwide. It remains a major public health issue in the UK with more than two million people suffering the symptoms, most commonly angina. IHD accounts for more than 82,000 deaths each year and has a major impact on the economy, costing the UK £30 billion per annum (1).

It remains the chief cause of death in the UK despite advances in its management contributing to a decline in mortality rates of more than 50% since 1961 (2). Reduction in modifiable cardiovascular (CV) risk factors, in particular smoking, has contributed to this decline. A number of significant therapeutic advances including the use of aspirin (3), cholesterol-lowering statins (4) and anti-hypertensive agents (5) have been shown to improve prognosis and reduce major CV events.

Revascularisation of the myocardium with coronary artery bypass grafting (CABG) has also demonstrated prognostic benefit over medical therapy in patients with obstructive left main stem IHD, three-vessel IHD and significant left-ventricular (LV) function impairment (6). Percutaneous coronary intervention (PCI) has been shown to reduce symptoms and event rates in IHD, though the evidence for the prognostic benefit remains controversial (7,8).

### Management of IHD

The decision for revascularisation in IHD was traditionally based upon the anatomical assessment of the coronary arteries and the degree of coronary stenosis caused by atheroma. Treating the anatomical narrowing does not take into account the coronary blood flow or the myocardial perfusion and its viability, which is fundamental to the pathophysiology of IHD. It is widely accepted that the degree of coronary stenosis and its functional significance correlate poorly (9).

The early evidence for the performance of coronary revascularisation was based upon animal models with mechanical constrictors. These demonstrated a 40-85% reduction in coronary artery diameter (equivalent to a coronary stenosis) and induced a reduction in myocardial blood flow and perfusion, causing ischaemia (10). However, this model does not incorporate the complexity of IHD, which may involve multiple or diffuse stenoses, varying compositions of calcification in atherosclerosis, dynamic changes in vasomotor tone, and collateralisation. Longer lesions have been shown to produce greater haemodynamic change (11).

Guidelines exist on decision making for revascularisation (8) (Figure 1). Recognition of these limitations is reflected in current guidelines, which recommend the use of functional testing prior to revascularisation (Figure 2). A number of diagnostic tests, both invasive and non-invasive techniques, are available to assess the presence of IHD and can be used to guide clinical treatment. Cardiovascular magnetic resonance (CMR) is one technique that has recently generated much interest as imaging modality to detect myocardial ischaemia and its use is now reflected in international guidelines (Figure 2). This thesis addresses further advances in perfusion CMR.

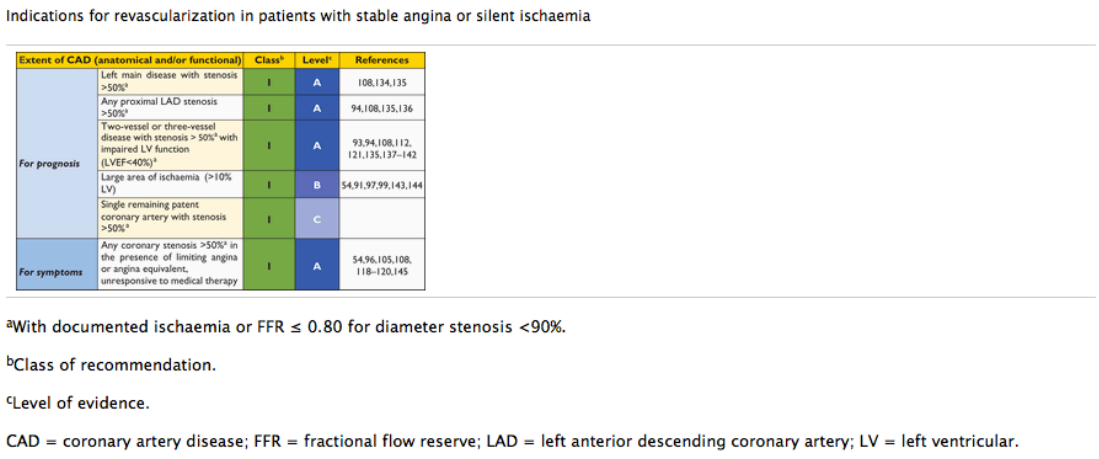

Indications for revascularization in patients with stable angina or silent ischaemia

| Extent of CAD (anatomical and/or functional) | | Class[b] | Level[c] | References |
|---|---|---|---|---|
| *For prognosis* | Left main disease with stenosis >50%[a] | I | A | 108,134,135 |
| | Any proximal LAD stenosis >50%[a] | I | A | 94,108,135,136 |
| | Two-vessel or three-vessel disease with stenosis > 50%[a] with impaired LV function (LVEF<40%)[a] | I | A | 93,94,108,112, 121,135,137–142 |
| | Large area of ischaemia (>10% LV) | I | B | 54,91,97,99,143,144 |
| | Single remaining patent coronary artery with stenosis >50%[a] | I | C | |
| *For symptoms* | Any coronary stenosis >50%[a] in the presence of limiting angina or angina equivalent, unresponsive to medical therapy | I | A | 54,96,105,108, 118–120,145 |

[a]With documented ischaemia or FFR ≤ 0.80 for diameter stenosis <90%.

[b]Class of recommendation.

[c]Level of evidence.

CAD = coronary artery disease; FFR = fractional flow reserve; LAD = left anterior descending coronary artery; LV = left ventricular.

**Figure 1 ESC guidelines on indications for revascularisation in patients with stable angina or silent ischaemia. Adapted from (8). The indication for myocardial revascularisation should included documented ischaemia or FFR <0.80 for all lesions between 50- 90% or >10% ischaemia**

Indications for diagnostic testing in patients with suspected CAD and stable symptoms

| | Asymptomatic[a] | | Symptomatic | | | | | | |
|---|---|---|---|---|---|---|---|---|---|
| | | | Probability of significant disease[b] | | | | | | |
| | | | Low (<15%) | | Intermediate (15–85%) | | High (>85%) | | |
| | Class[c] | Level[d] | Class[c] | Level[d] | Class[c] | Level[d] | Class[c] | Level[d] | Ref[e] |
| **Anatomical detection of CAD** | | | | | | | | | |
| Invasive angiography | III | A | III | A | IIb | A | I | A | 50–52,54 |
| CT angiography[f,g] | III | B | III | C | IIa | A | III | B | 57–62 |
| **Functional test** | | | | | | | | | |
| Stress echo | III | A | III | A | I | A | III | A | 63–65 |
| Nuclear imaging | III | A | III | A | I | A | III | A | 60,66–70 |
| Stress MRI | III | B | III | C | I | A | III | B | 71–75 |
| PET perfusion | III | B | III | C | I | A | III | B | 67,69,70,76,77 |
| **Combined or hybrid imaging test** | | | | | | | | | |
| | III | C | III | C | IIa | B | III | B | 78–83 |

CAD = coronary artery disease; CT = computed tomography; MRI = magnetic resonance imaging; PET = positron emission tomography.

[a]Screening for silent (asymptomatic) myocardial ischaemia may be considered in selected high-risk patients, such as those with diabetes mellitus.[84]

[b]Pre-test probability of CAD. Low 0—15%; intermediate 15—85%; high >85% as assessed using the criteria based on ESC Guidelines of SCAD.[47]

[c]Class of recommendation.

[d]Level of evidence.

[e]References.

[f]This refers to CT angiography, not calcium scoring.

[g]CT is considered to perform best in the lower range of pre-test probability (15—50%).[47]

**Figure 2 ESC guidelines on investigation of IHD. The current guidelines have recommended the use of functional testing prior to revascularisation. Stress CMR testing has now been included as one of the functional tests.**

## Mechanisms of IHD - Atherosclerosis

Atherosclerosis is hypothesised to be a multi-factorial inflammatory process as a result of environmental and genetic factors that disrupt the architecture of the vasculature leading to the development of atherosclerotic plaque and artery obstruction (12). The endothelium of the arterial wall responds to inflammatory stimuli to produce damaging chemokines, leading to deposition of inflammatory matter including smooth muscle cells, macrophages, T-lymphocytes, cholesterol, phospholipids and extracellular connective tissue, largely consisting of collagen (13). Endothelial dysfunction can therefore impair coronary blood flow.

This process can occur from early life, with evidence from necropsy studies of early streaks of plaque in the aorta and coronary arteries (14). Despite early pathophysiological changes, clinical manifestation can be many years later. The coronary circulation displays a number of physiological principles, which compensate for luminal stenosis to maintain a sufficient supply of oxygen.

## Coronary Physiology

The myocardium receives 5% of the cardiac output under basal conditions. It is efficient at extracting oxygen from blood, and at rest more than two-thirds of the available blood is utilised (15). Efforts to meet increased myocardial demand for oxygen are met by increasing blood flow. In the absence of coronary stenosis, blood flow can increase linearly with oxygen consumption. Flow predominantly occurs during diastole, as vascular resistance significantly increases during systolic contraction. Coronary flow is determined by diastolic (driving) pressure, vascular tone (resistance) and to a lesser extent elastic recoil within the conduit and capacitance vessels.

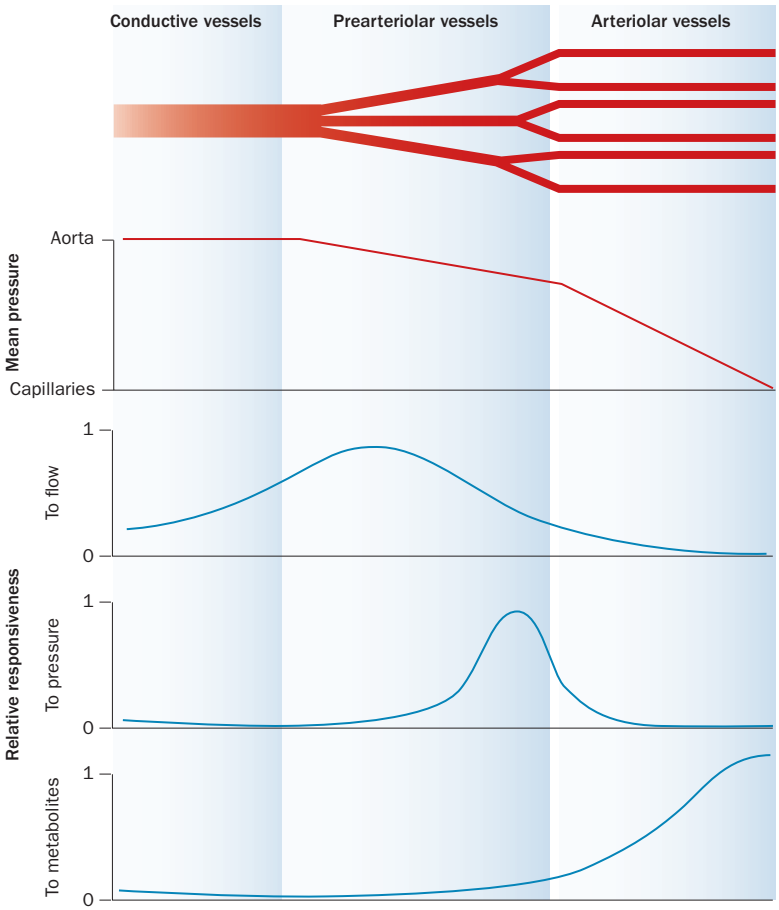


**Figure 3 Functional compartments of the coronary circulation.** Adapted from (16). Functional compartments of the coronary system summarising the pressure changes and the response to metabolites, pressure and shear stress.

Coronary artery circulation consists of three main components (Figure 3): epicardial arteries (conductive), pre-arterioles (100-300 μm) and pre-capillary arterioles (<100 μm).

The epicardial arteries under normal conditions make a minimal contribution to coronary vessel resistance (<5%) and have a capacitance function. The larger arterioles (100-300 μm) maintain a constant blood flow despite changes in perfusion pressure through autoregulation. They have a high resting tone and are thought to dilate in response to neurogenic and myogenic stimulation (17). The majority of resistance in the coronary vasculature is produced by arterioles less than 100 μm in size and is controlled by metabolic regulation, which allows for an increase in coronary blood flow with exercise. At rest blood flow is usually in the range of 0.6-1.2 ml/g/min (10). Myocardial blood flow can increase three- to five-fold. The increase in blood flow compared with baseline flow is defined as the coronary flow reserve (CFR) (Figure 4).

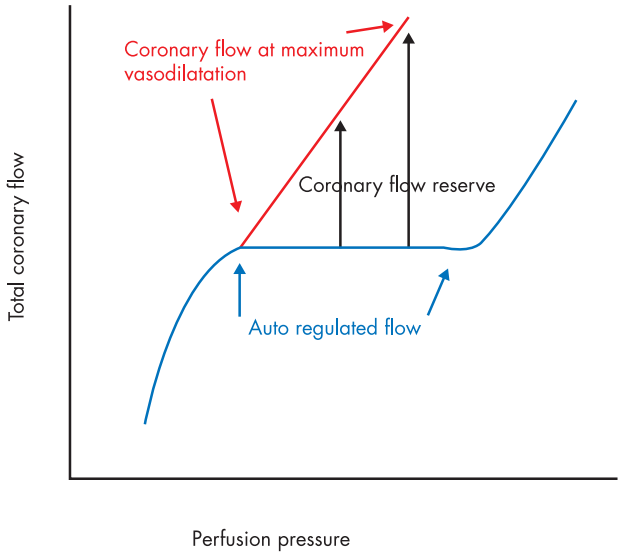


**Figure 4 Coronary blood flow vs. perfusion pressure.** Reproduced from (17). The coronary flow reserve represents the difference between the basal autoregulated blood flow (blue) and maximum flow (coral).

Under normal conditions, epicardial arteries have no significant influence on the degree of coronary vascular resistance. In the presence of a stenosic lesion, as flow is inversely proportional to the fourth power of the radius a small reduction in diameter can significantly affect blood flow. For an epicardial coronary stenosis of up to 85% (10)

resting blood flow is well maintained due to autoregulatory mechanisms in the arteriolar system compensating for the increased vascular resistance. Flow-mediated arteriolar dilatation maintains a constant blood flow and oxygen supply through the release of vasodilators, including nitric oxide, endothelium-derived relaxation factor, and prostacyclin, by the endothelial cells (18) (19).

Atherosclerosis disrupts the endothelium and impacts the compensatory vasodilator mechanisms. During hyperaemia, reduced blood flow will occur at lower magnitudes, typically from 40% stenosis. The variability in CFR is most marked in intermediate (50-70%) coronary stenosis (20) (21). Myocardial perfusion imaging must therefore be performed during hyperaemia in order to detect flow-limiting IHD. Early reduction in CFR can therefore represent early objective evidence of physiologically significant IHD.

The direction of the coronary circulation flow is from the epicardium to the endocardium; blood flow is thus heterogeneous across the ventricle. The endocardial layer is more susceptible than the epicardium because of the extravascular compression from the myocardial contraction, higher oxygen consumption and workload (22) (23). In the absence of epicardial stenosis, earlier reduction in subendocardial flow may reflect dysfunction in the microvasculature due to systemic disease including atherosclerosis, hypertension or diabetes. Higher-resolution imaging techniques may allow more sensitive differentiation than lower-resolution techniques.

In summary, the relationship between the degree of epicardial stenosis and CFR is complex and dependent upon multiple factors. A functional assessment is necessary to correctly assess the significance of coronary stenosis.

**Ischaemic Cascade**

When myocardial oxygen demand exceeds supply, a sequence of biochemical, haemodynamic and electrophysiological changes leads to angina. The earliest effect of atherosclerosis is endothelial dysfunction, which leads to subendocardial ischaemia. The resultant reduction in coronary perfusion leads to diastolic dysfunction and metabolic abnormalities, and progresses to electromechanical dysfunction along this cascade until symptoms of angina occur (Figure 5).

Early detection of this cascade is the goal of non-invasive testing. Detecting early changes in ischaemia may help prevent the disease from becoming symptomatic, and is useful for monitoring the progression over time. Inducing coronary vasodilatation physically or pharmacologically may enable this cascade to be exploited and allow earlier detection of ischaemia. This concept forms the basis of non-invasive detection of IHD.

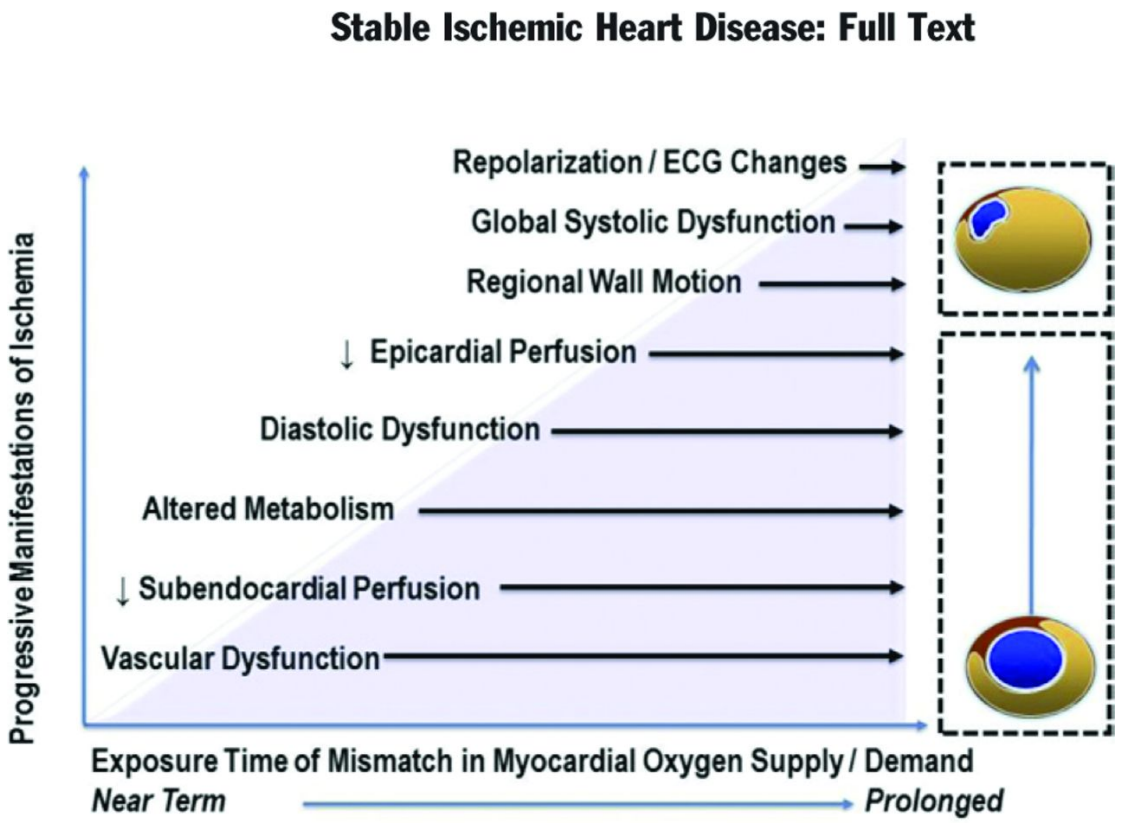


**Figure 5 The ischaemic cascade.** Reproduced from (24). The ischaemic cascade describes the transition from the earliest recognisable changes in the myocardium that ultimately lead to clinical symptoms of angina.

### Physical Stress

Exercise offers important information on CV physiology independent of imaging. Physical exercise increases myocardial oxygen demand and causes coronary vasodilatation. There is an increase in heart rate and contractility, and reduced afterload. Exercise allows concurrent evaluation of symptoms, haemodynamic and metabolic parameters, exercise capacity and electrocardiographic changes.

A treadmill or bicycle is used with set protocols based on increasing intensity with duration. Each technique has its own merits; however, peak oxygen consumption is lower using bicycle exercise in an untrained subject (25). Methods are often combined with exercise electrocardiogram (ECG) testing, exercise stress echocardiography (ESE), and single photon emission computed tomography (SPECT). Exercise in the CMR environment was previously difficult because of safety issues due to a lack of compatible equipment, but MRI-compatible bicycle ergometers have been designed and used for research purposes (26). However, there are a number of limitations including patient discomfort leading to early muscle fatigue, not reaching peak stress and movement during the scan affecting image quality.

The problem of motion during scanning was overcome recently with an MR-compatible non-ferrous hydraulic-powered treadmill. Its feasibility and safety have been demonstrated in healthy volunteers showing that perfusion and cine imaging could be performed rapidly after exercise (27). More recently, a pilot study showed treadmill exercise CMR can be performed at least as rapidly as ESE (28). To allow free movement, the patient is pulled out of the scanner for exercise. During this, the coil and patient location may move relative to the starting position resulting in changes to slice location and introduce artefact. Due to the impact of exercise on breathing and breath-holding, there is greater respiratory motion and temporal blurring, which can lead to reconstruction artefacts due to loss of coil sensitivities limiting the possibility of using temporal undersampling methods. Exercise in the CMR scanner is challenging and is a currently a niche area.

**Pharmacological Stress**

Patient factors including disability, lack of motivation or poor conditioning may prevent the achieving of maximal hyperaemia from being achieved through exercise, which may lead to a non-diagnostic test. Pharmacological stress can be used to mimic physiological exercise and induce coronary hyperaemia. Pharmacological agents can differentiate haemodynamically important obstructive and non-obstructive significant lesions during maximal vasodilatation, as CFR is impaired with flow-limiting coronary stenosis. Some protocols, particularly in SPECT stress perfusion imaging, combine exercise with pharmacological stress, firstly to overcome the issue of submaximal exercise and

secondly because exercise can ameliorate the non-cardiac side effects of vasodilators (adenosine and dipyridamole) as well as major arrhythmias (29). Two groups of pharmacological agents are widely used: vasodilators and sympathomimetics.

**Adenosine**

Adenosine is a naturally ubiquitous purine nucleoside, which is formed by the breakdown of adenosine triphosphate (ATP). ATP is the major energy source at a cellular level, needed for transfer of energy. It is metabolised by a process of dephosphorylation in the mitochondria through aerobic or anaerobic metabolism. Adenosine also has a role in signal transduction as cyclic adenosine monophosphate. Adenosine exerts its physiological effects by cellular signalling on four main receptors: A1, A2a, A2b and A3 (30). Adenosine A2 receptors are found most commonly within the coronary arteries (Figure 6). Adenosine acts upon the coronary arterioles and mediates metabolic blood flow regulation. It is formed in the myocytes through the action of ATP. Coronary vasodilatation occurs mainly through activation of A2a receptors leading to vascular smooth muscle cell relaxation. The role of A2b receptors in causing coronary vasodilatation remains controversial.

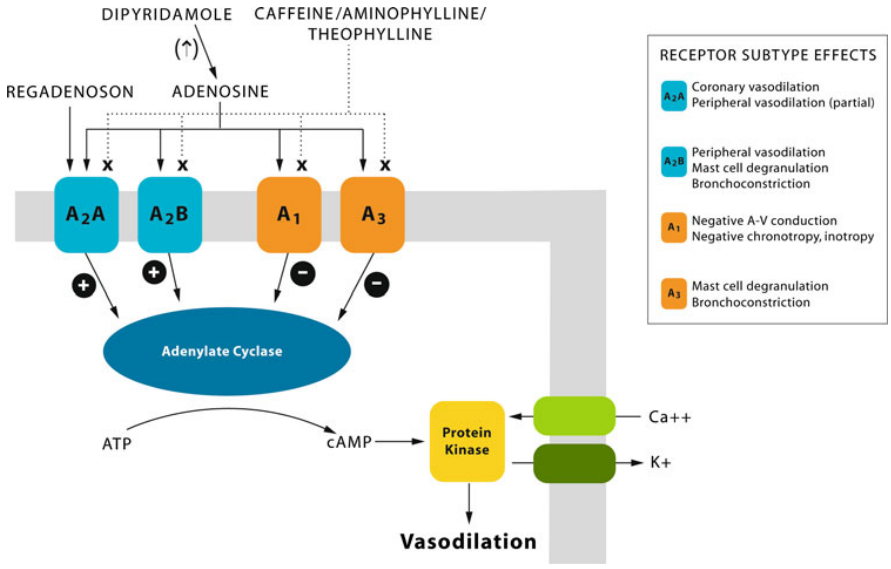


**Figure 6 Adenosine receptor subtypes.** Adapted from (29). Adenosine receptor subtypes and their mechanisms of action and clinical effects. There are three main adenosine receptors, with two subtypes of A2 receptors. Activation of the A2 receptors causes activation of adenylate cyclase, causing downstream activation of the potassium and calcium channels and consequently hyperpolarisation and then relaxation and vasodilation of smooth muscle.

The net effect is an increase in interstitial adenosine concentration with an increase in coronary blood flow. Infusion of adenosine can produce near-maximal hyperaemia of the coronary microcirculation, with an increase in coronary flow reserve.

Adenosine has a short half-life of less than 10 seconds and can be administered via IV infusion or intracoronary injection. For perfusion CMR studies, adenosine is given as a peripheral infusion for four minutes. In areas supplied by a significantly stenotic coronary artery, arteriolar resistance falls further in order to preserve capillary hydrostatic pressure. This is maintained until capillaries de-recruit as a decompensatory mechanism to preserve the compromised hydrostatic pressure; the net result leads to a rise in capillary resistance in the area supplied by the stenotic artery. As the surface area of capillaries is reduced, there is reduced perfusion and lower concentration of contrast agent compared with the normal supply of myocardium, which is represented and visualised by a perfusion defect (31).

For invasive investigation of the haemodynamic significance of a coronary stenosis, fractional flow reserve (FFR) can be measured. Intracoronary injections are often used due to simplicity, cost, few side effects and ability to perform multiple measurements. However, there are several limitations with this method including reproducibility of FFR (32) and the fact that pressure drop across a diffusely diseased artery cannot be measured.

The A2 receptor effects of systemic and peripheral vasodilatation cause undesirable effects including facial flushing, hypotension and dizziness. Activation of other receptors (A1) leads to reduced chronotropy and dromotropy, which may cause atrioventricular (AV) nodal blockade. Chest discomfort, nausea and dyspnoea are frequently experienced but the mechanisms are considered multi-factorial (A1, A2b, A3). Adenosine stimulates increased respiration via pulmonary C-fibre stimulation through activation of A1 receptors. Asthmatics can develop bronchospasm via activation of A1 (mast-cell-independent), A2b and A3 receptors (mast-cell-dependent).

Adenosine is therefore relatively contraindicated in asthmatics and contraindicated in patients with higher-degree AV block (second or third degree) and severe hypotension.

Treatment of these complications involves stopping the infusions and the additional use of theophylline, salbutamol and atropine.

**Dipyridamole**

Dipyridamole was the earliest pharmacological stress agent used in the diagnosis of IHD. It is an agent which indirectly acts by the same mechanism to cause coronary vasodilation by increasing endogenous adenosine levels. This occurs by inhibition of cellular reuptake and deamination of adenosine. It has multiple additional effects, including inhibition of platelet activation and thrombosis by phosphodiesterase inhibition. It can be given orally but owing to its reduced potency and pharmacokinetics the IV route is preferred. Peak vasodilation usually occurs within four to eight minutes following a four minute infusion, and has a longer half-life of 30 to 45 minutes. The usual dose is 0.56 mg/kg; at higher doses it can precipitate angina in patients due to the coronary steal phenomenon and increased myocardial oxygen demand (33). The side-effect profile is similar to adenosine; however, due to the anti-thrombotic and anti-inflammatory effects, prolonged bleeding, nosebleeds and gastrointestinal upset can also occur.

**Selective A2a Receptor Agonist**

Most (>80%) patients experience side effects from adenosine or dypiridamole through non-selective activation of adenosine receptors (34) (35). Coronary vasodilation is primarily mediated by stimulation of the A2a receptors, whereas stimulation of the other receptors causes undesired side effects. More selective A2a receptor agonists have the potential to cause hyperaemia whilst reducing these side effects. A number of selective agents have been proposed including regadenoson, binodenoson (36) and ATL313.

Regadenoson was the first selective A2a receptor agonist to be approved as a pharmacological stress agent for use with radionuclide myocardial perfusion imaging. It is more potent than adenosine at the A2a receptor. It has a number of advantages including a standard fixed dose (400 micrograms), independent of the patient's bodyweight. It is an adenosine derivative that is less rapidly metabolised and therefore

can be administered as a slow bolus over 10 seconds. This avoids the need for an infusion pump, reducing the duration of the stress protocol, and has implications for efficiency of laboratory resources and physician time. Hyperaemia typically occurs within a minute and lasts for two to three minutes; the haemodynamic effects are seen quicker than with adenosine, with heart rate being more marked (36,37).

In clinical studies, regadenoson has demonstrated similar diagnostic values to adenosine but an improved safety profile. The randomised, double-blinded, ADVANCE MPI 1 and 2 trials demonstrate non-inferiority of regadenoson to detect reversible perfusion defects with SPECT imaging (38,39). They demonstrate a significant reduction in major side effects (complete heart block), favourable side-effect profile and tolerability. The major limitation is that these trials exclude patients who have contraindications to adenosine and patients with significant symptoms on adenosine only. Further studies have demonstrated the safety of regadenoson in patients with asthma and COPD (40,41), although caution should be exercised if the airway disease is more marked.

ATL313 is another selective potent adenosine receptor agonist that has been used in the assessment of murine perfusion CMR, with encouraging results (42). This agent has pleotropic immuno-modulatory effects and its use has been investigated in lymphoma and multiple sclerosis.

**Limitations of Adenosine and Analogues**

Caffeine (methylxanthines) can attenuate the response through blockade of the A2a receptor – which may mask ischaemia. This has been demonstrated in dipyridamole (43) but controversy exists as to whether it applies to adenosine (44), as it is thought at the dose used there are sufficient additional adenosine molecules to competitively occupy the receptors. In clinical practice patients are asked to abstain from xanthine-rich products. Where xanthine-rich products have been consumed, high-dose adenosine has been shown to overcome the attenuation of myocardial perfusion defect size caused by caffeine (45).

**Dobutamine**

Dobutamine is a synthetic predominantly Beta 1 agonist with mild agonistic effects on the Alpha 1 and Beta 2 receptors. It has variable responses according to its dose of administration. It has a half-life of less than two minutes and is rapidly metabolised in the liver. At low doses (<10 mcg/kg/min) dobutamine increases cardiac contractility and causes some coronary vasodilation. It is used in stress studies to assess wall motion of the myocardium for the assessment of myocardial viability (46).

At higher doses (20-40 mcg/kg/min) it causes systemic vasodilatation (from stimulation of the alpha receptors) coupled with increased contractility, usually leading to a net increase in blood pressure and heart rate (47). The increased myocardial oxygen demand is thought to cause a secondary increase in coronary blood flow. In haemodynamically important epicardial stenosis this may induce heterogeneity of blood flow by competitive horizontal and vertical steal mechanisms. In accordance with the ischaemic cascade, dobutamine is used for the assessment of wall motion as a surrogate marker of ischaemia; it can also be used for the assessment of myocardial perfusion. To improve the detection of ischaemia by achieving the individual target heart rate during stress, atropine (0.6 mg), a muscarinic antagonist, blocks the vagus, resulting in a tachycardic response.

However, a number of side effects can occur including non-cardiac (nausea, headaches, anxiety), which are usually well tolerated. Cardiac side effects include hypotension (2%) and arrhythmias including supraventricular (2%) and ventricular tachycardias (2%) (48).

## 1.2 Invasive Detection and Assessment of Ischaemia

Detection of ischaemia can be performed with exercise or pharmacological stress using non-invasive imaging techniques. The diagnosis of IHD however can be performed either invasively or non-invasively. Each technique has its own merits and limitations.

### Coronary Angiography

Invasive coronary angiography remains the clinical standard for identifying coronary stenosis related to IHD. The technique of selective coronary arteriography was first performed over 50 years ago (49) and around 250,000 procedures are now performed in the UK annually (50). The procedure is performed under local anaesthesia using guide catheters to selectively cannulate the coronary arteries. Iodine-based contrast media is injected selectively into the left and right coronary arteries with multiple two-dimensional X-ray images stored to enable visualisation of the coronary arteries without superimposition of the other vessels. With developments in technical equipment, major complications are relatively low (<1%) (51) in diagnostic procedures. Common complications include vascular injury related to the arterial puncture, contrast allergy reaction, exacerbation of kidney function, myocardial infarction (MI), stroke, arrhythmias and death.

### Analysis of Coronary Stenosis

Film-based cine angiography has been superseded by digital technology and high-resolution X-ray imaging is now used for improved visualisation of the coronary tree and side branches. Despite significant improvements in the quality of the image acquisition and displaying methods, the analysis remains largely unchanged. The majority of decisions estimating the severity of IHD are based upon visual analysis.

It is recognised that visual estimates of severity of stenosis are not accurate or reproducible (9) (52). To reduce these inaccuracies quantitative coronary angiography (QCA) systems are used to model the geometry of coronary artery abnormalities. QCA

improves accuracy in assessment of lesion dimension, but errors can occur in the estimation as it only visualises contrast within a vessel narrowing (53). Vessel overlap, cardiac motion causing blurring lesion shortening, X-ray angle projection and the asymmetric nature of atherosclerotic lesions can also affect the estimation in QCA. Difficulties can occur when the disease is located at a bifurcation junction or diffuse for point of referencing.

## Invasive Indices of Ischaemia

Patients with more extensive IHD have a worse prognostic outcome (54,55), but these patients are thought to benefit most from revascularisation (56). Combining quantitative analysis with quantitative angiographic scoring systems allows semi-quantitative estimation of the extent and severity of IHD. The Duke Jeopardy Score (57) combines assessment of severity and location of vessel stenosis and provides an estimate of the amount of myocardium at risk. The scoring systems demonstrate the importance of anatomical location. The more proximal the lesion is, the greater the amount of myocardium at risk. Scoring systems including the BCIS Jeopardy Score (58) and the Myocardial Jeopardy Index described in the Bypass Angioplasty Revascularization Investigation (BARI) (59), have been validated as independent predictors of mortality.

### Limitations of Invasive Indices of Ischaemia

The main limitation is that the scores do not encompass the concept of viable myocardium. A culprit vessel in a large infarcted area could represent a high jeopardy score or a large amount of myocardium at risk, but may not reflect significant ischaemic burden or viability. A recanalised vessel subtending a large area of myocardial scar and peri-infarct ischaemia may have no jeopardy score but a large ischaemic burden. Furthermore, in lesions with an intermediate stenosis, the functional significance may not reflect the anatomical invasive indices of IHD (9).

Older scoring systems, including the Duke Jeopardy Score, did not include a score for left main stem lesions. No contingency was made for patients with coronary artery bypass

grafts. Anatomical variations of coronary arteries could not be incorporated easily to give a true representation of the amount of myocardium subtended by that artery. Finally, there was selection bias of patients as the studies were performed on registry data which excludes data on patients over 80 years old.

**FFR**

Coronary pressure can be used as a surrogate for coronary flow in conditions of stable resistance. FFR provides objective physiological evidence of IHD, in particular of intermediate epicardial lesions (60,61). It is a technique used to measure the pressure difference across a coronary stenosis to determine whether it is functionally significant. A guidewire with a highly sensitive pressure- and temperature-sensed tip is passed to the distal end of the coronary artery where it is used to measure distal coronary pressure. A simultaneous pressure is recorded from the guide catheter to establish the pressure proximal to the lesion (62). The FFR is calculated from the distal coronary pressure divided by the aortic pressure at maximal hyperaemia. In a normal coronary artery where there is no IHD and no pressure drop the FFR is 1.

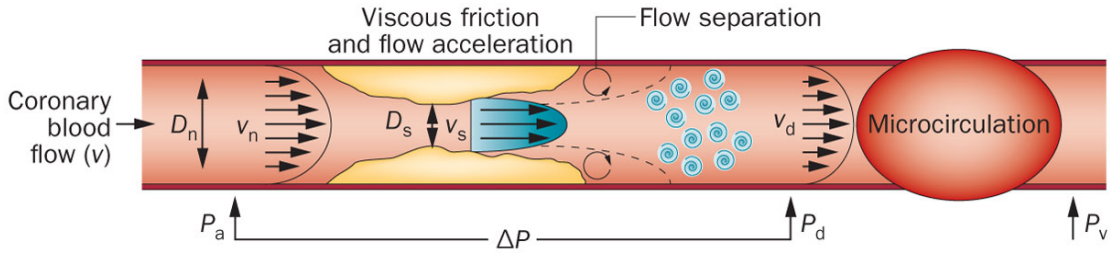


**Figure 7 FFR as a surrogate marker for inducible ischaemia.** Adapted from (62). FFR = Pd/Pa (Pd = pressure distal to the lesion, Pa = pressure proximal to the lesion)

As FFR is a continuous variable, an FFR cut-off value of 0.75 has a positive predictive value of 100%, a negative predictive value of 88% and a diagnostic accuracy of 93% to determine the presence of ischaemia (9). An FFR >0.8 is associated with negative ischaemia testing with a predictive accuracy of 95% (63). An FFR of between 0.75 and 0.8 is considered in the "grey zone", which requires clinical judgement (63). In post-PCI

measurements an FFR value <0.75 has a five-fold increase in adverse events compared with a post-FFR value of 0.9 (64).

In the DEFER study (65), which used FFR to determine the appropriateness of angioplasty in moderate coronary stenosis, if the FFR was ≥0.75 patients were randomised to either a medical treatment (defer group, n=91) or a PCI group (perform group, n=90). A five-year follow-up demonstrated no difference in event-free survival between the defer and PCI groups with FFR >0.75 (80% and 73%) and no difference in patients who were free of chest pain. Patient outcomes with deferral of PCI conferred an event rate (death and acute MI) of <1% per year (3.3% at five years), giving similar results in a negative stress test. The study suggested that patients with a stenosis and FFR ≥0.75 did worse if treated by PCI and supported the use of FFR to guide decisions on revascularisation.

The Fractional Flow Reserve versus Angiography for Multivessel Evaluation (FAME) study (63) was a multi-centre study of 1005 patients randomised to either visually guided PCI or FFR (<0.8)-guided PCI. Despite similar frequency of stenosis between the groups there were fewer stents used per patient in the FFR arm (2.7±1.2 and 1.9±1.3, respectively). The FFR group had significantly reduced adverse events and combined death or MI. Additional analysis also demonstrated a reduction in cost and hospital stay. Subgroup analysis showed that of all the patients with angiographic triple-vessel disease, only in 14% was this functionally significant (66). There were a number of criticisms of this study including the use of a threshold of FFR <0.8 and that differences may have related to inappropriate stenting of lesions in the visually guided arm rather than the FFR-guided PCI.

Functional guided revascularisation (including FFR) strategies were listed as a Class 1A recommendation in the 2014 European Guidelines in Myocardial Revascularisation (8). The follow-up FAME 2 (67) study included 1220 patients with a significant flow-limiting lesion (FFR <0.8, N=888) randomised into either PCI or optimal medical therapy (OMT). Patients with non-flow-limiting lesions were put into a registry and treated with medical therapy (N=332). The trial was stopped early, as patients with PCI were less likely to require urgent revascularisation (primary endpoint). Death and MI rates were similar

between the groups. Criticisms included that the study was not blinded and dual anti-platelet therapy was only used in the PCI group.

**Limitations of FFR**

Patients with unstable coronary syndromes were excluded from the large randomised studies. Furthermore, FFR may be overestimated in infarcted myocardium due to microvascular impairment (68) (69). Myocardial mass is reduced, and as it becomes fibrotic the relative demand from the supplying artery is also reduced due to less functional myocardium. In the presence of a moderate stenosis, its functional significance may therefore reduce according to the presence of scar. Viability testing by invasive measurement is limited, but the use of wave-intensity assessment in infarcted myocardium (70) has recently shown promising results.

As FFR measures pressure drops across an epicardial artery, the index does not take into consideration the contribution of abnormal microvasculature. In microvascular disease and LV hypertrophy ischaemia may still be present with an FFR of >0.8 (71). Technical issues may also occur including insignificant hyperaemia according to the route of administration (intra-cardiac [IC] vs. intra-venous [IV]), dampening of the guide catheter and signal drift by the guide catheter or the pressure wire (72), which need to be flushed and pulled back, respectively. Lastly, as this is an invasive test there is increased risk of complications and additional cost of set-up and pharmacological testing.

Overall, FFR is a useful technique and has advantages over conventional visual assessment of coronary lesions to determine functional significance. The cut-off is not strictly dichotomous but more likely a continuous variable for which the likelihood of ischaemia is significantly higher with a value of 0.75 or lower. Conversely, above 0.8 the likelihood of ischaemia is significantly lower. Between 0.75 and 0.8, the value is considered a “grey zone” where decisions should be made based on clinical evaluation.

**Instantaneous wave-free ratio (iFR)**

The instantaneous wave-free ratio (iFR) has been proposed as a method to measure the severity of coronary stenosis without adenosine hyperaemia. The concept of iFR was derived from wave-intensity analysis using both intracoronary pressure and flow velocity data. During diastole there is a "wave-free" period when microvascular resistance is low and stable, and measurement of the Pd/Pa ratio at this period in the resting state does not require hyperaemia (73). The ADVISE study demonstrated iFR correlated closely with FFR ($r=0.9$, $p<0.001$) and an iFR value of ≤0.83 was suggested to achieve comparable diagnostic accuracy for an FFR cut-off of ≤0.80 (74).

Further studies of diagnostic accuracy and validity during the wave-free period have been under debate particularly around moderate coronary stenosis(75,76). The RESOLVE study recruited 1768 patients from 15 centres and showed that there was no difference in diagnostic performance for resting Pd/Pa and iFR(77).

iFR may confer benefit in that it may obviate a recognised limitation of FFR. When coronary vessels have multiple stenosis it can be difficult to establish the haemodynamics of a specific lesion. iFR-Pullback has been proposed to permit the assessment of the haemodynamic impact of an individual stenosis in vessels with tandem lesions(78). This may be advantageous in planning coronary intervention in complex disease and predicting the impact of removing the stenosis on coronary haemodynamics.

At present, although it is a promising area, more evidence is needed to support the routine use of iFR, given the simplification and assumptions in its calculation and the variability observed in current studies.

## 1.3 Non-Invasive Assessment of Ischaemia

### Exercise Testing

Exercise ECG was the first line non-invasive method of detecting ischaemia. The major advantages are its wide availability, lack of requirement of technical expertise and the reduced cost of stratifying patients according to their risk of future events.

The presence and extent of significant IHD has been shown to correlate with the stage of Bruce Protocol (79) achieved. Notably, 10% of patients achieved level 3 or greater with a negative ECG but three-vessel IHD. The Duke Treadmill Score incorporates exercise capacity and exercise-induced ischaemia and showed that patients with a low risk had a low annual event rate (<0.5%) (80). A meta-analysis of 24,074 patients showed a mean sensitivity of 68% and a mean specificity of 77% (81). There are differences in the diagnostic accuracy in females (82). With newer diagnostic and more encompassing tests including CMR, NICE has removed exercise testing from its guidelines (83).

There are a number of contraindications to exercise testing (unstable angina, severe hypertension, severe aortic stenosis) and approximately 40% of patients are unable to achieve an appropriate level of stress for diagnostic purposes. Pre-existing ECG abnormalities may also preclude interpretation of exercise testing caused by bundle branch block, LV hypertrophy, paced rhythms or medications including digoxin.

### Echocardiography

Echocardiography uses a transducer to generate high-frequency sound waves of 1-5 MHz. The sound waves travel through the body until they reach a boundary and reflect an echo. A two-dimensional (2D) image is produced based on the distance and intensity of the echo. Millions of echoes are transmitted and received per second using a probe that utilises the piezoelectric effect. The probe usually contains quartz piezoelectric crystals, which change shape and polarity following the application of an electric current. The electric current can be adapted by changing the frequency and duration of the

pulses. Most transducers have multiple crystal elements to generate an ultrasound wave. The combination of these elements is called an array and the signal generated by the echo is then digitally transformed to produce a 2D image.

***Stress Echocardiography***

Two-dimensional echocardiography is used to assess the presence of stress-inducible myocardial ischaemia and in the detection of myocardial viability. Stress echocardiography can be performed in conjunction with exercise (physiological stress) or dobutamine (pharmacological stress). They have similar diagnostic accuracies. Physiological stress allows assessment of exercise capacity and symptoms. It may be considered to have fewer side effects than a pharmacological infusion of beta agonists. There is a delay from the exercise to acquisition of images as well as limitations with acquisition due to the respiratory motion and acoustic windows from hyperventilating during exercise. For patients unable to exercise or achieve appropriate physiological stress levels, dobutamine may be preferable.

***Diagnostic and Prognostic Performance***

Performance varies according to the stress protocol but sensitivity values were shown to be 85%, 80%, and 78% with specificities of 77%, 86% and 91% for exercise, dobutamine and dipyridamole stress, respectively – with no overall difference between the three (84) (85). In a meta-analysis the technique sensitivity varied significantly according to the coronary territory, with values of 72%, 55%, 76% for the left anterior descending (LAD), circumflex (Cx) and right coronary artery (RCA), respectively (86). This technique has demonstrated prognostic data. A negative stress echocardiogram yields a survival rate of >99% at one year and >97% at three years (87) (88). An abnormal scan is associated with a >10% risk of adverse cardiac events over subsequent years (89).

***Contrast Echo Perfusion***

Small highly echogenic microbubbles with a gas core (<10 microns) are administered intravenously as an infusion. They remain in the microcirculation without uptake or

influence on haemodynamics and can provide an assessment of myocardial perfusion (90). When a frequency signal is applied, the microbubbles compress, oscillate and reflect a harmonic frequency signal that can be distinguished from the surrounding tissues. An infusion at the rate of replenishment reflects myocardial perfusion. During hyperaemic stress, regions of hypoperfusion can be observed as they have a slower return of microbubbles.

### *Diagnosis and Prognosis*

Single-centre studies comparing myocardial perfusion with wall motion during dobutamine stress have confirmed improved sensitivity (91). Similar accuracies between perfusion echo and SPECT (92) have been demonstrated in studies and meta-analysis from 10 studies showed a sensitivity of 87% and a specificity of 72% in of 795 patients (93). Several studies have also demonstrated the prognostic impact of a positive perfusion scan (94) (95).

Advantages and Limitations

### *Advantages*

The lack of ionising radiation and portability is advantageous over other imaging techniques. Spatial resolution has improved with the use of harmonic imaging and IV ultrasound contrast agents. It is possible to derive both anatomical and functional information on the location, extent and severity of ischaemia. Concomitant assessments of valve and ventricular function can be made.

### *Disadvantages*

Disadvantages include that the interpretation of results can be subjective and operator-dependent. Foreshortening and incomplete coverage of the ventricle can lead to false negative scans. The image quality can vary dramatically and can be affected by patient factors including obesity and respiratory conditions. Anaphylaxis of the contrast agent is recognised. Intensive monitoring of patients with cardiopulmonary disorders and close observations of those without have been recommended (96). No contrast agents have been approved to date.

***Developments***

Limited ventricular coverage can also increase variability and reduce reproducibility. 3D echo techniques may overcome some of these problems by covering the whole heart simultaneously. Such techniques allow rapid image acquisition and require less skilled operators, and their feasibility for stress acquisition has been demonstrated. They may obviate the time-consuming serial acquisition of different imaging planes, which has to be performed in a narrow window of time during peak stress or whilst wall motion abnormalities exist. Unfortunately 3D techniques have lower temporal and spatial resolution and are more susceptible to artefacts than 2D methods; they also require longer analysis time. However, they may hold promise for the future (97).

**Nuclear Perfusion Techniques**

Nuclear perfusion techniques involve the administration of a radionuclide agent, which emits gamma photons by means of decay. A gamma camera is used to acquire a number of 2D projections of the emitted radiation from multiple angles. The projections are then tomographically reconstructed to produce a 3D dataset.

Radioisotopes of potassium, rubidium, ammonia and thallium are used for the evaluation of myocardial perfusion. The uptake of these agents within the myocytes is proportional to blood flow, myocyte integrity and the potassium pool. A reduction in myocardial perfusion, disturbance in cell membrane transport and lack of energy production or utilisation results in diminished uptake of these radionuclide traces. In infarction, cells are damaged and unable to uptake the tracers even if flow is preserved, and this is used as the basis of viability testing. Studies are gated to an ECG assisting with discrimination between true infarcts, viable myocardium and image artefacts (98). Stress-induced hyperaemia is usually achieved using adenosine, or regadenoson in combination with exercise. When there are contraindications, dobutamine can be used as the pharmacological stressor.

### *SPECT Myocardial Perfusion Scintigraphy (MPS)*

SPECT MPS is conventionally considered the clinical standard for perfusion imaging due to its extensive availability and use. Three radiotracers are commonly used in SPECT MPS: Thallium-201 (Tl-201), Technetium-99m (Tc-99m) sestamibi and Tc-99m tetrofosomin.

#### *Tl-201*

Tl-201 is a radioactive potassium analogue generated in a cyclotron. It therefore needs to be delivered from a radiopharmacy. It has a high first-pass extraction >85% at rest. Extraction is proportional to flow but plateaus and becomes non-linear at higher flow rates, thereby underestimating absolute values. Tl-201 is taken up via Na+/K+ in the ATP transport system intracellularly. This diffuses out of the cell. The characteristics of uptake and redistribution are used to differentiate ischaemia from scar.

Tl-201 emits low-energy 80 keV gamma radiation leading to attenuation artefacts and reduced-quality images in obese individuals. The long half-life (72 hours) also limits the maximum dose of radionuclide agent that can be safely administered. Tl-201 exhibits certain re-distribution characteristics that require acquisition within 15 minutes of completion of stress. As the radionuclide does not remain within the cell, it is in constant flux with the systemic circulation. With time (three to four hours), Tl-201 is taken up from the systemic circulation into hypoperfused myocardium. Viable and hypoperfused myocardium will therefore have homogenous normalised uptake of the perfusion tracer after several hours. Scar tissue will remain constant as a “fixed” defect – therefore this can be determined following a single injection of the tracer.

#### *Tc-99m sestamibi and Tc-99m tetrofosomin*

Tc-99m is eluted from molybdenum Mo-99m in a generator, and binds to compounds of sestamibi or tetrofosomin as a labelled agent. There is less attenuation with higher-energy radiation emission of magnitude 140 keV.

Tc-99m has a shorter half-life (six hours), allowing the use of a higher dose of tracer. Tc-99m perfusion agents are cleared from the hepatobiliary system and gastrointestinal tract, which causes a delay in its transmit. This may cause scattering of activity into the inferior wall of the heart, though this is usually corrected with post-processing software. Allowing for the transit of the radionuclide, images are usually taken 45-60 minutes following injection.

Tc-99m sestamibi binds to the mitochondrial membranes due to electrostatic interactions and minimally redistributes after initial uptake. Tc-99m sestamibi has a higher first-pass extraction (65%) than tetrofosomin (55%) at rest (99). Tetrofosomin is a newer radionuclide (available in the UK since 1994), which is favoured for SPECT MPS because of its lower radiation burden compared to sestamibi (8 vs. 11 mSv), ease of manufacture and low production cost. Several studies have shown no overall difference in the diagnostic detection of IHD between the three-perfusion radionuclide agents (100) (101).

***Image Analysis***

Analysis of images can be visual, based on the heterogeneity of stress and rest images, or semi-quantitative (102). This provides important measurements of disease extent, severity and reversibility and allows an estimation of ischaemic burden, which has been shown to have independent risk stratification value. The scoring uses a five-point semi-quantitative system based on a 17-segment model of the LV wall standardised by the American Heart Association (103,104).

A number of commercial packages are available (105) based upon the relative uptake of a tracer and have been validated prognostically for quantification of ischaemic burden (103). The Cedar-Sinai software is the most widely available and is based on sampling patients' short-axis and vertical long-axis tomograms using a maximum-count circumferential profile and then comparing these against a database of normal patients. If the profile falls below a set number of standard deviations, it is considered abnormal (Figure 8). The program will display a polar map compressing the 3D image into two dimensions with a percentage of abnormal pixel count in the regions of abnormal

myocardium. However, this software is dependent upon an institution's normal database; references will vary between institutions and according to the tracer and stress protocol used. Furthermore, estimations of the extent of ischaemia have been shown to vary according to the software package used (105).

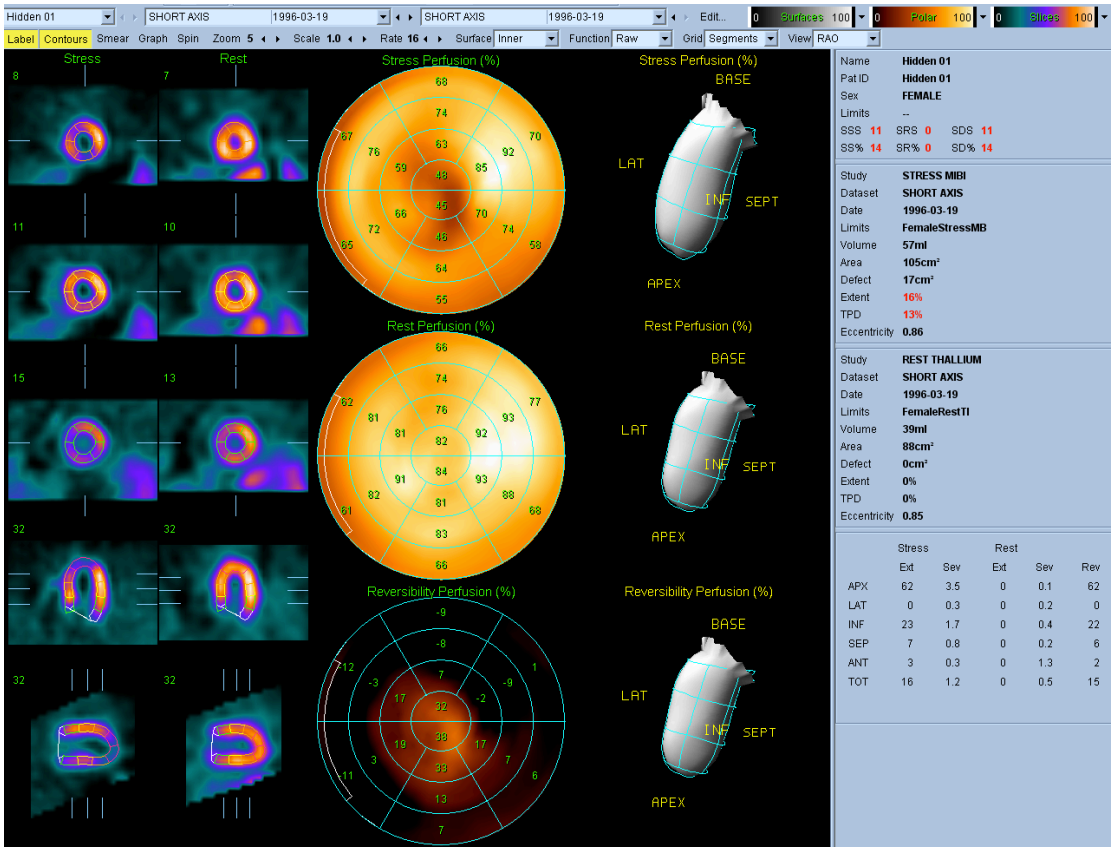


**Figure 8 SPECT MPS.** Adapted from http://cedars-sinai.edu. SPECT MPS showing semi-quantitative scores and an overall summary polar plot of homogeneity of tracer at stress, and demonstrating an apical perfusion deficit.

### *Diagnostic Accuracy*

There are a number of studies demonstrating the diagnostic performance of SPECT MPS. In a meta-analysis of 32 studies including 4480 patients, the sensitivity and specificity of exercise stress SPECT MPS were 87% and 73%, respectively (106). The corresponding values for vasodilator stress SPECT MPS imaging are similar (107) (89% and 75% respectively). It is noteworthy that the disease prevalence in the study population these studies were high (>75%).

A more recent meta-analysis of MPS imaging included 1323 patients from 13 studies, and showed the sensitivity and specificity were 83% and 77%, respectively (92).

***Prognostic Information***

Patients with a normal SPECT MPS study have a low risk of cardiac death or non-fatal infarction. A normal scan or a low-risk stress MPS were associated with an event rate of 0.6% per year (108). Patients with normal pharmacological stress have a higher annual cardiac event rate than patients with normal exercise scans (109). In a meta-analysis of 69,655 patients, at least moderately abnormal scans had an annual cardiac death or infarction rate of 5.9% per year (110). Additional studies have also shown higher event rates in patients with diabetes and chronic kidney disease (111).

MPS identifies patients who are likely to benefit from revascularisation compared with medical therapy in patients without prior known IHD (112) (113). Using MPS, the magnitude of ischaemic disease has been demonstrated to be associated with higher cardiac event rates. SPECT has been used to identify which patients could benefit from revascularisation on prognostic grounds. In the nuclear substudy (114) of the COURAGE (Clinical Outcomes Utilizing Revascularization and Aggressive Drug Evaluation) trial, ischaemic burden was reduced by PCI plus OMT over OMT alone. This study was not powerful enough to detect any difference in CV events. Subgroup analysis of a retrospective observational study in 13,969 patients showed that the presence of significant inducible ischaemia (an ischaemic burden >10% of the myocardium) was associated with a higher survival benefit with revascularisation than medical therapy alone (Figure 9). Conversely, patients without significant ischaemia or scar did better with OMT without revascularisation (115).

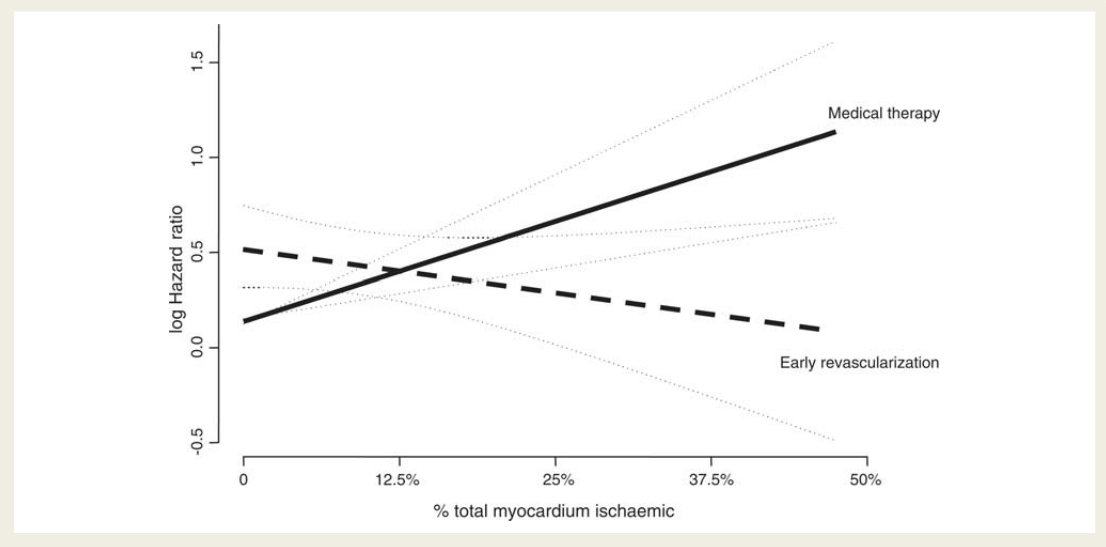


**Figure 9 Log hazard ratio of revascularisation vs. medical therapy.** Adapted from (115).
The lines intersect around 10-12.5%, above which the survival benefit for revascularisation over medical therapy increases with increasing amounts of inducible ischaemia. Conversely, with small amounts of ischaemia, medical therapy has a survival advantage over revascularisation.

### *Advantages*

SPECT MPS is widely used and the technique has been extensively validated for management of patients with IHD. A number of software and hardware advances have been made (116,117) (118). A number of studies have demonstrated the cost-effectiveness of this technique (119) (120). There may be less potential for technical errors in the study acquisition. In contrast to other techniques, which acquire over the first pass of the contrast agent, SPECT MPS imaging occurs over the uptake of multiple passes of the tracer. With multiple passes there is improved signal over a longer time period and less need for high temporal resolution.

### *Disadvantages*

As the technique often requires a double injection and adequate time period between the first and second scan, the duration of a protocol can take several hours. The spatial resolution is also considerably less (10x10 mm), making it difficult to detect subendocardial ischaemia.

The test involves significant doses of radiation exposure depending on the tracer tetrofosomin (10 mSv) and thallium (25 mSv). When the ischaemia is balanced, SPECT has reduced sensitivity to three-vessel disease or left main disease (121).
A number of causes of artefacts reduce the diagnostic accuracy of the perfusion images. These include the presence of left bundle branch block, respiratory motion, partial volume artefacts, scatter related to gastrointestinal activity and soft tissue attenuation, typically from the breast in women and diaphragm in men (122).

***Image Quality, Artefacts and Future Developments***

A number of practical strategies exist with an aim to overcome the potential for imaging artefacts. In men, an additional view of the left lateral decubitus can reduce the attenuation effects. The taping of breasts can also minimise attenuation. Analysis of the raw images helps to distinguish artefacts. Attenuation correction hardware uses two collimated line sources with Gadolinium 153. Emission and transmission projection images are obtained for each angular position and perfusion images are corrected for attenuation (123).

A number of software and hardware developments have reduced these limitations (118) (116). Post-processing software tools for motion artefact correction are available. Improvements in reconstruction methods and resolution recovery software have led to better image quality and spatial resolution (5x5 mm). Developments in hardware with the use of solid-state cameras using NaI or cadmium-zinc-telluride crystals and smaller zinc-based detectors are now available. These detectors are restricted to the cardiac field of view (FOV) surrounding the patient. They have the potential to increase count sensitivity five to 10 fold with a potential gain in resolution. A standard dose of injection allows acquisition within two to three minutes.

***Stress Perfusion Computed Tomography (CT)***

Despite the advantage of combining non-invasive coronary imaging with high spatial resolution, CT perfusion techniques have limitations. The main concern is the significant radiation burden – particularly when all imaging protocols (function and scar) are combined. Image quality is limited by patient heart rate and cardiac motion. During

stress perfusion the quality of images is reduced due to the tachycardia response to adenosine or alternative stress agents. Finally, the use of iodinated contrast agents limits its use in patients with allergies or renal dysfunction.

### *Positron Emission Tomography (PET)*

PET uses positron-emitting radiotracers. The net effect is that the positrons collide with electrons in their shell and form an annihilation reaction with the emission of two photons at 180 degrees to each other. When the paired photons are detected, the PET scanner registers events. N-13 ammonia, O-15 water, Rubidium-82 (Rb-82), and F-18 are the most commonly used tracers for PET cardiac perfusion imaging. Radio-labelled fluorodeoxyglucose (FDG) can be used to evaluate myocardial metabolic activity and viability.

### *Diagnosis and Prognosis*

PET has been shown to be more accurate than SPECT for the detection of ischaemia. A meta-analysis of 11,862 patients and 117 studies (only nine of which included PET) showed superior sensitivity of PET vs. SPECT MPS (92.6% vs. 88.3%, respectively) but no difference in specificity (81.3% vs. 75.8%) using angiography as the reference standard (124). In another meta-analysis of 1442 patients the sensitivity was 92% and specificity 85% (125). In a study comparing PET against perfusion CMR there was no overall difference in the detection of IHD (126).

The prognostic value of PET perfusion imaging has been demonstrated in multiple studies and is similar to that of SPECT MPS imaging. A normal PET scan was associated with <1% annual cardiac mortality, and a rate of 4.3% in those with abnormal scans (127). There are limited prognostic data on PET for ischaemic burden (summed stress scores <4) (128).

***Advantages and Disadvantages of PET***

PET offers improved spatial resolution and shorter duration protocols compared to SPECT. It is considered the reference standard to quantify absolute myocardial blood flow (129). Despite PET being an older technique than SPECT, there is limited availability and significant cost of PET scanners in the UK. Their use is primarily limited to research. Due to the nature of the radionuclide agent N-13 ammonia, it is also necessary to have a cyclotron on-site. Newer agents including Rubidium-82 may be generated through simple means and overcome the cyclotron issue. Rubidium has a comparable ionising radiation burden to SPECT radionuclide agents (14 mSv).

## 1.4 CMR

### Principles

Magnetic resonance (MR) describes a physical property of elements which have an uneven number of protons and neutrons and therefore possess an ability to spin around their axis. When an external magnetic field is applied, the spins align along the field in either a parallel or an anti-parallel direction, and an overall excess of spins occurs leading to a net magnetisation vector. A number of elements possess this physical property including 19F, 31P, 13C, 23Na, and 17O. Clinical imaging is based on hydrogen nuclei owing to their abundance (80%) in both intra and extracellular tissue compartments in humans.

Radiofrequency (RF) waves are delivered to the heart (RF pulse) and cause the aligned nuclei to tilt away from the magnetic field. The effect of the generated RF wave distorts the longitudinal direction out of alignment with the external magnetic field and also causes the spins to rotate in phase in the transverse direction. The subsequent relaxation and realignment leads to the transmission of a measureable RF signal, which is detected by the receiver coils and converted by Fourier transformation into digital signals to generate images.

Following the excitation, the net magnetisation vector returns to baseline. The relaxation occurs in an exponential method and the rate of relaxation is defined by the times T1 and T2. T1 describes the time it takes for 63% of the longitudinal magnetisation to recover after a 90-degree displacement. T2 describes the transverse relaxation as the spins go out of phase. The T1 and T2 values vary according to the tissue of interest, and this can be exploited to produce an intrinsic difference in contrast between the tissues (130,131).

CMR is considered the gold standard imaging modality for the assessment for LV volume and function (132). CMR has a number of advantages in comparison with other modalities. The technique avoids the need for ionising radiation and provides a

complete comprehensive assessment of the LV for function, perfusion and viability with high temporal and spatial resolution.

## Dobutamine Stress CMR

### *Use and Diagnosis*

Dobutamine stress CMR provides accurate detection of contractile reserve and ischaemia at low-dose dobutamine and assessment of viability and perfusion at higher doses. The technique is highly accurate due to the high spatial resolution, reproducibility and coverage of the LV. Single-centre studies have demonstrated its diagnostic value with a sensitivity of 78 to 96% and a specificity of 70 to 100% (133). A meta-analysis of 13 studies and 735 patients showed an overall sensitivity of 83% and specificity of 86% (134).

### *Dobutamine Stress CMR vs. Echo and Viability*

Viable myocardium can be assessed with CMR to determine its potential to recover its function over time or following revascularisation. The principle is similar to echocardiography using lower-dose dobutamine stress, but CMR yields a higher diagnostic accuracy due to the improved image quality and fewer problems with patient anatomy limiting imaging, in particular of the inferolateral segments or with bundle branch block (135) (136) (137).

Low-dose dobutamine (2.5-10 mcg/kg/min) is infused to assess LV myocardial thickening. A lack of thickening is considered to indicate myocardium that will not improve following revascularisation and lacks viability. A thickening response <1 mm has been shown to be a better predictor of residual metabolic activity than PET. For the assessment of viability, CMR had a sensitivity of 88% and a specificity of 87% when compared to PET (138). A wall thickening >2 mm for low-dose dobutamine was found to predict LV segmental functional recovery four to six months after coronary revascularisation (139).

***Prognosis***

Dobutamine CMR has shown its value for risk stratification and prognostication. A negative study confers an excellent prognosis (<0.6%) of CV events at least comparable to the other imaging modalities (140). Several studies have shown that a positive stress test confers an adverse prognosis (141). This risk increased with incremental ischaemic burden. Conversely, patients with an inducible wall motion abnormality following early revascularisation have a lower cardiac event rate than patients with medical therapy alone (142).

***Comparison with Perfusion***

Direct comparison of dobutamine against perfusion CMR for the detection of significant IHD showed no overall difference. The specificity for detection of IHD is marginally better with dobutamine at the cost of worse sensitivity (134). Due to vasodilatory effects of dobutamine at high dose, perfusion imaging can be combined with wall motion assessment (143). This has been shown to improve sensitivity, in particular in patients with ventricular hypertrophy and remodelling (144).

***Safety Profile***

For CMR dobutamine stress testing, the major adverse effects were similar to those reported with stress echocardiography, with an event rate of approximately one per 1000 (145) (146). Caution should be exercised, as patients are often in the MRI scanner without direct visualisation. Guidelines for the appropriate safety requirements have been published (147). Although similar diagnostic performance has been demonstrated against perfusion CMR for the detection of IHD, due to the increased duration of scan, tolerance, potential risk profile and experience, perfusion imaging is preferred (148).

**Late Gadolinium Enhancement (LGE)**

LGE has a high sensitivity and specificity to detect and quantify the magnitude of fibrotic tissue due to MI (149) (150). The presence of LGE in ischaemic and non-ischaemic myocardium confers an adverse prognosis (151) (152).

LGE techniques are based on gadolinium-DTPA contrast agents. Free Gadolinium is toxic; it competes with calcium and can pass intracellularly. It is therefore chelated with either linear or cyclic DTPA and is rapidly distributed in the intravascular and extracellular compartments. In infarcted tissue and non-viable tissue which is poorly perfused, there is an expanded collagen extracellular space (scar). Compared with healthy myocardium, Gd takes longer to wash into infarcted myocardium and longer to wash out. After 10 mins more Gd will have washed out of well-perfused healthy than infarcted/non-viable myocardium.

Gadolinium compounds have unpaired electrons, which interact with neighbouring protons in water to produce rapid relaxation indirectly. T1 and T2 relaxation times of water protons are inversely proportional to the local gadolinium concentrations (153). Late enhancement in infarction is due to increased volume of distribution and slow concentration washout. Early enhancement and myocardial perfusion differ due to delayed contrast wash-in. In evaluating cardiac perfusion, areas that are well perfused have a shorter T1 and appear bright on T1-weighted imaging. Hypoperfused regions have longer T1 and appear hypoperfused (154).

Black areas indicate normal myocardium that has undergone a wash-in, wash-out phase. In non-viable myocardium, there is an increase in penetration and distribution of the contrast agent and larger concentration of the gadolinium contrast leading to a bright image. The bright and high signal enables LGE imaging to accurately quantify the extent and severity of myocardial injury with excellent contrast and sub-millimetre resolution allowing for detection of microinfarcts of below 2 g (155). LGE scar imaging correlates closely with post-mortem infarcts in animal models and with PET imaging in humans (156).

Transmural thickness of scarred tissue and the prediction of recovery of a segment of myocardium following coronary revascularisation are inversely related (157). Scarred segments of myocardium with <25% transmurality of scar have a positive and negative predictive value of 88% and 89% of recovery following revascularisation. If a value of <50% transmurality is used the negative predictive value increases to 92% but the positive predictive value falls to 66% (Figure 10). The prediction of functional recovery after revascularisation with low-dose dobutamine combined with LGE improves the accuracy of CMR for determining myocardial viability (158).

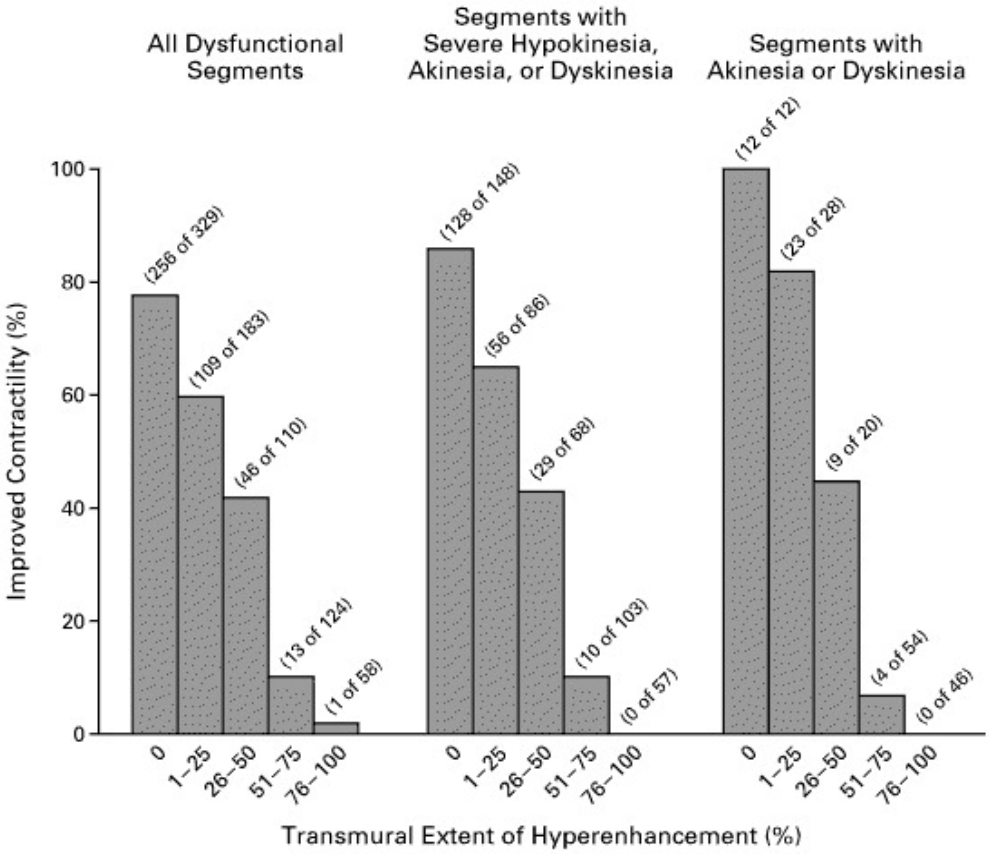


**Figure 10**

**Transmural hyperenhancement vs. revascularisation.** Adapted from (157). Relation between the transmural extent of hyperenhancement before revascularisation and the likelihood of increased contractility after revascularisation.

## Perfusion CMR

Over the past decade, myocardial perfusion imaging with CMR has become recognised as an accurate method for the detection of IHD (159) (160) (161) (134). Myocardial perfusion CMR can be performed with a number of methods, including blood oxygen level-dependent (BOLD) imaging (162) or arterial spin labelling (ASL) (163), although in practice dynamic first-pass methods with gadolinium-based contrast agents are by far the most commonly used.

Myocardial perfusion CMR has a number of advantages over other non-invasive tests including absence of ionising radiation, high spatial resolution, speed of acquisition and the fact that it is largely independent of the patient's body habitus. In addition, the method can in principle provide quantitative estimations of myocardial blood flow.

### *Principle of first pass myocardial perfusion CMR*

First-pass myocardial perfusion CMR tracks the passage of a contrast agent through the heart and myocardium. Data acquisition is synchronised with the cardiac cycle using ECG gating. Current methods allow for the acquisition of at least three sections of the heart in each R-R interval, typically positioned in the LV short-axis orientation. Additional short-axis or orthogonal long-axis images may be added. Data acquisition typically extends over 40-60 heartbeats, timed to coincide with the cardiac passage of an intravenously injected bolus of contrast agent (Figure 11).

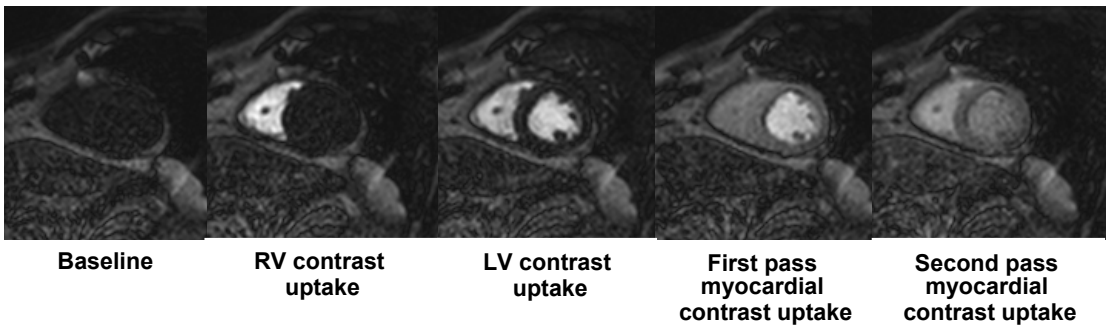


**Figure 11 CMR first-pass perfusion imaging.** CMR first-pass perfusion imaging at the mid-level of the myocardium during progressive time points following injection of gadolinium-based contrast agent. The contrast passes from the venous phase into the right ventricle, into the pulmonary circulation, then into the LV, and washes in and out of the myocardium.

Contrast agents in clinical use are generally gadolinium-based and shorten the T1 magnetisation recovery of blood. Acquisition pulse sequences for myocardial perfusion CMR are therefore T1-weighted. They are designed so that myocardial tissue appears dark before contrast arrival with signal in normal tissue enhancing homogenously during the myocardial contrast passage. Myocardium with reduced perfusion shows a lower and delayed signal enhancement. In clinical practice, the most common indication for perfusion CMR is the detection of myocardial ischaemia. For this purpose, blood flow to the myocardium is increased through coronary vasodilatation, which is most commonly achieved pharmacologically with IV infusion of a vasodilator such as adenosine. Reduced perfusion at hyperaemia due to flow-limiting ischaemic heart disease causes a delay and reduction in contrast delivery, identified as a dark or hypo-enhanced region on perfusion CMR (Figure 12).

(A) Stress Perfusion Imaging

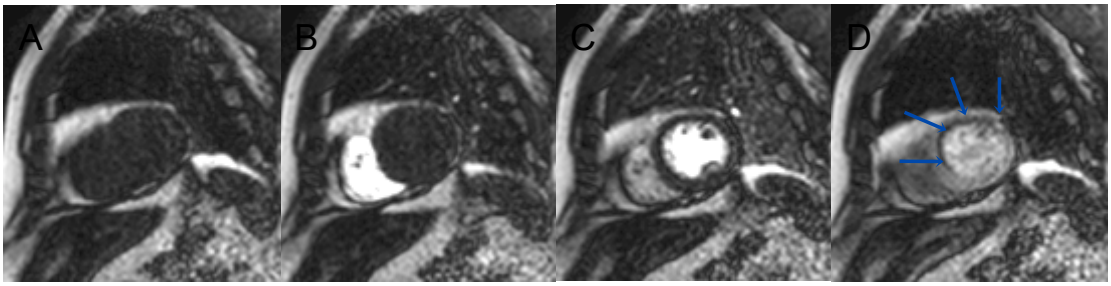


(B) Rest Perfusion Imaging

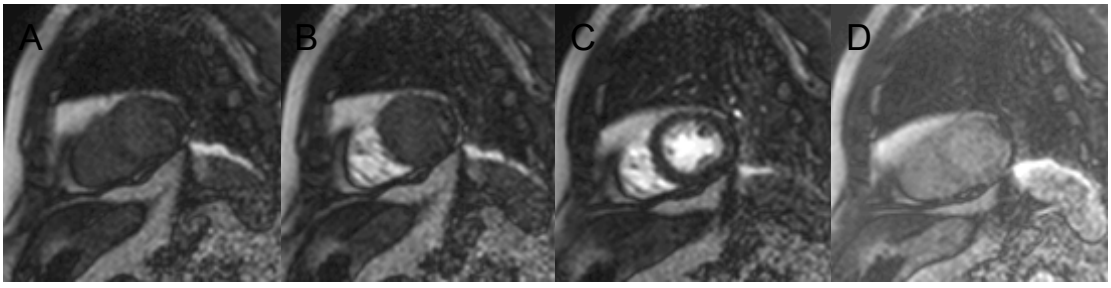


**Figure 12 Hyperaemic stress perfusion imaging.** Example of a hyperaemic (A) induced perfusion defect in the antero-septal region when compared with rest imaging (B) during the first-pass injection of gadolinium-based contrast agent (A-D). Coronary angiography demonstrated a severe stenosis of the LAD artery. Flow-limiting IHD corresponds to a reduction in contrast delivery as represented by a hypo-enhanced anterior wall during hyperaemia.

## Analysis of Myocardial Perfusion CMR and Contrast Dosing

### *Qualitative Analysis*

A variety of methods have been proposed for the analysis of perfusion CMR, including qualitative (164), semi-quantitative (165) and fully quantitative assessment (126) (166,167). In clinical practice, qualitative analysis by visual review of the acquired data is the most commonly used and most rapid analysis method. Conventionally, stress and rest data are compared to detect inducible perfusion defects and distinguish them from artefacts. Additional correlation is made with LGE data to detect scar and determine peri-infarct ischaemia. While the major clinical studies have used visual analysis, limitations of this analysis method are observer-dependence and the potential to underreport multi-vessel disease. In balanced ischaemia it is theoretically possible for all three vessels to have the same magnitude of ischaemia, but in reality this is exceptionally rare. Furthermore, the high spatial resolution of CMR usually permits detection of transmural perfusion gradients or greater relative differences in perfusion in the coronary territories. In lower-resolution modalities such as SPECT, large pixels are less able to discriminate and depict subtle differences in the magnitude of ischaemia as the abnormality between the arteries becomes smoothed out.

### *Qualitative Analysis and Dosing*

For qualitative analysis high signal is desirable within the myocardium, as there is greater differentiation between hypoperfused and normal myocardium. In summary, a dose of 0.05 to 0.1 mmol/kg is deemed appropriate for visual assessment of myocardial perfusion.

In an early dose-comparing study using an echo planar imaging (EPI) pulse sequence, there was no significant difference in diagnostic accuracy of perfusion CMR using 0.05, 0.1 and 0.15 mmol/kg doses of gadodiamide (Omniscan). There was a trend towards improved accuracy in the 0.1 mmol/kg group but higher doses were associated with increased artefacts (168). Another study which used gadopentetate dimeglumine (Magnevist) and a sequence of echo planar pulses showed similar efficacy between low doses (0.05 mmol/kg) and higher doses (164). The MR-IMPACT study analysed the

diagnostic performance of CMR myocardial perfusion in 228 patients using varying doses of Omniscan and found that a dose of 0.1 mmol/kg led to the highest diagnostic performance by visual analysis. The lowest dose (0.01 mmol/kg) was significantly inferior to the other doses (160) (Figure 13).

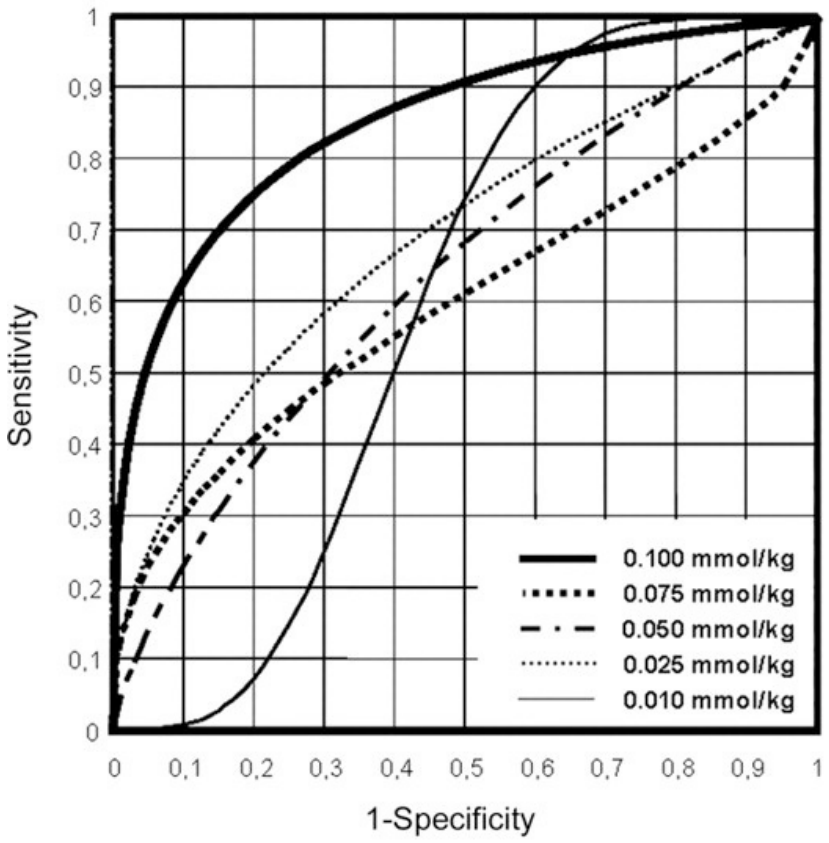


**Figure 13 Perfusion CMR accuracy vs. contrast dose.** Reproduced from (160). Qualitative diagnostic accuracy of perfusion CMR by contrast agent dose. Gadodiamide doses ranged from 0.01 to 0.1 mmol/kg in the MR-IMPACT study and the best diagnostic accuracy was observed in the higher 0.1 mmol/kg dose.

### *Semi-Quantitative Analysis*

For semi- and fully quantitative analysis epicardial and endocardial contours are manually drawn around the LV and copied to the dynamic frames. TIC can be derived for a defined pixel of myocardium (Figure 14).

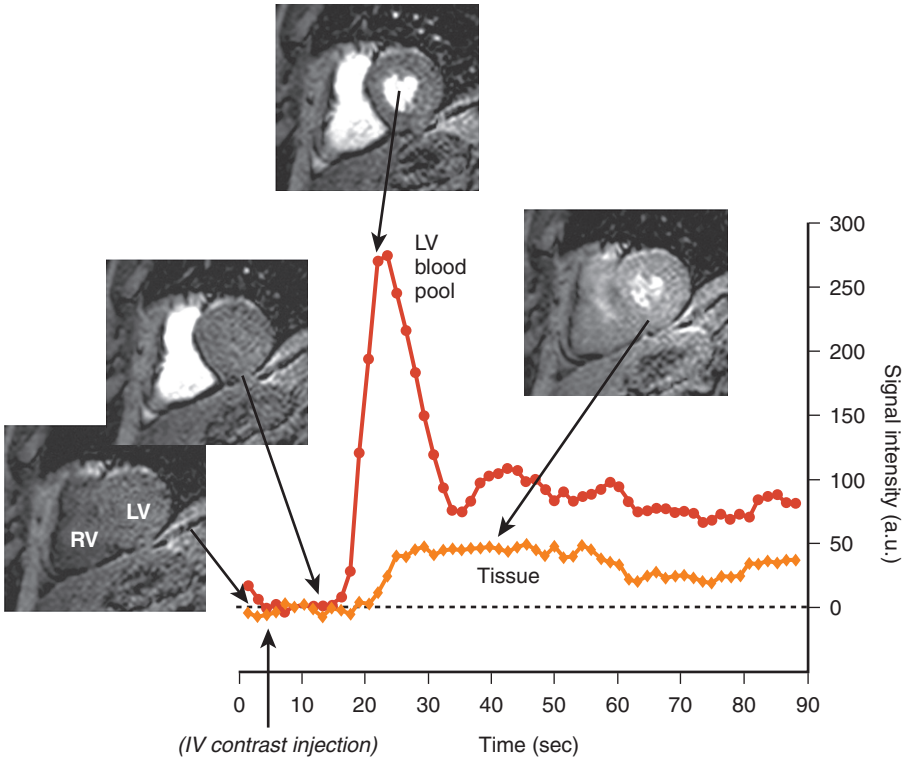


**Figure 14 Signal intensity vs. time.** Reproduced from *Cardiovascular Magnetic Resonance*, Manning and Pennell, second edition, 2010. Signal intensity curve against time showing the first pass of a gadolinium-based contrast agent in the inferior wall of the myocardium and the LV cavity. Injection was performed after four dynamics of pre-contrast acquisition. The peak concentration and signal intensity of gadolinium is higher in the LV bloodpool than the myocardium due to the larger intracellular space within the myocardium, to which gadolinium does not distribute.

Semi-quantitative methods are based upon the assessment of the signal intensity changes over the course of the first pass of the contrast through the myocardium. The myocardial time-intensity curve is compared at stress and rest to calculate an index or perfusion reserve.

A number of methods have been proposed including peak myocardial enhancement, time to peak enhancement, contrast enhancement ratio, upslope of the signal or the upslope integral and the calculation of a myocardial perfusion index (MPI) (Figure 15) (169). The upslope integral of the signal intensity curve is the most commonly used and has shown improved diagnostic accuracy over visual analysis (165). The analysis may also be influenced by differences in the contrast agent's pharmacokinetics and pharmacodynamic properties. In clinical practice, semi-quantitative analysis is less

frequently used, and in research studies quantitative analysis methods have become the methods of choice.

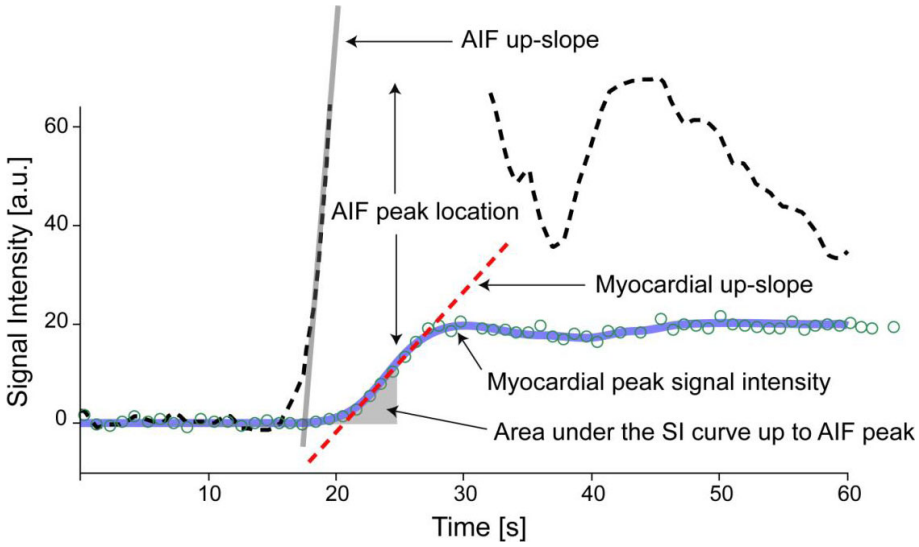


**Figure 15 Signal intensity curve of myocardial contrast enhancement.** Reproduced from (169). Signal intensity curves of myocardial contrast enhancement, which have been used as a semi-quantitative marker of tissue perfusion.

### *Linearity and Quantitative Perfusion*

At lower doses of gadolinium-based contrast agents, there is an approximate linear relationship between contrast agent concentration and signal intensity. At higher doses, which are necessary for higher myocardial contrast-to-noise ratio as well as visual analysis, T1 saturation effects occur with loss of linearity (170) (Figure 16). Maximum signal intensity response will not change despite increased concentration of gadolinium contrast.

Due to the increase in concentration of gadolinium in the LV bloodpool compared with the myocardium, contrast agents behave with non-linearity (0.01 mmol/kg) at lower concentrations than the myocardium (0.05 mmol/kg) (170). Signal attenuation is a particular problem in the LV as the signal intensity curve represents the arterial input function (AIF).

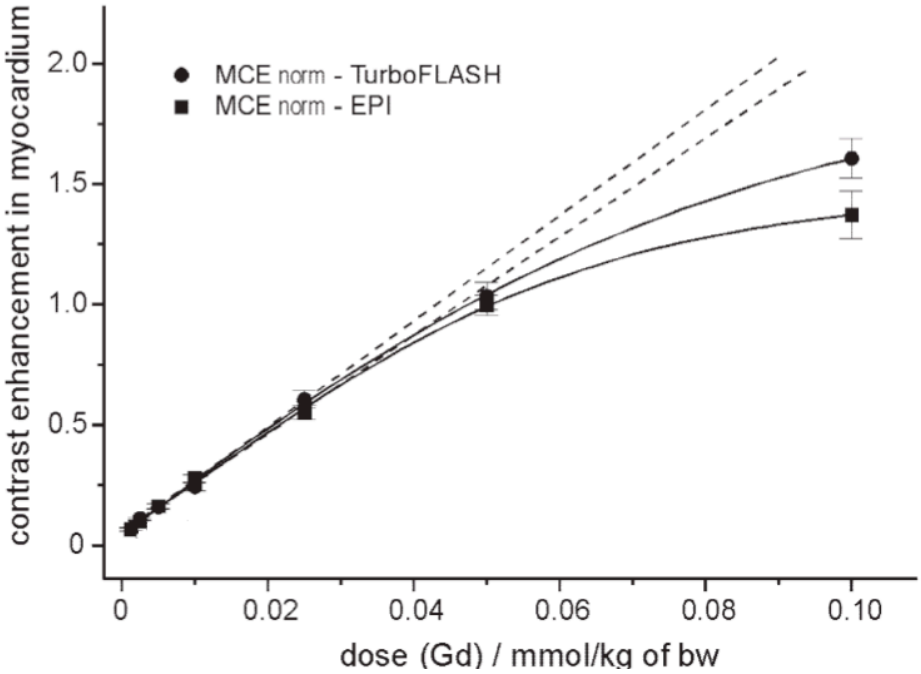


**Figure 16 Signal intensity vs. contrast dose.** Reproduced from (170). Signal intensity approaches linearity at lower doses. At higher doses, the signal intensity may not increase despite higher concentrations of gadolinium contrast.

A number of strategies have been proposed to overcome the problem of arterial signal saturation. First, dual-bolus methods use a low contrast dose (typically 0.0025-0.005 mmol/kg) to generate an AIF that is still in the linear 'contrast to signal range', followed by a higher dose (0.05-0.1 mmol/kg) bolus to improve myocardial enhancement. The lower dose allows an accurate assessment of the AIF from the LV bloodpool and the higher dose enables both visual and quantitative assessment of myocardial perfusion. This method has been used in animal studies over a range of blood flow rates (171). When comparing single and dual-bolus methods, both showed close correlation with perfusion, but greater signal and contrast was seen in the dual-bolus images (172). Furthermore, in smaller areas where myocardial signal was reduced, the dual-bolus methods appeared to provide more accurate results. Subsequent studies have demonstrated that the dual-bolus technique was more accurate than the single-bolus technique (173) for the assessment of myocardial perfusion reserve.

Second, the use of dual-contrast sequences permits the derivation of an accurate AIF from the LV bloodpool. In summary, two images are acquired – a low-resolution image

with a short saturation, followed by a higher-resolution image with a long saturation recovery (SR) time – in order to measure the myocardial signal (174).

### *Quantitative Perfusion*

Full quantification of myocardial perfusion CMR is based on modelling of the signal intensity profiles. A number of methods have been proposed, which can be broadly divided into the linear time-shift model, including Fermi constrained deconvolution, and the compartment model.

#### The Linear Time-Invariant Model

This is based on the calculation of the quantity of gadolinium in a region of myocardium. The contrast enhancement can thus be modelled and the myocardial impulse response can be calculated by deconvolution of the measured tissue response with an arterial input. The myocardial impulse response gives a direct estimate of myocardial blood flow. This technique is relatively robust to the effects of extracellular accumulation of the contrast agent during the first pass of the contrast (167) (175) (Figure 17).

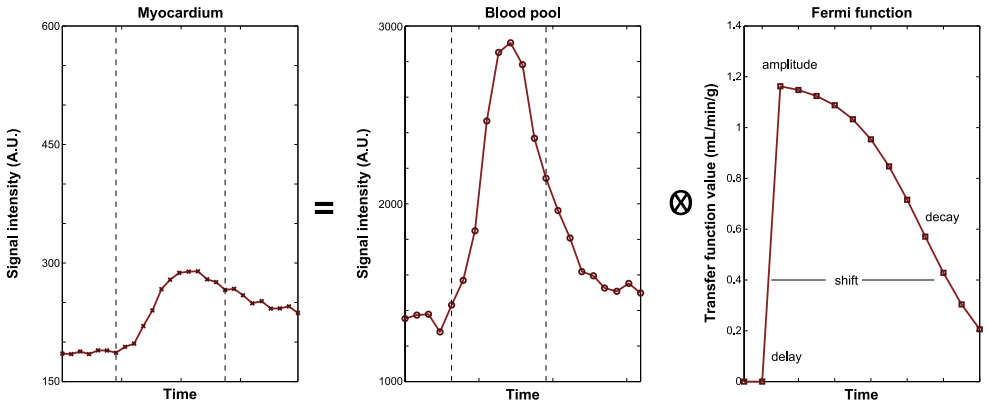


**Figure 17 Fermi function deconvolution.** Reproduced from (175). The myocardial time-intensity curves (TIC) (left) equal the bloodpool TIC (middle) convolved with the Fermi transfer function. The maximal amplitude of the transfer function equals absolute myocardial blood flow. The areas between the dashed lines of the TICs are used for analysis; these have also been corrected for coil effects, baseline signal intensity and conversion to gadolinium concentration.

Compartment Models

The compartmental model establishes the quantity of gadolinium shifting from the blood to the myocardium to establish absolute blood flow (166,176) (177) (Figure 18).

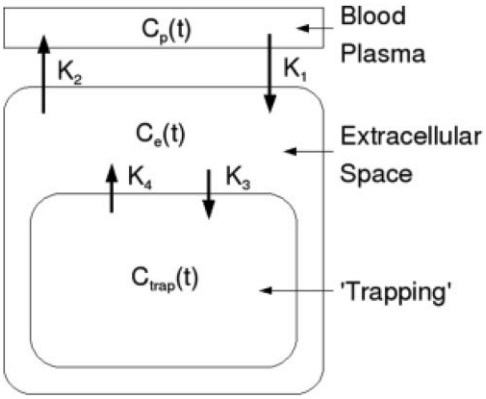


**Figure 18 Compartmental model.** Adapted from (177). The CV system is divided into distinct compartments (intravascular, interstitial and intracellular space). As gadolinium is an extracellular agent a two-compartment model is used. The concentration of gadolinium varies as the compound moves from one space into another. The shift from blood to myocardium is convolved to establish absolute blood flow.

***Clinical Quantitative Perfusion***

Quantitative analysis of myocardial perfusion CMR to derive absolute estimates of myocardial blood flow MBF has been validated in experimental models (166) and in clinical studies (176). Estimates of MBF reserve by CMR agree well with microspheres (171) and with PET, although in one recent study the correlation was less strong for stress MBF (126). Quantitative analysis methods offer increased objectivity compared with visual analysis and may be particularly useful to detect multi-vessel ischaemic heart disease if ischaemia is balanced, leading to global perfusion reduction. Quantitative analysis also enables definitions of thresholds associated with myocardial ischaemia and robust monitoring of disease progression as well as assessment of treatment efficacy. However, quantitative analysis is time-consuming and no agreed standards exist for it. Limitations to modelling of the complex distribution of MRI contrast agents need to be considered, as these complicate quantitative perfusion assessment. The clinical benefit of quantitative over visual analysis has been described recently, suggesting a promising role in clinical perfusion assessment (178).

Quantitative analysis of stress perfusion outperformed semi-quantitative measures of perfusion and qualitative methods with high diagnostic accuracy for the assessment of IHD.

## Pulse Sequences

There are two main components of pulse sequence techniques used in contrast-enhanced perfusion imaging: magnetisation preparation for T1 weighting, and image read-out.

### *Preparation Pulses*

CMR first-pass perfusion imaging is performed with T1-weighted pulse sequences. Gadolinium-containing blood and myocardium have shorter T1s and recover quicker, while non-enhancing myocardium and other tissues remain relatively saturated. To provide T1 contrast, RF saturation preparation pulses are delivered prior to image acquisition to suppress non-enhancing tissue. The inversion time (TI) is the time taken between the tissue preparation and the centre of the *k*-space of image acquisition. A short TI allows more slices to be acquired but influences signal-to-noise ratio (SNR) and contrast-to-noise ratio (CNR) as there is less contrast between enhanced and unenhanced tissue. A longer TI increases T1 contrast for visualisation of perfusion defects. Consequently, there is an increased acquisition time and the maximum number of slices that can be acquired in a given R-R interval is reduced.

Inversion recovery (IR) was the first contrast preparation to be used. The pulse sequence nulled the pre-contrast blood to maximise the contrast effect. Imaging duration was longer, often restricting imaging to a single slice per heartbeat (179). As the signal was not reset to zero for each R-R interval there was variation in contrast-to-noise ratios and signal intensities for each acquisition. IR perfusion imaging is also more vulnerable to R-R variation or missed triggers due to incomplete magnetisation recovery leading to greater differences in signal intensity. A magnetisation-driven steady-state preparation was also proposed. Non-selective RF pulses were used to achieve nulling prior to image acquisition (180). This technique produced better linearity of signal intensity to gadolinium concentration compared with the IR sequence, but at the cost of

reduced CNR. The preparation time was long, limiting the acquisition to one slice per heartbeat.

SR pulses are the most commonly used preparation pulses. The SR pulse is applied using a non-selective 90-degree RF excitation followed by a gradient crusher; the resultant signal is therefore independent of the magnetisation "history". SR sequences are relatively insensitive to changes in heart rate and have shorter preparation times (181) (Figure 18). SR pulses however may be sensitive to variations in the transmitted RF field (182), particularly at higher field strength, where there may be insufficient magnetisation saturation due to the increased B1 inhomogeneities. Newer SR preparation pulses including the adiabatic BIR4 pulse (insensitive to B1 - dynamic and B0 - static) and water suppression enhanced through T1 effects (WET) pre-pulse provide more uniform saturation, though with increased power deposition causing RF heating effects and increased performance time (182).

***Multi-slice Imaging***

To achieve multi-slice imaging the magnetisation preparation pulse can be applied in a number of different combinations. Single SR preparation per slice allows the same image contrast for each slice; however, the slices are acquired at different cardiac phases. Cardiac motion and wall thickness will vary, with the heart being less prone to motion artefacts during mid-diastole and end-systole. Shared SR preparation for multiple slices allows more slices to be acquired, but each slice has a different T1 contrast behaviour, as each slice has a different saturation and TI. Multiple interleaved slices per SR preparation allow greater efficiency of acquisition and therefore spatial coverage. However, the imaging time per slice is longer and the potential for motion artefacts is increased. In an alternative scheme using notched RF pulses to saturate adjacent slices, the TI is longer as the saturation pulse is performed prior to the previous slice read-out; there is consequently improved SNR at the cost of increased motion artefact. The first slice may be of poorer quality due to preparation pulse occurring during the preceding R-R interval, which may negate some of the efficiency gain.

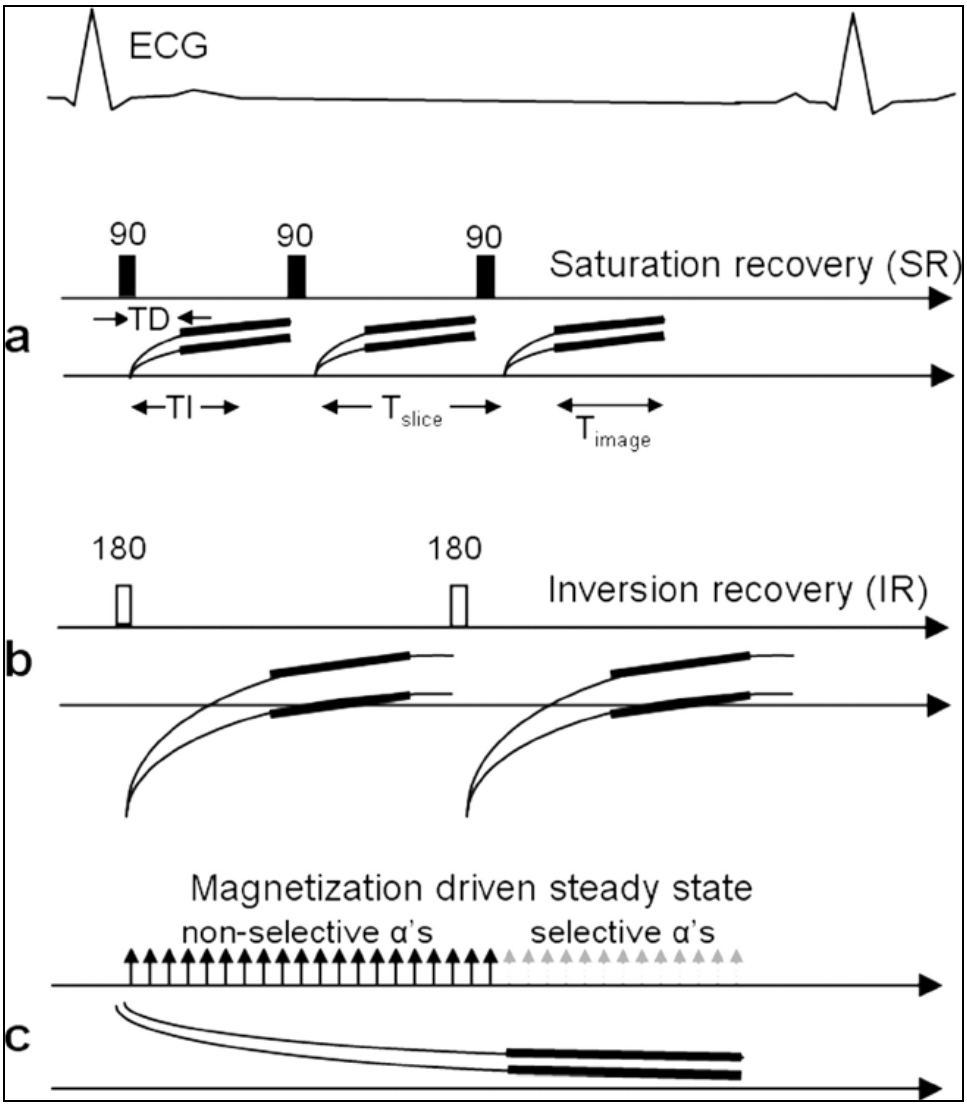


**Figure 19 Magnetisation preparation scheme.** Adapted from (179). Magnetisation preparation schemes for T1-weighted myocardial perfusion imaging: (a) SR (b) IR (c) magnetisation-driven steady-state.

***Read-out***

SR pre-pulses are followed by an acquisition imaging module with either gradient echo (GRE), balanced steady-state free precession (bSSFP) or hybrid gradient echo-planar imaging (GRE-EPI). All three sequences are ultra-fast and have a short repetition time (TR).

***GRE***

GRE sequences produce an image by delivering individual RF pulses in succession to sample lines of *k*-space. Improvements in gradient switching speeds and slew rates have led to "turbo" GRE sequences, which have significantly reduced acquisition times to milliseconds. With a short delay between successive RF pulses and the spoiling of transverse magnetisation after each pulse, the flip angle has to be kept low. As a result, there is a lower SNR compared with the other sequences. Initial feasibility of first-pass perfusion CMR (183) was based on this technique and it remains the most used sequence. Advantages include reduced susceptibility-induced image artefacts, as there is a new signal for each line of *k*-space. Image acquisition is inefficient; as a result, it takes longer and SNR is lower.

***Steady-State Free Precession (SSFP)***

SSFP uses repeated delivery of excitatory RF pulses to maintain a steady-state transverse magnetisation. bSSFP sequences have the highest signal of the methods due to the higher flip angle. SSFP is reported to have a greater occurrence of susceptibility artefact, ghosting and Gibbs ringing. Despite the improved SNR, SSFP perfusion imaging is more difficult for field strengths >1.5T due to limitations with artefacts and specific absorption rate (SAR) (184) (185).

***Hybrid GRE-EPI***

EPI allows faster acquisition of an image than GRE, as multiple lines of *k*-space are acquired with each RF pulse. EPI techniques have better temporal resolution (186) but are limited by their sensitivity to susceptibility and motion artefacts. Hybrid GRE-EPI was developed to include the faster gradient switching of GRE. This allowed excitation by multiple pulses and acquisition of multiple lines for each pulse using fast-switching magnetic gradient hardware. The improved acquisition without requiring shorter TR

(which would reduce SNR) was demonstrated using a hybrid GRE-EPI perfusion sequence with an echo train length of 4 (i.e. four lines of *k*-space acquired per excitation pulse). This sequence was less prone to the artefacts associated with EPI and had similar linearity in signal intensity response to GRE sequences (187). More recently, EPI techniques have been reported to suffer from ghosting artefacts from periodic fluctuations of the *k*-space signal and frequency offset (188).

#### *Comparison of Techniques*

Comparisons of the techniques have resulted in no overall consensus on the optimal imaging protocol. Published results have shown similar diagnostic values. The most consistent findings are that bSSFP offers the highest SNR and CNR of the three pulse sequence designs, thought in part to be due to the higher flip angles used (189) (190) (191). In a direct comparison, bSSFP was shown to have higher sensitivity for the detection of perfusion defect but also an increased sensitivity to susceptibility artefacts. It should be noted that this study only included nine patients (192).

In a comparison of GRE-EPI and GRE sequences in 15 patients with IHD, GRE-EPI sequences showed improved CNR and temporospatial resolution (186). A study comparing all three sequences in 15 patients referred for coronary angiography showed GRE-EPI allowed the greatest diagnostic confidence and demonstrated fewer artefacts. CNR was lower than bSSFP and also GRE images. The discrepancy in CNR with EPI in comparison with previous studies was thought in part to be due to the flip angle used (193). There are technical limitations in comparing the methods due to contrast dosing, flip angle and effects of field distortion (189).

### Artefacts

A number of artefacts can impede diagnostic interpretation of perfusion CMR studies, in particular for inexperienced observers.

#### *Dark-Rim Artefacts*

Dark-banding artefacts at the endocardial border can impede diagnostic interpretation of perfusion CMR studies, in particular for inexperienced observers. The cause of the dark-rim artefacts is multi-factorial (194) and includes myocardial motion (195) and Gibbs ringing (196) caused by reduced spatial resolution (197) and susceptibility from the passage of contrast at the myocardial wall and LV cavity (198)[32,33]. The extent of the dark-rim artefacts is dependent on spatial resolution and is diminished with high-resolution methods (199).

***Wrap Artefacts***

Wrap artefacts occur when the size of the object being imaged exceeds the FOV in the phase-encode direction. The outside regions are wrapped in the opposite edge of the FOV, producing wrap-around or aliasing artefacts. This is due to failing of the Nyquist sampling of the *k*-space signal for parts of the object outside the FOV. In perfusion imaging a large FOV is used to cover the chest with some aliasing; this is considered acceptable, as it does not superimpose on the heart. Methods to reduce the artefacts include using saturation bands (200).

***k-t-related Artefacts***

Motion-related artefacts appear to be the main problem with *k-t* undersampling accelerated imaging methods due to respiratory and cardiac movement causing blurring and ghosting from nearby structures. This problem is exacerbated during the effects of stress perfusion and in patients who have tachyarrhythmias or poor breath-holding. To reduce these problems, fewer dynamics are acquired compared with conventional methods and greater emphasis is placed on focussed breath-holding during contrast passage (201) (202).

Newer technical developments which incorporate motion correction may allow free-breathing data acquisition. Acceleration techniques using *k-t* PCA are less sensitive to respiratory motion and improve temporal fidelity (203). Finally, reconstruction algorithms assume the heart remains rather static; however, due to the acquisition window of 100-200 ms some cardiac motion artefacts are invariable.

## Limitations of Myocardial Perfusion CMR

### *Patient Factors*

A small proportion of patients will not be suitable for stress perfusion CMR (204). Claustrophobia remains an issue with a small minority of patients (<2%), though developments in newer wide-bore magnets should lead to a reduction in this number. The presence of pacemakers remains a contraindication to CMR. Implantable devices that are CMR-conditional are now increasingly available. Guidance is readily available to screen patients (www.mrsafety.com) with devices and foreign bodies with regard to suitability for CMR imaging.

### *Pharmacological Contraindications*

Intolerance to adenosine as a stress agent in patients with higher-degree block, hypotension and severe airway disease restricts its use in this subgroup of patients. However, this also applies when adenosine is used during other diagnostic tests. Newer selective A2 agents have been proposed with more favourable tolerability and easier administration, and have been shown to be of comparable diagnostic accuracy (38).

### *Technical Limitations*

Cardiac arrhythmias can be problematic, as scans are gated to a time point in the cardiac cycle and variations in the R-R interval during arrhythmias including ectopy and atrial fibrillation introduce blurring and artefacts and affect image quality. This limitation may apply less to 3D methods, as all data are acquired in a single acquisition and during systole, which is less affected by heart-rate variations. Tachyarrhythmias can cause

constraints on data acquisition and so compromises have to be made on resolution and dynamic acquisition.

**Diagnostic Performance of Myocardial Perfusion CMR**

Numerous single-centre studies and a small number of multi-centre trials have reported on the diagnostic performance of myocardial perfusion CMR. In a meta-analysis of 24 studies and 1516 patients, Nandalur et al. calculated a sensitivity of 91% (95% CI 88 to 94%) and a specificity of 81% (95% CI 77 to 85%) of CMR against X-ray coronary angiography (134). It is noteworthy that there was a relatively high prevalence of IHD (57.4%) in the pooled population. In a meta-analysis by Hamon et al. (205), which included 55 studies, the sensitivity and specificity of CMR were similar at 89% (95% CI: 88-91%) and sensitivity was 80% (95% CI 78-83%). A meta-analysis by De Jong et al. based on 28 studies and 2970 patients showed perfusion CMR to be superior for the diagnosis of obstructive IHD to EPI and SPECT (92). The most recent meta-analysis, by Jaarsma et al., pooled 17,901 patients from 143 studies (105 SPECT, 27 CMR, 11 PET) to determine the diagnostic accuracies of three imaging modalities. All techniques demonstrated high sensitivity (SPECT 88%, CMR 89%, PET 84%), though the specificity was lower with SPECT (61%) in comparison with CMR (76%) and PET (81%). The diagnostic accuracy of PET and CMR was similar (206).

Following the relatively small studies summarised in the meta-analyses listed above, the CE-MARC study was the first with adequate statistical power to directly compare the diagnostic performance of CMR with SPECT. Of 752 recruited patients with suspected angina, 628 underwent SPECT, CMR and X-ray angiography. The sensitivity (CMR 86.5% vs. SPECT 66.5%), negative predictive values (90.5% vs. 79.1%) and receiver operator characteristics (0.89 vs. 0.74) were significantly higher for CMR compared to SPECT (159).

The findings of the single-centre CE-MARC study were largely reproduced in MR-IMPACT 2, to date the largest multi-centre trial comparing CMR and SPECT for the detection of myocardial ischaemia (161). This study was conducted in 33 centres and included 465 patients. The overall performance (0.75 vs. 0.69, P=0.018) and sensitivity of myocardial perfusion CMR to detect IHD on quantitative X-ray coronary angiography

was higher than for gated SPECT (0.67 vs. 0.59, P=0.024), but specificity of CMR was lower (0.61 vs. 0.72, P=0.038).

One of the difficulties in validating non-invasive functional imaging methods against an anatomical test for the detection of IHD is that the degree of stenosis and its haemodynamic significance correlate poorly. Several studies have therefore used functional measures, in particular pressure-wire-derived FFR, as the reference standard. These studies have reported sensitivities of CMR against FFR ranging between 88.0 and 92.9% and specificities in the range of 56.7%-94.0% (207,208) (209). The MR-INFORM study is an ongoing randomised controlled study assessing perfusion CMR against FFR. The outcome of patients with stable angina managed with FFR guidance vs. those managed with CMR guidance is the primary endpoint (210).
Overall, evidence from clinical studies to date suggests that the diagnostic performance of myocardial perfusion CMR is at least comparable to that of SPECT and similar to PET.

**Prognosis**

A wealth of data regarding the prognostic value of myocardial perfusion CMR is now available. In a study by Jahnke et al., 513 patients with known or suspected IHD were investigated. An abnormal perfusion scan was associated with a 16.3% event rate (cardiac death or non-fatal MI) while a normal scan was associated with a <1% annual event rate (211). These data are comparable with those reported for other non-invasive imaging modalities (110). In a study of 1229 patients with anginal symptoms, a reversible defect on perfusion CMR was the strongest independent predictor for an event. The presence of a reversible perfusion was associated with a more than three-fold increased risk of death or non-fatal MI. In the same study, five-year event-free survival was 95.6% in patients with a normal perfusion study, demonstrating a high negative predictive value of CMR (212). In 135 patients presenting acutely with troponin-negative chest pain, perfusion CMR had a sensitivity of 100% and a specificity of 93% for predicting major adverse cardiac events (MACE) at one year. This suggests that perfusion CMR may also have a role in the stratification of patients with chest pain in the emergency department (213).

A more recent meta-analysis summarised data from 19 studies and 11,636 patients, followed up for a mean of 32 months. Fourteen of these studies used adenosine perfusion CMR; four used dobutamine cine CMR and one used both. The event rate of a positive test was 4.9% vs. 0.8% for a negative stress test (P<0.0001). The odds ratio of CV death or MI for a positive vs. negative stress test was 6.5. The presence of LGE was associated with a poorer outcome of CV death and MI (odds ratio 3.8, P<0.00001) (214).

Previous studies have also shown that late gadolinium predicts adverse prognosis in patients with IHD (151). The combined assessment of ischaemia by myocardial perfusion CMR and LGE can offer complementary prognostic information. This was demonstrated in a study by Steel et al., who followed up 254 patients over a median of 17 months and showed that the presence of reversible perfusion defects was most strongly associated with MACE (hazard ratio 10.9, P<0.0001). Reversible perfusion abnormalities and LGE both maintained a more than three-fold association with CV death or acute MI when corrected for age and gender (215).
In the coming years, outcome data from the recent larger clinical perfusion studies (159-161) will become available and will provide a better picture of the prognostic potential of perfusion CMR. In addition, the EuroCMR Registry (216) is expected to deliver further insight into the prognostic yield of myocardial perfusion and other CMR methods.

## Technical Advances and Challenges in Perfusion Techniques

### *High Field Strength*

3T MR systems have been increasingly introduced in clinical practice and offer higher SNR compared with 1.5T systems . They are of particular benefit for relatively SNR-limited applications including perfusion CMR.
The higher field strength increases the SNR due to increased magnetisation of nuclear spins and higher resonance frequency. The longitudinal relaxation times T1 lengthen at 3T, whereas T2 values are similar or slightly diminished (217). The increased T1 times are more marked in hypoperfused areas of myocardium, resulting in an increased contrast between normal and hypoperfused myocardium (184). Myocardial perfusion at 3T has been shown to be highly accurate and to improve the SNR, contrast enhancement,

image quality (218) and spatial resolution (219) compared with 1.5T. A number of clinical studies have also demonstrated improved detection of ischaemia compared with imaging at 1.5T (220) (221).

Higher field strength also poses challenges, including increased susceptibility artefacts, field inhomogeneity, and limitations on SAR (184) (185).

### *Field Homogeneity and Susceptibility*

Susceptibility effects are greater at higher field strength. Homogeneity of the main magnetic field (B0) varies to a greater magnitude than with 1.5T. Increased field strength causes a linear increase in the susceptibility-induced field variations, particularly at tissue interfaces (185). This can lead to off-resonance and manifest as a susceptibility artefact and signal loss in an image at tissue interfaces. This is more marked with bSSFP sequences, causing more banding artefacts, and may be reduced with the use of frequency scout sequences (222)

### *Larmor Frequency and Di-Electric Effect*

At higher field strength the resonant frequency (Larmor frequency) increases proportionally. Doubling the field strength doubles the frequency difference and this leads to a wider separation of resonant frequencies. These changes cause a shift in the phase of the MR signal and will be most prominent at tissue interfaces – resulting in intra-voxel dephasing (223).

The higher resonant frequency at 3T also requires higher RF excitatory pulses (B1). At 3T, the wavelength for proton imaging becomes smaller than the patient (224). B1 inhomogeneity occurs with variable absorption of RF power across the patient, due to the changing permittivity and conductivity of tissues (dielectric effects) and standing waves in tissues. This results in a non-uniform flip angle across the imaging volume, which can lead to dielectric shading and areas of poorly nulled myocardium (218).

Newer techniques such as dual-source parallel RF transmission are beginning to address these challenges and can improve image homogeneity, image contrast and diagnostic confidence compared with conventional RF transmission at 3T (225) (226). Techniques including advanced sequence design, adiabatic pulses and improved shimming techniques (227) have been proposed to overcome some of these issues.

***SAR***

SAR describes the potential for heating a subject's tissue through the application of RF pulses. Inhomogeneity of the RF field leads to local adsorption of RF energy to local areas of tissue region rather than uniform distribution. Higher-frequency pulses increase the power deposition required to acquire at a specified flip angle. The SAR of a sequence at 3T will be four times the SAR of the identical sequence at 1.5T. The International Electrotechnical Commission specifies an average whole-body maximum SAR of 2 W/kg/6 minute exposure. The SAR can be reduced by a decrease in flip angle or an increase in the TR. Short TR and sequences place constraints on perfusion imaging.

In principle, more data could be acquired faster with even stronger gradient systems, but adverse physiological effects such as peripheral nerve stimulation limit these developments beyond current levels. Undersampling can provide further acceleration of data acquisition.

## Accelerated Cardiac Perfusion Imaging

### *Principles*

Current perfusion CMR methods produce a lower spatial resolution than other CMR techniques (159-161). Acquisition of other methods including cine and LGE images is typically segmented and acquired over several cycles to improve spatial resolution and SNR. Data acquisition for dynamic perfusion CMR imaging is limited to short intervals within each cardiac cycle to minimise the effect of cardiac motion and to track the passage of contrast agent.

### *Accelerating Imaging*

Accelerating data acquisition is of fundamental relevance for the improvement of myocardial perfusion. If data are acquired faster and more efficiently, a larger image matrix can be used to improve spatial resolution, with cardiac coverage increased, acquisition at higher heart rates achieved or SNR improved.

Data acquisition has been accelerated with innovative acquisition pulse sequences and reconstruction algorithms. In particular, the development of high-number parallel imaging techniques and multi-coil arrays has allowed a more flexible use of parallel acquisition schemes. The introduction of spatiotemporal undersampling has led to dramatic acceleration of data acquisition, and forms the basis of this thesis.

### *Multi-channel Coils*

Multi-channel or phased-array coils receive and or transmit the RF signal. With perfusion imaging, they are used as receive-only coils and the body coil as a transmitter. Increasing the number of surface coils has the potential advantages of improving SNR and FOV coverage and therefore allowing higher spatial resolution or faster acquisition times. Typically, clinical scanners have between six and 32 channels. Increasing the number of surface coils can also lead to an increase in time taken for image

reconstruction. The number of independent channels is also limited to the development of parallel imaging techniques.

The use of multiple-coil arrays can be efficiently tailored to a specific target anatomy by deriving the optimal virtual coil configuration (228). Increasing the number of receiver coils will improve the detection of spin but will also increase the amount of noise received. Gains in SNR can only be achieved by limiting the volume of tissue contributing to the noise. Increasing the number of channels beyond 32 has been shown not to significantly increase SNR (229), though the use of a 128-channel coil still holds promise.

***Parallel Imaging – Sensitivity Encoding (SENSE)***

Parallel imaging exploits the spatial signal variation across the multiple receiver coils in a phase array (202,230). This reduces the number of phase encoding steps to fill the *k*-space lines. The multiple sets of undersampled coil-component data will then be reconstructed to generate a final image. Parallel imaging techniques do not require improved gradient hardware to increase imaging acquisition time or increase spatial and temporal resolution. The use of parallel imaging techniques can reduce the total number of RF pulses required to complete the acquisition and therefore to reduce the SAR.

SENSE is an example of a parallel imaging technique accelerating data acquisition using a Cartesian trajectory, which acquires one parallel line of *k*-space at a time (Figure 20). Subsets of the full image data are acquired and reconstructed. The missing information is completed by exploiting the differences in signals from the multiple receiver coils.

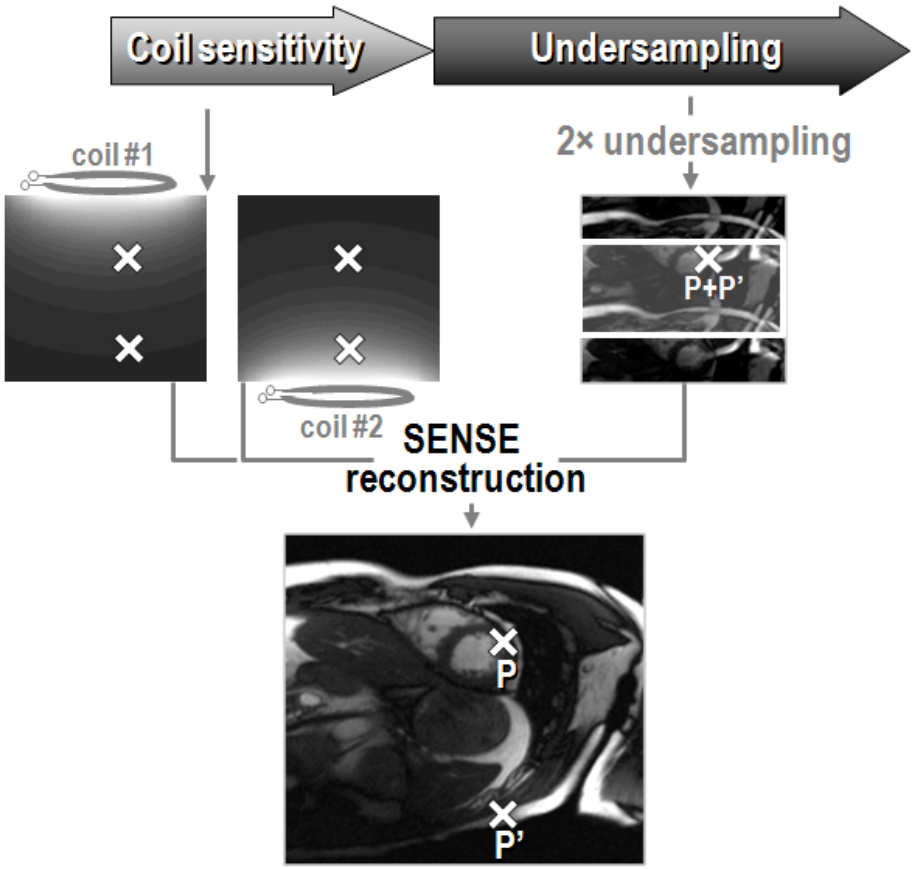


**Figure 20 Parallel imaging and SENSE acquisition.** Adapted from (202). Differences in the reception of the RF echoes from each of the receiver coils are used to reconstruct undersampled data sets. This reduces the number of phase encoding steps to fill the *k*-space lines. The overall size of the *k*-space and spatial resolution are preserved with the loss of FOV size. An aliased image is produced from each coil element, and is reconstructed by distinguishing the true and aliased signal from the receiver coils.

***SNR***

The reduction of phase encoding steps with respect to full Fourier encoding (filling all the lines) is described by the SENSE reduction (acceleration) factor R. The value of R is typically between 2 and 6 for multi-receiver elements of cardiac coils.
Parallel perfusion imaging techniques therefore result in a reduced SNR compared with baseline unaccelerated data, according to the following formula:

$$SNR^{accelerated} = \frac{SNR^{baseline}}{g\sqrt{R}}$$

R = Acceleration factor

g = Geometry factor

The g factor measures the noise amplification due to the imperfect geometrical relationship of the coil sensitivities. This results in a reduction that is greater than expected from acquiring fewer profiles with parallel imaging. A value of 1 or greater reflects the performance of the coil and imaging algorithm. At higher field strengths the higher frequencies and smaller wavelengths improve the effective coil separation and maintain g closer to 1 at higher acceleration factors. The acceleration factors achievable with 2D imaging are limited to acceleration factors of approximately three fold, beyond which SNR reduces markedly. With 3D imaging it is possible to accelerate higher degrees of acceleration than 2D imaging before significantly impacting SNR (Figure 21).

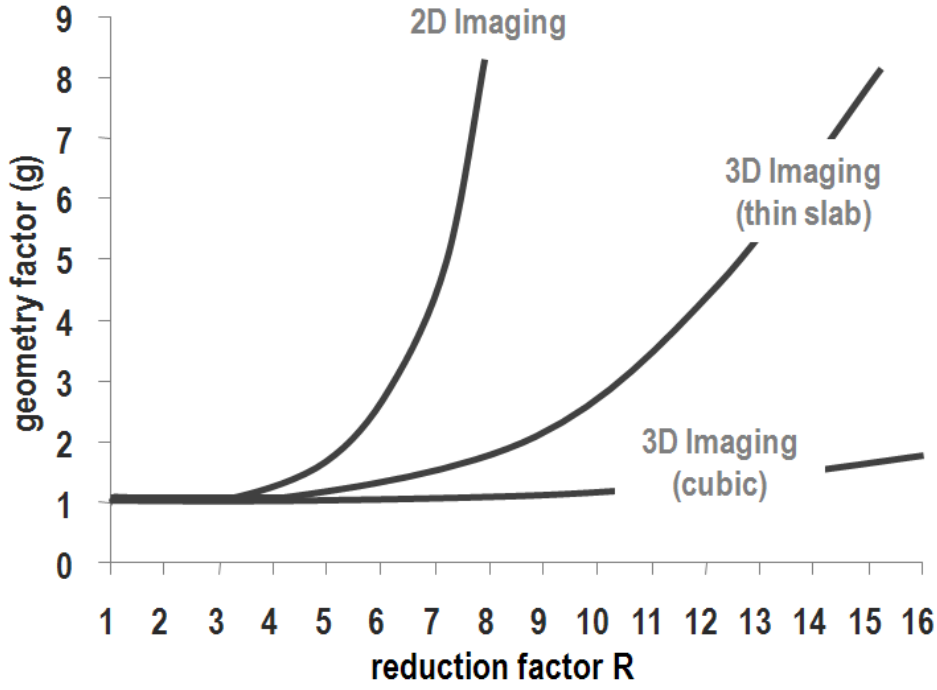


**Figure 21 Geometry factor vs. reduction factor with 2D and 3D imaging.** Adapted from (202). Three-dimensional imaging allows much higher acceleration before an additional noise penalty compromises SNR.

Due to the reduced FOV, SENSE parallel imaging is prone to "ghost" (aliasing or fold-over) artefacts (231). Alternative parallel techniques such as General Autocalibrating Partially Parallel Acquisition (GRAPPA) may reduce these artefacts. GRAPPA is another parallel imaging technique that differs from SENSE in how the coil sensitivity data are acquired. SENSE acquires coil sensitivities with an additional low-resolution reference scan. An "autocalibration" method is used in GRAPPA where additional lines for the full FOV are acquired during data acquisition for coil calibration. The theoretical advantage of this is the improved consistency between coil sensitivities and undersampled data,

minimising any errors with motion. The disadvantage is a reduction in acceleration factor due to an increase in image acquisition time (232).

***Spatiotemporal Undersampling***

The use of parallel imaging with a multi-coil array allows a more flexible use of parallel acquisition schemes at potentially much higher acceleration factors than are otherwise possible. Methods have been proposed and applied to myocardial perfusion CMR that allow much higher acceleration factors of up to 10 fold by exploiting the difference in coil sensitivities and spatiotemporal correlations in parallel. The acceleration schemes exploit data correlations in *k*-space and in time due to redundancies that exist between successive frames of a moving image. A large proportion of the images remain static and therefore a lot of the data acquired can be acquired quicker. If the redundant data follow a predictable trend, the pattern of acquisition can be learnt and used to compensate for undersampled data.

Unaliasing by Fourier-Encoding the Overlaps Using the Temporal Dimension (UNFOLD) uses a similar *k*-space sampling method to SENSE leading to a reduction in the FOV and image aliasing. Rather than coil sensitivity being used to summate the aliased images, UNFOLD uses time modulation, alternating odd and even phase encoding of lines of *k*-space to transfer data from the *k*-axis into *k*-*t* space (233).

TSENSE combines the sensitivity encoding of SENSE with the temporal filtering of UNFOLD to facilitate accelerated data acquisition. The combination of both methods reduces the necessary accuracy for coil sensitivity estimation and temporal low-pass filter selectivity compared to the use of the methods individually. There is no additional reference scan, as allowance is made for variation in coil sensitivity and chest wall motion. In perfusion imaging, the reduction in the number of phase encoding steps increases the range of contrast to signal intensity linearity by 40%, permitting quantification analysis with higher doses of contrast agents (191).

### *k-t* SENSE, *k-t* BLAST and *k-t* PCA

Newer spatiotemporal undersampling acceleration schemes allow much higher acceleration factors up to 10 fold. *k-t* SENSE and *k-t* Broad-use Linear Acquisition Speed-Up Technique (BLAST) reconstruct undersampled data in addition to training data based on a separate low-spatial-resolution scan at full temporal resolution. The result is multiple aliases of the original object, which are reconstructed into a higher resolution, unaliased image, with the aid of a model based on the acquired training data (234) (Figure 22).

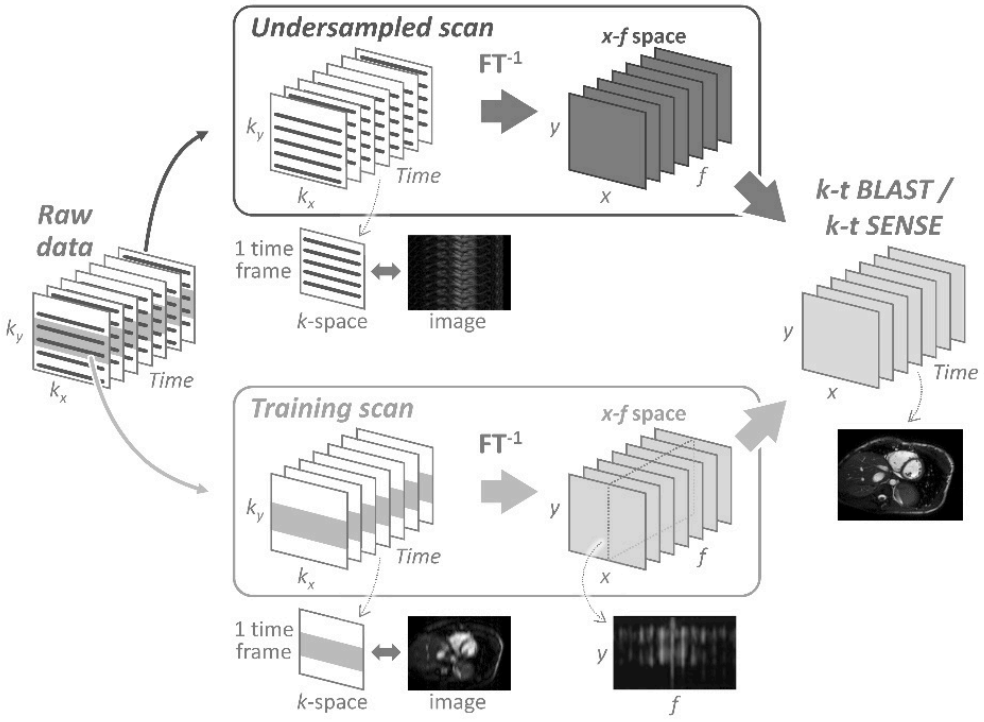


**Figure 21 *k-t* undersampling.** Adapted from (234). An undersampled scan is acquired at full spatial and temporal resolution in the x-f domain, contaminated by aliasing artefacts. A training scan is acquired from the central part of the *k*-space at low spatial but full temporal resolution, usually in an interleaved fashion. Both *k-t* BLAST and *k-t* SENSE unfold and reconstruct the two images to remove the aliasing artefacts and recover the missing data to reconstruct the final image.

The differences between the two reconstruction methods are based upon their use of receiver coil sensitivity during the image reconstruction. *k-t* BLAST uses multiple receiver coils as a single unit whereas *k-t* SENSE takes advantage of parallel imaging and

uses the individual sensitivities during reconstruction. This allows tighter signal packing in x-f space, improving acquisition efficiency (235) in the removal of aliasing artefacts.

*k-t* PCA is a development of *k-t* SENSE and *k-t* BLAST. Rather than reconstructing in the x-f space, it is performed in the x-PCS (principle component space) to permit better recovery of the overlapping signals in the aliased object (236). This has several advantages over the x-f space, with improved signal compaction and reduced Gibbs ringing, and has been shown to improve temporal fidelity (203) (Figure 23).

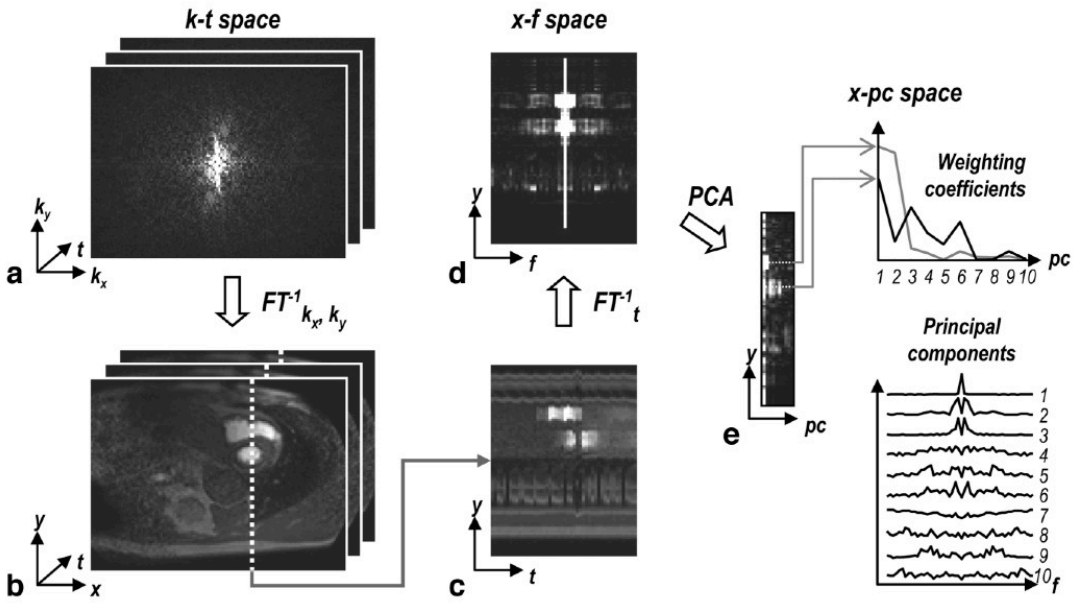


**Figure 22 *k-t* PCA.** Adapted from (236). Perfusion imaging with *k-t* PCA. The image series undergoes inverse Fourier transformation into the *x-f* representation. Each temporal frequency profile in the *x-f* space consists of a set of spatial weighting coefficients and a set of principle components, which separate the overlapping signals accurately, thereby maintaining high temporal fidelity.

The principle of highly constrained back-projection reconstruction (HYPR) method differs by acquiring a portion of radial trajectory during the cardiac phase and rotating an undersampling pattern with a high-resolution composite image made from a series of the undersampled projections. The image is reconstructed serially, from the fully sampled composite image and the undersampled data acquired at each time point. Developments in the reconstruction process using conjugate gradients (CG) minimise the error in signal intensity change (237). Sliding windows (SW) have also been proposed to update the changing signal during the reconstruction of the composite

image. SW-CG-HYPR has been used in small studies showing improved resolution and SNR in application to myocardial perfusion CMR (238).

Newer acceleration strategies have been proposed, including spiral imaging. This has been shown to be technically feasible, but clinical use has yet to be assessed (239-241).

## Clinical Application of Accelerated Perfusion Imaging

In earlier studies, GRE was combined with EPI and SENSE (242) (164) or TSENSE (191). Despite significant constraints for perfusion CMR imaging, these methods allowed three to four slices to be acquired at every heartbeat at an acquisition time of 100 ms per slice and a resolution of 2-3 mm. Using newer spatial and temporal acceleration schemes, the faster data acquisition afforded by these methods has been utilised in several ways. Accelerated imaging has been invested into improving the efficiency and quality of scans, acquiring images with increased coverage, higher spatial resolution and at higher heart rates.

### *High-Resolution Perfusion Imaging*

The introduction of the newer data acceleration schemes has facilitated the development of high-resolution perfusion CMR imaging. This allows a spatial resolution enabling direct comparison with other high-resolution forms of functional assessment. This is important when assessing viability in the context of peri-infarct ischaemia and revascularisation. The resolution may also allow better discrimination between the layers of myocardium to allow an evaluation of the microvascular perfusion in diseased states including syndrome X and diabetic and hypertensive heart disease.

Although arbitrary, standard resolution is considered approximately 2-3 mm. Less than 2 mm is often quoted as high resolution. Plein et al. demonstrated the feasibility of high-resolution perfusion in 10 volunteers by investing the acceleration into spatial resolution with preserved temporal resolution. Using five-fold k-t SENSE acceleration

they achieved an in-plane spatial resolution of 1.5 mm. The image acquisition window was 120 ms, similar to conventional resolution perfusion sequences. There were significantly reduced dark-rim artefacts; however, image quality was deemed similar (242).

Early studies have suggested improved diagnostic accuracy of high-resolution vs. standard-resolution myocardial perfusion. Using the same *k-t* SENSE acceleration sequence, Plein et al. demonstrated the high diagnostic accuracy (area under curve [AUC] 0.85) of this technique in 51 patients to detect significant IHD. This study also demonstrated discrimination of subendocardial defects with the higher spatial resolution, allowing the transmurality of ischaemia to be assessed (201). The technique was shown to be feasible at higher field strength and demonstrated better overall image quality and SNR than than the equivalent method at 1.5T (243). Using a 3T magnet and an eight-fold *k-t* SENSE acceleration produced an AUC of 0.94 for the detection of IHD (coronary stenosis >50%) (244). Given the poor relationship between anatomical and functional evaluation of IHD, Lockie et al. used FFR as the reference for functionally significant IHD in 42 patients. The diagnostic accuracy remained high (AUC 0.92), supporting the conclusion that high-resolution perfusion CMR can accurately determine haemodynamically important coronary stenosis (245). A summary of the diagnostic performance of high-resolution perfusion imaging is shown in Table 1.

The use of high-resolution perfusion CMR may also have added benefit in the detection of multi-vessel and balanced ischaemia. For visual assessment in these cases, the lack of homogeneity in high-resolution imaging may improve detection. In the only study in this area to date, Motwani et al. showed the superior diagnostic accuracy of high-resolution against standard-resolution perfusion CMR. In this study 100 patients underwent two separate perfusion CMR scans at 1.5T, one at standard resolution (2.5x2.5 in plane) and one with high resolution (1.6x1.6 mm in plane) using 8x *k-t* BLAST (199). The study by Ma et al. used a high resolution and six slices, and increased myocardial coverage in 56 patients. The results were impressive, suggesting a role for higher spatial resolution and greater myocardial coverage.

**Table 1 Performance of Advanced Accelerated Perfusion CMR Techniques**

| Study | N | Strength | Acceleration Method | Resolution | Sensitivity /% | Specificity /% | Diagnostic Accuracy |
|---|---|---|---|---|---|---|---|
| Plein (201) | 51 | 1.5T | 5 x *k-t* SENSE | 1.4 mm | 89 | 44 | QCA>50% |
| Plein (243) | 33 | 3T | 5 x *k-t* SENSE | 1.3 mm | 92 | 90 | QCA>50% |
| Meyer (219) | 60 | 3T | 3 x SENSE | 1.9 mm | 89 | 79 | QCA>70% |
| Klumpp (220) | 57 | 3T | 2 x GRAPPA | 1.9 mm | 88 | 93 | QCA>70% |
| Manka (244) | 20 | 3T | 8 x k-t SENSE | 1.1 mm | 90 | 90 | QCA>50% |
| Lockie (245) | 42 | 3T | 5 x k-t BLAST | 1.2 mm | 82 | 94 | FFR<0.75 |
| Motwani (199) | 100 | 1.5T | 8 x k-t BLAST | 1.6 mm | 91 | 80 | QCA ≥50% |
| Morton 2012 (246) | 17 | 1.5T | 5 x k-t BLAST | 1.7 mm | 78 | 80 | QCA >70% |
| Morton 2012 (126) | 41 | 1.5T | 5 x k-t BLAST | 1.7 mm | 86 | 76 | QCA>70% |
| Ma 2012 (238) | 50 | 3T | SW-CG-HYPR | 1.6 mm six slices | 96 | 82 | QCA ≥50% |

**Three-dimensional myocardial perfusion CMR**

Most myocardial perfusion CMR methods cover the heart in three short-axis slices, as required by international guidelines (104) (247). Three-dimensional acquisition methods may overcome some of the remaining limitations of myocardial perfusion CMR, specifically the limited myocardial coverage offered by conventional multi-slice 2D methods. Although conventional multi-slice imaging is accurate for diagnostic purposes, the selective coverage with variable gaps between slices limits accurate comparison with other whole-heart CMR measurements such as cine imaging and LGE. Two-dimensional imaging may also limit accurate measurement of ischaemic burden. In clinical practice, ischaemic burden is most commonly measured by MPS. It is an important prognostic factor in IHD in accordance with guideline recommendations (248) and may help identify and stratify patients who will benefit most from revascularisation compared with medical therapy (103).

With reduced artefacts in high-resolution imaging and greater coverage in whole-heart perfusion imaging there is less operatory dependence. Greater coverage and the ability to process imaging off-line mean the perfusion study can be performed rapidly with reduced training requirements.

As all data in 3D myocardial perfusion CMR are acquired in a single cardiac phase, inter-frame motion and undersampling are more robust. Three-dimensional acquisition is also more signal-to-noise efficient than 2D imaging, and, as all data are acquired in the same shot, fewer compromises regarding cardiac phase are necessary (Figure 24). This may have further relevance when quantifying perfusion and perfusion reserve.

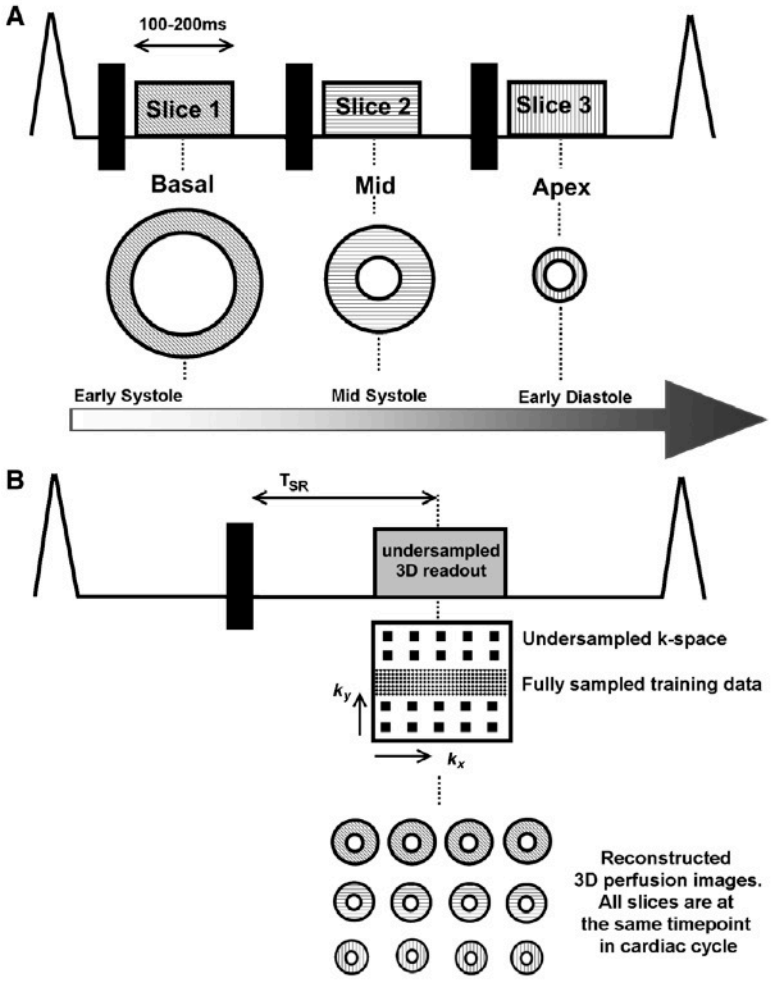


**Figure 23 Pulse sequence for 2D and 3D imaging.** Reproduced from (249). Pulse sequence for 2D and 3D perfusion imaging. For 3D imaging a single saturation pre-pulse is followed by an SR time and undersampled 3D perfusion data read-out. As all the data are acquired at the same time point in the cardiac cycle, the slices appear in the same cardiac phase.

Multi-slice acquisition with up to eight slices was already proposed early in the development of perfusion CMR, but at that time led to suboptimal image quality: resolution was significantly lower, breath holds were long and artefacts were frequent (250) (187). The feasibility of 3D myocardial perfusion CMR was first proposed by Shin et al. (251). They used six-fold SENSE to achieve the required data acquisition speed and validated the method in a phantom and a volunteer cohort. It was shown that whole-heart coverage was more accurate than conventional three-slice imaging in calculating the size of a perfusion deficit.

The acquisition window was in the order of 300 msecs, which meant images were prone to potential motion artefacts, particularly with higher heart rates (e.g. during stress perfusion). The same group presented further data from volunteers comparing systolic with diastolic 3D perfusion. These results demonstrated the feasibility of 3D perfusion imaging in systole, which is less prone to variations in heart rate than diastole. The implementation of 3D perfusion CMR in the study used a shorter acquisition window, compromising with a relatively low spatial resolution that would be unlikely to detect small or subendocardial perfusion defects (252). Alternative proposals for 3D acquisition were put forward by Vitanis et al. (203), who used *k-t* PCA reconstruction in their feasibility study and demonstrated improved temporal resolution based on one volunteer and one patient with IHD.

In clinical feasibility studies, 3D myocardial perfusion CMR using *k-t* PCA has been shown to be feasible and accurate in detecting IHD and in calculating ischaemic burden. Manka et al. (253) showed that the method can detect angiographically defined IHD with high diagnostic accuracy. Three-dimensional myocardial perfusion CMR yielded a sensitivity of 91.7% and a specificity of 74.3% on a patient basis. Analysis was not performed on a vessel basis and IHD was defined by a QCA stenosis >50%. In a subgroup of 48 patients ischaemic volume was significantly reduced from 14% +/-10% pre PCI to 3% +/-5% following revascularisation. In this study QCA was used as the reference standard for the detection of significant IHD. The study did not provide any information on the extent of myocardium at risk based on the magnitude and location of coronary stenosis, a separate marker of prognosis (57).

***Potential Clinical Role of 3D Myocardial Perfusion CMR***

Three-dimensional myocardial perfusion CMR is feasible. It provides promising diagnostic accuracy against QCA and allows calculation of the ischaemic burden compared with invasive and non-invasive methods. In addition, it can be directly correlated with LGE and may thus allow more accurate estimation of peri-infarct ischaemia in partial thickness scar. Compared with SPECT, higher-resolution 3D myocardial perfusion CMR without exposure of patients to ionising radiation is an ideal method for serial imaging and to assess the efficacy of treatment (e.g. revascularisation

or stem-cell therapy) designed to improve regional blood flow. Compared with 2D methods, with greater coverage the complete visualisation of inducible perfusion abnormalities observed in conditions including diabetes and LV hypertrophy may help in differentiation from epicardial obstructive IHD for improved risk stratification (254).

***Reproducibility***

The use of a non-ionising imaging technique with high resolution may allow accurate serial follow-up of disease progression. Reproducibility affects test precision and reliability, and is important to assess whether variations observed are due to the accuracy of the technique or biological factors. CV function is affected by diurnal variation, and changes in heart rate, blood pressure and ischaemic threshold are recognised (255).

However, reproducibility remains to be comprehensively evaluated. There are a few small, limited studies which have investigated reproducibility of perfusion. Muhling et al. reported good intra- (R=0.80-0.85) and inter-observer (R=0.83-0.88) agreement at 1.5T using a FLASH sequence and an acquisition time of 160-235 msec per slice (256). Elkington et al. assessed inter-study reproducibility in nine patients with IHD and seven healthy volunteers, revealing respective coefficients of variation of 41% and 21% for transmural magnetic resonance perfusion imaging (MRPI) by Fermi deconvolution (257). In 20 patients with suspected IHD, Chi et al. showed the reproducibility of MPRI was 19% (258). These studies were not performed using *k-t* accelerated methods or high resolution. The effects and the variability of perfusion CMR post processing and their clinical significance are yet to be completely elucidated.

Using higher resolution the inherent variability of the signal intensity and quantitative perfusion of the technique may change. Larger variations in repeatability may require future studies with increased sample sizes to reduce statistical error and ensure power.

**Myocardial perfusion CMR in preclinical studies**

Animal models are important to develop our understanding of the pathophysiology of CV disease and for the development of new therapies (259). While coronary autoregulation maintains resting MBF over a wide range of pathological conditions, MBF reserve during hyperaemic or chronotropic stress is impaired in several common disease processes including atherosclerosis (260), systemic hypertension (261) and diabetes mellitus (262) due to alteration of micro- or macro-vascular reserve. Rodent models in particular are widely used to develop novel therapies aimed at improving MBF in these disease states, making accurate non-invasive assessment of MBF and MBF reserve in rodent models of CV disease highly desirable.

Despite the obvious size difference, there are parallels between mice and humans with regard to CV function and physiology. There are advantages including the ability to manipulate the genome for the investigation of genetic knockout and transgenic models for disease pathogenesis (263). Pre-clinical work is broadly divided into in vitro or in vivo. In vitro describes using isolated components of the rodent to allow a more detailed study. This would include the use of microscopy for histological evaluation of cellular structure.

Invasive in vivo techniques including microsphere evaluation (264) and LV pressure catheters (265) are useful, but do not allow serial assessment. Non-invasive in vivo methods permit longitudinal assessment and thus permit observation of treatment effects. Currently, non-invasive in vivo estimates of myocardial perfusion in rodents may be obtained with nuclear perfusion imaging (SPECT) (266), PET, echocardiography (267), and spin labelling MR imaging. However, nuclear and echocardiographic perfusion methods are limited by relatively low spatial resolution. MR provides higher resolution and spin labelling MR methods have been proposed for myocardial perfusion MR in rodents, but require acquisition times of approximately 25 minutes for a single slice, thus precluding measurements during pharmacological stress (268). First-pass contrast-enhanced myocardial perfusion MR, which is the standard MR method for the estimation of MBF and MBF reserve in humans, has previously not been feasible in rodents because of the constraints related to the small heart size and very high heart rates in these animals (around 500 beats per minute in mice).

CMR studies are usually performed in non-clinical high-field MR magnets with field strengths ranging from 4.7 to 17.6T for murine CMR (268-270). The high field strengths provide increased SNR and spatial resolution required for adequate signal. There are inherent problems however with availability and cost of the specialised software of these systems. Despite these limitations and the reduced magnetic field strength, clinical scanners are increasingly being used (271). There are advantages of cost and availability in using newer pulse sequences and reconstruction algorithms. Clinical protocols are already being implemented and could potentially be directly translated and facilitated. Furthermore, lower field strength scanners may be more desirable for sequences including perfusion imaging, as the longitudinal relaxation times of gadolinium-based contrast agents decrease with increased field strength.

A number of considerations must be taken into account, as follows.

***MRI hardware***

Due to the size of the murine heart (longitudinal length 7 mm) in comparison to a human heart there are requirements for increased spatial resolution, despite the inherent SNR loss of between two to 10 fold. To compensate, small RF coils either purposely built or commercially available (wrist or carotid artery coils) are used (Figure 25). High temporal resolution is also required to acquire at high heart rates. A mouse heartbeat is approximately 120 ms (assuming a heart rate of 500 beats/minute); temporal resolution in a clinical scanner is typically 10-15 ms, compared with 5 ms in a dedicated animal scanner. Therefore, the clinical MRI system should have sufficient gradient strength and fast-switching coils. Current clinical systems have gradient strengths of 40-80 mT/m, and slew rates of 200 mT/m/ms can achieve similar spatial resolution of 200 μm.

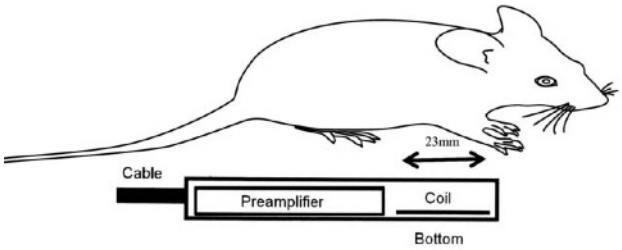


**Figure 24 Single circular-loop coil for murine perfusion imaging.** Adapted from (272). Illustration demonstrates the size and set-up of a single circular-loop coil used for murine perfusion imaging.

### *Animal Preparation*

UK law requires the obtaining of the appropriate personal and project licences to handle animals and perform procedures. Ethical approval is required for carrying out experiments within a specific site with the correct facilities. There is emphasis on strain and gender, in addition to meticulous planning of the procedure to avoid pain and distress. A consistent environment for the mice is required to ensure reproducible experimental conditions. Physiological monitoring of the animal is recommended in order maintain homeostasis; this includes monitoring temperature, heart rate, respiratory rate and blood pressure. The UK Home Office recommends that the maximum dose of animal blood volume that should be injected should be 200 µl for a mouse (approximately 10%-15% circulating volume).

### *Anaesthesia and Monitoring*

The choice of anaesthetic is important and should be considered carefully, as it may influence cardiac function (273). The mouse is induced in a closed container using 3-5% isoflurane and maintenance anaesthesia is delivered at between 0.5 and 1.5% isoflurane in oxygen at a flow rate of 1-2 ml/min via a nose cone or IV catheter used as an endo-tracheal tube.

Following induction of anaesthesia the mouse is transferred to a cradle in the prone position on the RF coil. The cradle allows reproducible positioning and is equipped with a nose cone for maintenance anaesthesia; it is designed to allow placement of ECG leads and IV catheters. During anaesthesia, with a large-bore scanner core body temperature

will decline. An MR-compatible rectal probe and heating system (SA instruments, Stony Brook, NY) is used to regulate temperature variations to less than 0.1°C.

ECG monitoring is used to monitor the heart rate and rhythm. Strong ECG signal and trigger are needed, as RF pulses and gradient switching may cause ECG signal interference. Methods to reduce this include shielding and twisting of the cables. ECG monitoring is important to synchronise the R-wave of the ECG in order to capture the myocardium at precise phases of the cardiac cycle. A number of MR-compatible electrodes are available. Subcutaneous electrodes are used commonly, or paediatric electrodes can be adapted by sticking them on the paws of the mice.

Respiratory motion is likely to degrade image quality and introduce artefacts; options during murine scanning are limited. Either software can be used to correct for respiratory motion by signal averaging, or pneumatic pillows can be employed. Alternatively, if the mouse is intubated a similar strategy to one employed in paediatric anaesthesia can be employed, transiently halting the animals' breathing.

***Imaging***

Using the cradle with the mouse at the isocentre of the magnet, the scan is usually performed in the anterior-posterior direction. An ungated low-resolution scout image is performed acquiring low-resolution, multi-planar images using a spoiled GRE pulse sequence. Using these images a short-axis image can be planned using an imaging plane perpendicular to a pseudo long-axis image parallel to the mitral valve, in preparation for perfusion imaging.

***Perfusion***

Due to the small size and high heart rates of rodents first-pass perfusion was considered unfeasible with conventional acquisition methods (274). ASL is a quantitative, contrast-free technique for measuring tissue perfusion. ASL uses the water in blood as an endogenous tracer. Perfusion is assessed by measuring the differences in myocardial T1 relaxation times and calculated by subtracting a control image from a tag image.

ASL has the advantages of not requiring challenging tail-vein cannulation and avoids missing the rapid wash-out of first-pass perfusion techniques. Among the disadvantages, most studies have been limited to small animals with healthy tissue. Problems exist with physiological noise, respiratory motion artefact, ECG triggering and the duration of scan time, precluding stress perfusion.

Compared with ASL, the dynamic nature of first-pass perfusion takes seconds to acquire. First-pass myocardial perfusion CMR in mice is challenging and compromises have to be made between acquisition speed and spatial resolution. Recent studies using spatiotemporal undersampling methods to meet the high requirements in these areas have used a clinical scanner (272), allowing facilitation of imaging protocols between rodent and human studies. Quantitative measurement of myocardial perfusion was performed before and after MI. No stress perfusion was performed. Van Nierop et al. used a dual-bolus method to estimate murine perfusion in a 4.7T non-clinical scanner (275). Myocardial perfusion was found to be comparable to that measured invasively by microspheres in mice. However, the technique was not validated against microspheres and stress perfusion was not assessed, limiting the translational applicability of the study. The major challenge will be the translation from in vivo work to clinical practice.

***Microspheres, Flow Cytometry and Microscopy***

Microspheres are considered a gold standard for the determination of regional tissue blood flow. Following the injection of microspheres they become trapped within the microcirculation in direct proportion to blood flow. A number of principles must hold for the technique to be accurate. It is assumed that all spheres mix with central circulation, that they are completely extracted in the first pass, and that they distribute homogenously within tissue.

To quantify absolute blood flow a reference blood sample is required to be withdrawn at a known rate. Originally, the methods involved using radioactive labelled microspheres – which has the advantage that the spheres do not need to be recovered after perfusion,

but are directly measured using a scintillation counter. The use of radioactive microspheres creates safety concerns for the animal and the researchers involved. They preclude the use of chronic studies and there are additional costs of storage and disposal; fluorescent microspheres are therefore increasingly preferred.

Fluorescent microspheres have been shown to correlate closely with radioactive microspheres for the determination of myocardial blood flow (276). They can be used for serial studies; however, the disadvantages include that the spectra from the different colours overlap, and that there is increased duration of tissue processing.

The standard method of quantitative analysis includes a destruction and extraction method (277). The tissue is digested, the spheres isolated, fluorophores extracted and fluorescence analysed. Fluorescent spheres are analysed using a flow cytometer. The sample moves through a flow cell through laser beams. The scattered light emitted from these particles produces fluctuations in brightness and provides information about their number, size, shape, granularity and fluorescence.

Fluorescent microspheres can also be examined using confocal microscopy (278). Unlike fluorescent microscopy, this technique has been shown to improve optical resolution and contrast by using a point illumination and a pinhole to remove out-of-focus light signals. Only fluorescence very close to the focal plane is detected, giving better optical resolution at the expense of reduced signal intensity – increasing scan duration. This facilitates reconstruction of images into larger stitched images or reconstruction of 3D structures.

# Chapter 2

## Validation of dynamic three-dimensional whole heart magnetic resonance myocardial perfusion imaging against fractional flow reserve for the detection of significant coronary artery disease

## 2.1 Abstract

Background

Three-dimensional (3D) myocardial perfusion cardiovascular magnetic resonance (CMR) overcomes the limited spatial coverage of conventional two-dimensional perfusion CMR methods and allows estimation of the extent of ischaemia. The method has shown good diagnostic accuracy for the detection of coronary artery disease (CAD) as defined by quantitative coronary angiography (QCA). However, QCA does not provide a functional assessment of CAD as available from pressure wire-derived fractional flow reserve (FFR). In the catheter laboratory, the Duke Jeopardy Score (DJS) can complement FFR to estimate the myocardium at risk.

Objectives

To determine the diagnostic accuracy of whole heart 3D myocardial perfusion CMR against invasively determined FFR and to establish the correlation between myocardium at risk defined by the invasive DJS and non-invasive 3D CMR.

Methods

Fifty-three patients referred for angiography underwent rest and adenosine stress 3D myocardial perfusion CMR at 3 Tesla. Perfusion was scored visually on a patient and coronary territory basis and ischaemic burden was calculated by quantitative segmentation of the volume of hypoenhancement. FFR was measured in vessels with >50% severity stenosis. The DJS was calculated from the coronary angiograms to quantify the myocardium at risk.

Results

In 64 of 159 coronary vessels FFR was measured and 39 had an FFR<0.75. Sensitivity, specificity and diagnostic accuracy of CMR for the detection of significant CAD were 91%, 90% and 91%, on a patient basis and 79%, 92% and 88%, respectively by coronary territory. There was a strong correlation between the DJS and ischaemic burden on CMR ($p<0.0001$, Pearson's $r=0.82$).

Conclusion

3D myocardial perfusion CMR accurately detects functionally significant CAD as defined by FFR and provides an assessment of ischaemia burden in agreement with the invasive DJS. The accurate detection of significant CAD combined with an estimation of ischaemia burden by 3D myocardial perfusion CMR holds promise for non-invasive guidance of therapy and risk stratification of patients with CAD.

## 2.2 Background

Cardiovascular magnetic resonance (CMR) is an evolving method for myocardial perfusion imaging[1,2]. Compared with the more frequently used single photon computed tomography (SPECT), CMR offers the advantages of higher in-plane spatial resolution and lack of ionising radiation. In a recent large single centre study CMR had higher sensitivity and negative predictive value than SPECT[3].

A limitation of myocardial perfusion CMR has been that the conventionally used two-dimensional (2D) acquisition methods cover the heart with a limited number (typically three) of non-contiguous imaging slices. This selective coverage potentially limits diagnostic yield and prevents quantitation of ischaemic burden. More recently, three-dimensional (3D) myocardial perfusion CMR methods have been proposed to overcome the limitation of spatial coverage[4]. 3D methods have shown good diagnostic accuracy for the detection of coronary artery disease (CAD) determined by quantitative coronary angiography (QCA)[5]. Since the original reports on 3D myocardial perfusion CMR, technological advances have led to improved signal homogeneity in particular at 3 Tesla and better reconstruction accuracy of temporally resolved signal intensity curves[6,7]. These second-generation 3D methods have not been tested in a clinical setting.

Furthermore, comparisons of myocardial perfusion imaging with QCA are inherently limited, because of the variable relationship between the severity of coronary stenosis and its functional significance[8]. A more appropriate validation of perfusion imaging can be made against invasive pressure wire-derived fractional flow reserve (FFR) measured during coronary angiography. FFR <0.75 correlates closely with objective evidence of reversible ischemia and FFR-guided PCI confers a prognostic benefit[9].

While one of the key advantages of FFR is that it is largely independent of vessel size and other confounders, this also implies that FFR provides no information on the extent of myocardium at risk, a separate marker of prognosis. For invasive estimation of ischaemic burden, the Duke Jeopardy Score (DJS)[10] which correlates the myocardium at risk with prognosis has previously been described.

The objective of this study was to determine the diagnostic accuracy of a state-of-the-art 3D perfusion CMR method against FFR to detect flow limiting coronary artery stenosis. A secondary aim was to establish the correlation between myocardium at risk defined by the DJS derived from angiographic data and ischemic burden as defined by the volume of hypoperfused myocardium on 3D whole heart myocardial perfusion CMR.

## 2.3 Methods

*Patient Population*

The study was approved by the local research ethics committee and all subjects gave written informed consent to participate. Fifty-five consecutive patients with known or suspected CAD were recruited prior to clinically indicated invasive coronary angiography studies. Exclusion criteria were recent (<3 months) acute coronary syndromes, coronary artery bypass grafting, and contraindications to CMR imaging (including pacemakers, claustrophobia) or adenosine stress testing (poorly controlled obstructive airway disease, second or third degree atrio-ventricular block).

On the angiography procedure day, a full medical history was taken and a physical examination undertaken. Symptoms of chest pain were recorded in accordance to the Canadian Cardiovascular Society angina grading scale. Baseline ECG was performed and analysed for the presence of Q waves or bundle branch block using defined Minesota criteria.

*CMR Protocol*

All subjects were scanned in supine position on a 3 Tesla MR scanner (Achieva, Philips Healthcare, Best, Netherlands) equipped with dual-source parallel RF transmission (multi-transmit) technology[7] and a 6-channel cardiac phased array receiver coil. Subjects were monitored throughout the scan with a 4-lead vectorcardiogram, respiratory belt and blood pressure monitoring. For perfusion imaging, a 3D spoiled turbo gradient echo sequence was used (TR/TE/flip angle 1.8ms/0.7ms/15°, saturation prepulse delay 150ms, acquisition timed to end-systole, partial Fourier acquisition, 10 fold *k-t* acquisition with 11 training profiles leading to a net acceleration of 7.0, *k-t*

principal component analysis reconstruction[6], reconstruction of 12-16 contiguous slices of 5mm thickness, field of view 350 x 350mm$^2$, acquired voxel size 2.3x2.3x5mm$^3$). Stress perfusion images were acquired during intravenous adenosine-induced hyperaemia administered for 4 minutes at 140 μg/kg/min. An intravenous bolus of 0.075 mmol/kg gadobutrol (Gadovist, Bayer, Germany) was administered at a rate of 4.0ml/s followed by a 20ml saline flush (Spectris Solaris power injector, Pennsylvania, USA).

Stress perfusion CMR was followed by cine imaging covering the left ventricle in 10-12 short axis sections and a rest perfusion scan performed 15 minutes later using the same concentration and volume of contrast agent (0.075 mmol/kg) as for stress perfusion. Late gadolinium enhancement (LGE) images (0.15mmol/kg cummulative dose) were acquired in the same short axis geometry after a further 15 minutes using a conventional method[11].

*Catheter laboratory protocol*

FFR was calculated as $(P_d - P_v) / (P_a - P_v)$ during hyperaemia induced by infusion of intravenous adenosine at 140mcg/kg/min, where $P_d$, $P_a$, $P_v$ are mean distal coronary, aortic and right atrial pressures, respectively[12]. FFR was performed in all coronary arteries with luminal stenosis >=50% in two orthogonal views. FFR<0.75 was considered to represent haemodynamically significant coronary stenosis. Vessels with chronic total occlusions were considered as significantly stenosed and FFR measurements were not attempted. Angiographic images were analysed quantitatively using QCA (Medcon Ltd., Tel Aviv, Israel) by a blinded observer. Significant CAD was defined as >70% diameter stenosis of the left anterior descending, circumflex or right

coronary arteries with >/= 2 mm luminal diameter or >50% diameter stenosis for the left main stem.

*Duke Jeopardy Score*

The Duke Jeopardy score was calculated using methods as originally described from myocardium at risk depending on the size and location. The coronary tree was divided into 6 segments of nearly equal myocardial perfusion (eg, left anterior descending artery, major septal perforator, major diagonal branch, circumflex artery, major obtuse marginal branch artery and posterior descending artery). A score of 2 for each significant lesion was given, so that a total maximal score of 12 can be derived. The cardiologists performing the coronary angiogram and all angiography-derived measurements were blinded to the CMR scan result.

*CMR analysis*

Two experienced observers blinded to clinical details, visually analyzed the CMR images using standard software (ViewForum, Philips Healthcare, Best, The Netherlands). Stress and rest perfusion scans and LGE images were viewed simultaneously. Image quality was graded on a scale from 1 to 4 (1=uninterpretable, 2=poor, 3= good, 4=excellent). Image artefacts were recorded and categorised as breathing related, subendocardial rim artifacts or related to the reconstruction of undersampled data. A perfusion defect was considered present if reduced contrast uptake was seen at stress with greater than 25% transmurality in more than one contiguous slice persisting for more than 4 consecutive dynamic time points but not present at rest. Ischemia was only reported if the perfusion defect extended outside of any scar noted on matching LGE images. Perfusion defects were scored on a scale from 0-3 [0=normal (all segments normal, no artefacts),

1=possibly normal (1 segment affected or suspected artefacts), 2=probably abnormal (2 segments affected or artefacts), 3=definitely abnormal (>2 segments affected and no artefacts)] for each perfusion territory to provide a summed stress score by each of the two reviewers. In case of disagreement, arbitration from a third observer was sought. For patient analysis, all normal and probably normal scores were classified as being "normal" and probably abnormal and definitely abnormal scores were grouped as "abnormal".

Perfusion defects were assigned to coronary territories using the AHA coronary arterial segment model[13]. In order to simulate a comparison of 3D whole heart with 2D three-myocardial perfusion CMR, in a separate analysis session only slices 3, 7, and 11, representing apical, mid-myocardial and basal sections, were reviewed by the observers and the resulting diagnostic values calculated on a per patient and vessel basis.

*Ischaemic Volume Calculation*

The ischaemic volume of myocardium was calculated by a separate blinded observer using GTVolume software (GyroTools, Zurich, Switzerland). A previously described method which defines ischaemic volume as tissue at an intensity threshold of <2 SDs below the signal of remote myocardium in the stress perfusion dynamic with the clearest delineation of a perfusion defect was used[5]. The total ischaemic volume was calculated by summation of the hypoperfused areas in each slice. In patients with scar on late gadolinum enhancement, scar volume was calculated in a similar fashion and peri-infarct ischaemia was derived as the difference between the ischaemia and scar volumes. The analysis was initially performed for all cases and the repeated for correctly identified cases only, i.e. excluding studies with false positive and false negative results.

To test reproducibility of detecting ischaemic volumes, interobserver variablity was assessed in a subset of ten patients by a second reader fully blinded to clinical details and previous results. For intraobserver variability the first reader repeated measurements of ischaemic volumes two weeks later.

*Statistical analysis*

Data analysis was performed using IBM SPSS, Version 19.0 (SPSS< Chicago, IL, USA). Analysis was performed on both a patient and coronary territory basis to determine sensitivity, specificity, negative and positive predictive values. These values were calculated for CMR to detect FFR<0.75. Receiver operator characteristics (ROC) analysis was performed using the summed perfusion scores of the visual analysis. The interobserver variability of perfusion analysis was calculated using the kappa coefficient. Inter- and intraobserver variability of ischaemic burden data as determined by CMR was calculated using Bland Altman analysis. Correlation between inter- and intraobserver variability, and the DJS and CMR ischemic burden was determined using Pearson's test of correlation with a two-tailed test of significance. For all analyses $P<0.05$ was considered significant.

## 2.4 Results

*Patient population*

Of the 55 patients recruited to the study, one study was incomplete because of claustrophobia and one was excluded because the CMR image quality was deemed uninterpretable. A total of 53 patients (41 men, mean age 63) thus formed the final population for analysis (Table 1).

*Coronary angiography*

Angiography was performed on average three (range 0-14) days after the CMR scan (Table 2). The overall disease prevalence in the study population was 64%. Of the 159 vessels analysed, 72 (45%) vessels contained >50% diameter stenosis on visual assessment. FFR was not performed in 2 vessels with heavily calcified long complex lesions, and in 6 vessels, which were either completely or subtotally occluded. These arteries were deemed significantly stenosed for the purpose of the study. FFR was performed in the remaining 64 arteries. Of these, 39 had an FFR <0.75 and 25 had an FFR>=0.75. The total number of diseased vessels was thus 47. Twenty-four patients had single-vessel disease, seven patients had two-vessel disease and three patients had three-vessel disease as defined by a FFR<0.75.

QCA was retrospectively performed in all vessels and did not reveal any vessel with >50% stenosis that was not assessed by FFR. In the vessels with FFR >0.75, mean diameter stenosis was 48.7% and in vessels with FFR</=0.75, diameter stenosis was 75.6%.

The mean FFR in vessels reported negative for ischaemia by perfusion imaging was 0.82, (range 0.68-0.95, median 0.83) and the diameter stenosis in these vessels was 56.6%. The mean FFR in vessels reported as positive for ischaemia by perfusion imaging was 0.61, (range 0.30-0.86, median 0.66) with a mean diameter stenosis of 71.7% (Figure 1). Statistical significance was observed between the FFR of the two groups ($p<0.0001$) and for QCA ($p=0.0013$).

*CMR imaging*

Average exam time per patient was 51 (+/- 4) minutes. Typical symptoms were experienced in 46 out of 53 of patients during adenosine stress with mean blood pressure changing from 131/71 to 124/70 mmHg (systolic $p<0.001$, diastolic $p=0.16$) and heart rates increasing from 68 to 81 beats/min ($p<0.01$). Subendocardial LGE was found in four patients and a small area of transmural scar was seen in one. There was no significant difference in rest or stress haemodynamic data between CMR perfusion and angiography (all p-values >0.05), (Tables 2 and 3).

*Image Quality*

The median image quality score was good (mean score 3.1+/-SD 0.5). The main artefacts seen were subendocardial dark rim related artefacts in 7 patients (13%) and breathing artefact in 8 patients (15%) – although the overall quality was deemed sufficient to make a diagnosis in all of these cases. Agreement between observers for the identification of abnormal perfusion per coronary territory showed a $\kappa$ of 0.94, indicating excellent agreement. In four patients (2.5% of coronary territories), a third reader was involved to arbitrate the remaining cases.

*CMR Analysis vs FFR*

When analysed per patient (Table 4a), visual analysis of CMR perfusion images yielded a sensitivity of 91.2% (95% CI: 75.2 to 97.7), specificity of 89.5% (95%CI 65.5 to 98.2) and diagnostic accuracy of 90.6% for the detection of significant coronary disease defined by a FFR <0.75. The likelihood ratio was 16 weighted by prevalence, with a positive predicative value of 93.9% (95% CI: 78.4-98.9) and a negative predictive value of 85.0% (95% CI: 61.1-96.0). ROC analysis showed an area under the curve of 0.89 (95%CI 0.785 to 0.991, p<0.0001). An example of a case is shown in figures 2a and 2b. When analysed per vessel territory (Table 4b), the sensitivity was 79% (95% CI: 62.0-87.0), specificity 92% (95% CI 84.9 – 96.0%) and diagnostic accuracy 88.1%. The positive predictive value was 80.4% (95% CI: 65.6-90.1) and negative predictive value 91.2% (95% CI 83.9-95.4). ROC analysis showed an area under the curve of 0.88 (95%CI 0.801 to 0.994, p<0.0001).

When using only three slices of the whole heart perfusion datasets for analysis, the sensitivity, specificity and diagnostic accuracy were 85.3% (95% CI 68.2% to 94.4%), 84.2% (95% CI 59.5% to 95.8%) and 84.9% on a patient basis. ROC analysis showed an area under the curve of 0.845. For the vessel analysis, sensitivity, specificity and diagnostic accuracy were 74.4% (95% CI 59.4% to 85.6%), 88.4% (95% CI 80.6% to 93.4%), and 84.3% with an area under the ROC curve of 0.81. None of these values were significantly different to the whole-heart analysis.

*CMR Analysis vs QCA*

Visual analysis of 3D-CMR perfusion images, on a patient basis, yielded a sensitivity, specificity, and diagnostic accuracy of 87.9% (95% CI: 70.9 to 96.0), 80.0% (95% CI:

55.7 to 93.4), and 84.9% respectively, for the detection of significant CAD defined by QCA. These data are summarized in Table 5.

*Ischaemic burden vs. Duke Jeopardy Score*

The mean percentage ichaemic volume (Table 6) on perfusion CMR was 9.9% (±10.9). The mean DJS was 4.0 (±3.9). The mean percentage of ischaemia volume for DJS of 0, 6, 12 were 0, 13.1% and 36.7% respectively.

Pearsons correlation coefficient showed a strong correlation (r=0.82, 95% CI 0.70 – 0.89) between the DJS and ischaemic volume on CMR (p<0.0001). If only patients correctly identified by perfusion CMR (48/53) were included in the analysis, the correlation was stronger (r=0.87, 95%CI 0.78 to 0.93, P<0.0001) (Figure 5). Mean bias on Bland-Altman analysis was 0.1ml (95% CI -3.1 to 3.3) for intra-observer and 0.05mls (95% CI -1.8 to 1.9) for and the intraobsever variability. Pearsons correlation was very strong for both interobserver (r=0.96) and intraobserver variability (r=0.98) (Figure 6).

## 2.5 Discussion

This study has shown that 3D whole-heart myocardial perfusion CMR accurately predicts the presence of haemodynamically significant coronary artery stenosis as measured by FFR. In addition, it has demonstrated close agreement between estimates of ischaemic volume by 3D CMR and an invasive index of ischaemic burden.

Three-dimensional acquisition methods overcome some of the remaining limitations of myocardial perfusion CMR, specifically the limited myocardial coverage offered by conventionally used 2D methods. Furthermore, 3D acquisition is more signal-to-noise efficient than 2D imaging and as all data are acquired in one shot, all images are acquired in the same cardiac phase. 3D myocardial perfusion CMR has become feasible as a result of recent advances in data acquisition speed, with several different methods proposed[14-16].

Following initial feasibility studies, a recent larger clinical study reported a sensitivity of 91.7% and a specificity of 74.3% of 3D myocardial perfusion CMR for the detection of coronary stenosis on QCA on a patient basis[5]. However, QCA correlates poorly with the hemodynamic effect of a coronary stenosis because of effects of lesion proximity and length, calcification, collateral vessels and dynamic changes in vasomotor tone[8]. Pressure-wire derived FFR, which was the endpoint in the present study, is considered the reference standard for assessing the haemodynamic significance of atherosclerotic coronary lesions and is a more appropriate comparator for ischaemia imaging than QCA.

Determining the functional significance of coronary stenosis is directly related to patient outcome, as shown for invasive assessment in the DEFER and FAME[17,9] cohorts and for

non-invasive imaging in COURAGE and other studies [18-20]. Furthermore, a substudy of FAME suggested visual and functional disparity, which highlights the need for functional assessment in patients with coronary artery disease[21]. For these reasons, current guidelines recommend the use of functional testing prior to elective revascularisation[22]. In clinical routine, however, less than one half of patients are evaluated non-invasively before revascularisation[23].

This study demonstrates excellent agreement between FFR and 3D myocardial perfusion CMR. Compared with the previous study that compared 3D myocardial perfusion CMR with QCA, the specificity in the present analysis was higher (89.5% vs 74.3%) while sensitivity was the same at 91% [5]. The increased specificity of our analysis, reflecting a lower false positive rate, is likely to relate to vessels that cause no functional flow limitation despite appearing significant on QCA.

In the present study, whole heart analysis did not statistically outperform the analysis of only three equally distributed slices of the 3D data set, intended to simulate conventional 2D myocardial perfusion CMR methods. However, selecting three slices of a 3D data set for analysis is not equivalent to the acquisition of a three-slice 2D data set. In a 3D data set, all images are acquired in one optimised cardiac phase (systole in our study), which cannot be achieved in a multi-slice 2D acquisition. On the other hand, 2D acquisition would yield a higher in plane spatial resolution in a shorter acquisition time than 3D acquisition if a similar undersampling factor was applied. Further technical differences exist between 2D and 3D acquisitions that affect signal and contrast behaviour of the acquired images. Our results can therefore only give an indication of the relative performance of 2D versus 3D myocardial perfusion CMR and only an

adequately powered head-to-head comparison of the two acquisition methods can give conclusive evidence of their relative diagnostic performance. However, as demonstrated in this study, 3D acquisition has other advantages, in particular the estimation of ischemic volume.

We observed a strong correlation between ischaemia burden on 3D myocardial perfusion CMR and the invasive DJS. Proximal lesions with a higher invasive score showed a higher volume of ischaemia on CMR. Although not frequently used, invasive scores of ischaemia burden have clinical legitimacy as the magnitude of myocardium at risk due to severe coronary stenosis is associated with an adverse prognosis[10,24,25] and ischaemia burden is not reflected in the FFR. The Duke Jeopardy score combines assessment of stenosis severity, location and five year survival of patients with scores of <2, 6 and 12 of 97%, 85% and 56% respectively as has been reported[10]. Non-invasive assessment of myocardium at risk has similar prognostic relevance and an ischaemic burden above 10% may serve as a threshold at which revascularisation conveys prognostic benefit over medical therapy alone[26].

Our study thus shows that 3D myocardial perfusion CMR allows both the detection of ischaemia and provides an estimate of the extent of myocardium at risk. Such a non-invasive assessment may convey clinical advantages over invasive assessment. Compared with FFR-guided revascularisation, non-invasive imaging is more suited for serial assessment and avoids potential iatrogenic complications, which could have economic implications in particular the multi-vessel setting[27]. Although not formally assessed in the present study given the low prevalence of prior myocardial infarction, the combination of 3D perfusion with late gadolinium enhanced CMR will also permit a

parallel assessment of ischaemia and infarction in equivalent imaging planes, which is not possible with invasive assessment. A comprehensive assessment with 3D CMR methods thus holds promise as a non-invasive diagnostic and risk assessment tool for patients with known or suspected CAD.

Although the sensitivity of this technique was high, it is possible the false negatives reflect inadequate stress response rather than diagnostic failure. Recently, splenic switch-off has been proposed as a simple and quick marker of stress adequacy[28]. It has been observed that during adenosine perfusion, there is little signal increase in the spleen while during rest perfusion the spleen enhances normally. Failure of splenic switch-off may reflect inadequate pharmacologic stress, which has the potential to identify patients at risk of false-negative examination results. In CMR perfusion images with proven false-negative results, failed splenic switch-off was four times more common than in perfusion scans with true-negative results. This test was not performed in our study, but retrospective analysis incorporating it could potentially influence diagnostic confidence in scan interpretation.

**Limitations**

This study investigated a population with a high disease prevalence. Future studies will be required to establish the diagnostic performance of 3D myocardial perfusion CMR in lower risk patient groups. In order to minimise patient complications and to be consistent with clinical practice, FFR was only measured in vessels with greater than >50% coronary stenosis. It cannot be excluded that some lesions of <50% luminal stenosis may have had an abnormal FFR. We chose an FFR value of 0.75 as significant,

but clinically a value of 0.8 is often used and the functional significance of "gray zone" FFR values (0.75-0.8) remains uncertain.

FFR measurement was not possible in eight vessels, accounted for by the six chronic total occlusions and two significantly calcified tortuous vessels. No attempts at FFR were made consistent with clinical practice and maintaining patient safety. These vessels were deemed positive for the purpose of analysis as in the FAME study. A limitation of FFR is that it may be influenced by the presence of major collateral vessels (we had measured any stenosis >50%); however, FFR in vessels supplying collaterals to the occluded vessels is thought to be overestimated and unlikely to affect overall patient analysis, as at least one vessel being abnormal makes the overall scan abnormal. This may in part account for the differences we observed in the sensitivity between patient and vessel analysis, originally proposed to be due to the appropriate assignment of perfusion to coronary territories. However, exclusion of these vessels and re-analysis to demonstrate statistical significance would be useful for focusing data analysis on patients with intermediate lesions and for whom functional investigation is recommended.

As in all studies comparing angiographic and imaging methods, we may not have correctly assigned all myocardial segments to the appropriate coronary artery. This limitation is likely to have accounted for some of the reduced sensitivity of per vessel territory compared with per patient analysis. Both CMR and the DJS have limitations for the calculation of the ischemia burden. 3D myocardial perfusion CMR is a novel method and no formal validation of estimates of ischemia volume with this method against a recognised reference test such as myocardial perfusion scintigraphy has been

performed to date. The method of estimating ischemic volume from a single frame of the dynamic CMR data that was used in the current study and the previous report by Manka et al[5] requires further validation. It should be noted that this method is not a substitute for quantitative estimation of myocardial blood flow, which has been used in other studies. Our analysis method provides a relatively fast but visual measurement of ischaemic burden, while quantitative analysis methods of myocardial blood flow are more time-consuming but offer higher objectivity and the detection of balanced ischaemia, but have not yet been applied to 3D data sets.

The 3D method we have used does not necessarily provide full heart coverage. We acquired 12-16 slices of 5mm thickness, thus covering 6-8cm in the z direction. As we acquired 3D perfusion images in systole, this coverage was generally sufficient to cover the LV myocardium from the apex to the mitral valve ring and LVOT. However in very large hearts, the number of acquired slices may not be sufficient for true whole heart coverage and in some patients the true apex or base of the heart was not included in the 3D volume. However the diagnostic value of image acquisition, immediately beneath the LVOT or at the true apex is limited by partial volume effects, so that the impact of this limitation on our findings should be small.

The DJS has several limitations, including the difficulty of predicting the haemodynamic significance of coronary disease from angiography alone, particularly for intermediate lesions and the fact that it does not take into account myocardial viability. For this reason, we excluded any patients with a history of recent myocardial infarction (<3/12), but five patients still had evidence of small infarcts on CMR. Furthermore, the DJS simply involves scoring the coronary tree segments and does not directly measure the size of

the myocardial territory supplied by each vessel. This can cause problems with true left and right coronary artery co-dominance, unusual anatomic variations and collaterization. However, whilst more precise scoring systems exist, they do not have the same attributes of simplicity and universal applicability.

**Conclusion**

Three-dimensional myocardial perfusion CMR accurately detects functionally significant coronary artery disease with excellent sensitivity, specificity, and positive and negative predictive values when compared with FFR. CMR estimates of ischaemic burden correlate closely with an invasive index. Multicentre studies to determine the use of 3D myocardial perfusion CMR as a non-invasive strategy for the diagnosis and risk stratification of patients with suspected CAD appear warranted.

## 2.6 References

1. Nandalur KR, Dwamena BA, Choudhri AF, Nandalur MR, Carlos RC. Diagnostic performance of stress cardiac magnetic resonance imaging in the detection of coronary artery disease: a meta-analysis. J Am Coll Cardiol 2007;50(14):1343-1353.

2. Hamon M, Fau G, Née G, Ehtisham J, Morello R, Hamon M. Meta-analysis of the diagnostic performance of stress perfusion cardiovascular magnetic resonance for detection of coronary artery disease. *J Cardiovasc Magn Reson.* 2010 May 19;12(1):29

3. Greenwood J, Maredia N, Plein S, et al. Cardiovascular magnetic resonance and single-photon emission computed tomography for diagnosis of coronary heart disease (CE-MARC): A prospective trial. Lancet 2011; S0140-6736(11)61335-4

4. Shin T, Hu HH, Pohost GM, Nayak KS. Three dimensional first-pass myocardial perfusion imaging at 3T: feasibility study. J Cardiovasc Magn Reson. 2008; 10: 57

5. Manka R, Jahnke C, Paetsch I, et al. Dynamic 3-dimensional stress cardiac magnetic resonance perfusion imaging: detection of coronary artery disease and volumetry of myocardial hypoenhancement before and after coronary stenting. J Am Coll Cardiol. 2011 Jan 25;57(4):437-44.

6. Pedersen H, Kozerke S, Ringgaard S, Nehrke K, Kim WY. k-t PCA: temporally constrained k-t BLAST reconstruction using principal component analysis. Magn Reson Med. 2009 Sep;62(3):706-16

7. Willinek WA, Gieseke J, Schild HH, et al. Dual-source parallel radiofrequency excitation body MR imaging compared with standard MR imaging at 3.0 T: initial clinical experience. Radiology. 2010 Sep;256(3):966-75

8. White CW, Wright CB, Marcus ML et al. Does visual interpretation of the coronary arteriogram predict the physiologic importance of a coronary stenosis? *N Engl J Med* 1984;310:819–824.

9. Tonino PA, De Bruyne B, Fearon WF, et al; FAME Study Investigators. Fractional flow reserve versus angiography for guiding percutaneous coronary intervention. N Engl J Med. 2009 Jan 15;360(3):213-24

10. Califf RM, Phillips HR 3rd, Wagner GS, et al. Prognostic value of a coronary artery jeopardy score. J Am Coll Cardiol. 1985 May;5(5):1055-63

11. Kim RJ, Wu E, Judd R, et al. The Use of Contrast-Enhanced Magnetic Resonance Imaging to Identify Reversible Myocardial Dysfunction N Engl J Med 2000; 343:1445-145

12. Perera D, Biggart S, Redwood S, et al. Right atrial pressure: can it be ignored when calculating fractional flow reserve and collateral flow index? J Am Coll Cardiol. 2004 Nov 16;44(10):2089-91

13. Cerqueira MD, Weissman NJ, Dilsizian V, et al. Standardized myocardial segmentation and nomenclature for tomographic imaging of the heart: a statement for healthcare professionals from the Cardiac Imaging Committee of the Council on Clinical Cardiology of the American Heart Association. Circulation 2002;105:539-542

14. Shin T, Hu HH, Pohost GM, Nayak KS. Three dimensional first-pass myocardial perfusion imaging at 3T: feasibility study. J Cardiovasc Magn Reson. 2008 Dec 11;10:57.

15. Shin T, Pohost GM, Nayak KS. Systolic 3D first-pass myocardial perfusion MRI: Comparison with diastolic imaging in healthy subjects. Magn Reson Med. 2010 Apr;63(4):858-64

16. Vitanis V, Manka R, Kozerke S, et al. High resolution three-dimensional cardiac perfusion imaging using compartment-based k-t principal component analysis. Magn Reson Med. 2011 Feb;65(2):575-87

17. Pijls NH, van Schaardenburgh P, de Bruyne B et al. Percutaneous coronary intervention of functionally nonsignificant stenosis: 5-year follow-up of the DEFER Study. J Am Coll Cardiol. 2007 May 29;49(21):2105-11.

18. Shaw L, Berman D, Boden W et al. Optimal medical therapy with or without percutaneous coronary intervention to reduce ischemic burden: results from the Clinical Outcomes Utilizing Revascularization and Aggressive Drug Evaluation (COURAGE) trial nuclear substudy. Circulation 2008;117:1283–

19. Jahnke C, Nagel E, Paetsch I, et al. Prognostic value of cardiac magnetic resonance stress tests: adenosine stress perfusion and dobutamine stress wall motion imaging. Circulation 2007;115: 1769 – 1776.

20. 1291Sicari R, Pasanisi E, Venneri L, Landi P, Cortigiani L, Picano E, Group EPICES, Group EDICES. Stress echo results predict mortality: a large-scale multicenter prospective international study. J Am Coll Cardiol 2003;41:589–595.

21. Tonino PA, Fearon WF, Pijls NH et al. Angiographic versus functional severity of coronary artery stenoses in the FAME study fractional flow reserve versus angiography in multivessel evaluation. J Am Coll Cardiol. 2010;55:2816 –2821

22. Smith SC Jr, Feldman TE, Riegel B, et al. ACC/ AHA/SCAI 2005 guideline update for percutaneous coronary intervention: summary article: a report of the American College of Cardiology/American Heart Association Task Force on Practice Guidelines (ACC/AHA/SCAI Writing Committee to Update the 2001 Guidelines for Percutaneous Coronary Intervention). Circulation. 2006;113:156–175.

23. Lin GA, Dudley RA, Redberg RF et al. Frequency of stress testing to document ischemia prior to elective per- cutaneous coronary intervention. JAMA. 2008;300:1765–1773.

24. Perera D, Thomas M, Redwood S et al; BCIS-1 Investigators. Elective intra-aortic balloon counterpulsation during high-risk percutaneous coronary intervention: a randomized controlled trial. JAMA. 2010 Aug 25;304(8):867-74

25. Seven-year outcome in the Bypass Angioplasty Revascularization Investigation (BARI) by treatment and diabetic status. J Am Coll Cardiol. 2000 Apr;35(5):1122-9

26. Hachamovitch R, Hayes SW, Friedman JD, Berman DS. Comparison of the short-term survival benefit associated with revascularization compared with medical therapy in patients with no prior coronary artery disease undergoing stress myocardial perfusion single photon emission computed tomography. Circulation 2003;107:2900–2907.

27. Fearon WF, Bornschein B, Siebert U, et al. Economic evaluation of fractional flow reserve-guided percutaneous coronary intervention in patients with multivessel disease. Circulation. 2010;122:2545–2550.

28. Manisty C, Ripley DP, Herrey AS, Captur G, Wong TC, Petersen SE, Plein S, Peebles C, Schelbert EB, Greenwood JP, Moon JC. Splenic Switch-off: A Tool to Assess Stress Adequacy in Adenosine Perfusion Cardiac MR Imaging. Radiology. 2015 Sep;276(3):732-40. doi: 10.1148/radiol.2015142059

## 2.7 Tables

### Table 1: Patient demographics

| Baseline Demographics of Patient Cohort (n=53) | |
|---|---|
| Parameter | Data (%) |
| Male | 41(77.3) |
| Age, years | 63.5 ± 10.8 |
| Range | 43 to 83 |
| BMI, kg/m$^2$ | 27.5 ± 4.1 |
| Previous coronary intervention | 14 (26.0) |
| Normal LV function | 49 (92.5) |
| Canadian Cardiovascular Society Angina Grading Scale | |
| No pain or Atypical Symptoms | 16 (30.2) |
| Class 1 | 24 (45.3) |
| Class 2 | 10 (18.9) |
| Class 3 | 3 (5.7) |
| Class 4 | 0 (0) |
| Baseline Electrocardiogram | |
| Q wave | 4 (7.5) |
| Left Bundle Branch Block | 3 (5.7) |
| Right Bundle Branch Block | 1 (1.9) |
| Cardiovascular Risk Factors | |
| Diabetes | 16 (30.2) |
| Dyslipidaemia | 44 (83.0) |
| Current Smoker | 9 (17.0) |
| Hypertension | 35 (66.0) |
| Family History | 20 (37.7) |
| Peripheral Vascular Disease | 3 (5.7) |
| Medications | |
| Aspirin | 51 (96.2) |
| Clopidogrel | 19 (35.8) |
| Beta Blocker | 35 (66.0) |
| Statin | 50 (94.3) |
| Angiotensin enzyme inhibitor or angiotensin receptor blocker | 32 (60.3) |
| Nitrate | 12 (20.7) |

**Table 2. X-ray angiography data**

| Angiogram Data | |
|---|---|
| Time from CMR scan, days | 3.2±3.3 (range 0-14, mode 0, median 2.0) |
| Resting systolic blood pressure | 128.7±20.4 |
| Resting diastolic blood pressure | 74.0±12.9 |
| Resting heart rate, beats/min | 66.5±13.4 |
| FFR systolic blood pressure | 121.3±19.3 |
| FFR diastolic blood pressure | 72.6±11.4 |
| FFR heart rate beats/min | 81.0±15.8 |
| Vessels FFR measured (per patient), n | 1.2±0.7 |
| Vessels with FFR >0.75 | 25 |
| Vessels with FFR ≤0.75 | 39 |
| LAD | 18 |
| Cx | 9 |
| RCA | 12 |
| Patients with FFR positive: | |
| One vessel disease | 24 (45.3) |
| Two-vessel disease | 7 (13.2) |
| Three vessel disease | 3 (5.7) |
| QCA in vessels with FFR>0.75 (% diameter stenosis) | 48.7±21.8 |
| QCA in vessels with FFR≤0.75 (% diameter stenosis) | 75.6±12.3 |

**Table 3. CMR data**

| CMR Data | |
|---|---|
| Scanning time, minutes | 50.8 ± 4.2 |
| Range | 42 to 66 |
| Resting systolic blood pressure | 131.1 ± 23.5 |
| Resting diastolic blood pressure | 70.8 ±12.7 |
| Resting heart rate, beats/min | 67.9 ± 16.7 |
| Stress systolic blood pressure | 124.5 ± 22.2 |
| Stress diastolic blood pressure | 70.1± 11.4 |
| Stress heart rate, beats/min | 81.1 ± 18.3 |
| Image quality | 3.1 ± 0.5 |
| Artefact | |
| Breathing | 8 (15.1) |
| Subendocardial rim | 7 (13.2) |
| Adenosine symptoms | 46(86.7) |
| Adenosine complications | 0 |
| Late Gadolinium Enhancement | |
| Full thickness | 1 (1.9) |
| Partial thickness | 4 (7.5) |

**Table 4a: Sensitivity and specificity of CMR vs. coronary angiography and FFR on patient basis (CAD=Coronary Artery Disease)**

| | Coronary Angiography/FFR | | Total |
|---|---|---|---|
| CMR 3D Perfusion | CAD –ve | CAD +ve | |
| Test Positive | 2 | 31 | 33 |
| Test Negative | 17 | 3 | 20 |
| Totals | 19 | 34 | 53 |

| | | 95% Confidence Interval | |
|---|---|---|---|
| | Value | Lower Limit | Upper Limit |
| Prevalence | 0.642 | 0.497 | 0.765 |
| Sensitivity | 0.912 | 0.752 | 0.977 |
| Specificity | 0.895 | 0.655 | 0.982 |

**Table 4b. Sensitivity and specificity of CMR vs. coronary angiography and FFR on coronary artery basis**

| | Coronary Angiography/FFR | | |
|---|---|---|---|
| CMR 3D Perfusion | Absent | Present | Totals |
| Test Positive | 9 | 37 | 46 |
| Test Negative | 103 | 10 | 113 |
| Totals | 112 | 47 | 159 |

| | | 95% Confidence Interval | |
|---|---|---|---|
| | Value | Lower Limit | Upper Limit |
| Prevalence | 0.296 | 0.227 | 0.374 |
| Sensitivity | 0.787 | 0.639 | 0.888 |
| Specificity | 0.920 | 0.849 | 0.960 |

**Table 5: Sensitivity and specificity of CMR vs. coronary angiography and QCA on a patient basis**

| | Coronary Angiography/QCA | | Total |
|---|---|---|---|
| CMR 3D Perfusion | CAD –ve | CAD +ve | |
| Test Positive | 4 | 29 | 33 |
| Test Negative | 16 | 4 | 20 |
| Totals | 20 | 33 | 53 |

| | Value | 95% Confidence Interval | |
|---|---|---|---|
| | | Lower Limit | Upper Limit |
| Prevalence | 0.642 | 0.497 | 0.765 |
| Sensitivity | 0.879 | 0.709 | 0.960 |
| Specificity | 0.800 | 0.557 | 0.934 |

**Table 6: Ischaemia Volumes by CMR and Jeopardy Scores**

| N=53 | LV volume Ml | Ischaemic Volume Ml | Myocardial Ischaemia % | Jeopardy Score |
|---|---|---|---|---|
| Minimum | 50.2 | 0.0 | 0.0 | 0 |
| Median | 68.0 | 8.1 | 11.5 | 4 |
| Maximum | 106.4 | 33.1 | 38.0 | 12 |
| Mean | 70.1 | 7.9 | 9.9 | 4.0 |
| Std. Deviation | 12.3 | 8.0 | 10.9 | 3.9 |

## 2.8 Figure legends

**Figure 1.**

Box plot FFR vs CMR: Relationship between 3D myocardial perfusion imaging vs. fractional flow reserve (n = 64 coronary arteries), the mean fractional flow reserve is marked with a black line; 0.61 with perfusion defect vs. 0.82 with normal myocardial perfusion (P <0.0001).

**Figure 2a**

Case example: Three-dimensional cardiac magnetic resonance (3D-CMR) perfusion scans during adenosine stress. A subendocardial defect is seen in the anterior and anteroseptal segments extending from the base to the apex. Invasive X-ray angiography demonstrated a proximal left anterior descending coronary lesion with a fractional flow reserve of 0.61.

**Figure 2a**

Case example: Three-dimensional cardiac magnetic resonance (3D-CMR) perfusion scans during adenosine stress. A transmural defect is seen from the lateral to infero-lateral segments extending from the base towards the apex. Invasive X-ray angiography demonstrated an ostial circumflex coronary lesion with a fractional flow reserve of 0.31.

**Figure 3**

Case example: Three-dimensional cardiac magnetic resonance (3D-CMR) perfusion scans during adenosine stress. A defect is seen in the inferior, infero-septal and infero-lateral segments of >50% transmurality extending from the base to apex is seen. Invasive X-ray angiography demonstrating a proximal right coronary lesion with a

fractional flow reserve of 0.67. The circumflex had a mid course lesion with a negative FFR 0.82. The ischaemic volume was calculated as 10.3% of the myocardium (marked in red). The area at risk calculated by the Jeopardy score was 4.

**Figure 4a**

Analysis per Patient: Receiver-operating characteristic (ROC) showing sensitivity and specificity of CMR perfusion visual analysis to detect a hemodynamically significant coronary stenosis using a dichotomous value of 0.75 for FFR. The area under the curve was 0.89.

**Figure 4b**

Analysis per coronary territory: Receiver-operating characteristic (ROC) showing sensitivity and specificity of CMR perfusion visual to detect a hemodynamically significant coronary stenosis using a dichotomous value of 0.75 for FFR. The area under the curve was 0.88.

**Figure 5**

Correlation between ischaemic volume vs Duke Jeopardy Score: The dotted line indicates the 10% threshold cut off previously quoted as being the point at which revascularisation may confer prognostic benefit.

**Figure 6 a and b**

Interobserver and intraobserver variabililty of ischaemic volume. A 10% MIB threshold is often quoted to stratify clinical management, this caution is particularly relevant at the lower end of the MIB spectrum. Small differences may be clinically significant in deciding how CAD is managed.

## Figures

### Figure 1. Box plot FFR vs CMR

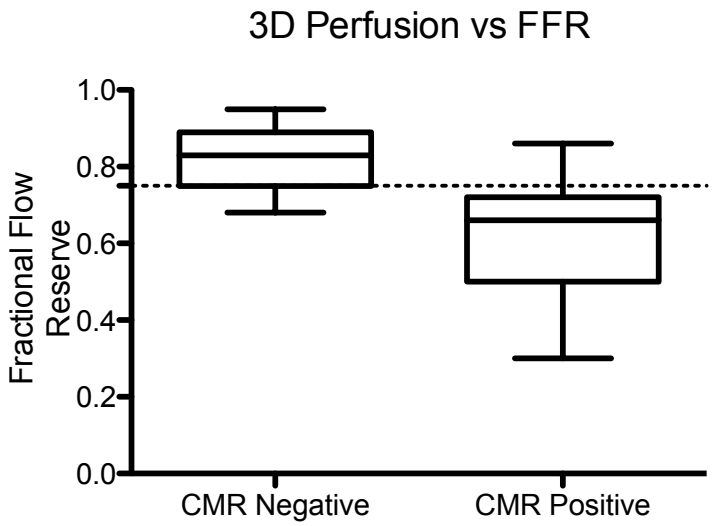

**Figure 2 a). Case example**

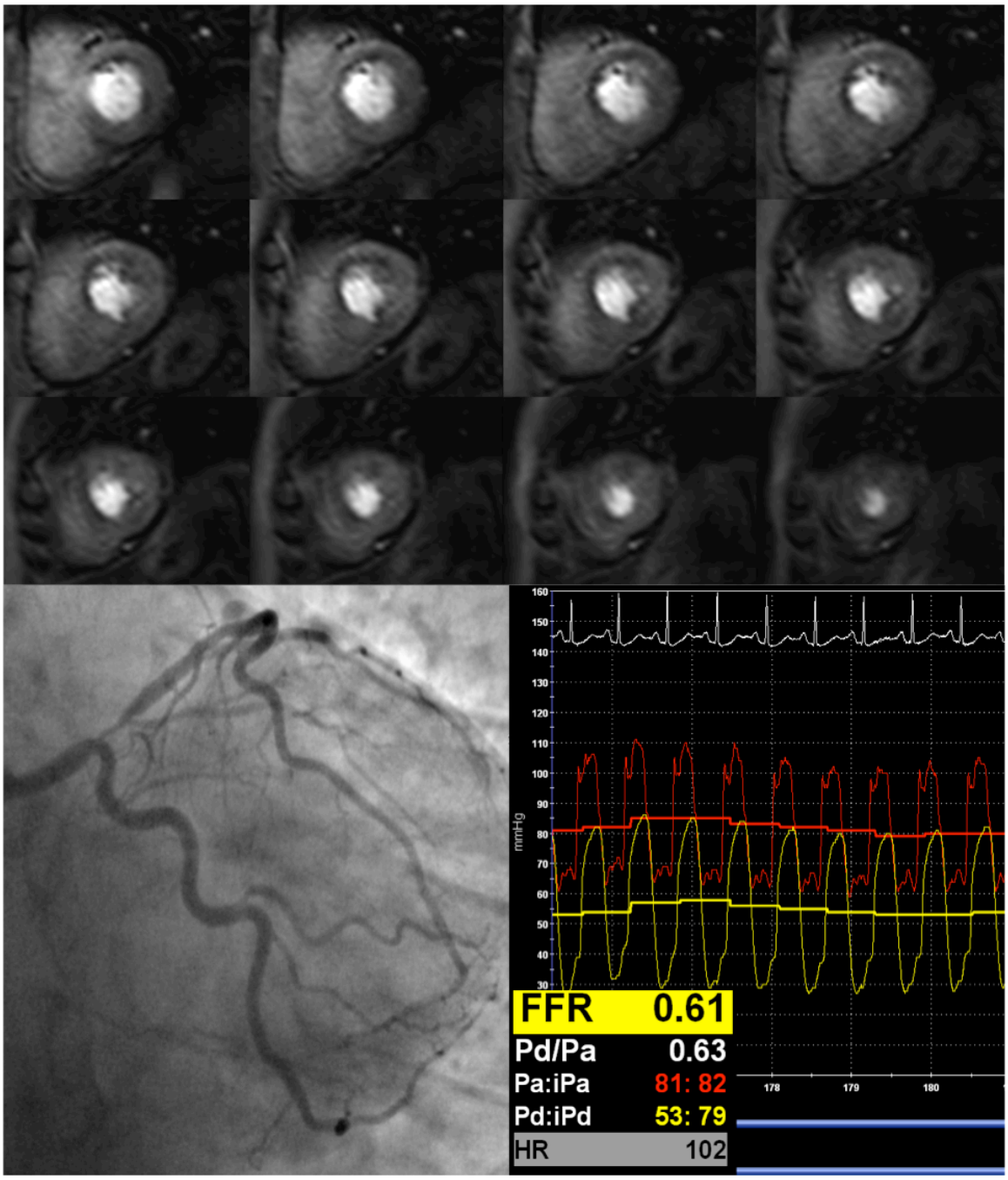

**Figure 2 b) Case example**

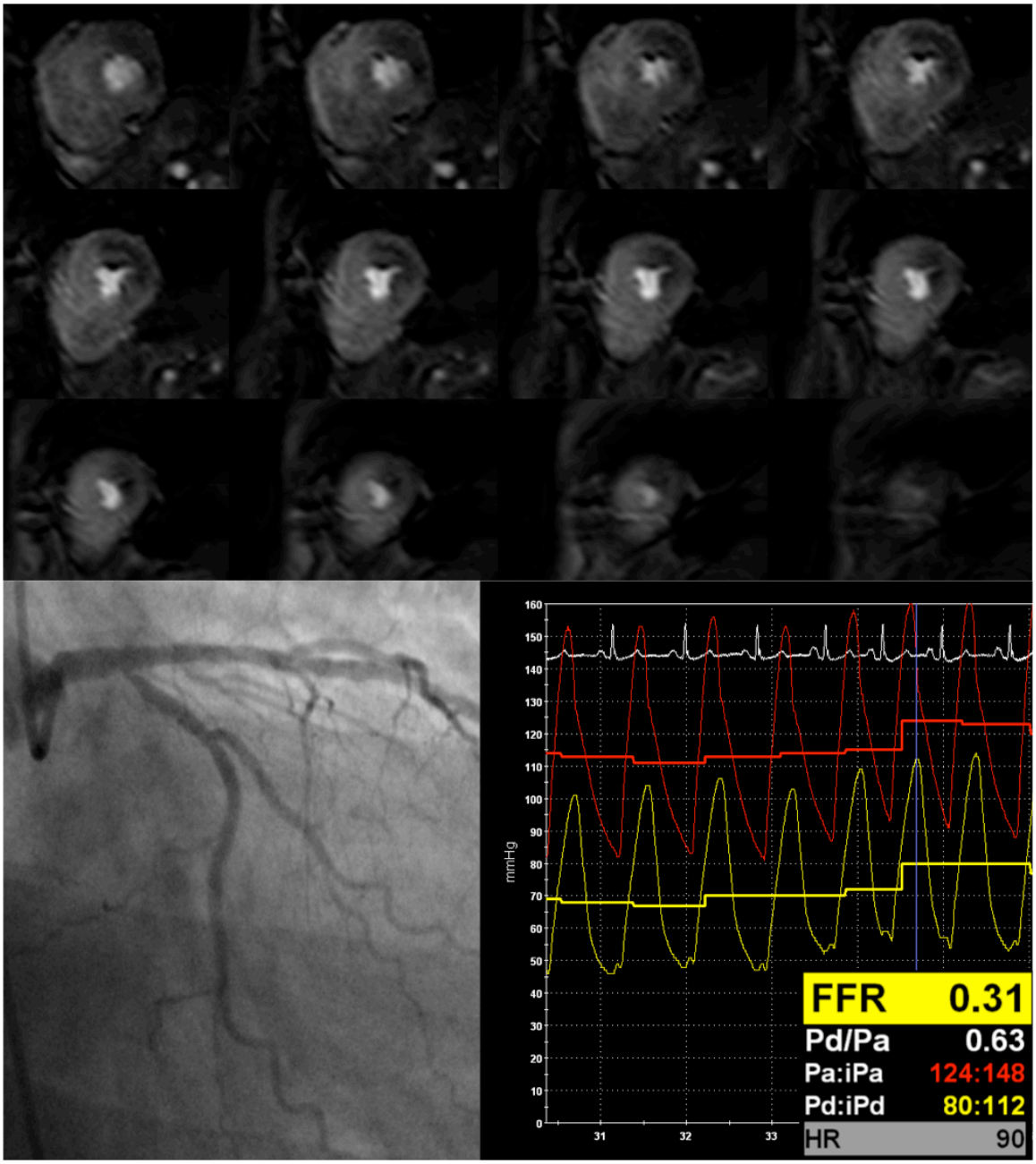

**Figure 3. Case example**

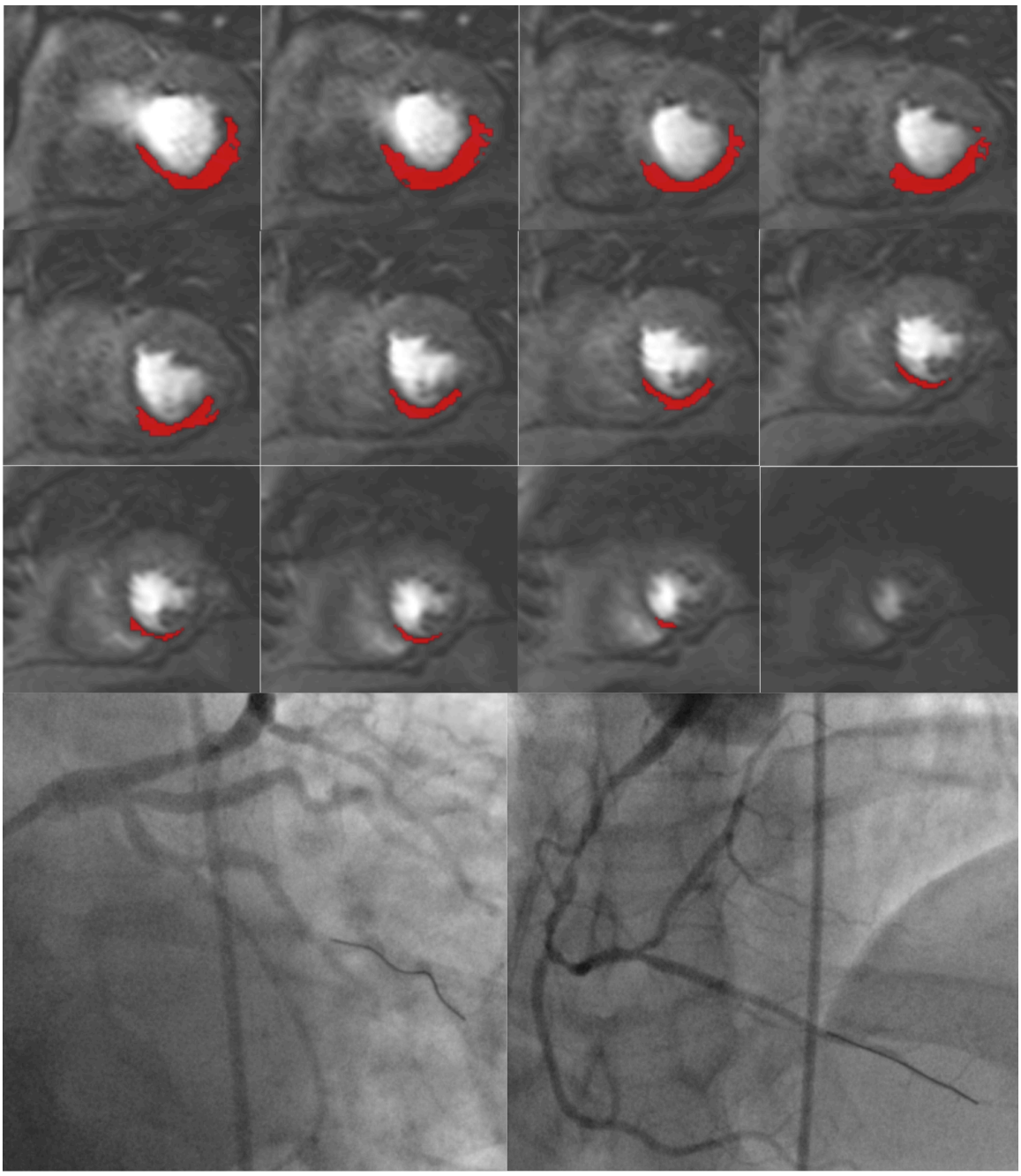

**Figure 4a) ROC Curve - Patient**

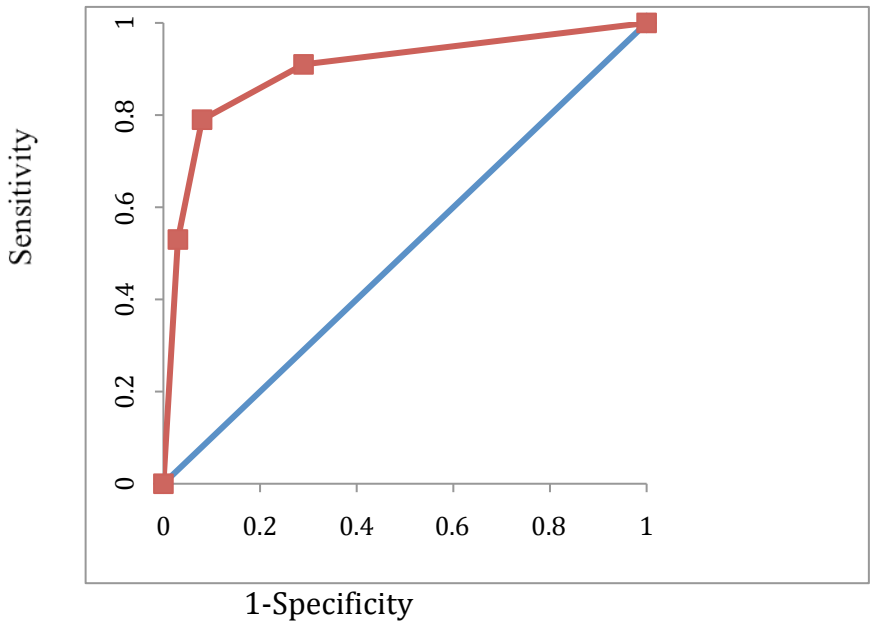

**Figure 4b) ROC Curve - Vessel**

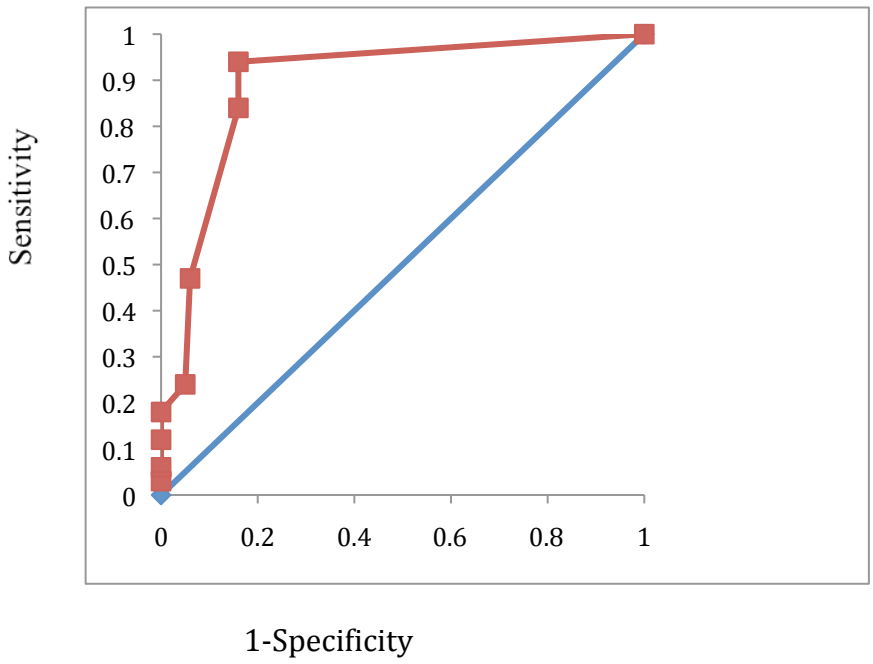

**Figure 5) Ischaemic Volume vs DJS**

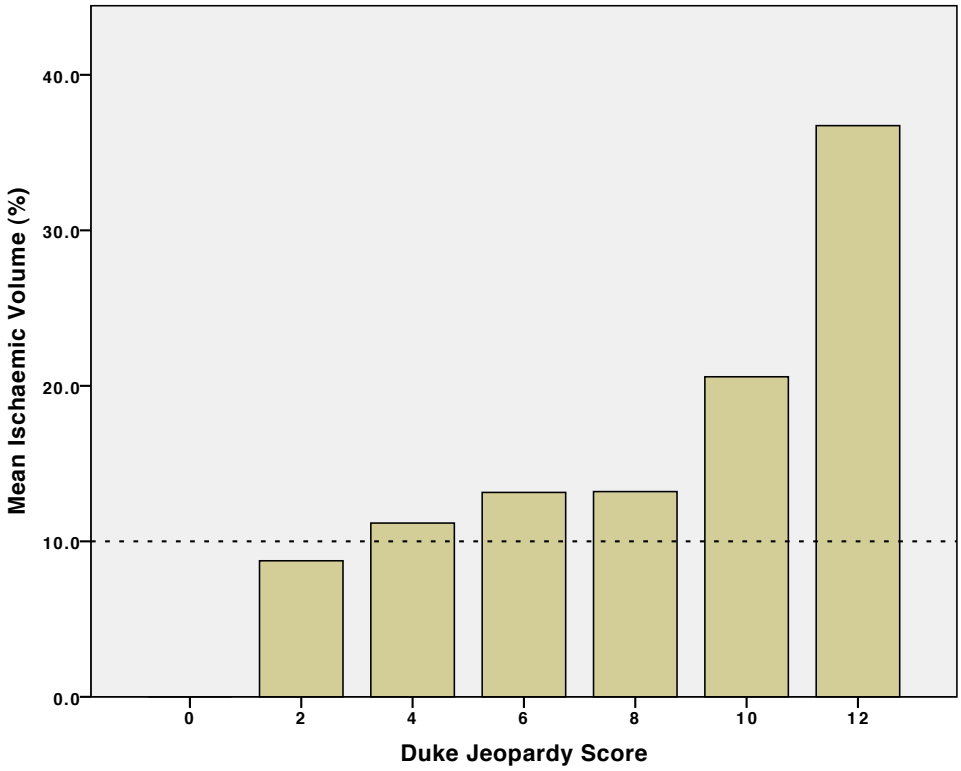

**Figure 6a)**

Bland-Altman of Interobserver variability for assesment of ischaemic volume

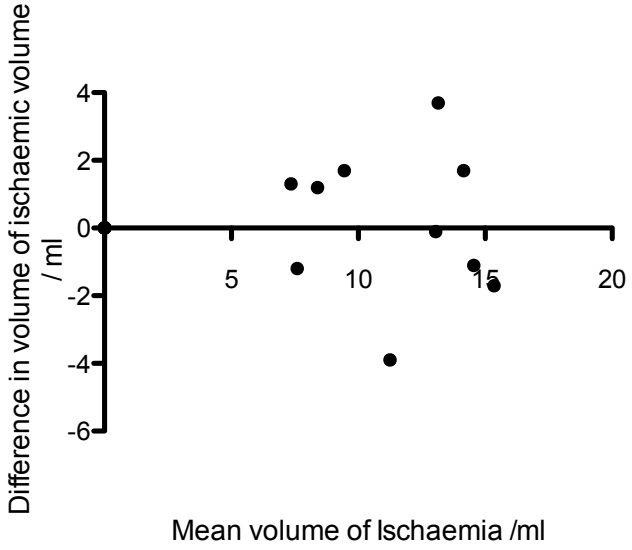


**Figure 6b)**

Bland-Altman of Intraobserver variability for assessment of ischaemic volume

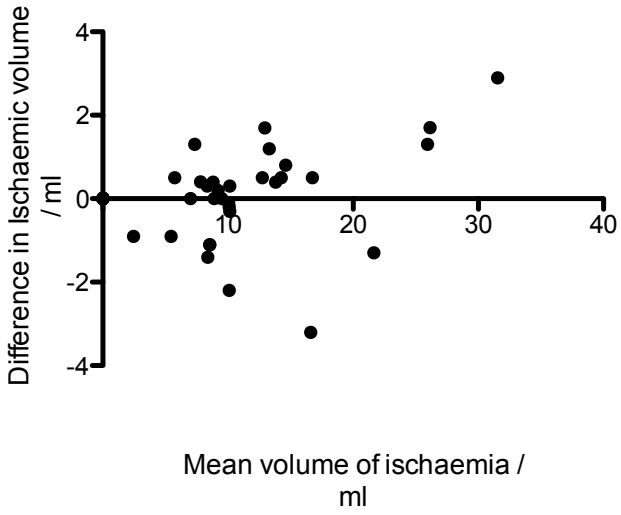

# Chapter 3

# Ischemic burden by three-dimensional myocardial perfusion CMR – comparison with myocardial perfusion scintigraphy

## 3.1 Abstract

*Background*

The extent and severity of ischemia on myocardial perfusion scintigraphy (MPS) is commonly used to risk-stratify patients with coronary artery disease (CAD). Estimation of ischemic burden by cardiovascular magnetic resonance (CMR) with conventional two-dimensional myocardial perfusion methods is limited by incomplete cardiac coverage. More recently developed three-dimensional (3D) myocardial perfusion CMR however provides whole heart coverage. The aim of this study was to compare ischemic burden on 3D myocardial perfusion CMR with $^{99m}$Tc-tetrofosmin MPS.

*Methods*

Forty-five patients who had undergone clinically indicated MPS underwent rest and adenosine stress 3D myocardial perfusion and late gadolinium enhancement CMR. Summed stress and rest scores were calculated for MPS and CMR using a 17-segment model and expressed as a percentage of the maximal possible score. Ischemic burden was defined as the difference between stress and rest scores.

*Results*

3D myocardial perfusion CMR and MPS agreed in 38 of the 45 patients for the detection of any inducible ischemia. The mean ischemic burden for MPS and CMR was similar (7.5+/-8.9% versus 6.8+/-9.5%, respectively, P=0.82) with a strong correlation between techniques (rs=0.70, P<0.001). In a subset of 33 patients who underwent clinically indicated invasive coronary angiography, sensitivities and specificities of the two techniques to detect angiographic CAD were similar (McNemar P=0.45).

*Conclusion*

3D myocardial perfusion CMR is an alternative to MPS for detecting the presence and rating the severity of ischemia with the added benefits of higher spatial resolution and no exposure to ionizing radiation.

## 3.2 Background

Myocardial perfusion cardiovascular magnetic resonance (CMR) has become an established method for the non-invasive diagnosis of coronary artery disease (CAD).[1,2] It is accurate and in recent studies was shown to be non-inferior to single photon emission computer tomography myocardial perfusion scintigraphy (MPS).[1,3] However, the cardiac coverage provided by conventional myocardial perfusion CMR methods is limited to three short axis sections that cover 16 of the 17 myocardial segments defined by guidelines but with variable gaps between the acquired sections.[4] While this may be sufficient for diagnostic purposes, the selective spatial coverage may prevent an accurate measurement of ischemic burden[5]. In clinical practice, ischemic burden is most commonly measured by MPS. It is an important prognostic factor in CAD[6,7] and in accordance with guidelines can help identify patients who will benefit most from revascularization compared with medical therapy.[8,9]

In a recent sub-analysis of the CE-MARC study, ischemic burden was compared between MPS and conventional two-dimensional CMR perfusion. Although there was good agreement for overall ischemic burden, discrepancies in the detection of ischemia versus scar were noted, thought to be related at least in part to the differences in cardiac coverage of perfusion CMR and perfusion MPS and also between perfusion and late gadolinium enhancement (LGE) CMR. [10]

Recently proposed three-dimensional (3D) myocardial perfusion CMR techniques overcome the problem of limited cardiac coverage and are also accurate in the detection of CAD.[5,11,12,13] Measurements of ischemic burden from 3D myocardial perfusion CMR have been shown to agree with invasive indices of myocardium at risk[12] and to reduce following PCI.[14] However, a direct comparison with MPS has not previously been

reported.

The main objective of this study was therefore to compare ischemic burden between MPS and 3D myocardial perfusion CMR. Diagnostic accuracy of the two methods against invasive coronary angiography was also assessed in a subset of patients.

## 3.3 Methods

*Patient population*

The study was approved by the local research ethics committee and all subjects gave written informed consent to participate. Forty-six patients routinely referred for MPS to the Royal Brompton Hospital, London, United Kingdom were consecutively recruited to undergo CMR within the following fourteen days. The MPS studies were reported as part of clinical routine and the report available to the referring physician to guide patient management. Exclusion criteria were contraindications to CMR or adenosine stress and the presence of atrial fibrillation. On the procedure day, a full medical history and examination were undertaken. Symptoms of chest pain were recorded in accordance with the Canadian Cardiovascular Society angina grading scale. A resting ECG was analyzed for the presence of Q waves or bundle branch block using defined Minnesota criteria[15].

*MPS qcquisition*

All patients underwent one-day stress-rest[16] ECG-gated $^{99m}$Tc-tetrofosmin MPS using a dual-headed gamma camera (Philips CardioMD) fitted with $^{153}$Gd transmission sources. Patients were asked to abstain from caffeine for 12 hours before the study and to have only a light breakfast. Adenosine was infused at 140µg/kg/min for 6 minutes combined with semi-supine exercise on a bicycle ergometer in 2 minute stages of 25W, 50W and 75W if tolerated. In patients with left bundle branch block or bifasicular block, adenosine was infused without exercise. Two hundred and fifty MBq $^{99m}$Tc-tetrofosmin were injected 2 min before the end of stress with imaging 45–60 min after injection. Three hours later, 750MBq $^{99m}$Tc-tetrofosmin were given at rest 5 minutes after 200µg

sublingual glyceryl trinitrate, with imaging 45–60 minutes later. The total effective radiation dose was 8mSv.

*MPS interpretation*

For the purpose of this study, all MPS studies were reported by an observer blinded to all clinical data and the previous clinical MPS report. The analysis undertaken for this study was not made available to the patient's clinician. Transverse tomograms of the left ventricle were reconstructed using iterative reconstruction on a Hermes workstation (Hermes Medical Systems, Stockholm). Transaxial slices were reoriented to obtain short-axis, horizontal long-axis, and vertical long-axis views of the left ventricle. Attenuation correction and resolution recovery were used. Unprocessed planar images were displayed in the cine format to assess quality and to assess patient motion and attenuation. Image artifact was scored on a four-point scale from 0 (none), 1 (mild), 2 (moderate) and 3 (severe). Image quality was scored on a similar scale using the reconstructed tomograms taking into account the severity of artifact score and overall clinical value as follows:

1) Q3: excellent quality images with no artifact

2) Q2: good quality images with total artifact score of 2 or less

3) Q1: adequate quality images with total artifact score of 3 or more

4) Q0: Inadequate quality images with artifact severe enough to affect diagnostic quality

The tomographic slices were divided into 17 segments[4] and mean segmental counts were graded semi-quantitatively by an experienced observer: 0 = normal uptake (≥70% of maximum activity), 1 = mild reduction (50-69%), 2 = moderate reduction (30-49%), 3 = severe reduction (10-29%) and 4 = absent uptake (0-9%). The summed stress score

(SSS) and summed rest score (SRS) were obtained by adding segmental scores and the summed difference score (SDS=SSS-SRS) expressed as a percentage of 68, the theoretical maximum score, was used as a measure of total ischemic burden.[17]

Each study was also classified as normal or showing reversible, fixed or mixed defects. A subjective confidence score of 3 (definite confidence), 2 (moderate confidence), 1 (mild confidence) to 0 (uncertain) was assigned to the classification.

*CMR acquisition*

All subjects were scanned in a supine position using a 3T MR scanner (Achieva, Philips Healthcare, Best, Netherlands) equipped with dual-source parallel RF transmission (multi-transmit) technology [18] and a 6-channel cardiac phased array receiver coil. Patients were asked to refrain from caffeine-containing substances for 12 hours before CMR. Subjects were monitored throughout the scan with a 4-lead vectorcardiogram, respiratory belt and blood pressure monitoring. For perfusion imaging, a 3D spoiled turbo gradient echo sequence was used (TR/TE/flip angle 1.8ms/0.7ms/15°, saturation prepulse delay 150ms, acquisition timed to end-systole, 75% partial Fourier sampling in the ky and kz direction and an elliptical k-space shutter, 10 fold k-t acquisition with 49 training profiles leading to a net acceleration of 7.0, total number of acquired profiles 106, which results in an acquisition time per heartbeat of 191 ms (106x1.8ms), *k-t* principal component analysis reconstruction[11,19], reconstruction of 12-16 contiguous slices of 5mm thickness, field of view 350 x 245mm$^2$, acquired voxel size 2.3x2.3x5mm$^3$, interpolated to 1.5x1.5x5mm$^3$).

Stress perfusion images were acquired during intravenous adenosine-induced hyperemia administered at 140µg/kg/min. An intravenous bolus of 0.075mmol/kg

gadobutrol (Gadovist, Bayer, Germany) was administered at a rate of 4.0ml/s followed by a 20ml saline flush (Spectris Solaris power injector, Pennsylvania, USA).

Stress perfusion CMR was followed by cine imaging covering the left ventricle in 10-12 short axis sections and a rest perfusion scan performed 15 minutes later using the same concentration and volume of contrast agent as for stress perfusion. Late gadolinium enhancement (LGE) images (0.15mmol/kg cumulative dose) were acquired in the same short axis geometry after a further 15 minutes using a conventional method.[20]

*CMR analysis*

An experienced observer blinded to all previous test results analyzed the CMR images using standard software (ViewForum, Philips Healthcare, Best, The Netherlands). The CMR data and analysis were not made available to the patient's clinician. Stress and rest perfusion scans were viewed simultaneously. Image artifacts were scored using a four-point scale from 0 (none), 1 (mild), 2 (moderate) and 3 (severe). The artifact was categorized as breathing related, subendocardial rim artifact or related to the reconstruction of undersampled data. Image quality was graded in the same way as MPS as 0 uninterpretable, 1 interpretable, 2 good or 3 excellent.

An inducible perfusion defect was considered to be present if there was reduced or delayed segmental delivery of contrast to the myocardium during stress persisting for more than 4 cardiac cycles, not present on the rest perfusion. This analysis strategy is consistent with recommended reporting guidance to exclude artefacts.[21] For calculation of ischemic burden, each segment was scored on a 5-point scale taking into account the transmurality of the stress perfusion defect: 0 normal (0-24%), 1 mild defect (25-49%), 2 moderate defect (50-74%), 3 severe reduction (75-100%) and 4 thinned with persistent absent contrast delivery. Viable myocardium was assessed using the LGE

images, scored in a similar way for transmurality of enhancement with 0 representing no enhancement, 1 mild enhancement (1-24%), 2 moderate enhancement (25-49%), 3 severe enhancement (50-74%) and 4 transmural enhancement (≥75%).
As for MPS, a confidence score of 3 (definite confidence), 2 (moderate confidence), 1 (mild confidence) to 0 (uncertain) was subjectively assigned to the classification.

In accordance with MPS analysis, the summed stress score (SSS) and summed rest score taken from the late gadolinium enhancement images (SRS) were obtained by adding segmental scores and the summed difference score (SDS=SSS-SRS) was expressed as a percentage of 68, the theoretical maximum score, was used as a measure of total ischemic burden.

*Whole heart versus three slice comparison*

We aimed to simulate as much a possible a comparison of 3D whole heart with 2D multislice myocardial perfusion CMR. Although no 2D data were acquired in this study, analysis of three slices of the whole heart data sets was considered a reasonable approximation to 2D acquisition for the purpose of quantification of ischemic burden. Several limitations of this approach relating to cardiac phase, spatial and temporal resolution were acknowledged and will be further discussed. For this purpose, all data sets were reanalyzed after 4 weeks by a reviewer blinded to all previous analyses and clinical data. In this analysis, only slices 3, 7, and 11, representing apical, mid-myocardial, and basal sections, were reviewed. All scoring was repeated using a 16 segment model that excluded the true apex.

*Reproducibility*

Analysis of MPS and CMR was repeated by the same reader at a remote time in a subset of sixteen patients.

*Coronary angiography*

Treating physicians decided the clinical management of patients including the referral for invasive angiography based on the clinical MPS report and all other clinical information. Data from this study were not released to treating physicians. Clinically indicated coronary angiography performed within 8 weeks of MPS were reviewed for this study. X-ray angiograms were reported by an experienced cardiologist blinded to the other studies. Significant CAD was defined as ≥70% stenosis of a first-order coronary artery measuring ≥2mm in diameter or LMS stenosis ≥50%, by quantitative coronary angiography (QCA) Medcon Ltd. Tel Aviv, Israel.

*Statistical analysis*

Data were analyzed using IBM SPSS v19 (SPSS, Chicago, IL, USA). Differences in mean ischemic burden used Bland Altman analysis and Wilcoxon's test. Comparisons of ischemic burden used Spearman's correlation. The comparison of ischemia burden compared of CMR perfusion with MPS in 45 patients will deliver a power of at least 80% at a 95% significance level to determine agreement between the tests. The intraobserver variability of perfusion analysis was calculated using the kappa coefficient. McNemar's test was used to compare the accuracy of the noninvasive test against the standard of coronary angiography. For all analyses $P<0.05$ was considered significant.

## 3.4 Results

*Patients*

Of the 46 patients recruited, one was excluded because of a technical fault during the CMR study, in which contrast was injected too early preventing acqusition of the first pass perfusion under hyperaemia. Forty five patients (31 men, mean age 59) thus formed the population for analysis. The indication for referral was diagnosis of CAD in 26 patients (58%) without a prior history. In this population the pre-test likelihood of underlying CAD was 37.8% (95% CI 31.8-43.9%). Nineteen patients had a previous history of CAD with 15 patients whom had previous documented myocardial infarction (Table 1). 39 patients experienced symptoms during CMR stress perfusion compared with 35 patients during MPS. There was no-significant difference (P=0.27).

*Myocardial Perfusion Scintigraphy*

Hemodynamic data are shown in table 2. All studies were considered interpretable with a median image quality score of 3 and a median confidence score of 2. The main artifacts reported were motion (6/45) and attenuation (6/45). Intraobserver variability showed agreement in 15/16 cases (κ 0.88) for the detection of ischemia.

*CMR imaging*

The mean time from MPS to CMR was 9 days (range 3-14 days). Mean scan time was 47 (SD 4) minutes. Hemodynamic data are shown in table 2. Compared with MPS there were significant differences in stress blood pressure and heart rate, reflecting the differing stress regimes. All 45 CMR studies were of interpretable quality. The median

image quality score was 3 and the median confidence score was 3. The main artifacts seen were subendocardial dark rim artifacts in 7 patients (16%) and breathing artifact in 4 patients (9%). There was 100% intraobserver agreement for the presence of ischemia (κ 1).

*Comparison of Ischemic Burden by MPS and CMR*

MPS and CMR agreed for the presence or absence of inducible ischemia in 38/45 patients (84%) (Figures 1 and 2). The mean ischemic burden by MPS in all 45 patients was 7.5% (SD 8.9, range 0-29.4)% and by CMR 6.8% (SD 9.5, range 0-33.8) with good correlation and no significant differences between methods (rs=0.70, P = 0.82). In the 38 patients in whom the tests agreed, the correlation for ischemic burden was stronger (rs=0.96, P < 0.0001) (Figure 3). The mean bias for ischemic burden between the two methods (CMR minus MPS) was
-0.62% (95% limit of agreement -14.3 to 13.1%) (Figure 4).

Twelve patients had an ischemic burden >10% on MPS and of these CMR ischemic burden was >10% in 11 patients. Conversely, 2 patients had CMR ischemic burden >10% but <10% by MPS, although the differences were small (10.3% and 10.3% by CMR vs 8.8% and 7.5% by MPS).

When only three short axis slices were used for analysis, the mean ischemic burden was lower at 5.7% (SD 8.2)%. There was no significant difference in the ischemic burden between MPS and 3 slice perfusion (P=0.12). However, there was a significant difference in ischemic burden between whole heart CMR and 3 slice CMR perfusion analysis

(P=0.03). There was good correlation between three-slice analysis and MPS ischemic burden (rs=0.72) and excellent correlation with whole heart CMR analysis (rs = 0.97).

Scar Burden

CMR and MPS agreed for the presence or absence of myocardial scar in 38 of 45 patients (84%). Scar was detected by LGE-CMR in 14 of 45 patients (31%) and in 11 of these also by MPS. Four patients had scar reported on MPS that was not present on LGE CMR. Taking CMR as the reference, the sensitivity of MPS for scar was 79% (95% CI 49 to 94%) and specificity 87% (95% CI 69 to 96%). The mean scar burden was higher with MPS than CMR (4.9% SD 10% versus 3% SD 6.8%) but this was not statistically significant (P = 0.06). In all 45 patients, the correlation between the two tests for scar burden was good (rs = 0.73) and in the 38 cases in which CMR and SPECT agreed, there was stronger agreement (rs=0.99).

*Diagnostic Accuracy Against Coronary Angiography*

Thirty-three (33) of the 45 patients underwent coronary angiography for clinical reasons, of whom 17 were found to have significant coronary disease (disease prevalence 52%). The overall sensitivity, specificity and diagnostic accuracy of MPS were 94% (95% CI 71 to 100%), 63% (95% CI 39 to 87%) and 79%. The positive and negative predictive values were 72.7% and 90.9% respectively. The sensitivity, specificity and diagnostic accuracy of CMR was 94% (95% CI 71 to 100%), 81% (95% CI 54 to 95%) and 88% (Table 3). The positive and negative predictive values were 84.2% and 92.9% respectively. Diagnostic performance of both tests depended on image quality and confidence scores (Table 4). The overall accuracy of the two techniques did not differ significantly (McNemar P = 0.45).

## 3.5 Discussion

3D myocardial perfusion CMR has become feasible because of increased speed of data acquisition.[11] Its value for the calculation of ischemic burden was first suggested in a phantom study, which showed that 3D imaging was more reliable than the conventional 2D techniques.[5] Subsequent studies demonstrated the feasibility of measuring ischemic burden, a reduction in ischemic burden after coronary intervention[14] and a strong correlation with the invasively derived Duke jeopardy score.[12] The current study has now shown that ischemic burden by 3D myocardial perfusion CMR agrees closely with the clinical reference standard of MPS and that both methods have similar accuracy for the detection of angiographically significant CAD.

The presence of myocardial ischemia is relevant prognostically and an ischemic burden over 10% of total myocardium is a threshold above which revascularization leads to better outcomes than with medical therapy alone.[17,22] Most data on ischemic burden have been derived from MPS,[6,7,17,22], justifying the comparison of 3D myocardial perfusion CMR with MPS in this study. In addition to the close overall agreement between the techniques we found that in 11 of 12 patients with an ischemic burden >10% by MPS the ischemic burden by CMR was also >10%. Conversely, CMR only slightly overestimated ischemic burden in two patients with an ischemic burden <10% by MPS. This suggests that the 10% MPS threshold for improved outcome with intervention might also be used for CMR but prospective studies will be required to confirm this.

*Scar Burden*

LGE-CMR is an established technique for the detection of myocardial scarring and it is sensitive to even small amounts of subendocardial scar.[20, 23] MPS is widely used for the detection infarction and it is well validated for its quantification although it is less sensitive than CMR for small areas of infarction because of its lower resolution.[24] In this study there was overall good correlation between CMR and MPS for the detection and quantification of scar, but numbers were too small to assess the relationship between infarct size and agreement.

*Detection of CAD*

In the subgroup of patients that underwent coronary angiography, the sensitivity of 3D perfusion CMR was similar to previous studies. MPS had a similar high sensitivity but the specificity was non-significantly lower because of six false positive cases. A breakdown into image quality and confidence scores showed that diagnostic performance was greater with better quality images for both tests.

*Whole-heart versus three slice analysis*

Because of its selective spatial coverage, estimates of ischemic burden from 2D CMR may be less accurate than 3D. We therefore compared analysis of three slices in slice positions that are typical for 2D acquisitions, with analysis of the whole heat data sets. Because no separate 2D data were acquired in this study, we used a simulation and analysed three of the equally distributed slices of the whole heart stack. We acknowledge that this approach is distinctly different to 2D acquisition. For example, as compared to a previously published 2D acquisition using *k-t* acceleration[25], the selected three slices of the 3D stack have lower in-plane spatial resolution (2.3mm vs 1.4mm), a

longer temporal window (193ms, vs 120 ms), but have thinner slices (5mm vs 10mm), require faster acceleration (10x vs 5x), and acquire all of the data in an end systolic heart phase instead of at 3 different phases. This may impact detection of subendocardial ischemia in slices acquired during diastolic time points or during rapid motion. Our analysis can therefore only give early indications of comparison between 2D and 3D perfusion CMR and direct comparisons are needed in the future.

Although there was a difference in ischemic burden between the 3 slice and whole heart analysis, there was no difference in assigning patients to either medical therapy when using a threshold of 10% ischemic burden. There was a trend towards a smaller ischemic burden from the three-slice CMR analysis (6.8% vs 5.7%, P=0.03). The lower ischemic burden is likely to be a consequence of reduced number of slices influencing reporting of ischemia, causing an underestimation of ischemia. Within its limitations, the comparison of whole heart versus three slice analysis raises questions about the relative benefits spatial resolution, temporal resolution, SNR and cardiac phase that need to be explored in future studies. Further differences between the techniques are discussed in more detail elsewhere.[26]

*Limitations*

This study investigated a population with a relatively high prevalence of scar but we were primarily interested in the assessment of ischemic burden independently of scar. The presence of scar may complicate the detection of superimposed inducible ischemia and it is possible that the assessment of ischemia would be more accurate in populations without scar.

There were inevitable differences in the acquisition and measurement of ischemic volume between MPS and CMR. We equated the transmurality of a CMR perfusion defect to the depth of the defect of tracer uptake on MPS. These two phenomena, while related, will not always be equivalent, potentially leading to differences in the estimation of ischemic burden. The method of establishing ischemic burden from the dynamic image series in first pass CMR is not identical to that used in MPS which is based upon multiple passes producing an average of distribution of tracer uptake.

The stress protocols differed slightly, leading to different haemodynamic parameters as reflected by the different rate pressure products. Although the use of rate pressure products has validation in stress imaging, its validity in vasodilator stress is questionable. Vasodilator stress using adenosine was used for both techniques because dynamic exercise was not possible during CMR. When adenosine is used for MPS it is desirable to combine it with submaximal dynamic exercise in order to reduce side effects and extracardiac uptake of tracer. The accuracy of adenosine MPS with and without additional exercise is similar and the difference between stress techniques would not be expected to have affected the findings.

Our results can only give an indication of the relative performance for conventional 3 slice 2D CMR perfusion imaging. Only an adequately powered head-to-head comparison of the two acquisition (2D vs 3D) methods can give conclusive evidence of their accuracy in determination of ischemic burden. However, as demonstrated in this study and observed in phantoms studies[5], 3D whole heart acquisition appears to provide a more accurate estimation of ischemic burden than using 3 slice acquisition.

Our analysis method used the clinical standard of visual measurement of ischemic burden. Quantitative analysis methods have important potential advantages such as higher objectivity and the detection of balanced ischemia. , but were not applied to 3D CMR perfusion data sets.

**Conclusions**

Estimates of ischemic burden from 3D myocardial perfusion CMR agreed closely with MPS. The technique was also accurate for the detection of angiographically defined coronary obstruction. Combined with CMR assessment of cardiac function and viability the technique holds promise as a complete non-invasive and radiation-free diagnostic and risk stratification tool for patients with known or suspected CAD.

Clinical Perspective

Myocardial perfusion cardiovascular magnetic resonance (CMR) has become an established method for the non-invasive diagnosis of coronary artery disease (CAD). While this technique may be useful for diagnostic purposes, the selective spatial coverage may prevent an accurate measurement of ischemic burden. In clinical practice, ischemic burden is most commonly measured by myocardial perfusion scintigraphy (MPS). It is an important prognostic factor in CAD and in accordance with guidelines can help identify patients who will benefit most from revascularization compared with medical therapy.

Three-dimensional (3D) myocardial perfusion CMR techniques overcome the problem of

limited cardiac coverage and are also accurate in the detection of CAD. Measurements of ischemic burden from 3D myocardial perfusion CMR have been shown to agree with invasive indices of myocardium at risk and to reduce following PCI. However, a direct comparison with MPS has not previously been reported.

This study compared ischemic burden between MPS and 3D myocardial perfusion CMR in 45 patients. The mean ischaemic burden was similar and there was a strong correlation between techniques. In a subset of these patients, the diagnostic accuracy of the two methods against invasive coronary angiography was also assessed and noted to be similar. 3D myocardial perfusion CMR may be considered an alternative to MPS for detecting the presence and rating the severity of ischemia with the added benefits of higher spatial resolution and no exposure to ionizing radiation.

In accordance with current guidelines the recently proposed 3D myocardial perfusion CMR may help identify patients who will benefit most from revascularization compared with medical therapy.

Due to the limited numbers it remains as to whether there is any difference in diagnostic performance comparing conventional 2D multi-slice imaging against 3D whole heart coverage.

Although intuitive it is unanswered as to if the same thresholds of 10% ischemic burden in determining optimal management in MPS hold for CMR. Multicentre studies powered to determine the use of 3D myocardial perfusion CMR as a non-invasive strategy for the diagnosis and risk stratification of patients with suspected CAD appear warranted.

## 3.6 References

1. Greenwood JP, Maredia N, Younger JF, Brown JM, Nixon J, Everett CC, Bijsterveld P, Ridgway JP, Radjenovic A, Dickinson CJ, Ball SG, Plein S. Cardiovascular magnetic resonance and single-photon emission computed tomography for diagnosis of coronary heart disease (CE-MARC): a prospective trial. Lancet 2012; 379:453 – 460.

2. Nandalur KR, Dwamena BA, Choudhri AF, Nandalur MR, Carlos RC. Diagnostic performance of stress cardiac magnetic resonance imaging in the detection of coronary artery disease: a meta-analysis. J Am Coll Cardiol 2007;50:1343-1353

3. Schwitter J, Wacker CM, van Rossum AC, Lombardi M, Al-Saadi N, Ahlstrom H, Dill T, Larsson HB, Flamm SD, Marquardt M, Johansson L. MR-IMPACT: comparison of perfusion-cardiac magnetic resonance with single-photon emission computed tomography for the detection of coronary artery disease in a multicentre, multivendor, randomized trial. Eur Heart J. 2008; 29:480-9

4. Cerqueira MD, Weissman NJ, Dilsizian V, Jacobs AK, Kaul S, Laskey WK, Pennell DJ, Rumberger JA, Ryan T, Verani MS. Standardized myocardial segmentation and nomenclature for tomographic imaging of the heart: a statement for healthcare professionals from the Cardiac Imaging Committee of the Council on Clinical Cardiology of the American Heart Association. Circulation 2002;105:539-542

5. Shin T, Hu HH, Pohost GM, Nayak KS. Three dimensional first-pass myocardial perfusion imaging at 3T: feasibility study. J Cardiovasc Magn Reson. 2008; 10:57

6. Brown KA, Boucher CA, Okada RD, Guiney TE, Newell JB, Strauss HW, Pohost GM. Prognostic value of exercise thallium-201 imaging in patients presenting for evaluation of chest pain. J Am Coll Cardiol 1983;1:994–1001.

7. Hachamovitch R, Berman DS, Shaw LJ, Kiat H, Cohen I, Cabico JA, Friedman J, Diamond GA. Incremental prognostic value of myocardial perfusion single photon emission computed tomography for the prediction of cardiac death. Circulation 1998;97:535–543

8. Task Force on Myocardial Revascularization of the European Society of Cardiology (ESC) and the European Association for Cardio-Thoracic Surgery (EACTS); European Association for Percutaneous Cardiovascular Interventions (EAPCI), Wijns W, Kolh P, Danchin N, Di Mario C, Falk V, Folliguet T, Garg S, Huber K, James S, Knuuti J, Lopez-Sendon J, Marco J, Menicanti L, Ostojic M, Piepoli MF, Pirlet C, Pomar JL, Reifart N, Ribichini FL, Schalij MJ, Sergeant P, Serruys PW, Silber S, Sousa Uva M, Taggart D. Guidelines on myocardial revascularization. Eur Heart J. 2010 31:2501-55.

9. Patel MR, Dehmer GJ, Hirshfeld JW, Smith PK, Spertus JA. ACCF/SCAI/STS/AATS/AHA/ASNC 2009 appropriateness criteria for coronary revascularization: a report by the American College of Cardiology Foundation Appropriateness Criteria Task Force, Society for Cardiovascular Angiography and Interventions, Society of Thoracic Surgeons, American Association for Thoracic Surgery, American Heart Association, and the American Society of Nuclear Cardiology J Am Coll Cardiol 2009;53:530-553

10. Plein S, Herzog B, Maredia N, Kidambi A, Motwani M, Uddin A, Ripley J, Brown JM, Nixon J, , Everett CC, Dickinson CJ, Greenwood JP. The ischaemic and scar burden

measured by cardiac magnetic resonance imaging in patients with ischaemic heart disease from the CE-MARC study. J Cardiovasc Magn Reson 2013; 15(suppl1):O105

11. Vitanis V, Manka R, Giese D, Pedersen H, Plein S, Boesiger P, Kozerke S. High resolution three-dimensional cardiac perfusion imaging using compartment based k-t principal component analysis. Magn Reson Med. 2011 2:575-87

12. Jogiya R, Kozerke S, Morton G, De Silva K, Redwood S, Perera D, Nagel E, Plein S . Validation of dynamic 3-dimensional whole heart magnetic resonance myocardial perfusion imaging against fractional flow reserve for the detection of significant coronary artery disease. J Am Coll Cardiol. 2012;60:756-65

13. Manka R, Paetsch I, Kozerke S, Moccetti M, Hoffmann R, Schroeder J, Reith S, Schnackenburg B, Gaemperli O, Wissmann L, Wyss CA, Kaufmann PA, Corti R, Boesiger P, Marx N, Lüscher TF, Jahnke C. Whole-heart dynamic three-dimensional magnetic resonance perfusion imaging for the detection of coronary artery disease defined by fractional flow reserve: determination of volumetric myocardial ischaemic burden and coronary lesion location. Eur Heart J. 2012; 16:2016-24

14. Manka R, Jahnke C, Kozerke S, Vitanis V, Crelier G, Gebker R, Schnackenburg B, Boesiger P, Fleck E, Paetsch I. Dynamic 3-dimensional stress cardiac magnetic resonance perfusion imaging: detection of coronary artery disease and volumetry of myocardial hypoenhancement before and after coronary stenting. J Am Coll Cardiol. 2011 57:437-44

15. Rose GA, for the World Health Organization. Cardiovascular Survey Methods. 2nd edition. Geneva: World Health Organization, 1982.

16. Anagnostopoulos C, Harbinson M, Kelion A, Kundley K, Loong CY, Notghi A, Reyes E, Tindale W, Underwood SR. Procedure guidelines for radionuclide myocardial perfusion imaging. Heart. 2004 90 Suppl 1:i1-10.

17. Hachamovitch R, Hayes SW, Friedman JD, Berman DS. Comparison of the short-term survival benefit associated with revascularization compared with medical therapy in patients with no prior coronary artery disease undergoing stress myocardial perfusion single photon emission computed tomography. Circulation 2003;107:2900–2907.
18. Willinek WA, Gieseke J, Kukuk GM, Nelles M, König R, Morakkabati-Spitz N, Träber F, Thomas D, Kuhl CK, Schild HH. Dual-source parallel radiofrequency excitation body MR imaging compared with standard MR imaging at 3.0 T: initial clinical experience. Radiology. 2010 256:966-75
19. Pedersen H, Kozerke S, Ringgaard S, Nehrke K, Kim WY. k-t PCA: temporally constrained k-t BLAST reconstruction using principal component analysis. Magn Reson Med. 2009 62:706-16
20. Kim RJ, Wu E, Rafael A, Chen EL, Parker MA, Simonetti O, Klocke FJ, Bonow RO, Judd RM. The Use of Contrast-Enhanced Magnetic Resonance Imaging to Identify Reversible Myocardial Dysfunction N Engl J Med 2000; 343:1445-145
21. Hundley WG, Bluemke D, Bogaert JG, Friedrich MG, Higgins CB, Lawson MA, McConnell MV, Raman SV, van Rossum AC, Flamm S, Kramer CM, Nagel E, Neubauer S. Society for Cardiovascular Magnetic Resonance guidelines for reporting cardiovascular magnetic resonance examinations. J Cardiovasc Magn Reson. 2009; 11:5
22. Hachamovitch R, Rozanski A, Shaw LJ, Stone GW, Thomson LE, Friedman JD, Hayes SW, Cohen I, Germano G, Berman DS. Impact of ischaemia and scar on the therapeutic benefit derived from myocardial revascularization vs. medical therapy among patients undergoing stress-rest myocardial perfusion scintigraphy. Eur Heart J. 2011 32:1012-24.
23. Wu E, Judd RM, Vargas JD, Klocke FJ, Bonow RO, Kim RJ. Visualisation of presence, location, and transmural extent of healed Q-wave and non-Q-wave myocardial infarction. Lancet. 2001 357:21-8.

24. Wagner A, Mahrholdt H, Holly TA, Elliott MD, Regenfus M, Parker M, Klocke FJ, Bonow RO, Kim RJ, Judd RM. Contrast-enhanced MRI and routine single photon emission computed tomography (SPECT) perfusion imaging for detection of subendocardial myocardial infarcts: an imaging study. Lancet. 2003 361;374-9

25. Plein S, Kozerke S, Suerder D, Luescher TF, Greenwood JP, Boesiger P, Schwitter J. High spatial resolution myocardial perfusion cardiac magnetic resonance for the detection of coronary artery disease. Eur Heart J. 2008 Sep;29(17):2148-55

26. Motwani M, Jogiya R, Kozerke S, Greenwood JP, Plein S. Advanced cardiovascular magnetic resonance myocardial perfusion imaging: high-spatial resolution versus 3-dimensional whole-heart coverage. Circ Cardiovasc Imaging. 2013 Mar 1;6(2):339-48

## 3.7 Tables

**Table 1: Patient Demographics**

| Parameter | Data (%) |
|---|---|
| Number | 45 |
| Male | 32(71.1) |
| Age, years | 58.9 ± 7.7 |
| Range | 44 to 76 |
| BMI, $kg/m^2$ | 25.8 ± 2.8 |
| Previous myocardial infarction | 15 (33.3) |
| Previous coronary intervention | 16 (35.6) |
| Normal LV function (EF>60%) | 41 (91.1) |
| Canadian Cardiovascular Society Angina Grading Scale | |
| No pain or Atypical Symptoms | 27 (60.0) |
| Class 1 | 9 (20.0) |
| Class 2 | 6 (13.3) |
| Class 3 | 3 (6.7) |
| Class 4 | 0 (0) |
| Baseline Electrocardiogram | |
| Q wave | 7 (15.6) |
| Left Bundle Branch Block | 5 (11.1) |
| Right Bundle Branch Block | 1 (2.2) |
| Cardiovascular Risk Factors | |
| Diabetes | 16 (35.6) |
| Dyslipidaemia | 41 (91.1) |
| Current Smoker | 12 (26.7) |
| Hypertension | 38 (84.4) |
| Family History | 22 (48.9) |
| Medications | |
| Aspirin | 41 (91.1) |
| Clopidogrel | 7 (15.6) |
| Beta Blocker | 27 (60.0) |
| Calcium Channel blocker | 5 (11.1) |
| Statin | 41 (91.1) |
| Angiotensin enzyme inhibitor or angiotensin receptor blocker | 33 (73.3) |
| Nitrate | 12 (17.8) |

**Table 2: Hemodynamic Data**

| | Rest | | | Stress | | |
|---|---|---|---|---|---|---|
| | MPS | CMR | P | MPS | CMR | P |
| HR | 72.9 ±11.6 | 72.0 ±11.6 | 0.42 | 102.2 ±17.7 | 89.5 ±13.6 | <0.0001 |
| SBP | 139.8 ±18.7 | 135.2 ±12.6 | 0.08 | 153.3 ±23.3 | 130.5 ±22.6 | 0.008 |
| DBP | 81.6 ±13.4 | 80.0 ±19.6 | 0.4 | 88.1 ±21.2 | 80.1 ±12.7 | <0.0001 |
| RPP | 10250 ±2408 | 9825±2769 | 0.19 | 15,810 ±4365 | 11,841 ±3568 | <0.0001 |

Table 3: **Sensitivity and specificity of MPS and CMR vs. coronary angiography**

| | Angiography – Significant Coronary Disease | | |
|---|---|---|---|
| | Absent | Present | Total |
| CMR + | 3 | 16 | 19 |
| CMR - | 13 | 1 | 14 |
| Total | 16 | 17 | 33 |

| | Angiography – Significant Coronary Disease | | |
|---|---|---|---|
| | Absent | Present | Total |
| MPS + | 6 | 16 | 22 |
| MPS - | 10 | 1 | 11 |
| Total | 16 | 17 | 33 |

**Table 4: Sensitivity and specificity of MPS and CMR vs. coronary angiography stratified by image quality and confidence scores**

| MPS | N | Sensitivity | Specificity | Accuracy |
|---|---|---|---|---|
| Confidence 3 | 10 | 100 | 80 | 90 |
| Confidence ≥2 | 27 | 94 | 82 | 89 |
| Confidence ≥1 | 33 | 94 | 63 | 79 |
| | | | | |
| Quality 3 | 19 | 100 | 83 | 94 |
| Quality ≥ 2 | 31 | 94 | 75 | 85 |
| Quality ≥ 1 | 33 | 94 | 63 | 79 |

| CMR | N | Sensitivity | Specificity | Accuracy |
|---|---|---|---|---|
| Confidence 3 | 18 | 100 | 100 | 100 |
| Confidence ≥2 | 28 | 100 | 80 | 89 |
| Confidence ≥1 | 33 | 94 | 81 | 88 |
| | | | | |
| Quality 3 | 19 | 100 | 90 | 94 |
| Quality ≥ 2 | 26 | 100 | 83 | 92 |
| Quality ≥ 1 | 33 | 94 | 81 | 88 |

## 3.8 Figure Legends

**Figure 1**

Images from a 47 year old male with atypical chest pain and multiple risk factors for CAD are shown. The patient had no known prior myocardial infarction.

(a) and (b) CMR perfusion scans during adenosine stress and late gadolinium enhancement CMR. A perfusion defect is seen in the anterior and anteroseptal segments from the base to the apex extending into the inferior wall. Late gadolinium enhancement shows subendocardial scar in the septal segments from the mid ventricle to the apex. The ischemic burden by CMR was 20.5 %.

(c) and (d) Rest and stress MPS. Stress MPS shows extensive and profound inducible ischemia involving most of the LAD territory and further inferior changes corresponding with the stress CMR images. Rest MPS shows reduced uptake in the LAD territory towards and including the apex that is less marked than on the stress images. The study was reported as showing partial infarction in the LAD territory with a large area of peri-infarct ischemia. The ischemic burden by MPS was 19.8 %.

Invasive X-ray angiography showed an occlusion of the proximal left anterior descending coronary artery with collateral supply from the right coronary artery, which had a mid course stenosis.

**Figure 2**

Images from a 58 year old male with a previous myocardial infarction and subsequent revascularisation with ongoing chest pain are shown.

(a) and (b) CMR perfusion scan during adenosine stress. A subendocardial defect is seen in the basal inferolateral wall extending to the mid inferolateral wall. Late gadolinium enhancement CMR shows a small area of subendocardial scar in the same region but the perfusion deficit extends beyond the equivalent imaging plane. The ischemic burden by CMR was 8.8 %.

C and D) Stress and rest MPS imaging shows corresponding limited partial-thickness scarring in the basal inferolateral region with mild superimposed and peri-infarct ischemia extending up to the mid inferolateral region. The coronary angiogram showed a significant stenosis in a large first obtuse mariginal branch. The ischemic burden by MPS was 7.4 %.

**Figure 3**

Correlation between MPS and CMR for ischemic burden in the patients where there was agreement between the techniques (38/45): The dotted line indicates 10% ischemic burden.

**Figure 4**

Bland-Altman analysis of ischemic burden between the techniques in the cohort of patients where there was agreement with the techniques (38/45). Blandt-Altman analysis showed a mean bias for ischemic burden between the two methods of 0.62% (95% CI -7.98% to 9.21%)

**Figure 1 Case example**

1a) 3D CMR stress perfusion

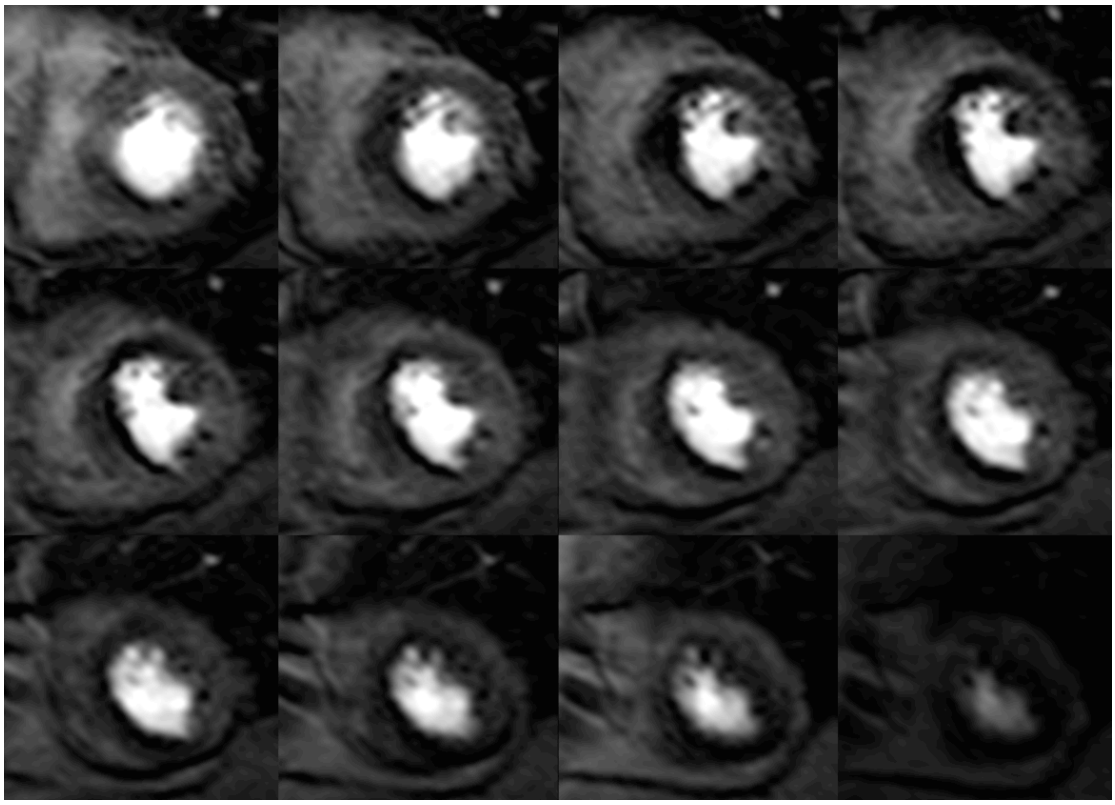

B) Late gadolinium enhanced CMR

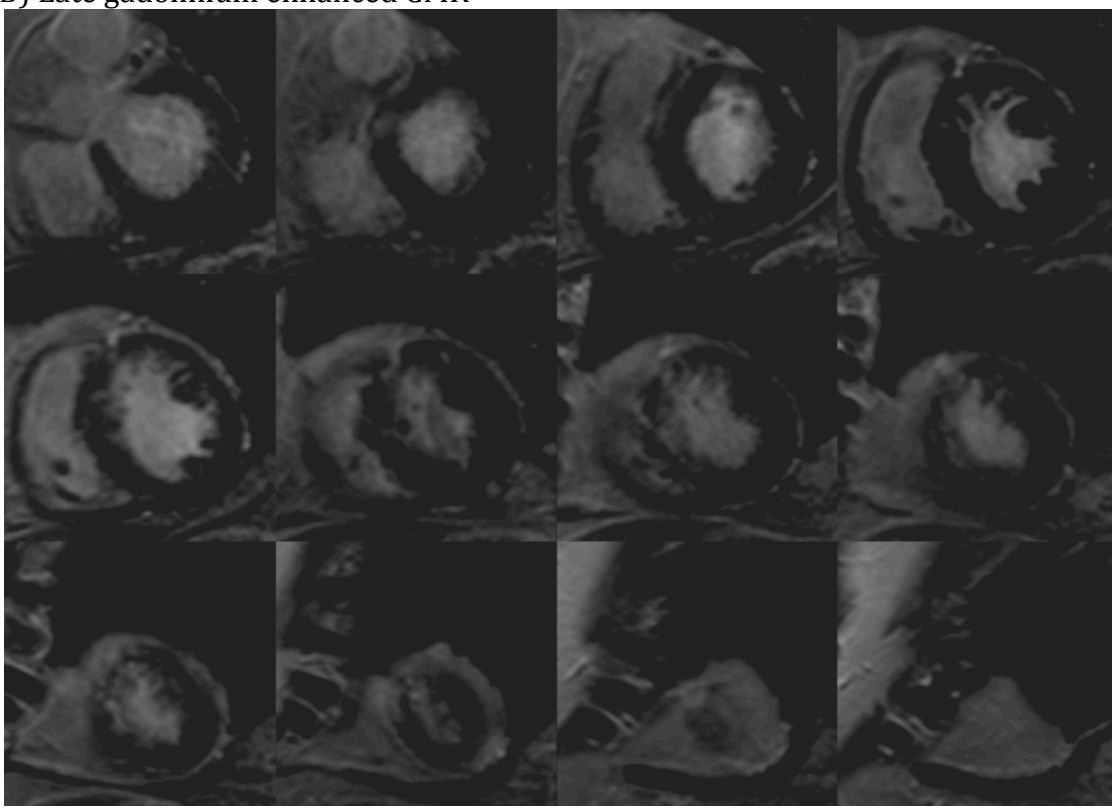

1c) MPS stress imaging

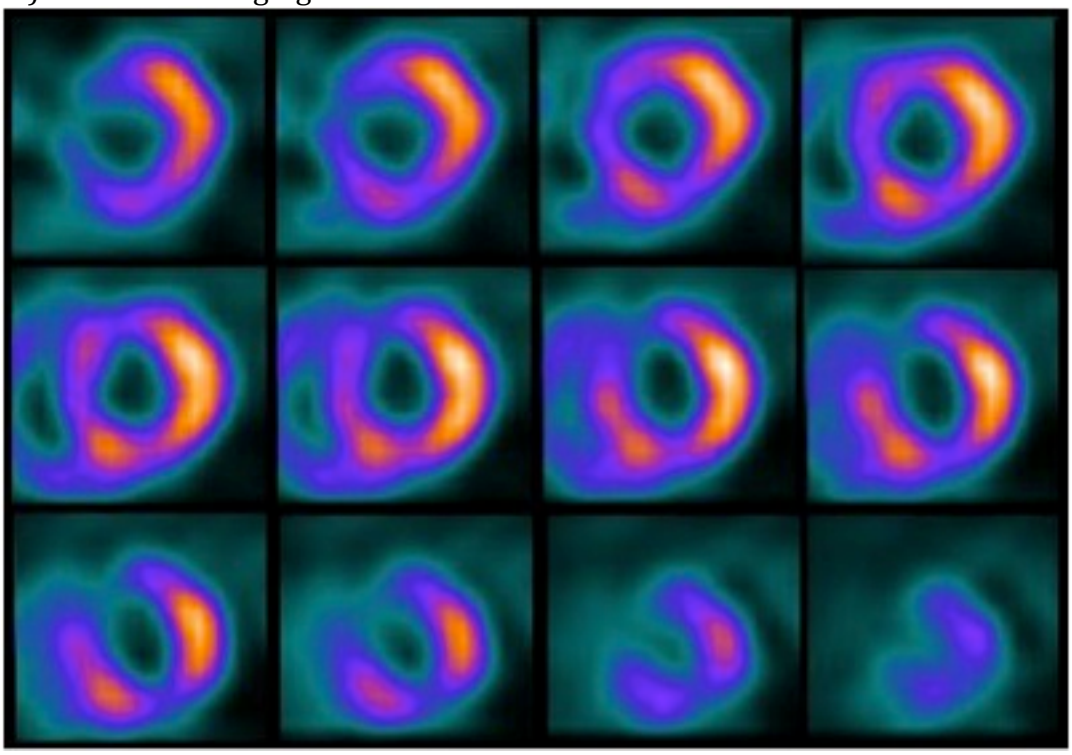

1d) MPS rest imaging

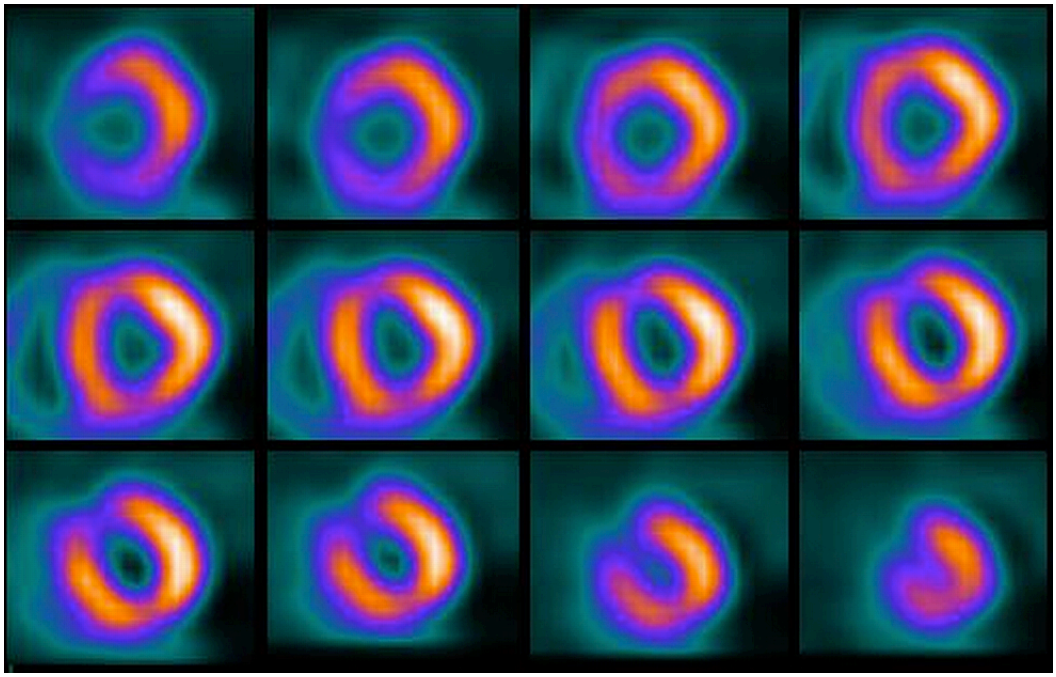

**Figure 2 Case Example**

a) 3D CMR stress perfusion

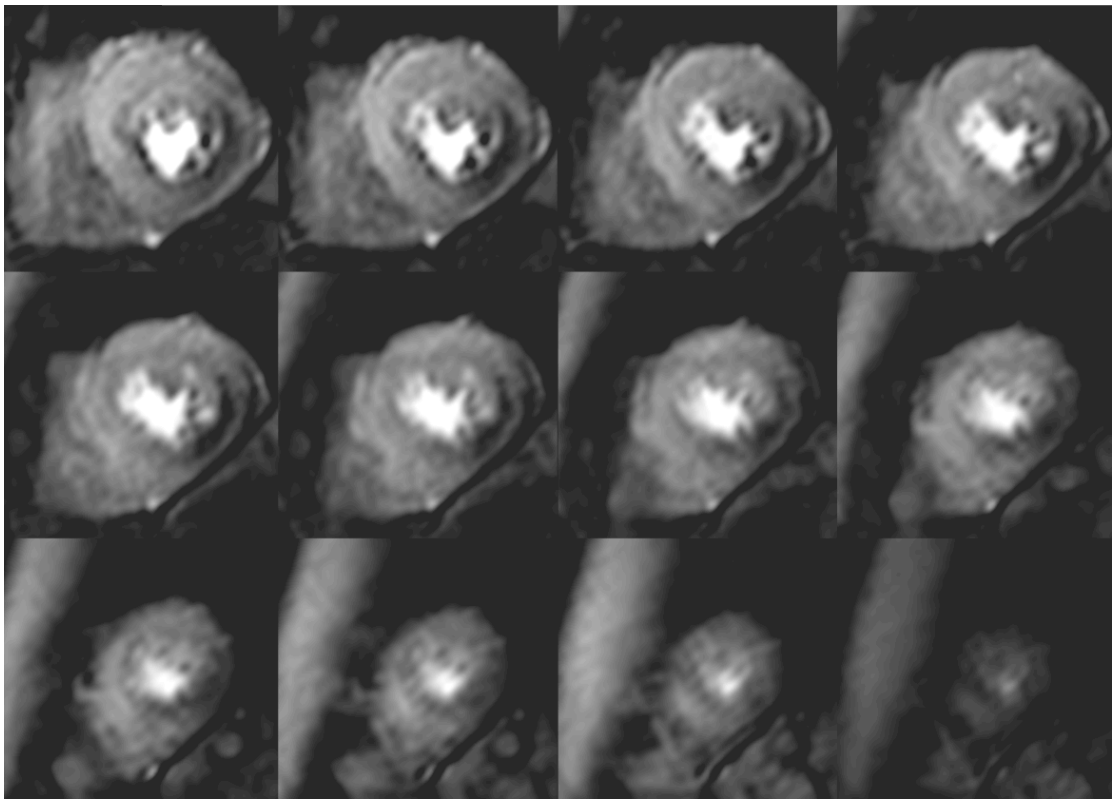

B) Late gadolinium enhanced CMR

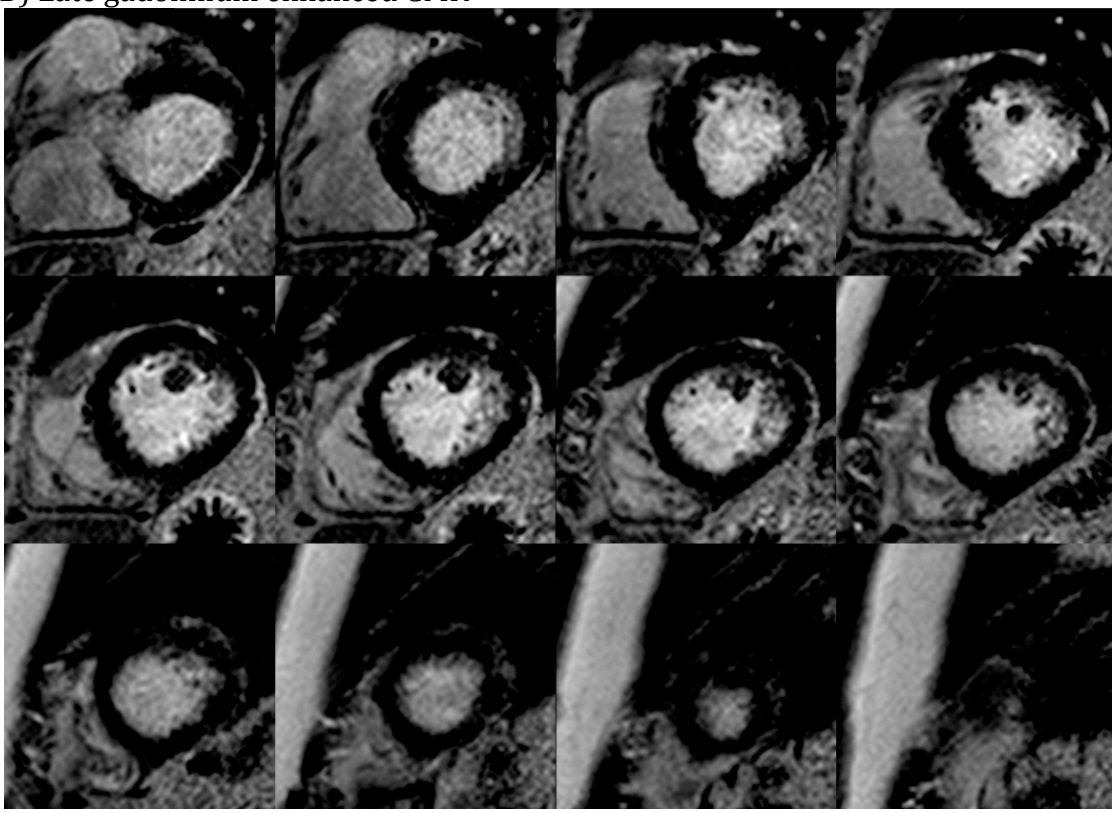

C) MPS stress imaging

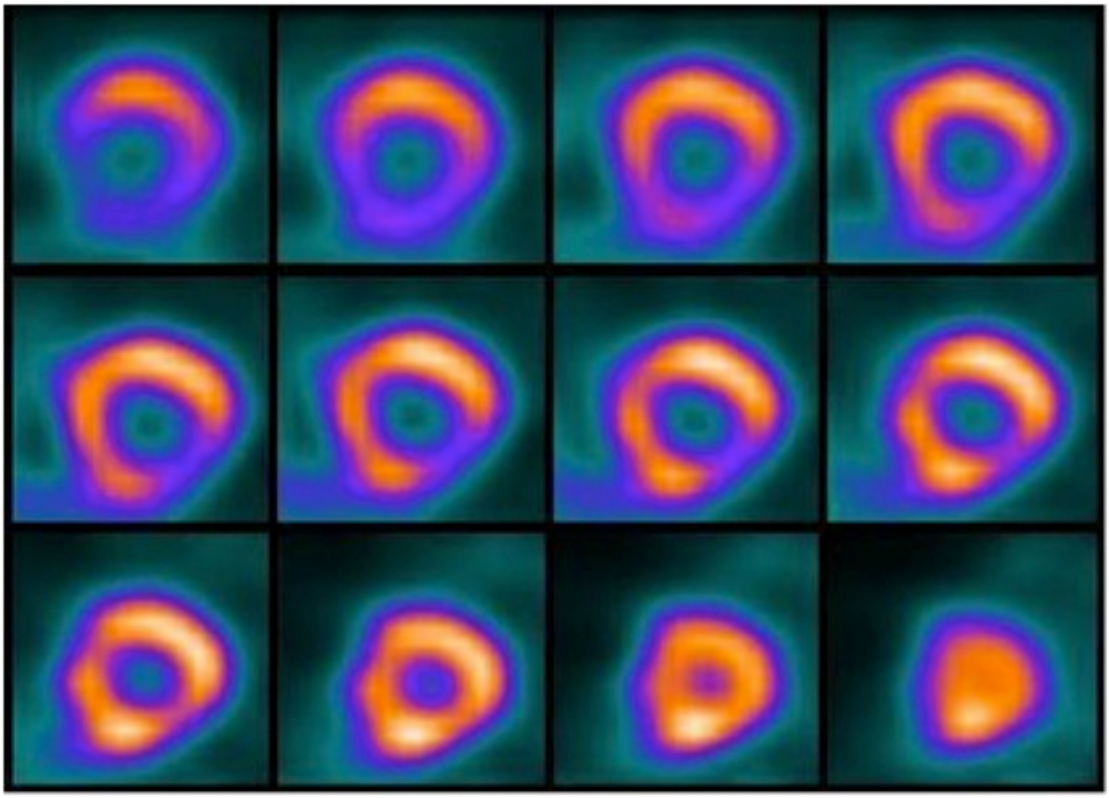

d) MPS rest imaging

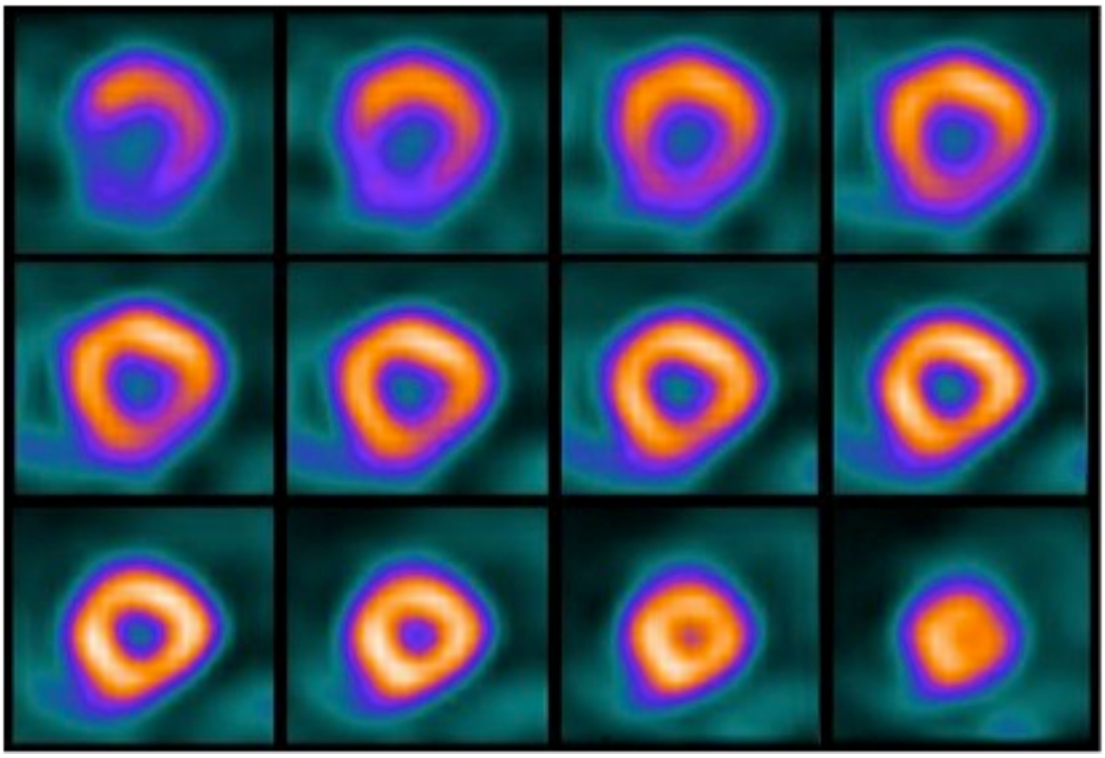

**Figure 3 Ischemic burden correlation**

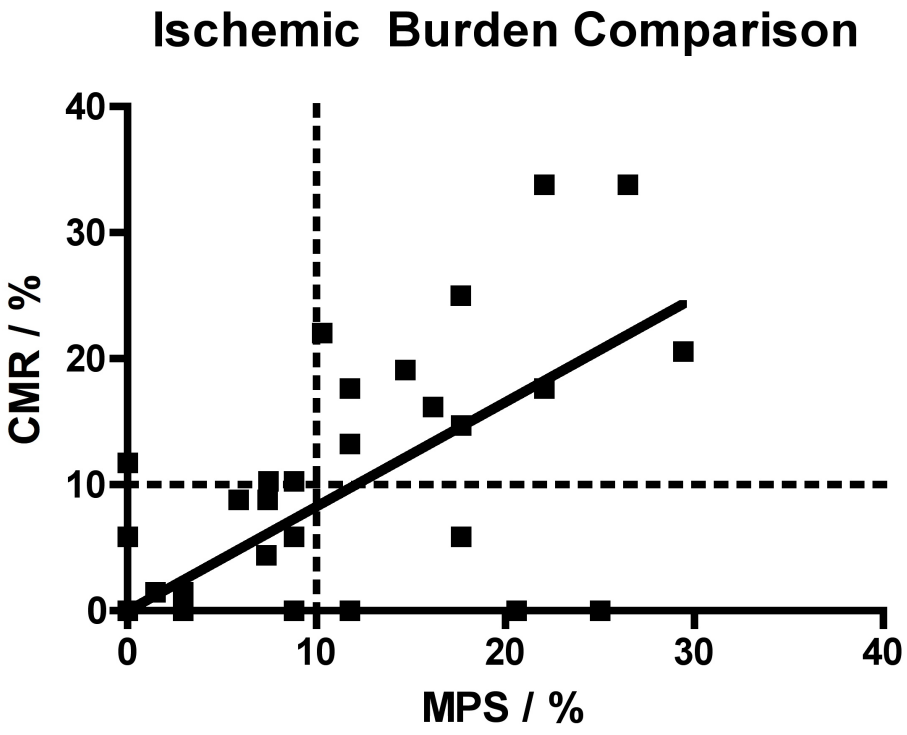

**Figure 4 Bland-Altman analysis for ischemic burden**

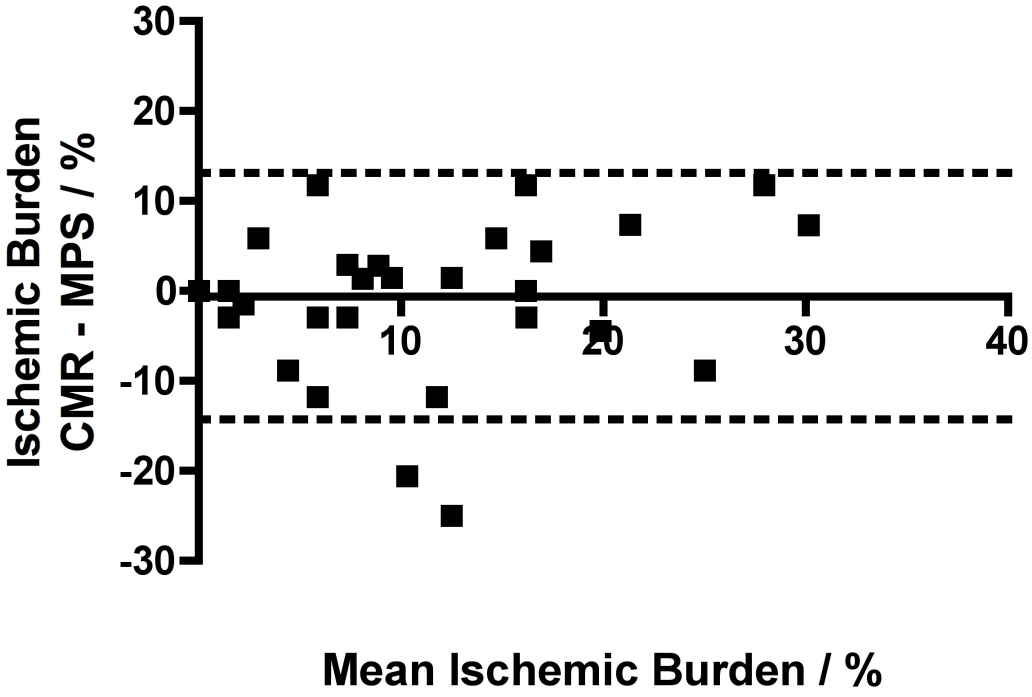

# Chapter 4

## Three-dimensional balanced steady-state-free-precession myocardial perfusion CMR at 3 Tesla using dual-source parallel RF transmission: An initial experience

## 4.1 Abstract

*Background*

The purpose of the study was to establish the feasibility of three-dimensional (3D) balanced steady-state-free-precession (bSSFP) myocardial perfusion CMR at 3T using local RF shimming with dual-source RF transmission, and to compare it with spoiled gradient echo (TGRE) acquisition.

*Materials and Methods*

Dynamic contrast-enhanced 3D bSSFP perfusion imaging was performed on a 3T CMR scanner equipped with dual-source RF transmission technology. Images were reconstructed using k-space and time broad-use linear acquisition speed-up technique (*k-t* BLAST) and compartment based principle component analysis (*k-t* PCA).

*Results*

In phantoms and volunteers, local RF shimming with dual source RF transmission significantly improved B1 field homogeneity compared with single source transmission (P=0.01). 3D bSSFP showed improved signal-to-noise, contrast-to-noise and signal homogeneity compared with 3D TGRE (29.8 vs 26.9, P=0.045; 23.2 vs 21.6, P=0.049; 14.9% vs 12.4%, p=0.002, respectively). Image quality was similar between bSSFP and TGRE but there were more dark rim artefacts with bSSFP. *k-t* PCA reconstruction reduced artefacts for both sequences compared with *k-t* BLAST. In a subset of five patients, both methods performed correctly identified those with coronary artery disease.

*Conclusion*

Three-dimensional bSSFP myocardial perfusion CMR using local RF shimming with dual source parallel RF transmission at 3T is feasible and improves signal characteristics compared with TGRE. Image artefact remains an important limitation of bSSFP imaging at 3T but can be reduced with *k-t* PCA.

## 4.2 Introduction

Two-dimensional (2D) myocardial perfusion cardiovascular magnetic resonance (CMR) imaging is increasingly used as a clinical tool for the assessment of myocardial ischemia[1,2,]. In recent years, 3T CMR scanners have become more widely available and the higher signal to noise ratio (SNR) at this field strength compared with 1.5T is particularly beneficial for myocardial perfusion CMR[3]. In parallel, more sophisticated data acceleration schemes have been introduced, such as space and time broad-use linear speed up technique (*k-t* BLAST) and *k*-space and time principal component analysis (*k-t* PCA), which allow acceleration of image acquisition ≥10 fold[4]. Together, these developments have facilitated the development of three-dimensional (3D) perfusion CMR[5].

Initial 3D myocardial perfusion studies have used spoiled turbo gradient echo (TGRE) acquisition. Balanced steady state free precession (bSSFP) has become popular for 2D myocardial perfusion CMR at 1.5T because it provides a gain in signal to noise ratio (SNR) of up to 85% and in contrast to noise ratio of up to 50% compared with TGRE[6]. However, bSSFP is more susceptible to artefacts relating to B0 inhomogeneities. In addition, limits on specific absorption rates (SAR) on CMR systems are often addressed by lower B1 amplitudes and hence longer TR, which compromise optimal bSSFP pulse sequences and higher flip angles. All of these effects are more prominent at higher field strength.

A potential solution to these challenges is local RF shimming using dual-source parallel RF transmission, which has been shown to improve image homogeneity, image contrast and diagnostic confidence compared with conventional RF transmission in cardiac cine bSSFP imaging at 3T[7]. The method reduces local SAR hot spots and optimizes the

homogeneity of RF deposition. These developments hold particular promise for bSSFP 3D CMR perfusion at 3T.

**Aim**

It was the aim of this study to develop an accelerated bSSFP pulse sequence for 3D whole heart myocardial perfusion CMR at 3T using dual-source parallel RF transmission with local RF shimming and to compare it with a TGRE method.

## 4.3 Methods

*Subjects*

The study was approved by the local research ethics committee and all subjects gave written informed consent to participate. Twenty-five healthy volunteers (mean age 28, range 20-57) and five patients (mean age 65, range 49-79) were included (Table 1). Subjects with contraindications to CMR and adenosine were excluded. Patients were recruited prior to clinically indicated invasive coronary angiography studies.

*CMR set up*

Subjects were scanned in supine position on a 3T MR scanner (Achieva 3T-TX, Philips Healthcare, Best, Netherlands) equipped with a Quasar Dual gradient system (60 mT/m; 200 mT/m/ms) and dual-source parallel RF transmission (MultiTransmit) technology[7]. A 6-channel cardiac phased array receiver coil, 4-lead vectorcardiogram, respiratory belt and blood pressure monitoring were used. For each perfusion scan, an intravenous bolus of 0.075 mmol/kg gadobutrol (Gadovist, Bayer, Germany) was administered followed by a 20ml saline flush (Spectris Solaris power injector, Pittsburgh, Pennsylvania, USA).

*RF Shimming and B1 maps*

A cardiac-triggered $B_1$ calibration scan was acquired as one transverse section through the middle of the left ventricle during end-diastole using a saturated double-angle method with a segmented echo-planar imaging readout in a single breath hold. This scan yields the $B_1$ maps for each independent transmit channel (sequentially acquired in the same breathhold), and is

used to obtain the phase difference and power ratio of the RF transmit channels for subsequent images with local RF shimming[7].

The RF shim for each scan was determined automatically by vendor-provided MR scanner software. This software uses an algorithm to minimize the coefficient of signal variation of the B1 field based on the linear combination of phase and amplitude of the two independent RF transmit channels, based on the B1 data from the calibration scan within the user-defined local shim area. An additional B1 map with RF shimming was acquired using the optimized RF shim settings[8].

*Pulse sequence design*

In phantom experiments and in five volunteers, a bSSFP pulse sequence was developed to match a previously validated and described TGRE method[5] with the following pulse sequence parameters (TR/TE/flip angle 1.8 ms/0.7 ms/15° with a B1-insensitive tailored composite water suppression enhanced through T1 effects (WET) prepulse, saturation prepulse delay 150 milliseconds, acquisition timed to end systole. Using partial echo and a 75% partial Fourier sampling in the ky-kz direction and an elliptical k-space shutter, 10-fold undersampled k-t acquisition with 49 training profiles leading to a net acceleration of 7.0, *k*-space and time broad-use linear speed up technique (*k-t* BLAST) and *k*-space and time principal component analysis (*k-t* PCA) reconstruction[5], reconstruction of 12 contiguous slices of 5 mm thickness, field of view 350×245 $mm^2$, acquired voxel size 2.3×2.3×5 $mm^3$, interpolated to 1.5×1.5×5 $mm^3$). Total number of acquired profiles was 106, which results in an acquisition time per heart-beat of 191 milliseconds [106×1.8 milliseconds]. Thirty dynamics were acquired in a single inspiratory breath-hold, with every dynamic covering one heart-beat.

Based on these parameters, the bSSFP pulse sequence was optimised to maximise the acquisition flip angle while keeping the TR minimal and the acquisition shot duration to approximately 200ms. The effect of local RF shimming using dual-source transmission was assessed by quantitative analysis of the B1 field homogeneity. B1 maps were acquired with and without RF shimming. These B1 maps are scaled as a percentage of nominal amplitude. A pixel value of 100 (%) means that the local flip angle corresponds exactly to the nominal (user defined) value.

*Comparison between TGRE and bSSFP acquisition*

In the next 15 volunteers, two resting perfusion scans were acquired in random order, using the previously described TGRE[5] and the bSSFP method separated by 20 minutes to allow contrast washout. Table 2 lists the key pulse sequence parameters of the two methods. Imaging was performed in the same plane for both acquisitions, using identical planning. In the last five volunteers of this group, noise maps were generated immediately after each of the contrast enhanced perfusion acquisitions. For this purpose, data were acquired with the excitation flip angle set to "zero" and with reconstruction coefficients inherited from the signal containing acquisition. Signal to noise ratio (SNR) was determined as the ratio of average absolute signal to standard deviation of the real channel of noise in the myocardial region-of-interest of the reconstructed *k-t* PCA images. Contrast-to-noise ratio (CNR) was calculated from the difference between the peak and baseline SNR.

Homogeneity of the reconstructed perfusion images was calculated in these five subjects based upon a previously described method[9]. Epicardial and endocardial borders (excluding papillary muscles, trabeculation and dark rim artefacts) were drawn in all ventricular slices. Myocardial mean and standard deviation of signal intensity were

measured in the dynamic image with peak signal intensity. The coefficient of variation of the myocardial pixel values taken was measured using the formula: coefficient of variation = standard deviation / mean signal (expressed as a percentage).

*Stress perfusion and detection of coronary artery disease (CAD)*

In the last 5 volunteers, bSSFP stress perfusion images were acquired during intravenous adenosine-induced hyperaemia administered for 4 minutes at 140mcg/kg/min and, following a 20 minute delay, repeated at rest. In addition, in five patients, both TGRE and bSSFP acquisitions at stress were performed in random order. Significant CAD was defined using quantitative coronary angiography (QCA) as >70% diameter stenosis of the left anterior descending, circumflex and right coronary arteries with >2 mm diameter or >50% diameter stenosis for the left main stem as described previously[5].

*Evaluation of image quality and artefacts of MR images*

Two experienced observers blinded to clinical details reviewed the CMR images (Extended Workspace, Philips Healthcare, Best, The Netherlands) in a randomised order. The whole heart images were displayed as a complete stack from base to apex and each slice was analysed to produce an overall unified score. Image quality was graded on a scale from 1 to 4 (1=uninterpretable, 2=poor, 3= good, 4=excellent) for both the standard *k-t* BLAST and reconstructed *k-t* PCA images. Image artefacts were categorised as breathing related, subendocardial dark rim artefacts[10] or related to the reconstruction of undersampled data.

*Statistical analysis*

Data were analysed using IBM SPSS, Version 19.0 (SPSS< Chicago, IL, USA). For all analyses $P<0.05$ was considered significant. Continuous data were expressed as the mean ± standard deviation. Comparisons between groups were made using two-tailed paired t test. No corrections were made for multiple comparisons. Image quality scores were compared using the Wilcoxon signed ranks test and McNemar's test. Discrete data were expressed as percentages.

## 4.4 Results

Baseline demographics of the 25 volunteers and five patients are given in Table 1. CMR examinations were completed in all subjects and no adverse effects occurred during stress acquisitions.

*Pulse sequence design*

Table 3 shows the minimum achievable TR, TE and maximal heart rate at increasing flip angles using the bSSFP sequence in the first five volunteers. The achievable TR shortening and hence the reduction in acquisition time using local RF shimming was very similar between subjects. A flip angle of 35 degrees was found to provide a balanced TR/TE design, a maximal achievable heart rate of 83 bpm and a shot duration of 211ms. These settings were used for all subsequent experiments. When switching to single source RF transmission, the same flip angle of 35 degrees required a minimum TR of 3.4 ms (range 3.4-3.5) resulting in a minimum shot duration of 301 ms and leading to increased motion artefact.

*RF Homogeneity*

Average B1 in the myocardium was higher for RF shimmed data. The mean percentage of the achieved flip angle in the myocardium was significantly higher and standard deviation lower at 91.1% ± 1.9 with dual source RF transmission compared with 74.2% ± 8.3 with single source mode (P=0.011). Figure 1 shows B1 maps acquired in one volunteer (a) without local RF shimming and (b) with local RF shimming.

*Image Quality and Artefacts*

Table 4 shows the image quality scores for the different sequences and reconstruction methods. The mean image quality (N=15) was similar between the two methods at 3.0

for TGRE and 2.8 for bSSFP (p=0.25) with *k-t* BLAST reconstruction and 3.2 for TGRE and 3.1 for bSSFP (p=0.5) with *k-t* PCA reconstruction. Figure 2 shows an example with both pulse sequences. Breathing related artefact occurred in one data set with both sequences (6.7%), *k-t* related artefact (eg image flickering) once with both sequences (6.7%) and subendocardial dark rim artefact in two of the TGRE (13.3%) and four of the bSSFP (26.8%) data sets with *k-t* BLAST reconstruction. With *k-t* PCA reconstruction this was reduced to one TGRE (6.7%) and two bSSFP (13.3%) cases and image flickering was not seen with either of the sequences. There was more dark rim artefact with the bSSFP cases (2 volunteers and 2 patients vs 1 patient and 1 volunteer for TGRE). This improved after *k-t* PCA reconstruction (bSSFP - 1 volunteer, 1 patient, TGRE 0 volunteers, 1 patient) (Figures 4a-d).

*Signal to noise and signal homogeneity*

The coefficient of variation of myocardial signal ("homogeneity index") was significantly higher with TGRE than bSSFP (14.9%, versus 12.4%, p=0.002), indicating more homogenous signal in bSSFP than in TGRE images (Figure 3). The mean SNR using bSSFP was 29.8 and with TGRE was 26.9 (Table 5 and Figure 5) (p=0.045). The mean CNR using bSSFP was 23.2 vs 21.6 (P=0.049) with TGRE.

*Stress acquisitions and patient studies*

Stress imaging was feasible and tolerated in all 5 volunteers and 5 patients without exceeding the maximum heart rate of the pulse sequences. Of the five patients, three had significant CAD on coronary angiography and all were correctly identified in both the TGRE and bSSFP sequences (Figure 6 – case example and supplementary material Video 1 and Video 2).

## 4.5 Discussion

This study has shown that the use of local RF shimming with dual source RF transmission significantly improves B1 field homogeneity and facilitates bSSFP 3D whole-heart myocardial perfusion imaging at 3 Tesla. Compared with a TGRE method, 3D bSSFP demonstrated significantly improved homogeneity, SNR and CNR but similar image quality. Artefact with bSSFP was more frequent but improved with *k-t* PCA reconstruction.

*High Field Strength*

High-field-strength CMR at 3 Tesla has rapidly gained acceptance for many clinical applications[11,12]. B1 inhomogeneity and restrictions related to local energy deposition pose particular challenges for cardiac imaging at 3 Tesla[13]. Compared with other applications, myocardial perfusion CMR poses additional challenges at high field strength as susceptibility effects increase the B0 inhomogeneity and accentuate banding artefacts, requiring higher order shimming or other corrective methods[14].

Previous studies have reported the use of bSSFP for two-dimensional myocardial perfusion CMR at 1.5T[15-17]. bSSFP provides higher SNR, but at 3T has also been associated with increased off resonance artefact in perfusion CMR and a non-uniform flip angle distribution[8] causing higher local SAR (due to the higher excitation flip angle). At 3 Tesla, these issues are particularly relevant as SAR increases fourfold compared with 1.5 Tesla. A shorter TR is desirable for bSSFP but impacts gradient hardware and SAR constraint by increasing the RF duty cycle. Using longer RF pulses prolongs the TR, making off resonance artefacts more prominent.

In the present study compromises were made between the achievable flip angle and maximal heart rate of the acquisition. A flip angle of 35° represented the best compromise between shot duration and reasonable TR in both phantoms and volunteers.

*Dual Source RF Transmission at 3T using bSSFP*

The dielectric effect is more pronounced at 3T than at 1.5T as the RF wavelength critically approaches the size of the body, influencing standing wave formation. As a consequence, flip angle variation at 3T is high and has previously been shown to range from 32-60% in the heart[18]. This effect contributes to reduced image homogeneity at 3T. Optimising RF shimming optimises power, amplitude, phase and waveform of each RF source to tailor the RF transmission to the patient's anatomy. Use of two independent RF sources, as in this study, allows local RF shimming with consequent homogenisation of flip angle distribution and optimised SAR distribution within the myocardium, thus reducing local SAR peaks. The use of RF shimming has been successfully demonstrated in spine[19], abdomen[20] and breast[21]. In the heart, B1 calibration imaging with local RF shimming and dual-source RF transmission at 3T has been described for bSSFP cine and black blood imaging with improved image quality[8]. The technique was also shown to improve image quality and reduce the number of non-diagnostic segments for dobutamine stress CMR[22].

In the current study, dual RF transmission allowed shortening of the TR for bSSFP acquisition compared with single source RF transmission at the same flip angle. This permitted an relatively tight acquisition shot duration of around 200ms for the bSSFP method, comparable to a previously described 3D TGRE myocardial perfusion method[4,5].

*SNR, CNR and homogeneity*

Homogeneity can vary in part due to the distance of tissue from the surface[23]. Differences in signal intensity between the septum and lateral wall have previously been described in both bSSFP and TGRE imaging[6]. Although regional differences are thought to be mainly due to B1 inhomogeneities, improved image homogeneity with bSSFP compared with TGRE observed in this study may in part be attributed to the pulse sequence characteristics including dependencies of flip angle variation.

In this study, the use of bSSFP improved SNR, CNR and homogeneity of myocardial signal, compared with an equivalent TGRE method. The increase in SNR and CNR over TGRE was consistent with previous studies at 1.5T[6,16]. The magnitude in gain of SNR of a bSSFP vs TGRE sequence was not as marked as observed at 1.5T due to several factors including the differences in the coil design, relaxation times of the tissues, flip angles implemented, artefact, SAR limitations and field inhomogeneity[24].

*k-t* PCA and *k-t* BLAST

Although beyond the scope of this article, differences in *k-t* PCA and *k-t* BLAST have been described[4]. In summary *k-t* PCA has a more efficient algorithm by defining spatial compartments within the 3D volume of a perfusion dataset. The number of overlapping signals is reduced and higher temporal frequency components are more accurately reconstructed. These effects are expected to improve temporal fidelity and reduce signal contamination artefact with *k-t* PCA and improve image quality. In this study, the use of *k-t* PCA reconstruction improved the amount of artefact but this was not associated with a significant improvement of image quality.

*Image quality and diagnosis of CAD*

Whilst increased signal of bSSFP acquisition should have advantages for diagnosis and analysis[6], in this study it did not translate into improved image quality. This was largely due to the higher rate of artefacts with bSSFP. The main artefact observed was subendocaridal dark rim artefact. Although in the 5 patients studied here, dark rim artefact did not affect the correct diagnosis of CAD, the presence of this artefact may lead to false positive reporting of ischemia.

*3D Myocardial Perfusion CMR*

3D acquisition has several potential advantages for myocardial perfusion CMR over the conventionally used 2D methods, including better coverage, higher signal-to-noise and fewer compromises regarding the cardiac phase in which data are acquired. Developing 3D myocardial perfusion CMR has been challenging and only recent technological developments including multi-element coils and spatio-temporal undersampling methods have permitted the very fast data acquisition required for 3D myocardial perfusion CMR. The use of bSSFP at 3Tesla, as shown in this study, is a promising further development and warrants evaluation in larger patient populations. Another recent study has reported the use of bSSFP for 3D myocardial perfusion CMR, but with a different implementation and at 1.5 Tesla[25]. Giri et al used no magnetization preparation but maintained the steady state by continuous application of the bSSFP kernel throughout the scan. This novel approach was feasible and demonstrated good signal characteristics. As the imaging was gated to mid-diastole, the acquisition was however limited to either single slice imaging or single slab 3D encoding and the read-out duration was longer than in our method, ranging between 300-380ms under rest conditions. In our study it was the aim to keep the acquisition as close to 200ms

comparable to previous published work, to avoid potential motion artefacts, which are more likely with a faster heart rate as seen during stress acquisitions.

Three-dimensional balanced steady-state free-precession myocardial perfusion imaging is feasible at 3.0 Tesla, but has a number of challenges including increased dark rim artefact, SAR limitations and longer acquisition times. The use of dual-source RF transmission mitigates some of these factors. Compared with TFE acquisition, image quality is similar, signal-to-noise ratio significantly higher and signal homogeneity significantly improved. Other factors including contrast dosing, optimised flip angles and greater reduction in TR require further study to solve the remaining challenges associated with high-field-strength SSFP perfusion imaging. bSSFP showed a modest but significant increase in SNR and CNR over TGRE, consistent with previous studies[6]. The increment may have not been as high as expected owing to the flip angle achieved but also because data was accelerated, which may have led to respective losses in SNR.

3D bSSFP myocardial perfusion imaging in our implementation was limited by the SAR model used by the scanner manufacturer, which restricted the achievable TR at higher flip angles. This led to longer acquisition times for 3D bSSFP. Acquisition parameters however, were designed to be closely matched with the spoiled GRE method. Higher flip angles may have incrementally improved the signal and image quality and future studies should explore the optimal compromise between flip angle, image resolution and acquisition duration further. It has however been shown previously (for non-contrast-enhanced imaging) that the effect of flip angle increases on bSSFP sequences is relatively minor, as the bSSFP contrast is not strongly dependent on flip angle beyond 35 degrees[26].

A shorter TR is desirable for balanced SSFP to avoid the effects of banding artefacts, but this has implications for SAR limitations and compromises have to be made with achieved flip angles. The use of RF shimming therefore is particularly helpful to homogenise the field but also to achieve a higher flip angle and shorter TR. Whilst increased signal provided by bSSFP should have advantages including the use of quantitative analysis, in this study it did not translate into improved image quality.

Compared with TGRE sequences, SSFP sequences are more vulnerable to banding artefacts because of off-resonance effects that cause variations in signal intensities across images. This is even more marked at 3T. Whenever the local off-resonance frequency is equal to a multiple of 1/TR, dark stripes appear in images. Clinically, dark banding artefacts with bSSFP may cause problems in patients where it may be difficult to differentiate artefacts from ischaemia.

*Implications for patient care*

Three-dimensional myocardial perfusion CMR offers better myocardial coverage than conventionally used 2D methods. 3D bSSFP myocardial perfusion CMR at 3 Tesla potentially offers further improvement of signal characteristics and may enhance the use of three-dimensional myocardial perfusion CMR for clinical application.

**Limitations**

The flip angle of 35 degrees we chose may not be optimal for bSSFP acquisition but was the maximal achievable within the restrictions of SAR, TR, heart rate and the desired acquisition shot duration. Higher flip angles may have improved the signal and image quality further and future studies should explore the optimal compromise between flip

angle, image resolution and acquisition duration further. The differences in acquisition window may also account for some of the image quality discrepancies as it was anticipated that there would be more temporal blurring in the bSSFP group. The use of k-t PCA may have mitigated some of this effect however.

The maximal heart rate of 83 bpm is a limitation, although it was not exceeded by volunteers and patients in this study even during stress studies. In many patients, however, higher heart rates will be encountered. A reduction of the read-out duration or saturation pulse delay, or acquisition at every other heartbeat can be relatively easily employed to deal with higher heart rates but the impact on diagnostic accuracy will need to be evaluated.

Lastly, we recognise the reduction in TR is the consequence of many factors not least the particular SAR model used by the vendor. We would not consider this "optimal" as the resulting long acquisition time led to poor image quality. As we have previously described, a number of approaches including dieletric cushions, post processing as well as a fixed anatomy dependent mode of RF shimming could have been used to improve B1 homogeneity. Many of these are vendor specific and were not available for the current study.

**Conclusion**

Three-dimensional bSSFP myocardial perfusion CMR using local RF shimming with dual source parallel RF transmission at 3 Tesla is feasible and improves signal characteristics compared with TGRE. Image artefact remains an important limitation of bSSFP perfusion imaging at 3 Tesla.

## 4.6 References

1: Hamon M, Fau G, Nee G, Ehtisham J, Morello R, Hamon M. Meta-analysis of the diagnostic performance of stress perfusion cardiovascular magnetic resonance for detection of coronary artery disease. J Cardiovasc Magn Reson. 2010 May 19;12(1):29.

2: Greenwood JP, Maredia N, Younger JF, Brown JM, Nixon J, Everett CC, Bijsterveld P, Ridgway JP, Radjenovic A, Dickinson CJ, Ball SG, Plein S. Cardiovascular magnetic resonance and single-photon emission computed tomography for diagnosis of coronary heart disease (CE-MARC): a prospective trial. Lancet. 2012 Feb 4;379(9814):453-60

3: Oshinski JN, Delfino JG, Sharma P, Gharib AM, Pettigrew RI. Cardiovascular magnetic resonance at 3.0 T: current state of the art. J Cardiovasc Magn Reson. 2010 Oct 7;12:55.

4. Vitanis V, Manka R, Giese D, Pedersen H, Plein S, Boesiger P, Kozerke S. High resolution three-dimensional cardiac perfusion imaging using compartment-based *k-t* principal component analysis. Magn Reson Med. 2011 Feb;65(2):575-8

5. Jogiya R, Kozerke S, Morton G, De Silva K, Redwood S, Perera D, Nagel E, Plein S. Validation of Dynamic 3-Dimensional Whole Heart Magnetic Resonance Myocardial Perfusion Imaging Against Fractional Flow Reserve for the Detection of Significant Coronary Artery Disease. J Am Coll Cardiol. 2012 Aug 21;60(8):756-6.

6. Wang Y, Moin K, Akinboboye O, Reichek N. Myocardial first pass perfusion: steady-state free precession versus spoiled gradient echo and segmented echo planar imaging. Magn Reson Med. 2005 Nov;54(5):1123-9

7. Mueller A, Kouwenhoven M, Naehle CP, Gieseke J, Strach K, Willinek WA, Schild HH, Thomas D. Dual-source radiofrequency transmission with patient-adaptive local

radiofrequency shimming for 3.0-T cardiac MR imaging: initial experience. Radiology. 2012 Apr;263(1):77-85.

8. Krishnamurthy R, Pednekar A, Kouwenhoven M, Cheong B, Muthupillai R. Evaluation of a subject specific dual-transmit approach for improving B1 field homogeneity in cardiovascular magnetic resonance at 3T. J Cardiovasc Magn Reson. 2013 Aug 6;15(1):68

9. Plein S, Bloomer TN, Ridgway JP, Jones TR, Bainbridge GJ, Sivananthan MU. Steady-state free precession magnetic resonance imaging of the heart: comparison with segmented k-space gradient-echo imaging. J Magn Reson Imaging. 2001 Sep;14(3):230-6.

10. Di Bella EV, Parker DL, Sinusas AJ. On the dark rim artifact in dynamic contrast-enhanced MRI myocardial perfusion studies. Magn Reson Med. 2005 Nov;54(5):1295-9.

11. Craven I, Griffiths PD, Hoggard N. Magnetic resonance imaging of epilepsy at 3 Tesla. Clin Radiol. 2011 Mar;66(3):278-86.

12. Kim PD, Truwit CL, Hall WA. Three-tesla high-field applications. Neurosurg Clin N Am. 2009 Apr;20(2):173-8.

13. Soher BJ, Dale BM, Merkle EM. A review of MR physics: 3T versus 1.5T. Magn Reson Imaging Clin N Am. 2007 Aug;15(3):277-90, v.

14. Wieben O, Francois C, Reeder SB. Cardiac MRI of ischemic heart disease at 3T: potential and challenges. Eur J Radiol. 2008 Jan;65(1):15-28

15. Morton G, Ishida M, Schuster A, Hussain S, Schaeffter T, Chiribiri A, Nagel E. Perfusion cardiovascular magnetic resonance: Comparison of an advanced, high-resolution and a standard sequence. J Cardiovasc Magn Reson. 2012 Jun 9;14:34.

16. Merkle N, Wöhrle J, Grebe O, Nusser T, Kunze M, Kestler HA, Kochs M, Hombach V. Assessment of myocardial perfusion for detection of coronary artery stenoses by steady-state, free-precession magnetic resonance first-pass imaging. Heart. 2007 Nov;93(11):1381-5.

17. Hunold P, Maderwald S, Eggebrecht H, Vogt FM, Barkhausen J. Steady-state free precession sequences in myocardial first-pass perfusion MR imaging: comparison with TurboFLASH imaging. Eur Radiol 2004;14:409–16

18. Sung K, Nayak KS. Measurement and characterization of RF nonuniformity over the heart at 3T using body coil transmission. J Magn Reson Imaging. 2008 Mar;27(3):643-8

19. Nelles M, Konig RS, Gieseke J, Guerand-van Battum MM, Kukuk GM, Schild HH, Willinek WA. Dual-source parallel RF transmission for clinical MR imaging of the spine at 3.0 T: intraindividual comparison with conventional single-source transmission. Radiology. 2010 Dec;257(3):743-53.

20. Rao RK, Riffel P, Meyer M, Kettnaker PJ, Lemke A, Haneder S, Schoenberg SO, Michaely HJ. Implementation of dual-source RF excitation in 3 T MR-scanners allows for nearly identical ADC values compared to 1.5 T MR scanners in the abdomen. PLoS One. 2012;7(2):e32613.

21. Rahbar H, Partridge SC, Demartini WB, Gutierrez RL, Parsian S, Lehman CD. Improved B,ÇÅ homogeneity of 3 Tesla breast MRI using dual-source parallel radiofrequency excitation. J Magn Reson Imaging. 2012 May;35(5):1222-6.

22. Strach K, Clauberg R, Müller A, Wonneberger U, Naehle CP, Kouwenhoven M, Gieseke J, Schild HH, Thomas D. Feasibility of high-dose dobutamine stress SSFP Cine MRI at 3 Tesla with patient adaptive local RF Shimming using dual-source RF transmission: initial results. Rofo. 2013 Jan;185(1):34-9.

23. Constantinides CD, Westgate CR, O'Dell WG, Zerhouni EA, McVeigh ER. A phased array coil for human cardiac imaging. Magn Reson Med. 1995 Jul;34(1):92-8

24. Gutberlet M, Noeske R, Schwinge K, Freyhardt P, Felix R, Niendorf T. Comprehensive cardiac magnetic resonance imaging at 3.0 Tesla: feasibility and implications for clinical applications. Invest Radiol 2006;41(2):154–67.

25. Giri S, Xue H, Maiseyeu A, Kroeker R, Rajagopalan S, White RD, Zuehlsdorff S, Raman SV, Simonetti OP. Steady-state first-pass perfusion (SSFPP): A new approach to 3D first-pass myocardial perfusion imaging. Magn Reson Med. 2013 Feb 25. doi: 10.1002/mrm.24638

26. Scheffler K, Lehnhardt S. Principles and applications of balanced SSFP techniques. Eur Radiol 2003;13(11):2409-2418

## 4.7 Tables

**Table 1: Study population demographics**

| | Volunteers | Patients |
|---|---|---|
| N | 25 | 5 |
| Male | 15 (60%) | 4 (80%) |
| Age, Years | 28.0 +/- 8.1 | 64.6 +/-13.7 |
| Range | 20-57 | 49-79 |
| BMI, $kg/m^2$ | 23.8 +/- 2.6 | 23.7 +/-1.9 |

**Table 2: Pulse sequence parameters**

| | TGRE | bSSFP |
|---|---|---|
| | | |
| TR | 1.8ms | 2.2ms |
| TE | 0.70ms | 1.04ms |
| Flip angle | 15° | 35° |
| RF Shimming | Yes (local) | Yes (local) |
| Partial Echo , Halfscan (Partial Fourier) in x-y and z planes | Yes 0.75/0.75 | Yes 0.75/0.75 |
| Spatial resolution | 2.3x2.3x10mm$^3$ | 2.3x2.3x10mm$^3$ |
| No slices | 12 | 12 |
| Acquisition | 191ms | 211ms |
| SAR | <30% | <88% |

**Table 3. Pulse sequence optimisation with dual source RF transmission in first five volunteers**

| Flip Angle (°/range) | Maximal Heart Rate (bpm) | Repetition Time (ms) | Echo Time (ms) |
|---|---|---|---|
| | | | |
| 10 (10-12) | 144 | 1.77 | 0.76 |
| 15 (15-17) | 144 | 1.77 | 0.76 |
| 20 (20-22) | 132 | 1.83 | 0.79 |
| 25 (25-26) | 109 | 1.97 | 0.86 |
| 30 (30-31) | 94 | 2.10 | 0.93 |
| 35 (35-36) | 83 | 2.20 | 1.04 |
| 40 (40-41) | 72 | 2.40 | 1.08 |
| 43 (43-43) | 63 | 2.51 | 1.15 |

**Table 4. Image quality scores for the *k-t* BLAST *and k-t* PCA images**

| Subject | bSSFP *k-t* BLAST | TGRE *k-t* BLAST | bSSFP *k-t* PCA | rTGRE *k-t* PCA |
|---|---|---|---|---|
| 1 | 3 | 3 | 3 | 4 |
| 2 | 2 | 3 | 3 | 3 |
| 3 | 3 | 3 | 3 | 3 |
| 4 | 2 | 3 | 3 | 3 |
| 5 | 3 | 3 | 3 | 3 |
| 6 | 3 | 3 | 3 | 3 |
| 7 | 3 | 3 | 3 | 3 |
| 8 | 3 | 3 | 3 | 3 |
| 9 | 3 | 3 | 4 | 4 |
| 10 | 3 | 3 | 3 | 3 |
| 11 | 3 | 3 | 3 | 3 |
| 12 | 3 | 3 | 3 | 3 |
| 13 | 3 | 3 | 4 | 4 |
| 14 | 2 | 3 | 2 | 3 |
| 15 | 3 | 3 | 3 | 3 |

**Table 5. Signal-to-noise and contrast-to-noise ratio in 5 volunteers**

| Volunteer number | Pulse Sequence Order | SNR | CNR |
|---|---|---|---|
| | | | |
| **1.** | BSSFP | 34.17 | 27.11 |
| | TGRE | 32.13 | 25.42 |
| | | | |
| **2.** | BSSFP | 31.53 | 27.12 |
| | TGRE | 29.33 | 26.29 |
| | | | |
| **3.** | TGRE | 27.78 | 21.44 |
| | BSSFP | 27.80 | 21.67 |
| | | | |
| **4.** | TGRE | 21.24 | 16.55 |
| | BSSFP | 26.92 | 18.30 |
| | | | |
| **5.** | TGRE | 24.10 | 18.20 |
| | BSSFP | 28.40 | 21.90 |
| | | | |
| **Mean** | TGRE | 26.9 | 21.6 |
| | BSSFP | 29.8 | 23.2 |
| **P Value** | | 0.045 | 0.049 |

## 4.8 Figure legends

Figure 1: Example of the effect of local RF shimming on B1 map in a volunteer. Image (a) shows conventional RF transmission without RF shimming. Image (b) shows the use of dual source RF transmission with local RF shimming. The mean percentage of flip angle achieved was 74.6% with conventional RF transmission and 91.3% with dual source RF transmission demonstrating improved homogeneity.

Figure 2: Case example of a volunteer who underwent (a) TGRE 3D whole heart perfusion followed by (b) bSSFP 3D whole heart perfusion. Both images had local RF shimming with dual source RF transmission applied and demonstrated similar image quality overall using *k-t* BLAST reconstruction. Image quality was scored as 3 in both sequences due to the presence of band artefacts.

Figure 3: Myocardial homogeneity index. The lower index in bSSFP indicates significantly improved (p=0.022) homogeneity of the myocardial signal compared with TGRE 3D whole heart perfusion.

Figure 4 a-d. Single slice Volunteer example of 3D spoiled gradient echo (TGRE) and balanced steady state free precession (bSSFP) acquisition using *k-t* PCA and *k-t* BLAST reconstruction – demonstrating reduced banding artefacts following reconstruction using *k-t* PCA (a) compared with standard *k-t* BLAST reconstruction (b). Using a bSSFP sequence SNR was demonstrated to be higher (c) and showed improved temporal fidelity compared with a standard *k-t* BLAST sequence with (d) similar picture quality.

Figure 5: Signal to noise ratio of bSSFP and TGRE 3D whole heart perfusion using *k-t* PCA reconstruction.

Figure 6: Case example of a 79 year old patient who underwent (a) TGRE 3D whole heart perfusion followed by (b) bSSFP 3D whole heart perfusion. Both images were reconstructed with *k-t* PCA and show significant ischemia of variable transmurality in the anterior and inferior wall extending from base towards the apex. Angiography showed an occluded proximal left anterior descending coronary artery (QCA=100%) and a significant proximal stenosis of the right coronary artery (QCA=85%). The circumflex artery was not considered flow limiting (QCA=50%). Image quality was scored as 3 for both sequences using *k-t* PCA reconstruction.

**Figure 1. B1 images without RF shimming and with local RF shimming**

B1 map without RF shimming

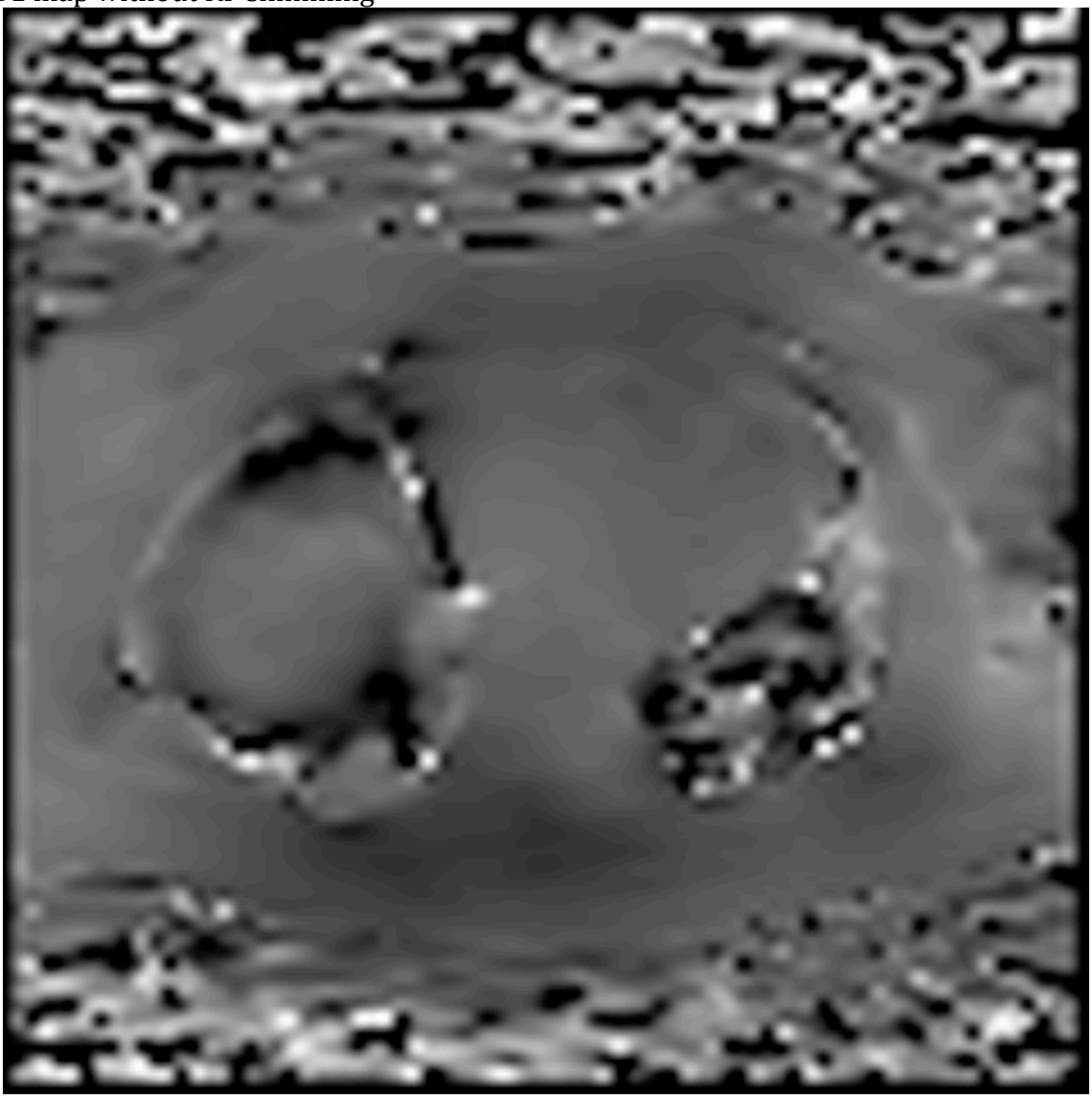

B1 map after local RF shimming of the heart

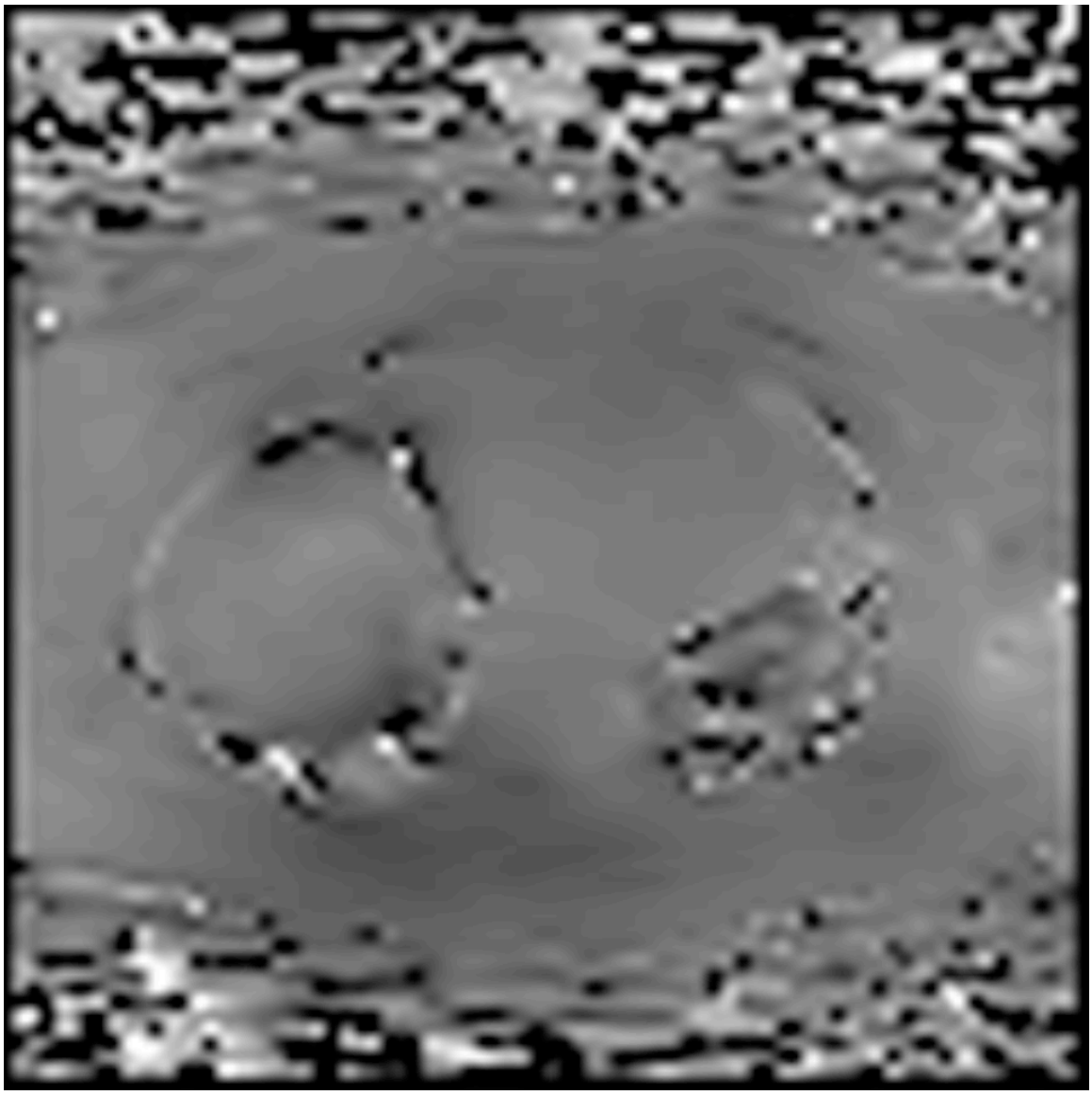

**Figure 2. Volunteer example of 3D spoiled gradient echo (TGRE) and balanced steady state free precession (bSSFP) acquisition**

a. TGRE

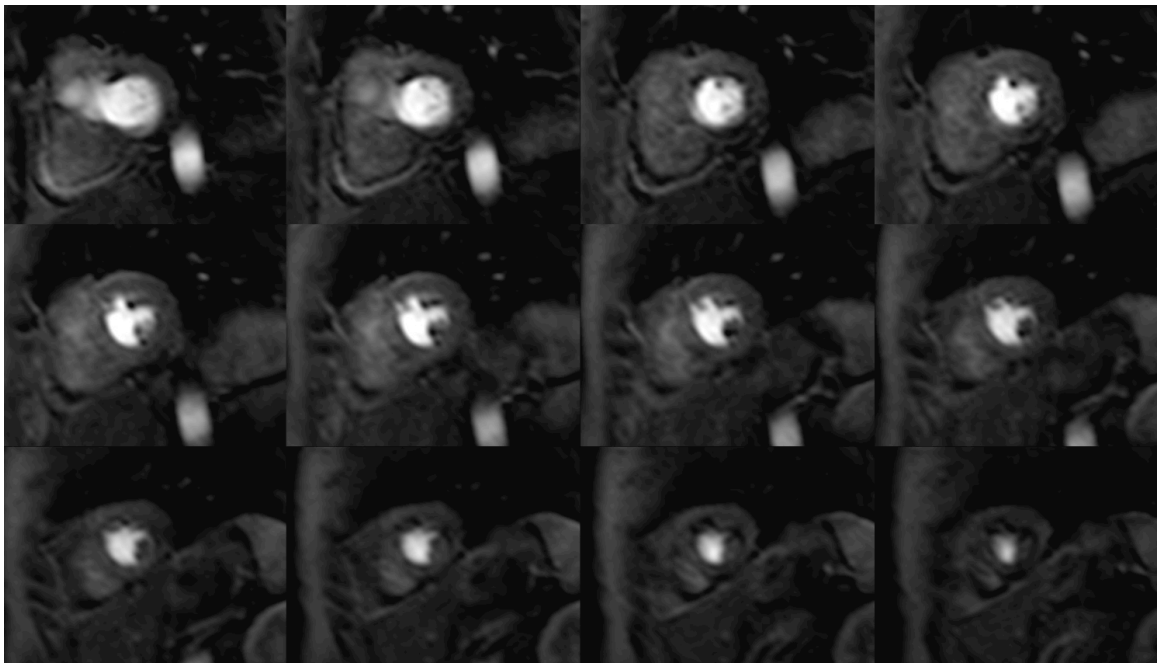

b. bSSFP

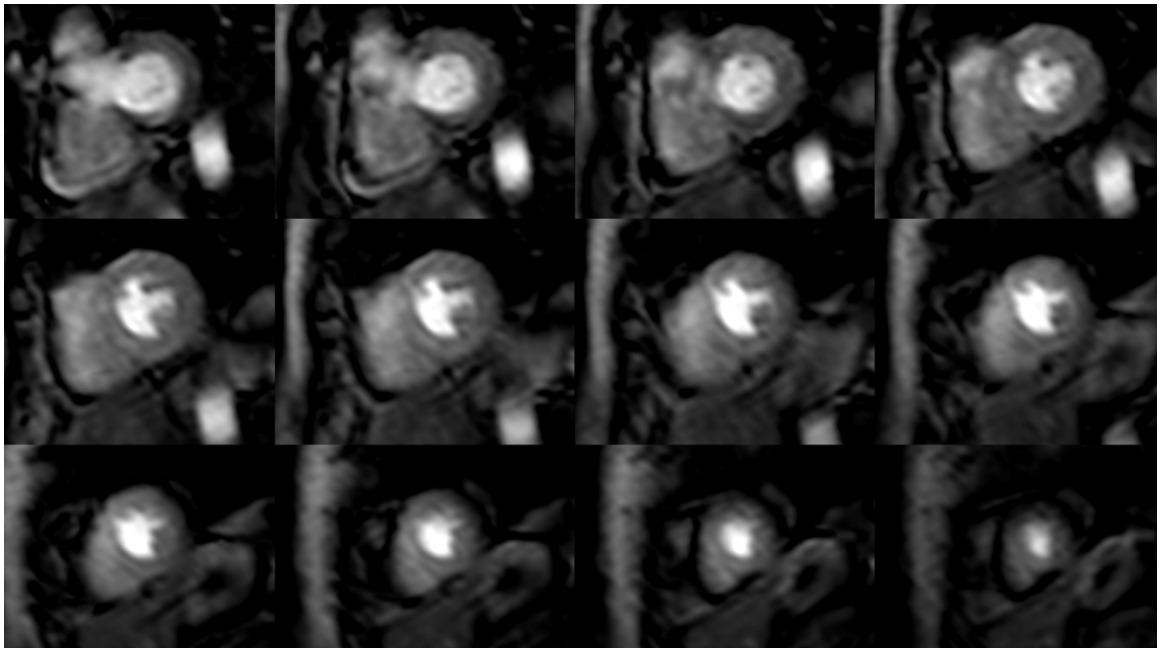

**Figure 3. Coefficient of Variation (Homogeneity Index)**

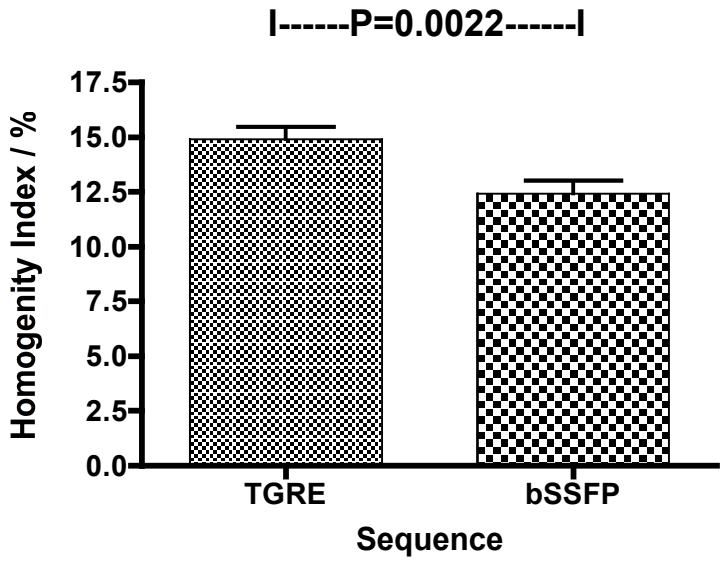

**Figure 4 a-d. Volunteer example of 3D spoiled gradient echo (TGRE) and balanced steady state free precession (bSSFP) acquisition using *k-t* PCA and *k-t* BLAST reconstruction**

**a.** *k-t* PCA TGRE

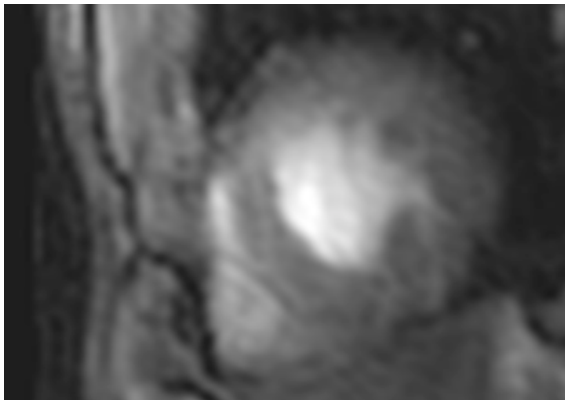

**b.** TGRE *k-t* BLAST

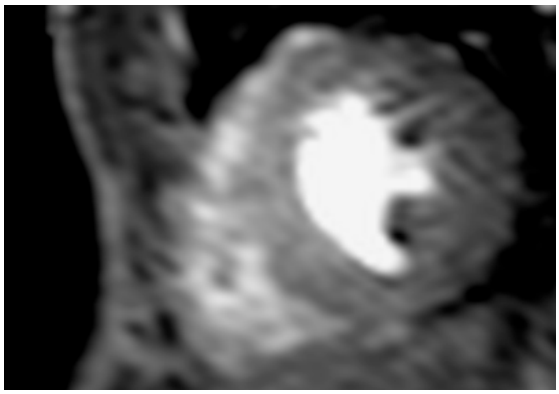

**c.** *k-t* PCA BSSFP

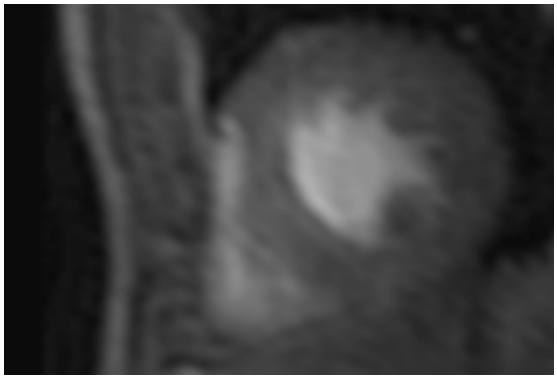

**d.** *k-t* BLAST BSSFP

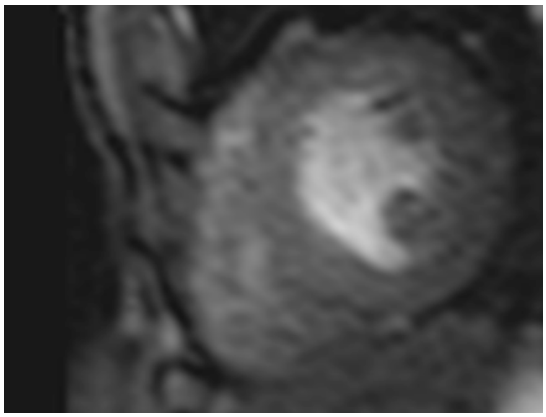

**Figure 5. Signal to Noise Ratio**

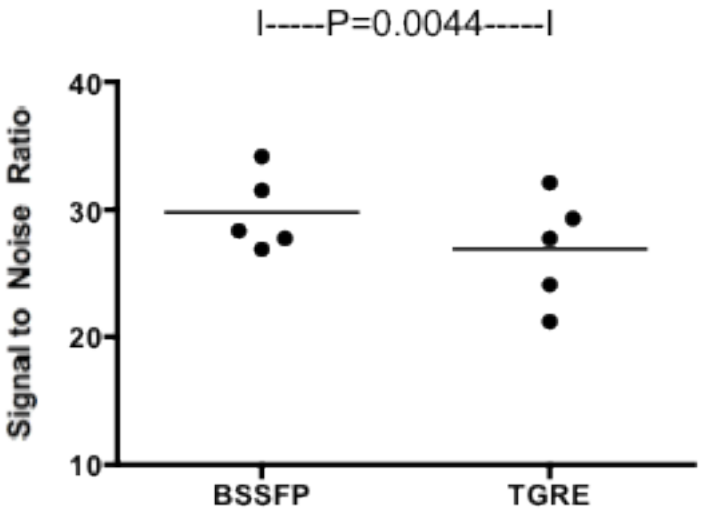

**Figure 6. Patient example of 3D spoiled gradient echo (TGRE) and balanced steady state free precession (bSSFP) acquisition**

a. TGRE

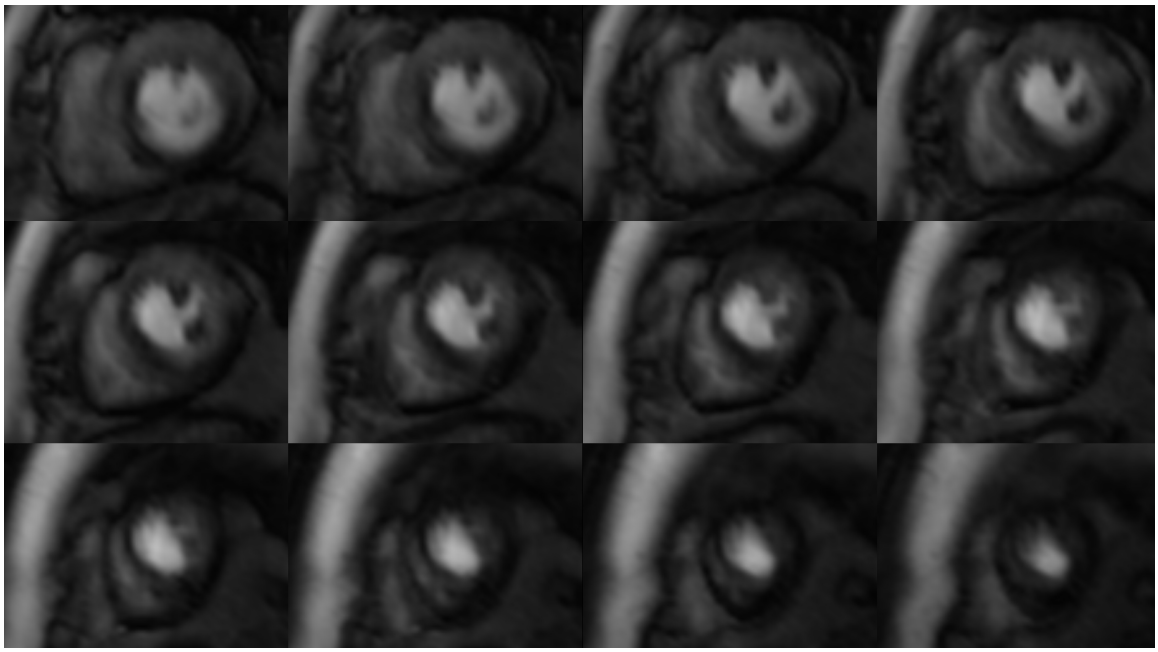

b. bSSFP

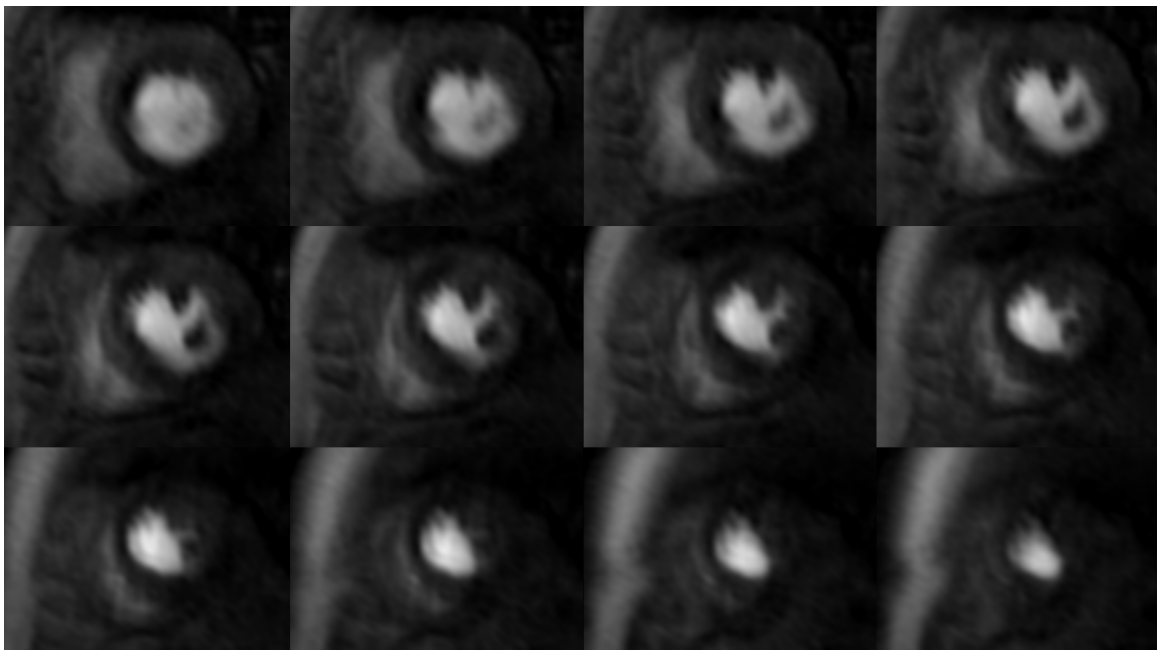

# Chapter 5

## Hyperemic stress myocardial perfusion CMR in mice at 3 Tesla: Initial experience and validation against microspheres

## 5.1 Abstract

Introduction

Dynamic first pass contrast-enhanced myocardial perfusion is the standard CMR method for the estimation of myocardial blood flow (MBF) and MBF reserve in man, but it is challenging in rodents because of the high temporal and spatial resolution requirements. Hyperemic first pass myocardial perfusion CMR during vasodilator stress in mice has not been reported.

Methods

Five C57BL/6J mice were scanned on a clinical 3.0 Tesla Achieva system (Philips Healthcare, Netherlands). Vasodilator stress was induced via a tail vein catheter with an injection of dipyridamole. Dynamic contrast-enhanced perfusion imaging (Gadobutrol 0.1mmol/kg) was based on a saturation recovery spoiled gradient echo method with 10-fold k-space and time domain undersampling (*k-t* PCA). One week later the mice underwent repeat anaesthesia and LV injections of fluorescent microspheres at rest and at stress. Microspheres were analysed using confocal microscopy and fluorescence-activated cell sorting.

Results

Mean MBF at rest measured by Fermi-function constrained deconvolution was 4.1±0.5ml/g/min and increased to 9.6±2.5ml/g/min during dipyridamole stress (P=0.005). The myocardial perfusion reserve was 2.4 ±0.54. The mean count ratio of stress to rest microspheres was 2.4 ±0.51 using confocal microscopy and 2.6 ± 0.46

using fluorescence. There was good agreement between CMR and microspheres with no significant difference (P=0.84).

## Conclusion

First-pass myocardial stress perfusion CMR in a mouse model is feasible at 3Tesla. Rest and stress MBF values were consistent with existing literature and perfusion reserve correlated closely to microsphere analysis. Data were acquired on a 3 Tesla scanner using an approach similar to clinical acquisition protocols, potentially facilitating translation of imaging findings between rodent and human studies.

## 5.2 Background

Myocardial blood flow (MBF) is one of the most relevant parameters in cardiovascular disease. While coronary autoregulation maintains resting MBF constant over a wide range of physiological and pathological states, MBF reserve is impaired in several disease processes including atherosclerosis[1], systemic hypertension[2] and diabetes mellitus[3]. Rodent models play a key role in developing our understanding of cardiovascular disease and the development of novel therapies[4,5]. Accurate non-invasive assessment of MBF and MBF reserve in rodent models of cardiovascular disease is therefore highly desirable. Currently used methods include nuclear perfusion imaging[6], echocardiography[7], and spin labelling cardiovascular magnetic resonance (CMR)[8]. However, nuclear and echocardiographic perfusion methods are limited by relatively low spatial resolution and spin labelling CMR methods require long acquisition protocols.

In human studies, dynamic contrast-enhanced myocardial perfusion imaging during vasodilator stress is the method of choice for the detection of ischemia with CMR. Clinical studies have demonstrated high diagnostic accuracy of the method for the detection of coronary artery disease [9,10]. While in clinical settings, data are usually interpreted by visual analysis, estimations of MBF and MBF reserve can also be derived from the acquired data.[11,12] Such quantitative analysis methods increase the objectivity of the analysis and allow monitoring of disease progression and assessment of treatment efficacy, which is an important consideration in developing translatable rodent models of cardiovascular disease. In rodents, dynamic contrast-enhanced myocardial perfusion CMR is challenging because of the high temporal and spatial resolution requirements.

Making use of new data acquisition acceleration schemes, quantitative murine first pass myocardial perfusion at rest has recently been described[13,14,15]. Hyperemic myocardial first pass stress perfusion CMR in mice has however not been reported or validated against microspheres.

The aim of this study was to test the feasibility of myocardial perfusion CMR in C57BL/6J mice during dipyridamole-induced hyperemia and validate the method against the reference test of injectable microspheres.

## 5.3 Methods

*Animal Model*

Five 6-month-old homozygous C57BL/6J male mice (weight 25-30g) were acquired from Charles Rivers Laboratories (Edinburgh, UK) and housed within the Animal Unit of the Rayne Institute at King's College London. The housing and care of the animals and all the procedures used in these studies were performed in accordance with the guidelines and regulations of the United Kingdom Home Office under the Animals (Scientific Procedures) Act, 1986.

*Preparation and Sedation*

Mice were anesthetized and maintained under inhalational anesthesia via a nose cone (1.5% isoflurane/medical oxygen). Rectal temperature was monitored continuously and a warm air flow (using an MR-compatible heater system; SA Instruments, Stony Brook, NY) was adapted to maintain temperature at 37°C. All experiments were conducted at a similar time of the day and in the same climate conditions. Two ECG leads (SA Instruments, Stony Brook, NY) were placed subcutaneously on the left and right side of the thorax. For electrocardiogram (ECG) synchronization a dedicated small-animal ECG device, 1025-MR (SA Instruments, Stony Brook, NY) and for signal reception, a microscopy receive coils (23mm diameter, single circular loop; Philips Healthcare, Hamburg, Germany) was used.

*CMR Protocol*

Imaging was performed on a clinical 3.0-T system (Achieva; Philips Healthcare, Best, The Netherlands) equipped with a clinical gradient system (30mT/m; 200mT/m/ms). Mice were imaged under isofluorane anesthesia and in prone position. The in-built ECG

triggering unit of the CMR scanner was modified to permit synchronization of heart rates of up to 600 beats/min.

All data were acquired during free breathing of the animals. For localization of the heart, low-resolution gradient echo scout scans were acquired in the coronal and transverse orientations followed by pseudo two- and four-chamber gradient echo cine scans acquired with a prospective ECG-triggered spoiled gradient echo sequence (field of view 35 × 35mm$^2$, matrix 160, slice thickness 1mm, 5 fold k-t *SENSE* acceleration with 11 interleaved training profiles, pulse repetition time/echo time 12/6.3msec, flip angle 20°). From these images, a true mid-ventricular short-axis view of the left ventricle was planned for subsequent perfusion imaging.

*MR perfusion pulse sequence*

The perfusion pulse sequence parameters were similar to a previously published method[15]: two-dimensional saturation recovery spoiled gradient echo (Turbo Filed Echo/TFE), repetition time/echo time 6.7 msec/1.0 msec, flip angle 20°, 10-fold *k-t* undersampling with three densely sampled training profiles interleaved with the undersampled data, 62.5% partial Fourier and partial echo acquisition, one slice acquired during each RR interval, field of view 25 × 25mm$^2$, slice thickness 1.5mm, matrix 128 × 128, spatial resolution 0.2 × 0.2mm$^2$ (reconstructed to 0.13 × 0.13mm$^2$), preparation pulse delay 100 msec (to the centre of k-space), acquisition window 43 msec. The preparation pulse delay was reduced if required to enable acquisition at higher heart rates, particularly when during stress. Data were acquired for 200 heart beats. To improve temporal fidelity of the data at the high undersampling factors, *k-t* principal component analysis (*k-t* PCA) was used for image reconstruction[16].

*Contrast Delivery*

A customised catheter was placed in the tail vein of the mouse and 0.1 mmol/kg bodyweight Gadobutrol (Gd-DTPA) (Gadovist, Bayer, Germany) was injected after the perfusion scan was started (volume of contrast injection 2.5 to 3.0μL based on the weight of the mouse). To ensure a reproducible bolus injection, the contrast agent, as well as 25 μL of saline, was preloaded into small-bore tetrafluoroethylene tubing and injected manually.

*Stress Agent*

For stress perfusion imaging, dipyridamole (Persantine, Boehringer Ingelheim,UK) 0.56mg/kg was injected via a tail vein catheter 1 minute prior to the perfusion acquisition and into the same tail vein catheter as used for contrast delivery. Contrast injection was performed in the same standardized way as for rest scans. Stress and rest scans were performed in random order to minimize any potential bias from residual contrast agent and were separated by 15 minutes. Following imaging of stress perfusion, a slow hand injection of intravenous aminophylline (Hospira, UK ltd, 5mg/kg diluted in a 25μL saline flush) was given in order to minimize any effects of dipyridamole on subsequent estimation of resting blood flow. The total volume of injection during CMR perfusion imaging was 105-106μL.

*CMR Analysis*

Image quality was scored from 1 to 4 (1=uninterpretable, 2=satisfactory, 3=good, 4=excellent). Quantitative analysis of MBF was performed using custom prototype image analysis software (Philips Healthcare, Best, The Netherlands). Endocardial and

epicardial contours were drawn on images with best blood to myocardium contrast and copied to all other dynamic images. Any subendocardial dark rim artifacts were excluded from the contours. The myocardium was divided into four eqiangular sectors, starting from a reference point placed at the anterior septal insertion of the right ventricle. To obtain the arterial input function, a region of interest was drawn inside the left ventricular (LV) blood pool. Signal intensity (SI)/time curves were generated for the LV blood pool, for the four myocardial sectors and an average for the myocardium as a whole. The maximal upslope of the profiles was generated using best-point fitting. SI profiles were then generated for each sector and the region of interest in the LV blood pool. Enhancement ratio of signal increase and normalized SI upslope ratios between the blood pool and myocardium were calculated as (enhancement ratio = (SI max – SI baseline)/SI baseline) and (normalized SI upslope = upslope myocardium/LV).
In addition, absolute MBF was computed from the LV blood pool and myocardial tissue SI vs. time curves, using in-house software, with previously described methods based on Fermi constrained deconvolution[17].

*Microspheres and confocal microscopy*

One week after MR scanning, all 5 mice mice underwent repeat anesthesia and injection of fluorescent microspheres at dipyridamole hyperemic stress and at rest in the same order and using the same stress regime as for the CMR scans. 25µl ($1.0x10^6$ beads/ml) of yellow-fluorescent microspheres (10µm diameter, Invitrogen, NY) (excitation/emission 515/534nm) were injected at rest. One minute following dipyridamole stress, 25µl ($1.0x10^6$ beads/ml) scarlet (excitation/emission 645/680nm) microspheres were injected, followed by a slow hand injection of intravenous aminophylline (5mg/kg

diluted in a 25μL saline). The total volume of injection for the microsphere experiment was 77.8-78.4μL.

Animals were sacrificed and the myocardium stored in phosphate buffer saline. To match the CMR protocol, a 1.5mm mid ventricular slice was later sectioned using a vibratome to obtain 150μM sections. Ten individual slices were analysed and the fluorochromes identified and enumerated manually using confocal microscopy (Leica TCS SP5; Deerfield, IL) to establish the absolute number of microspheres injected at rest and stress. This was used to establish a myocardial perfusion reserve (MPR = total number of spheres detected at stress / total number of spheres at rest) for each mouse.

*Flow Cytometry*

The remaining myocardium was processed using standardised methods[18] and analysed using flow cytometry to establish the ratio of microspheres at stress and rest. Briefly, the hearts were digested by incubation in a cocktail of collagenase IV, DNAse and hyaluronidase at 37°C for 1 h, followed by trituration and filtration through a 30μM nylon mesh. The relative number of microspheres in each cell suspension was measured on FACS Canto II flow cytometer (BD biosciences, UK) FACS Canto and analysed using FlowJo software (TreeStar Inc). The flow cytometer was calibrated to detect the spheres in accordance with their excitation/emission wavelengths using the allophycocyanin (APC) and fluorescein isothiocyanate channels (FITC). The perfusion ratio was calculated by measuring the relative number of microspheres acquired in each channel.

*Statistics*

Statistical analysis was performed using SPSS 19.0 (SPSS, Inc, Chicago, IL, USA). All data were expressed as mean ± standard deviation. For comparing hemodynamics and continuous variables a t-test was used. For linear regression a Pearson's correlation coefficient was used and for comparison of multiple variables a one-way analysis of variance (ANOVA) was used. Bonferroni post-hoc analyses were used to compare the calculation of the perfusion reserve using different techniques. A Bland-Altman analysis was performed to determine the mean bias and limits of agreement between CMR and microsphere estimates of MPR. Statistical significance was considered for $P < 0.05$ and high significance was considered for $P < 0.01$.

## 5.4 Results

All mice tolerated the scanning without complication and rest/stress first-pass myocardial perfusion imaging was successfully performed. The mean overall imaging time was 34.6 minutes (± 7.4 minutes).

*Stress perfusion imaging*

Dipyridamole was successfully injected in all 5 mice via the tail vein. The mean heart rate increased following the injection, but not to a statistically significant degree (rest perfusion: 480 ± 27 beats/min, stress perfusion 503 ± 42 beats/min, p=0.08).

*Visual interpretation of perfusion images*

Overall image quality was 2.6±0.5 and quality was sufficient to outline myocardial contours for quantitative analysis in all studies (Figure 1). Breathing did not pose a significant problem as respiratory motion correction is incorporated into the *k-t* PCA algorithm. Typical transient subendocardial dark rim artifacts were noted in 2 studies, affecting in particular the inferolateral segments. These banding artifacts persisted for three to seven heartbeats during peak signal in the LV and affected 30–60% of the myocardial thickness.

*Perfusion Measurements*

In three animals, stress imaging was performed first, and in two animals rest was performed first. Signal intensity/time profiles derived during stress and rest showed similar features to human profiles (Figures 2). At rest, mean LV signal increased from 129± 24 (arbitrary units) before contrast delivery to a peak of 1777±253, resulting in an

enhancement ratio of 13.3. Mean myocardial signal increased from 120±6 before contrast to 518±79, with an enhancement ratio of 3.3. The mean resting MBF by Fermi-constrained deconvolution across the four myocardial segments was 4.1 ± 0.5 mL/g/min. There were no significant differences between the segments.

At hyperemic stress, mean LV signal increased from 118±37 before contrast delivery to a peak of 1854±209, resulting in an enhancement ratio of 15.9. Mean myocardial signal increased from 91±34 to 787±187, with an enhancement ratio of 8.0. The mean estimated hyperemic MBF was 9.6 ± 2.5 mL/g/min (Figure 3) (Table 1). There were no significant differences between the four segments. The increase in MBF during stress-induced hyperemia compared with rest MBF was significant (P=0.0054) with a derived myocardial perfusion reserve of 2.4 ±0.54.

*Confocal microscopy*

In the midventricular slices matching the perfusion imaging, both fluorescent colored microspheres were identified using confocal laser microscopy (Figures 4a and 4b). The cumulative mean of microspheres injected at rest was 162±32 and 397±115 at stress (p=0.0045) (Figure 5), with a mean count ratio of 2.4±0.51. Using Pearson's correlation, there was a strong association between MPR estimated by CMR and count ratio by confocal microscopy (R=0.79) and no significant difference was observed. On Bland-Altman analysis, the mean bias between CMR and microscopy was -0.07 (95% limit of agreement -0.73 to 0.59) (Figure 6a).

*Flow cytometry analysis*

The remaining myocardium was digested and sampled for flow cytometry analysis to calculate the relative number of microspheres and to determine a perfusion reserve (Figure 7). The overall mean perfusion reserve was 2.6±1.01, which showed good agreement, but higher variability, compared with the other techniques (Figure 8). Using Pearson's correlation, there was a strong association between MPR estimated by CMR and count ratio by flow cytometry (R=0.74) and no significant difference was observed. On Bland-Altman analysis, the mean bias for MPR estimation between CMR and microscopy was -0.26 (95% limit of agreement -1.69 to 0.73) (Figure 6b).

Using ANOVA to compare the perfusion reserve using the different techniques, there was no significant difference between the quantitative CMR data, manual counting of spheres and using confocal microscopy, (P=0.84, $R^2$=0.03). Bonferroni post-hoc testing did not show any significant difference between the results derived from different techniques (CMR and histology).

## 5.5 Discussion

This study has shown that dynamic contrast enhanced myocardial perfusion CMR during dipyridamole-stress in a murine model is feasible at 3 Tesla. MBF and MBF reserve estimates were derived in good agreement with the existing literature and the reference standard of microsphere injection.

The use of first-pass dynamic contrast enhanced myocardial perfusion CMR in rodent models has only recently been reported. The studies published to date used different methods to acquire myocardial perfusion data and in all data were acquired under resting conditions only. Coolen et al[14] performed acquisitions on a 9.4T Bruker animal scanner. Data acquisition extended over three heart-beats, with a temporal resolution of approximately 400 ms and a 15 ms acquisition window within the cardiac cycle. Acquisition was feasible and detected reduced regional blood flow in an LAD ligation model. This study, however, did not attempt absolute quantification and comparisons with the existing literature could not be made. Makowski et al[15] performed dynamic contrast enhanced myocardial perfusion CMR in five healthy C57BL/6J mice and four mice with induced myocardial infarction using a similar acquisition method as in our current study. Resting MBF in remote myocardium and control mice was 7.3 ± 0.9 ml/g/min with a reduction in resting MBF in infarcted myocardium matching histology. Nierop et al[13] performed resting imaging in a cohort of nine healthy C57BL/6 mice. They applied a dual-bolus approach for contrast delivery, applied in two separate scans, and demonstrated good repeatability of the method for estimation of resting MBF with a mean MBF of 7.3 ± 0.9 mL/g/min.

Previous studies have derived stress MPR in rodent models using other methods[7,19,20]. Jacquier et al[19] used arterial spin labeling to estimate MBF at rest and during adenosine stress in rats. Because of the long acquisition times of spin labeling techniques, rodents required prolonged anaesthesia and exposure to the stress agent. Moreover, the animals were divided into two separate groups to acquire the rest and stress data. The myocardial perfusion reserve was found to be 2.5±0.6. Raher et al[7] measured rest and adenosine stress myocardial perfusion in wild-type and nitric oxide synthase 3 deficient mice using echocardiography. They found a 2.5 fold increase in MBF estimated with echocardiography and microspheres in the wild-type mice. Murine contrast echocardiography however poses several limitations especially with regards to the spatial resolution, as high frequency probes (14MHz) preclude the use of harmonic imaging. Furthermore the validation in the study by Raher was not directly performed against closed chest mice and did not quantify absolute blood flow due to the saturation of signal in the LV cavity, which precluded normalization of the blood flow estimate.

The present study used a first pass CMR technique on a clinical scanner with a high spatial ($0.2mm^2$) and temporal resolution (43msec and acquisition at every heart beat) by using highly accelerated data acquisition. The *k-t* PCA framework for image reconstruction has been shown to improve temporal fidelity and in this study allowed reliable assessment of signal enhancements in the blood pools and in the myocardium and quantitative MBF measurements. The rapid acquisition (<30 seconds) of a first pass method compared with spin labeling methods meant that both stress and rest acquisition could be performed in the same study and in the same animals.

Estimates of both resting and stress in the current study were at the lower end of values reported in the previous literature. We measured a mean resting MBF of 4.1mL/g/min, compared with previously reported values of 4–7 mL/g/min[8,15,21-24] and a mean stress perfusion MBF of 9.6 ml/g/min compared with a value of 11.5 mL/g/min in the literature[25]. Myocardial perfusion reserve, calculated as the ratio of stress over rest MBF, however was consistent with the literature at 2.4, compared with 2.5 in the studies by both Jacquier[19] and Raher[7] and in excellent agreement with microsphere analysis. There are multiple potential reasons for the relatively low estimates of both resting and stress MBF in the current compared with previous studies, including the age of our murine model, the methods (including anaesthesic regime and greater heat loss from the large bore of clinical scanner over preclinical one, despite having temperature regulation), the acquisition and analysis method used. A small increment in isoflurane from 1.25% to 2% for example has been shown to increase myocardial perfusion[24] by at least two fold. We therefore chose a low isoflurane flow rate. In addition, acquisition with temporal undersampling methods can be associated with low pass filtering effects, which may have led to an underestimation of MBF.

In a recent clinical study[26] in patients with suspected ischaemic heart disease, which used a similar acquisition regime and quantification tool, absolute CMR estimates of MBF were lower than those obtained by PET. Consistent with our preclinical study, both stress and rest perfusion values were lower and cancelled out in the calculation of the MPR.

In both previous studies and our data, MBF reserve was lower than that reported for humans. A potential explanation for this observation is that mice do not increase their oxygen consumption by more than two fold during peak excercise[27]. Oxygen

consumption is a major trigger that increases myocardial blood flow[28]. Heart rate (which is predominantly under sympathetic control) does not increase by more than 50%[29] at maximal exercise in mice and therefore may need less coronary reserve than humans to respond to increased myocardial oxygen requirements[30].

In this study, we used dipyridamole as the stress agent. Dipyridamole has previously been used as an alternative or in conjunction with exercise for the evaluation of coronary artery disease in the clinical setting. In our study, dipyridamole caused an insignificant increase in heart rate and the slow injection regime was well tolerated. Compared with adenosine, dipyridamole has the advantage that it can be administered prior to contrast agent administration, so that only one venous access is required. However, our data show a variable response to dypyridamole in the five animals and it is noted that it may be less potent than adenosine[31]. More recently, the stress agent regadenoson has become available for clinical use. This agent was originally validated in rats and is reported to have fewer side effects than adenosine and to cause more marked hyperemia[32]. Like dipyridamole it can be infused as a bolus prior to giving the contrast agent. Future studies are warranted to test this agent, although questions still remain as the optimal timing with injection in as the hyperemic response is not as sustained as with dipyridamole.

In this study absolute perfusion was calculated by Fermi-deconvolution of the myocardial signal response with the arterial input function and applying previously described methods[17]. An important assumption for this technique is the linearity between signal intensity and contrast agent concentration. Particularly for the arterial input function this condition is not easily met because of saturation of the signal by high

contrast agent concentrations in the blood. To overcome this problem for the second injection of contrast we applied baseline correction[33] and randomized the order of rest and stress acquisitions, but saturation effects especially in the input function may have underestimated MBF. Other methods using a dual bolus strategy have been reported mainly in clinical studies. One recent report by van Nierop acquired dual bolus data under resting conditions and in two separate settings[13]. The method is challenging to perform in rodent models in addition to stress, but may present a future option for improved MBF estimation. Both single-bolus and dual-bolus perfusion methods have been shown to correlate closely with MBF in particular when myocardial perfusion is normal[34].

**Limitations**

Contrast and stress agent were delivered by hand. This process can in principle be automated to improve reproducibility. Our perfusion method acquires only a single slice, but more slices could be acquired at the expense of temporal resolution or in consecutive experiments. We did not perform true quantification of absolute MBF by microspheres because there are concerns about the validity of this technique in rodents[35]. We were therefore not able to establish if CMR systematically underestimated MBF, but were able to demonstrate good agreement for the more robust MBF reserve. Further refinements of the quantitative tool may be required for estimation of absolute MBF in murine models, however values for MPR appear to be consistent with the literature. Few investigators have used the microsphere method using the reference sample approach for absolute quantification[21,22,36,37].

## Conclusion

Dynamic contrast enhanced myocardial perfusion CMR during hyperemic stress in a mouse model is feasible. In this study, data were acquired on a 3 Tesla scanner using an approach similar to clinical acquisition protocols, thus facilitating translation of imaging findings between rodent and human studies. This may in future help elucidate mechanisms and develop therapies for cardiovascular disease. The rapid data acquisition of dynamic contrast enhanced myocardial perfusion CMR compared with arterial spin labeling will facilitate its incorporation into more comprehensive in vivo CMR protocols.

## 5.6 References

1. Schwitter J, Nanz D, Kneifel S et al. Assessment of myocardial perfusion in coronary artery disease by magnetic resonance: a comparison with positron emission tomography and coronary angiography. Circulation 2001;103:2230–2235.

2. Laine H, Raitakari OT, Niinikoski H et al. Early impairment of coronary flow reserve in young men with borderline hypertension. J Am Coll Cardiol 1998;32: 147–153.

3. Pop-Busui R, Kirkwood I, Schmid H et al. Sympathetic dysfunction in type 1 diabetes: association with impaired myocardial blood flow reserve and diastolic dysfunction. J Am Coll Cardiol. 2004; 44: 2368-74.

4. Geisterfer-Lowrance AA, Christe M, Conner DA et al. A mouse model of familial hypertrophic cardiomyopathy. Science 1996;272:731–734.

5. Gilson WD, Yang Z, French BA, Epstein FH. Measurement of myocardial mechanics in mice before and after infarction using multi-slice displacement-encoded MRI with 3D motion encoding. Am J Physiol Heart Circ Physiol 2005;288:H1491–1497.

6. Hirai T, Nohara R, Hosokawa R et al. Evaluation of myocardial infarct size in rat heart by pinhole SPECT. J Nucl Cardiol. 2000 ;7:107-11

7. Raher MJ, Thibault H, Poh KK et al. In vivo characterization of murine myocardial perfusion with myocardial contrast echocardiography: validation and application in nitric oxide synthase 3 deficient mice. Circulation 2007;116:1250–1257.

8. Kober F, Iltis I, Cozzone PJ, Bernard M. Myocardial blood flow mapping in mice using high-resolution spin labeling magnetic resonance imaging: influence of ketamine/xylazine and isoflurane anesthesia. Magn. Reson. Med. 2005; 53: 601–606.

9. Greenwood JP, Maredia N, Younger JF, Brown JM, Nixon J, Everett CC, Bijsterveld P, Ridgway JP, Radjenovic A, Dickinson CJ, Ball SG, Plein S. Cardiovascular magnetic

resonance and single-photon emission computed tomography for diagnosis of coronary heart disease (CE-MARC): a prospective trial. The Lancet. 2012; 379:453-460.

10. Schwitter J, Wacker CM, Wilke N, Al-Saadi N, Sauer E, Huettle K, Schönberg SO, Luchner A, Strohm O, Ahlstrom H, Dill T, Hoebel N, Simor T. MR-IMPACT II: Magnetic Resonance Imaging for Myocardial Perfusion Assessment in Coronary artery disease Trial: perfusion-cardiac magnetic resonance vs. single-photon emission computed tomography for the detection of coronary artery disease:a comparative m. Eur. Heart J. 2012;:doi:10.1093/eurheartj/ehs022.

11. Lockie T, Ishida M, Perera D, Chiribiri A, De Silva K, Kozerke S, Marber M, Nagel E, Rezavi R, Redwood S, Plein S. High-resolution magnetic resonance myocardial perfusion imaging at 3.0-Tesla to detect hemodynamically significant coronary stenoses as determined by fractional flow reserve. J Am Coll Cardiol. 2011 Jan 4;57(1):70-5.

12. Jerosch-Herold M, Wilke N, Stillman AE. Magnetic resonance quantification of the myocardial perfusion reserve with a Fermi function model for constrained deconvolution. Med Phys. 1998 Jan;25(1):73-84

13. Van Nierop BJ, Coolen BF, Dijk WJ,et al. Quantitative first-pass perfusion MRI of the mouse myocardium. Magn Reson Med. 2012 Aug.

14. Coolen BF, Moonen RP, Paulis LE, Geelen T, Nicolay K, Strijkers GJ. Mouse myocardial first-pass perfusion MR imaging. Magn Reson Med. 2010; 64:1658-63

15 Makowski M, Jansen C, Webb I et al. First-pass contrast-enhanced myocardial perfusion MRI in mice on a 3-T clinical MR scanner. Magn Reson Med. 2010;64:1592-8.

16. Pedersen H, Kozerke S, Ringgaard S, Nehrke K, Kim WY. k-t PCA: temporally constrained k-t BLAST reconstruction using principal component analysis. Magn Reson Med 2009;62:706–716.

17. Hautvast G, Chiribiri A, Zarinabad N, Schuster A, Breeuwer M, Nagel E. Myocardial blood flow quantification from MRI by deconvolution using an exponential approximation basis. *IEEE Trans Biomed Eng*. 2012;59:2060-2067

18. Swirski FK, Wildgruber M, Ueno T, Figueiredo JL et al. Myeloperoxidase-rich Ly-6C+ myeloid cells infiltrate allografts and contribute to an imaging signature of organ rejection in mice. J Clin Invest. 2010; 120:2627-34.

19. Jacquier A, Kober F, Bun S, Giorgi R, Cozzone PJ, Bernard M. Quantification of myocardial blood flow and flow reserve in rats using arterial spin labeling MRI: Comparison with a fluorescent microsphere technique. *NMR Biomed*. 2011;24:1047-1053

20. Waller C, Kahler E, Hiller KH, Hu K, Nahrendorf M, Voll S, Haase A, Ertl G, Bauer WR. Myocardial perfusion and intracapillary blood volume in rats at rest and with coronary dilatation: MR imaging in vivo with use of a spin-labeling technique. Radiology. 2000 Apr;215(1):189-97

21. Richer C, Domergue V, Gervais M, Bruneval P, Giudicelli JF. Fluospheres for cardiovascular phenotyping genetically modified mice. J Cardiovasc Pharmacol. 2000 Sep;36(3):396-404

22.Trabold F, Pons S, Hagege AA, Bloch-Faure M, Alhenc-Gelas F, Giudicelli JF, Richer-Giudicelli C, Meneton P. Cardiovascular phenotypes of kinin B2 receptor- and tissue kallikrein-deficient mice. Hypertension. 2002 Jul;40(1):90-5

23. Antkowiak P, Janiczek R, Gibberman L, Xu C, Kramer C, Meyer C, French B, Epstein F. Quantitative first-pass perfusion CMR of the mouse heart. *J Cardiovasc Magn Reson* 2010; **12**( Suppl 1): M10

24. Vandsburger MH, Janiczek RL, Xu Y, French BA, Meyer CH, Kramer CM, Epstein FH. Improved arterial spin labeling after myocardial infarction in mice using cardiac and

respiratory gated look-locker imaging with fuzzy C-means clustering. Magn Reson Med. 2010; 63:648-57.

25. Vandsburger MH, French BA, Helm PA, Roy RJ, Kramer CM, Young AA, Epstein FH. Multi-parameter in vivo cardiac magnetic resonance imaging demonstrates normal perfusion reserve despite severely attenuated beta-adrenergic functional response in neuronal nitric oxide synthase knockout mice. Eur Heart J. 2007 Nov;28(22):2792-8

26. Morton G, Chiribiri A, Ishida M, Hussain ST, Schuster A, Indermuehle A, Perera D, Knuuti J, Baker S, Hedström E, Schleyer P, O'Doherty M, Barrington S, Nagel E. Quantification of absolute myocardial perfusion in patients with coronary artery disease: comparison between cardiovascular magnetic resonance and positron emission tomography. J Am Coll Cardiol. 2012 Oct 16;60(16):1546-55

27.Kemi OJ, Loennechen JP, Wisloff U, Ellingsen O. Intensity-controlled treadmill running in mice: cardiac and skeletal muscle hypertrophy.J Appl Physiol. 2002;93:1301–1309.

28. Tune JD, Gorman MW, Feigl EO. Matching coronary blood flow to myocardial oxygen consumption. J Appl Physiol. 2004;97:404–415.

29. Just A, Faulhaber J, Ehmke H. Autonomic cardiovascular control in conscious mice. *Am J Physiol Regul Integr Comp Physiol*. 2000;279:R2214-2221.

30. Rohrer DK, Schauble EH, Desai KH, Kobilka BK, Bernstein D. Alterations in dynamic heart rate control in the beta 1-adrenergic receptor knockout mouse. Am J Physiol. 1998; 274: H1184–1193.

31. Rossen JD, Quillen JE, Lopez AG, Stenberg RG, Talman CL, Winniford MD. Comparison of coronary vasodilation with intravenous dipyridamole and adenosine. J Am Coll Cardiol. 1991;18:485-491

32. Cerqueira MD, Nguyen P, Staehr P, Underwood SR, Iskandrian AE; ADVANCE-MPI Trial Investigators. Effects of age, gender, obesity, and diabetes on the efficacy and safety

of the selective A2A agonist regadenoson versus adenosine in myocardial perfusion imaging integrated ADVANCE-MPI trial results. JACC Cardiovasc Imaging. 2008 May;1(3):307-16

33. Jerosch-Herold M, Seethamraju RT, Swingen CM, Wilke NM, Stillman AE. Analysis of myocardial perfusion MRI. J Magn Reson Imaging 2004;19:758 –70.

34. Christian TF, Aletras AH, Arai AE. Estimation of absolute myocardial blood flow during first-pass MR perfusion imaging using a dual-bolus injection technique: comparison to single-bolus injection method. J Magn Reson Imaging. 2008;27:1271-29.

35. Decking UK, Pai VM, Bennett E et al. High-resolution imaging reveals a limit in spatial resolution of blood flow measurements by microspheres. *Am J Physiol Heart Circ Physiol*. 2004;287:H1132-1140

36. Prinzen FW, Bassingthwaighte JB. Blood flow distributions by microsphere deposition methods. Cardiovasc Res. 2000;45:13-21.

37. Zhang H, Qiao H, Frank RS et al. Spin-Labeling Magnetic Resonance Imaging Detects Increased Myocardial Blood Flow After Endothelial Cell Transplantation in the Infarcted Heart. Circulation: Cardiovascular Imaging. 2012;5:210-217

## 5.7 Tables

Table 1. MR derived measurements of signal intensity (SI) and perfusion values

| N | Scan | AIF SI Baseline | AIF SI Max | Enhancement Ratio | LV SI Baseline | LV SI Max | Enhancement Ratio | MBF/ ml/g/min | MPR |
|---|---|---|---|---|---|---|---|---|---|
| 1 | stress* | 115±24 | 2220±412 | 18.30 | 81±20 | 945±210 | 10.67 | 9.2 | 2.71 |
| | rest | 113±27 | 2199±460 | 18.46 | 116±26 | 650±144 | 4.60 | 3.4 | |
| | | | | | | | | | |
| 2 | stress | 170±36 | 1780±330 | 9.47 | 146±29 | 1021±243 | 5.99 | 8.7 | 2.12 |
| | rest* | 159±29 | 1602±313 | 9.08 | 111±22 | 440±97 | 2.96 | 4.1 | |
| | | | | | | | | | |
| 3 | stress* | 83±18 | 1690±331 | 19.36 | 66±15 | 580±106 | 7.79 | 12.5 | 2.98 |
| | rest | 138±26 | 1637±362 | 10.86 | 125±26 | 490±99 | 2.92 | 4.2 | |
| | | | | | | | | | |
| 4 | stress | 137±35 | 1777±367 | 11.97 | 100±23 | 704±142 | 6.04 | 6.2 | 1.59 |
| | rest* | 97±26 | 1616±369 | 15.66 | 122±27 | 520±102 | 3.26 | 3.9 | |
| | | | | | | | | | |
| 5 | stress* | 84±19 | 1804±391 | 20.48 | 64±16 | 684±121 | 9.69 | 11.6 | 2.42 |
| | rest | 138±22 | 1832±393 | 12.28 | 125±23 | 489±94 | 2.91 | 4.8 | |
| | | | | | | | | | |
| | | | | | | | | | |
| Mean | Stress | 118±37 | 1854±209 | 15.92±4,89 | 91±34 | 787±187 | 8.04±2.12 | 9.64±2.5 | 2.36±0.54 |
| Mean | Rest | 129±24 | 1777±254 | 13.27±3,78 | 120±6 | 518±79 | 3.33±0.72 | 4.08±0.5 | |

* denotes which scan was performed first
LV = Left ventricle
AIF = Arterial input function
MBF = Myocardial blood flow
MPR = Myocardial perfusion reserve

## 5.8 Figure legends

Figure 1. Series of dynamic images after contrast bolus injection (0.1 mmol/kg body weight Gd-DTPA) in a short axis section of a mouse . Spatial resolution was 0.2x0.2mm$^2$ (reconstructed to 0.13 × 0.13mm$^2$),Images demonstrate the baseline scan (a), as well as the passage of the contrast agent in the RV (b), LV (c), and in the myocardium (d).

Figure 2. Mean SI/phase profile from five mice at rest and stress. The different color codes represents the passage of the contrast agent (CA) within the LV and myocardial cavity.

Figure 3. Ladder plots demonstrating the increase in MBF by CMR between rest and dipyridamole stress.

Figure 4a. Stitched image of a confocal short axis mid section of murine myocardium following microspheres injected at stress, depicted in red.

Figure 4b. Stitched image of a confocal short axis mid section of murine myocardium following microspheres injected at rest, depicted in green. Fewer spheres are observed than in comparison the stress images.

Figure 5. Absolute number of microspheres counted using confocal microscopy at stress and rest using sectioned mid ventricular slices.

Figure 6a: Bland-Altman analysis of MPR demonstrating agreement by CMR and confocal microscopy.

Figure 6b: Bland-Altman analysis of MPR demonstrating agreement by CMR and flow cytometry.

Figure 7. Histogram showing the number of stress (blue) vs rest (red) microspheres in a sample of remaining myocardium showing a relative increased detection of stress to rest microspheres.

Figure 8. Comparison of the different methods (confocal microscopy, MR and flow cytometry) of assessing perfusion reserve.

Figure 1. Example images

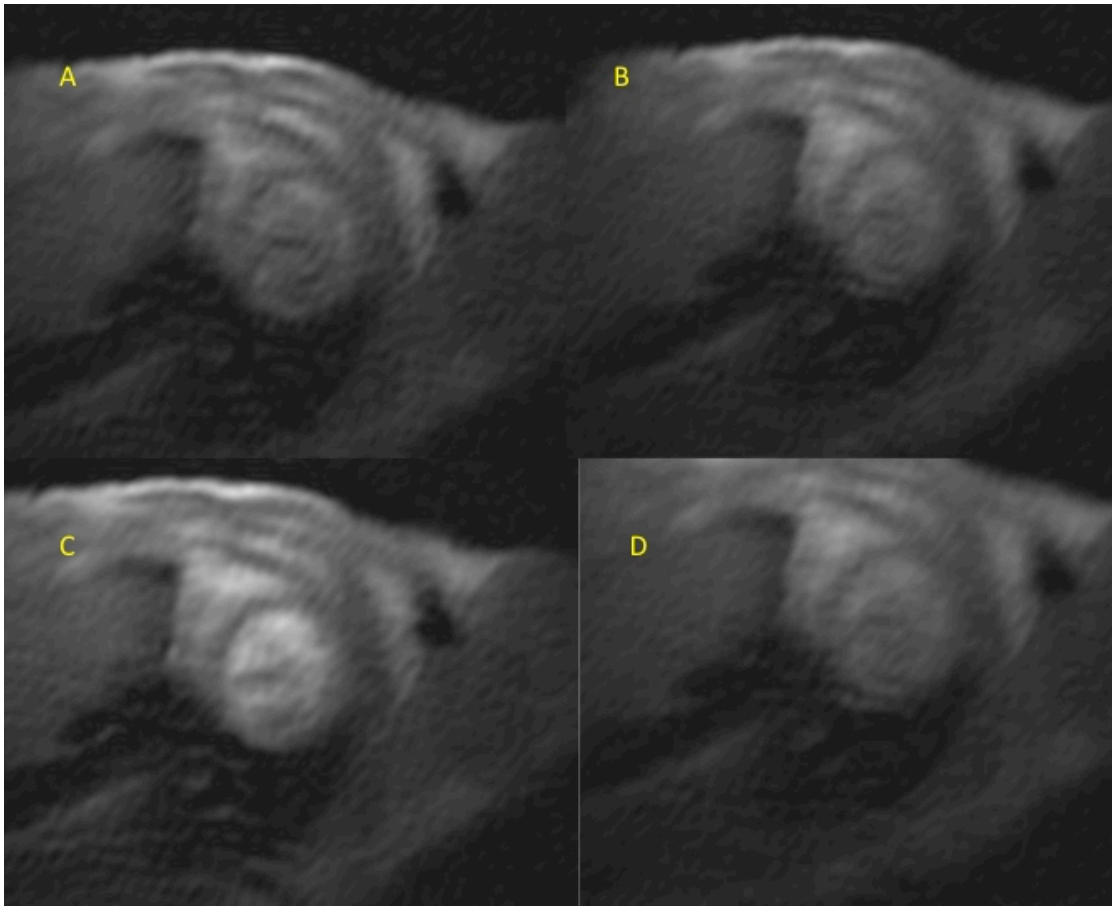

Figure 2. Mean signal intensity/time plots (n=5)

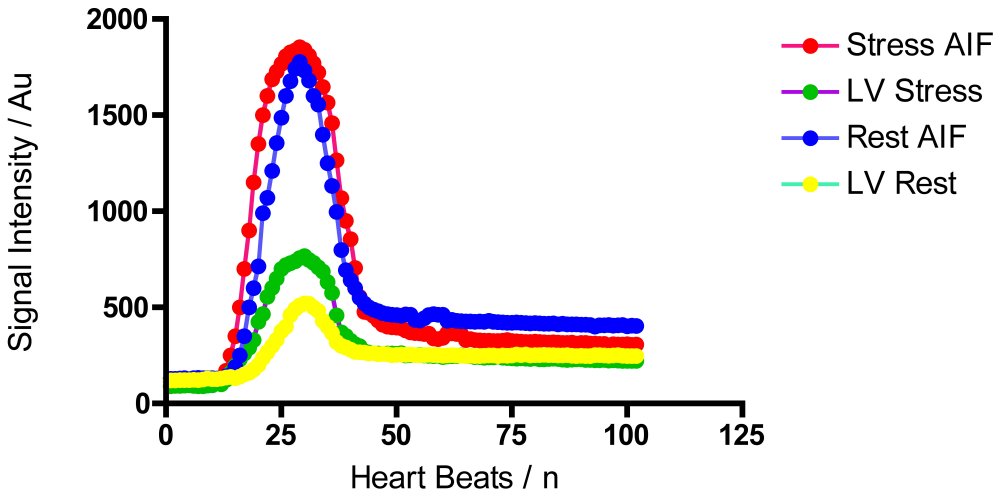

Figure 3. MBF by CMR between rest and dipyridamole stress

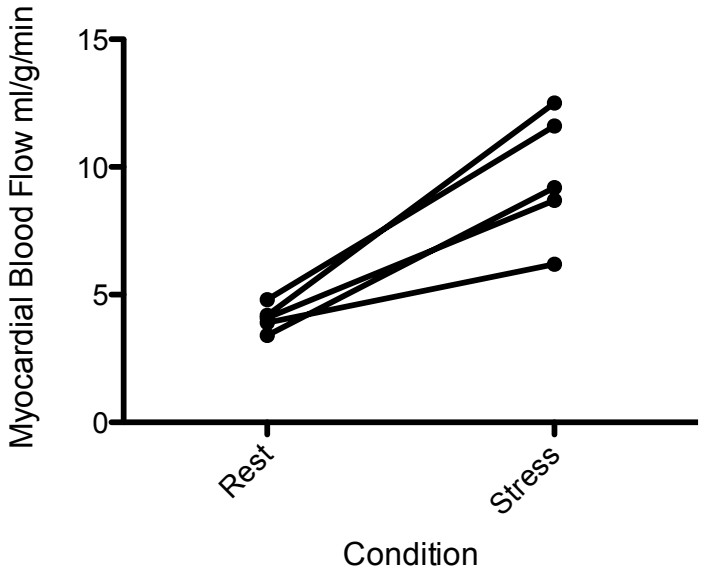

Figure 4a. Confocal image at stress

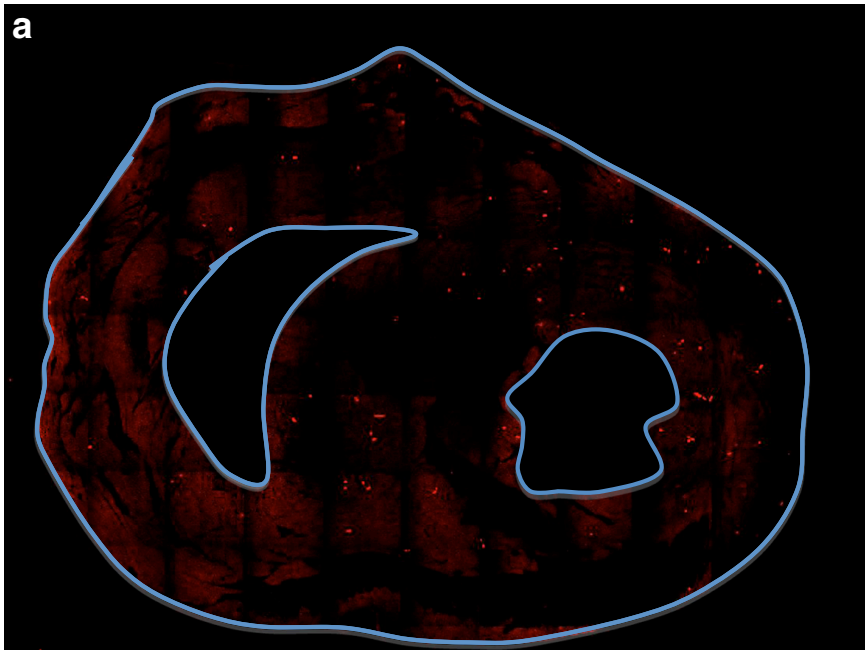


Figure 4b. Confocal image at rest

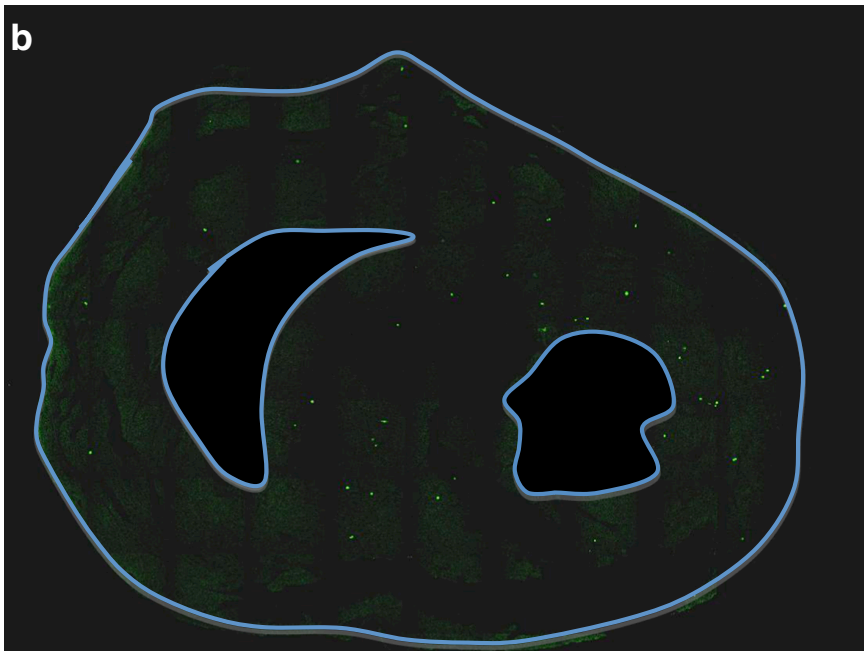

Figure 5. Absolute number of microspheres with confocal microscopy at stress and rest

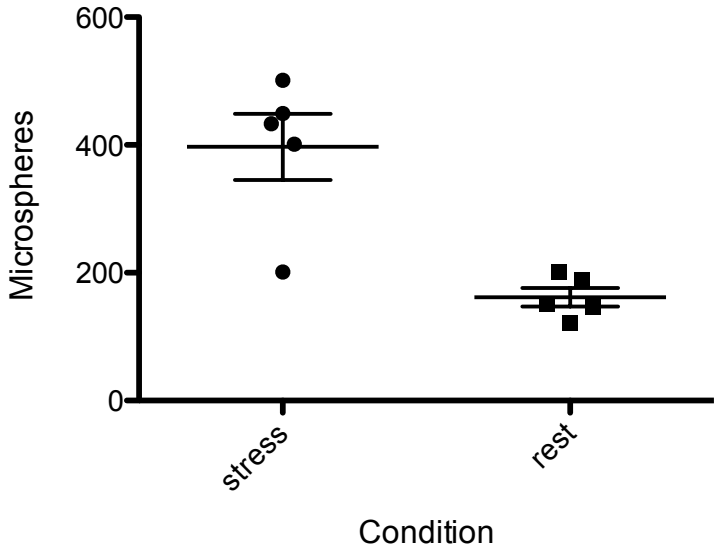

Figure 6a: Bland-Altman analysis of MPR (CMR-Confocal Microscopy)

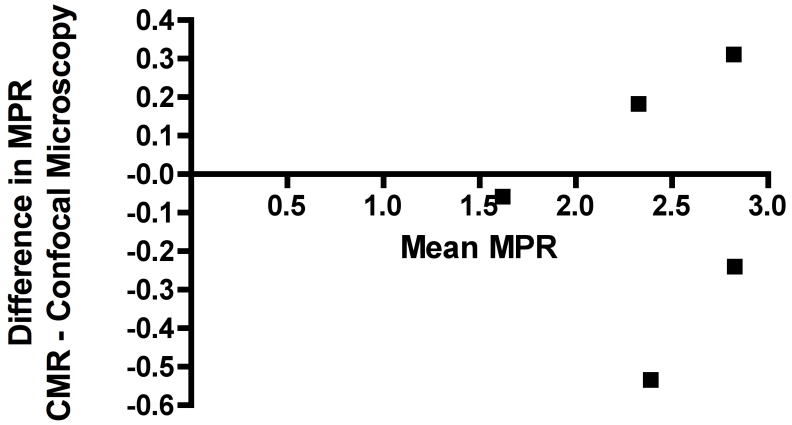

Figure 6b: Bland-Altman analysis of MPR (CMR-Flow Cytometry)

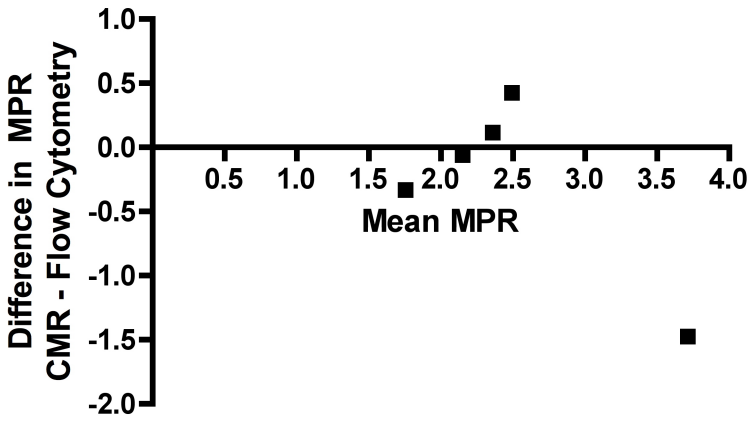

Figure 7: Histogram of numbers of stress (blue) vs rest (red) microspheres

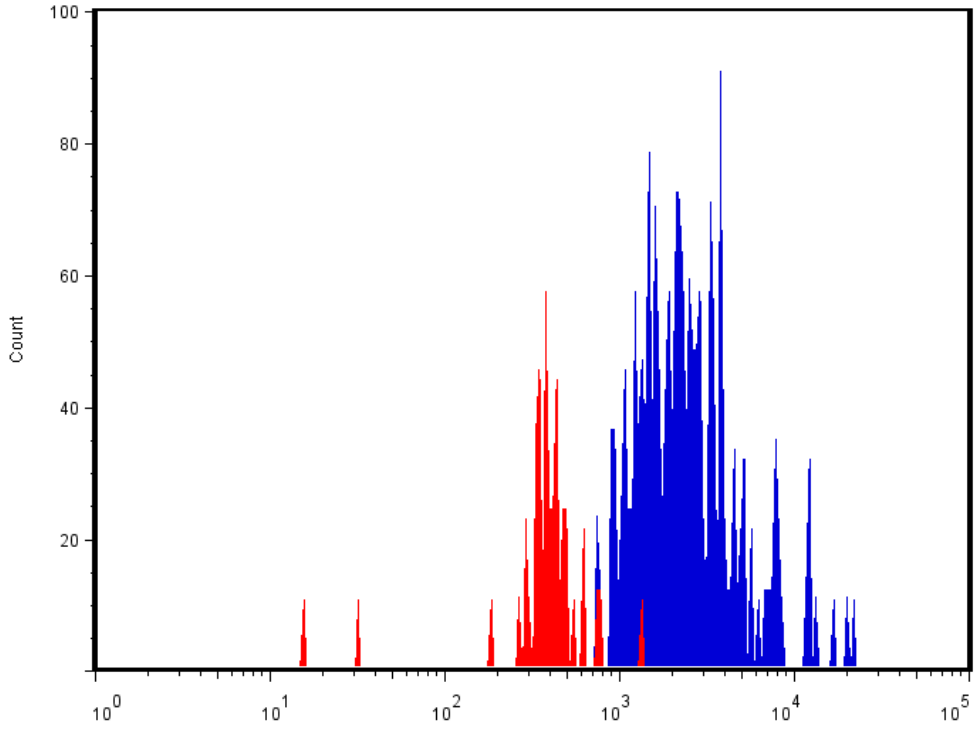

Figure 8: Comparisons of myocardial perfusion reserve (MPR) between Confocal Microscopy, Quantitative CMR and Flow Cytometry

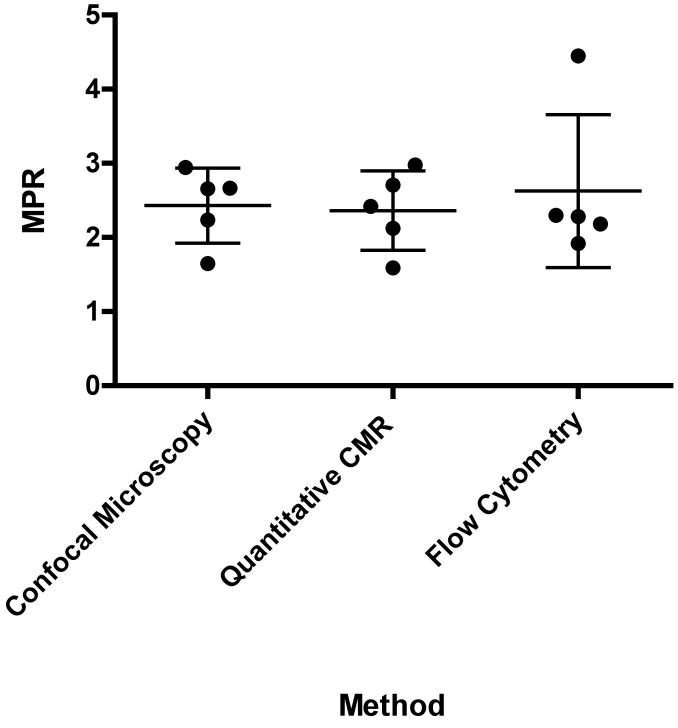

# Chapter 6 Conclusion

## 6.1 Introduction

Perfusion CMR imaging is an expanding field, which has been demonstrated to establish the diagnosis (159-161) and prognosis (213,214) of patients with IHD. A number of technical developments have been achieved including the use of higher-field-strength (221) scanners, faster gradient systems, receiver coils and pulse sequence design. Despite these advances, limitations exist due to constraints on acquisition because of the high temporal and spatial resolution requirements as well as the relatively large cardiac coverage. In this thesis we present the use of *k*-*t* PCA spatiotemporal acceleration methods in both a clinical and pre-clinical model.

## 6.2 Accelerated Imaging

The nature of dynamic imaging allows scan acceleration by exploiting spatiotemporal redundancy combined with complex reconstruction methods (202,235). Accelerated imaging is achieved by skipping data points in both time and space. The missing data are recovered based on the data at the neighbouring *k*-space positions and time points using prior assumptions of the correlation of the data. Increased skipping leads to higher acceleration at the potential expense of increased artefacts. The choice of skipping pattern will also influence the imaging artefacts (234).

Most accelerated methods adopt a variable density approach sampling the centre of the *k*-space more frequently than the periphery, as it contains the strongest signals. Acquiring higher-intensity signals will result in less marked artefacts. Non-Cartesian including radial and spiral acquisition approaches may minimise dark-rim artefacts and are more robust to motion, as they take a large sample from the centre of the *k*-space. Artefacts will appear more diffuse and subtle but are computationally demanding and images are often reconstructed offline, which precludes clinical use (234).

Techniques for exploiting spatiotemporal redundancy continue to evolve and have been implemented in routine clinical practice. These methods have also been utilised in other modalities including cardiac CT for X-ray dose reduction (279) and PET imaging for noise reduction (280).

The conventional and commonly used speed-up techniques *k-t* BLAST and *k-t* SENSE have previously been used in perfusion CMR imaging. They have particular use where there is compact representation in the *x-f* space. In myocardial perfusion imaging this is more of a problem due to respiratory and cardiac motion which leads to temporal blurring and redundant signal aliasing in the reconstructed images (234). *K-t* PCA constrains the reconstruction as it exploits the *x*-PC space as an alternative method to correlate the training data, which are acquired at full temporal resolution (236). The mathematical correlations within the *x*-PC space compared with the *x-f* space allow *k-t* PCA to acquire at higher acceleration with improved temporal fidelity (203).

## 6.3 Aims and Validation of *k-t* PCA with 3D Perfusion CMR

In this thesis, *k-t* acceleration with PCA reconstruction was used to demonstrate the feasibility of 3D whole-heart coverage. The high diagnostic accuracy of this technique was validated against the reference standard FFR (281). Following this, a comparison for determination of ischaemic burden was made against the clinical reference standard SPECT. This demonstrated the advantages of whole-heart coverage without the use of ionising radiation (282). Further technical developments to improve image characteristics were made in a feasibility study of bSSFP 3D perfusion CMR with *k-t* PCA acceleration. Although signal characteristics were improved, there was a trade-off with more image artefacts, which did not necessarily translate to improved image quality (283).

Since the earliest studies on perfusion CMR, a number of refinements have been made to optimise the sequences and methodology. Initial attempts were focused on single-slice (284) sequences but were sensitive to heart-rate variability and poor coverage. Most current myocardial perfusion CMR methods cover the heart in three short-axis slices, as recommended by international guidelines (104). Efforts are ongoing to improve cardiac

coverage. Three-dimensional acquisition methods overcome the limited myocardial coverage offered by 2D methods.

**Development of 3D Perfusion CMR**

Following the initial validation study a number of studies have been published investigating the use of 3D perfusion CMR imaging (Table 2). *CS=compressed sensing

| Author | Year | Acceleration Method | Factor | Trajectory | Resolution /mm | Acquisition Window/ms | Field Strength /T | Notes |
|---|---|---|---|---|---|---|---|---|
| Shin (251) | 2008 | TSENSE | 6 | Cartesian | 3.0x4.5x10.0 | 304 | 3 | |
| Shin (252) | 2010 | TSENSE | 6 | Cartesian | 2.8x4.2x10.0 | 254-305 | 3 | |
| Manka (253) | 2011 | *k-t* SENSE | 6 | Cartesian | 2.3x2.3x10.0 | 200 | 3 | |
| Vitanis (203) | 2011 | *k-t* PCA | 7 | Cartesian | 2.3x2.3x10.0 | 225 | 3 | |
| DiBella (285) | 2012 | CS temporal | 14 | Radial | 2.2x2.2x10.0 | 310 | 3 | Ungated |
| Manka (286) | 2012 | *k-t* PCA | 7 | Cartesian | 2.3x2.3x10.0 | 225 | 1.5 | |
| Jogiya (281) | 2012 | *k-t* PCA | 7 | Cartesian | 2.3x2.3x5.0 | 225 | 3 | |
| Chen (240) | 2012 | CS spatiotemporal | 10 | Radial | 2.2x2.2x8 | 300 | 3 | Gated |
| Shin (241) | 2013 | *k-t* SENSE | 5 | Spiral | 2.4x2.4x9.0 | 230 | 1.5 | |
| Giri (287) | 2014 | GRAPPA | 4 | Cartesian | 2.2x2.8x8.0 | 300-380 | 1.5 | SSFP |
| Motwani (288) | 2014 | *k-t* PCA | 7 | Cartesian | 2.3x2.3x5.0 | 192 | 3 | Free-breathing |
| Schmidt (289) | 2014 | *k-t* PCA | 7 | Cartesian | 2.3x2.3x10.0 | 205-225 | 3 | Motion-corrected |
| Akcakaya (290) | 2014 | Localised CS Spatiotemporal | 10 | Cartesian | 2.3x2.3x10.0 | 250 | 1.5 | |
| Jogiya (282) | 2014 | *k-t* PCA | 7 | Cartesian | 2.3x2.3x5.0 | 191 | 3 | |
| Jogiya (283) | 2014 | *k-t* PCA | 7 | Cartesian | 2.3x2.3x5.0 | 191 | 3 | |
| Wang (291) | 2015 | CS spatiotemporal | 11 | Cartesian | 2.4x2.4x6.0 | 255 | 3 | |
| Manka (292) | 2015 | *k-t* PCA | 7 | Cartesian | 2.3x2.3x5.0 | 200 | 3 | |
| McDiarmid (293) | 2015 | *k-t* PCA | 7 | Cartesian | 2.3x2.3x5.0 | 192 | 3 | 3D vs. 2D |

Table 2 Summary of 3D perfusion CMR literature

Since the early feasibility studies using TSENSE acceleration methods, Shin et al. (251) have demonstrated the potential benefits of 3D whole-heart coverage as compared to 2D imaging methods. The imaging protocols had a number of limitations, including significant dark-rim artefacts from the lower spatial resolution and motion artefacts due to the long acquisition window. There was also flickering in the TIC due to the use of early temporal acceleration methods. Significant advances were made using *k-t* parallel imaging techniques. These techniques allowed improvements in many of the parameters including shorter acquisition windows and a greater spatial resolution of 2.3 mm.

Using a *k-t* SENSE acceleration method, Manka et al. showed that 3D perfusion CMR can detect angiographically defined IHD with high diagnostic accuracy (253). One of the main limitations of this study was the use of a functional test compared against an anatomical test as the gold standard. The degree of coronary stenosis and its haemodynamic consequence correlate poorly.

In this thesis, a new and updated *k-t* PCA method was applied alongside additional newer technologies including local RF shimming techniques. This achieved a similar high diagnostic accuracy with a sensitivity of 91%, specificity of 90% and diagnostic accuracy of 91% at 3T in 53 patients. FFR was used as the reference standard for the detection of significant IHD. CMR estimation of ischaemic burden and the invasive Duke Jeopardy Score was also compared and a strong correlation between the two methods was demonstrated ($r = 0.82$; 95% CI: 0.70 to 0.89; $p<0.0001$) (281).

Manka et al. validated 3D perfusion CMR at a lower field strength of 1.5T with FFR as the reference for IHD (286). Recruiting 120 patients across two centres,, the technique yielded a sensitivity of 90%, specificity of 82% and diagnostic accuracy of 87%. The authors also demonstrated high reproducibility in measuring ischaemic burden in a subset of patients.

The measurement of ischaemic burden was validated as part of this thesis against the clinical standard SPECT. There was no difference between the modalities in the comparison of ischaemic burden (282). In a sub-study, a simulated three-slice analysis was performed against whole-heart imaging and did not demonstrate any difference in ischaemic burden. The limitations of this method have been acknowledged namely,

selecting three slices of a 3D data set was not equivalent to acquiring a three-slice 2D data set.

McDiarmid followed on from this study and compared 27 patients with stable angina undergoing coronary angiography (293). Patients underwent both high-resolution 2D and whole-heart 3D perfusion CMR. The authors' findings were similar to those presented here. There was no difference in the magnitude of ischaemic burden and there was a strong correlation between the techniques. Image quality, artefacts and diagnostic confidence scores were similar for both. The limits of agreement were relatively wide in this study. This highlights the small size of the study, but also the limitations of applicability around the 10% clinically relevant threshold. A larger study is therefore warranted.

In parallel, a multi-centre evaluation of 3D perfusion CMR was performed with FFR as the comparator, across five single-vendor sites. One hundred and fifty-five patients were scanned; the largest source of recruitment in this study was from works in this thesis. All analysis was performed in a core laboratory and image quality was reported as good. The sensitivity and specificity of 3D perfusion CMR was 84.7% and 90.8%, respectively, against FFR. QCA (≥50%) yielded a disease prevalence of 65.3% and a sensitivity and specificity of 76.5% and 94.2%, respectively (292).

Additional clinical studies have focused on the functional assessment of 3D quantitative perfusion. Motwani et al. demonstrated the feasibility of quantitative perfusion in 35 patients when comparing MPR in systole and diastole (288). Although diagnostic accuracy was similar there was better image quality in systole. The study also proved consistent with previous studies in concluding that myocardial blood flow was greater in systole than diastole.

Two clinical reports have shown the potential benefit of hybrid imaging combining 3D perfusion CMR imaging with non-invasive MR coronary imaging (Figure 26) (294,295). Current guidelines recommend hybrid imaging for planning myocardial revascularisation. There are however limitations with the other techniques, as SPECT imaging has inferior sensitivity compared with perfusion CMR. There is a radiation

burden associated with CT imaging. This new method is an exciting development in the dual assessment of coronary anatomy and its functional significance.

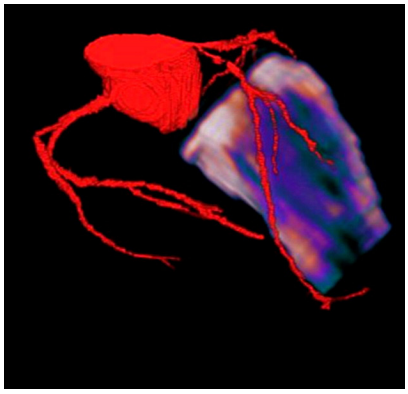

**Figure 25 Three-dimensional hybrid imaging.** Adapted from (295). Three-dimensional hybrid imaging of MR coronary angiography with 3D perfusion, demonstrating a combined anatomical and functional assessment of a patient with proximal LAD stenosis and anterior wall ischaemia**.**

A number of technical developments have been proposed, which attempt to overcome problems with respiratory motion artefacts. Akcakaya used "compressed sensing" to allow free breathing with an acquisition window of 250 ms and similar spatial resolution to current studies (290). Imaging was not performed with stress, which is likely to increase heart and respiratory rate and further reduce the durations of minimal cardiac motion. Schmidt used an iterative *k-t* PCA method and demonstrated the feasibility of correction of respiratory motion for 3D perfusion imaging (289).

As an alternative to Cartesian read-out newer techniques have been based on spiral and radial trajectories and have shown promise. None of the studies to date have been performed under stress. Initial feasibility studies by DiBella, demonstrat some of the highest spatial resolutions reported to date. A spatial resolution up to 2.0 mm was achieved at the cost of an increased window acquisition of 310 ms (285). This study was limited to phantoms and a volunteer, and the images were ungated. Subsequently, a gated study was reported with a variable FOV, with improved spatial resolution up to 1.8 mm with an acquisition window of 300 ms (240).

Spiral sequences have been proposed as a more efficient sampling of *k*-space with the smallest undersampling factor applied (five fold). Shin et al. demonstrated the feasibility

of this technique in seven volunteers and demonstrated similar signal characteristics of 2D single-slice and 3D imaging (241).

A novel study reported the use of bSSFP for 3D myocardial perfusion MRI, using no magnetisation preparation but maintaining steady state by continuous application of the bSSFP kernel throughout the scan (287). This approach was feasible and demonstrated good signal characteristics. As imaging was gated to mid-diastole, the acquisition was limited to either single-slice imaging or single-slab 3D encoding, and the read-out duration ranged between 300 and 380 ms. As demonstrated in this thesis, bSSFP imaging has some advantages including favourable signal characteristics (283). It was also feasible to perform stress perfusion studies with similar image quality. Unfortunately, this paper has shown that these benefits can often be mitigated by artefacts affecting interpretation, as has been described with 2D perfusion imaging (296).

**Advantages of 3D Perfusion CMR**

Although conventional multi-slice imaging is accurate for diagnostic purposes, the selective coverage with variable gaps between slices limits its comparison with other whole-heart CMR measurements including cine imaging and LGE. Matching a stress 3D perfusion CMR scan with the corresponding stack of LGE images may improve delineation and quantification of peri-infarct ischaemia.

As all data in 3D myocardial perfusion CMR are acquired in a single cardiac and respiratory phase, it is robust to inter-frame motion. The 3D acquisition is also more signal-to-noise efficient than 2D imaging, and, as all data are acquired in the same shot, fewer compromises regarding cardiac phase are necessary. This may have further relevance when quantifying perfusion and perfusion reserve.

Improved coverage of inducible perfusion abnormalities observed in conditions of microvascular dysfunction including diabetes and LV hypertrophy can help in differentiation from epicardial obstructive IHD for the purpose of improved risk stratification (254).

Two-dimensional imaging in comparison with continuous coverage by 3D imaging has been shown to be less accurate in measuring ischaemic burden (251). In clinical practice, ischaemic burden is most commonly measured by MPS. It is an important prognostic factor in IHD and in accordance with guidelines (248) (297) may help identify and stratify patients who will benefit most from revascularisation compared with medical therapy.

Compared with SPECT, the higher resolution of 3D myocardial perfusion CMR without exposure of patients to ionising radiation make the latter an ideal method for serial imaging and to assess the efficacy of treatment designed to improved regional blood flow (298).

**Disadvantages of 3D Perfusion CMR**

Three-dimensional perfusion is more vulnerable to respiratory and cardiac motion artefacts due to the longer acquisition window compared with 2D multi-slice imaging. Two-dimensional imaging also allows spatiotemporal acceleration methods to enable higher-spatial-resolution acquisition. Higher spatial resolution offers several benefits including detection of subendocardial ischaemia and reduced dark-rim artefacts (199). The comparative benefits of investing acceleration methods into improved cardiac coverage against spatial resolution remain a source of debate (249).

**Clinical role of 3D myocardial perfusion CMR**

Three-dimensional myocardial perfusion CMR is feasible at both currently used field strengths. It provides diagnostic accuracy comparable to 2D methods against QCA and FFR, and allows accurate calculation of the ischaemic burden compared with invasive and non-invasive methods. Preliminary results from multi-centred studies are promising and support its use in the detection of IHD.

## 6.4 Accelerated myocardial perfusion CMR in preclinical studies

In parallel, in this thesis, *k-t* PCA was applied in a pre-clinical model to demonstrate that fully quantitative, accelerated stress first-pass perfusion imaging was feasible to meet the high requirements of extreme heart rates, spatial resolution and acquisition speed in a clinical scanner (299).

Rodent models play a key role in the development of our understanding of CV disease and novel therapies. Due to the small size and high heart rates (up to 600 beats per minute in mice), first-pass perfusion imaging in murine models is challenging. Pre-clinical CMR studies in murine models are usually performed in non-clinical high-field MR magnets with field strengths ranging from 4.7 to 17.6T (268-270). The high field strengths provide increased SNR and spatial resolution required for adequate signal.

However, there are inherent problems with the availability and cost of the specialised software of these systems. As an alternative, clinical scanners have been used for murine CMR, with obvious disadvantages of lower field strength and less optimised set-up. Despite this, advantages include a wider availability the possibility to translate existing clinical pulse sequences and apply existing spatiotemporal acceleration methods. For myocardial perfusion CMR, lower-field-strength scanners also have advantages, as the longitudinal relaxation times of gadolinium-based contrast agents decrease with increased field strength.

### Advances in murine perfusion imaging

Spatiotemporal undersampling methods to meet the high requirements of extreme heart rates, spatial resolution and acquisition speed in murine first-pass perfusion CMR have been reported using a clinical scanner (272) and dedicated non-clinical MR scanner (275). Makowski et al. (272) used 10-fold *k-t* acceleration quantitative measurement of myocardial first-pass perfusion at rest before and after MI. Myocardial perfusion was comparable to that measured invasively by microspheres in mice (300). Coolen used a

segmented ECG-triggered acquisition in combination with parallel imaging acceleration at 9.4T (301). Van Nierop later used a dual-bolus approach with the previously described parallel imaging technique and showed good repeatability (275). Using this imaging protocol it was later shown that myocardial perfusion was significantly reduced in murine models of LV hypertrophy (302).

This thesis has been able to demonstrate the feasibility of accelerated imaging techniques to enable acquisition of fully quantitative CMR stress perfusion in a murine model in a clinical scanner, and to validate this against the reference standard of microspheres (299). Naresh proposed using a dual-contrast technique based upon signal saturation with $k_y$-t undersampling. Similar to the findings presented here, using a coronary vasodilator absolute perfusion and MPR were significantly increased in control mice (42). In a diet-induced obese model, both stress perfusion and MPR were significantly reduced. Using the same methodology a comparison of first-pass perfusion against ASL demonstrated the speed gain benefits of this technique. The acquisition time for first-pass perfusion imaging was less then a minute but approximately 40 minutes for ASL (303), which remains one of the main limitations of this alternative technique.

**Outlook for pre-clinical perfusion imaging**

Advances in accelerated CMR imaging techniques for evaluation of murine cardiac perfusion are now enabling previous limitations to be overcome. The techniques have until now been used in diseased-state models but in the future could be applied in genetically modified models, in order to study mechanisms which underpin early changes in perfusion for earlier detection and management of IHD. Validation and feasibility assessment using widely available clinical scanners may also allow greater scope for facilitation of imaging protocols in rodent and human studies.

## 6.5 High-Resolution, Quantification and Reproducibility Studies

Although not the primary aim of the thesis, it has also been shown that spatiotemporal speed-up techniques can be invested to improve the in-plane spatial resolution of perfusion CMR to <2 mm. *k-t* acceleration was used for high-resolution and three-slice coverage with every heartbeat at higher heart rates. The main benefits of high-resolution imaging include a reduction in dark-rim artefacts (304) and better detection of subendocardial ischaemia, which has been shown to improve diagnostic accuracy (199). The use of higher resolution has also been shown to quantify transmural gradients accurately as an alternative method for detecting IHD (305). With higher resolution, direct comparison can be made with other functional methods including LGE and cine imaging for the assessment of viability. Lower temporal resolution is known to influence the accuracy and calculation of MPR index (306).

Quantitative perfusion CMR analysis is a promising technique, which gives robust assessment and greater objectivity over qualitative assessment. Inter-study reproducibility has been shown to be reliable using current methods.

Knowing the inherent variability of a technique is critical for interpreting the significance of changes in measurements. Using spatiotemporal acceleration methods for higher resolution this thesis has assessed the inter-study reproducibility of segmental and global quantitative perfusion and the influence of diurnal variation (307). Perfusion scans were performed three times on a single day in 11 volunteers achieving a spatial resolution of up to 1.3 mm. Inter-study reproducibility was reasonable and demonstrated to be best for global rest perfusion. There was significant diurnal variation in perfusion values.

Larghat et al. used two-fold SENSE and showed reproducibility was affected by variability between intra-observer, inter-observer and inter-study comparisons (308). Notably, semi-quantitative measures were more reproducible than quantitative analysis. Goykhman later retrospectively studied the inter- and intra-observer reliability of commercially available software for the calculation of MPRI (309). This study showed

there was also measurement variation in the post-processing of perfusion CMR. Although not fully understood, the variation was thought to be multi-factorial. These factors include variations in data acquisition, stress response, image quality and the determination of myocardial contours and AIF. The clinical and research significance of this remains to be established but highlights some of the current limitations of this technique.

Currently, no quantitative analysis techniques are used in routine clinical practice. Qualitative analysis by experienced reporters is still the main method of image assessment. Consensus is required on standardising interpretation and quantitative assessment with emphasis on a highly reproducible and accurate tool for analysis of perfusion CMR.

## 6.6 Future Work

The use of accelerated imaging techniques has allowed advances in perfusion imaging with higher resolution and greater myocardial coverage. Both techniques have their distinct advantages and clinical benefits. The choice between 3D and high-resolution perfusion CMR may allow the opportunity to tailor scans specifically to the patient depending on the clinical question and the distribution of IHD.

Full coverage with full temporal and high spatial resolution would be desirable, but at present is not feasible. Future developments with accelerated imaging may establish the optimal balance with spatial resolution and cardiac coverage.

The results of the multi-centre study are promising and warrant a multi-centre, multi-vendor trial to investigate clinical utility both cross-modality and compared with 2D first-pass perfusion methods. Clinical questions regarding the diagnostic accuracy in a direct comparison remains. The interchangeability of the ischaemic burden between 2D and 3D methods remains unanswered, particularly around the clinically relevant 10% threshold due to the wide limits of agreement. This could be addressed with a larger study but one difficulty will be the absence of a reference standard. It is critically

important to define the optimal prognostically relevant ischaemic burden threshold for both techniques.

Initial results with improving signal characteristics with bSSFP have been shown in this thesis, but the clinical benefits remain unconfirmed due to compromises with image artefacts. Combined with technical advances in computational hardware, the use of non-Cartesian trajectories and acceleration methods including the recently proposed *k-t* SPIRiT may improve some of these issues (310).

Finally, hybrid fusion imaging can correlate coronary anatomy with functional significance of perfusion assessment, and is an exciting development which may further obviate the need for invasive assessment of IHD.

## 6.7 Summary

In conclusion, dynamic perfusion imaging exhibits significant spatiotemporal redundancy. This allows scan acceleration because it enables recovery of some of the data points that are skipped during acquisition. Higher acceleration factors are achieved by skipping larger amounts of data. Increased acceleration and the method by which *k*-space data are acquired will affect the image artefacts. Thus, compromises between increasing acceleration and improving coverage and spatiotemporal resolution have to be made. This thesis has demonstrated techniques exploiting this redundancy to enable and validate new and broader advanced applications of first pass perfusion CMR.

## References:


1. Group BHFHPR. Coronary Heart Disease Statistics. European Cardiovascular Disease Statistics 2012 2012.
2. Unal B, Critchley JA, Capewell S. Explaining the decline in coronary heart disease mortality in England and Wales between 1981 and 2000. Circulation 2004;109:1101-7.
3. Collaborative meta-analysis of randomised trials of antiplatelet therapy for prevention of death, myocardial infarction, and stroke in high risk patients. Bmj 2002;324:71-86.
4. Randomised trial of cholesterol lowering in 4444 patients with coronary heart disease: the Scandinavian Simvastatin Survival Study (4S). Lancet 1994;344:1383-9.
5. Effects of treatment on morbidity in hypertension. Results in patients with diastolic blood pressures averaging 115 through 129 mm Hg. Jama 1967;202:1028-34.
6. Hampton JR. Coronary artery bypass grafting for the reduction of mortality: an analysis of the trials. Br Med J (Clin Res Ed) 1984;289:1166-70.
7. Boden WE, O'Rourke RA, Teo KK et al. Optimal medical therapy with or without PCI for stable coronary disease. N Engl J Med 2007;356:1503-16.
8. Kolh P, Windecker S. ESC/EACTS myocardial revascularization guidelines 2014. Eur Heart J 2014;35:3235-6.
9. Pijls NH, De Bruyne B, Peels K et al. Measurement of fractional flow reserve to assess the functional severity of coronary-artery stenoses. N Engl J Med 1996;334:1703-8.
10. Gould KL, Lipscomb K, Hamilton GW. Physiologic basis for assessing critical coronary stenosis. Instantaneous flow response and regional distribution during coronary hyperemia as measures of coronary flow reserve. Am J Cardiol 1974;33:87-94.
11. Feldman RL, Nichols WW, Pepine CJ, Conti CR. Hemodynamic significance of the length of a coronary arterial narrowing. Am J Cardiol 1978;41:865-71.
12. Hansson GK. Inflammation, atherosclerosis, and coronary artery disease. N Engl J Med 2005;352:1685-95.
13. Ross R. Atherosclerosis--an inflammatory disease. N Engl J Med 1999;340:115-26.
14. Napoli C, D'Armiento FP, Mancini FP et al. Fatty streak formation occurs in human fetal aortas and is greatly enhanced by maternal hypercholesterolemia. Intimal accumulation of low density lipoprotein and its oxidation precede monocyte recruitment into early atherosclerotic lesions. J Clin Invest 1997;100:2680-90.
15. Feigl EO. Coronary physiology. Physiol Rev 1983;63:1-205.
16. Camici PG, d'Amati G, Rimoldi O. Coronary microvascular dysfunction: mechanisms and functional assessment. Nat Rev Cardiol 2015;12:48-62.
17. Crossman DC. The pathophysiology of myocardial ischaemia. Heart 2004;90:576-80.
18. Griffith TM, Edwards DH, Davies RL, Harrison TJ, Evans KT. EDRF coordinates the behaviour of vascular resistance vessels. Nature 1987;329:442-5.
19. Jones CJ, Kuo L, Davis MJ, DeFily DV, Chilian WM. Role of nitric oxide in the coronary microvascular responses to adenosine and increased metabolic demand. Circulation 1995;91:1807-13.

20. Demer LL, Gould KL, Goldstein RA et al. Assessment of coronary artery disease severity by positron emission tomography. Comparison with quantitative arteriography in 193 patients. Circulation 1989;79:825-35.
21. Uren NG, Melin JA, De Bruyne B, Wijns W, Baudhuin T, Camici PG. Relation between myocardial blood flow and the severity of coronary-artery stenosis. N Engl J Med 1994;330:1782-8.
22. Algranati D KG, Lanir Y. Why is the subendocardium more vulnerable to ischemia? A new paradigm. Am J Physiol Heart Circ Physiol 2011;300(3):H1090-100.
23. Toyota E OY, Hiramatsu O, Tachibana H, Kajiya F, Yamamori S, Chilian WM. Dynamics of flow velocities in endocardial and epicardial coronary arterioles. Am J Physiol Heart Circ Physiol 2005;288(4):H1598-603.
24. Fihn SD, Gardin JM, Abrams J et al. 2012 ACCF/AHA/ACP/AATS/PCNA/SCAI/STS guideline for the diagnosis and management of patients with stable ischemic heart disease: a report of the American College of Cardiology Foundation/American Heart Association task force on practice guidelines, and the American College of Physicians, American Association for Thoracic Surgery, Preventive Cardiovascular Nurses Association, Society for Cardiovascular Angiography and Interventions, and Society of Thoracic Surgeons. Circulation 2012;126:e354-471.
25. Miyamura M, Honda Y. Oxygen intake and cardiac output during maximal treadmill and bicycle exercise. J Appl Physiol 1972;32:185-8.
26. Gusso S, Salvador C, Hofman P et al. Design and testing of an MRI-compatible cycle ergometer for non-invasive cardiac assessments during exercise. Biomed Eng Online 2012;11:13.
27. Foster EL, Arnold JW, Jekic M et al. MR-compatible treadmill for exercise stress cardiac magnetic resonance imaging. Magn Reson Med 2012;67:880-9.
28. Thavendiranathan P, Dickerson JA, Scandling D et al. Comparison of treadmill exercise stress cardiac MRI to stress echocardiography in healthy volunteers for adequacy of left ventricular endocardial wall visualization: A pilot study. J Magn Reson Imaging 2014;39:1146-52.
29. Pennell DJ, Mavrogeni SI, Forbat SM, Karwatowski SP, Underwood SR. Adenosine combined with dynamic exercise for myocardial perfusion imaging. J Am Coll Cardiol 1995;25:1300-9.
30. Gemignani AS, Abbott BG. The emerging role of the selective A2A agonist in pharmacologic stress testing. J Nucl Cardiol 2010;17:494-7.
31. Jayaweera AR, Wei K, Coggins M, Bin JP, Goodman C, Kaul S. Role of capillaries in determining CBF reserve: new insights using myocardial contrast echocardiography. Am J Physiol 1999;277:H2363-72.
32. Petraco R, Sen S, Nijjer S et al. Fractional flow reserve-guided revascularization: practical implications of a diagnostic gray zone and measurement variability on clinical decisions. JACC Cardiovasc Interv 2013;6:222-5.
33. Schaper W. Dipyridamole, an underestimated vascular protective drug. Cardiovasc Drugs Ther 2005;19:357-63.
34. Cerqueira MD, Verani MS, Schwaiger M, Heo J, Iskandrian AS. Safety profile of adenosine stress perfusion imaging: results from the Adenoscan Multicenter Trial Registry. J Am Coll Cardiol 1994;23:384-9.
35. Lette J, Tatum JL, Fraser S et al. Safety of dipyridamole testing in 73,806 patients: the Multicenter Dipyridamole Safety Study. J Nucl Cardiol 1995;2:3-17.

36. Johnson SG, Peters S. Advances in pharmacologic stress agents: focus on regadenoson. J Nucl Med Technol 2010;38:163-71.
37. Ghimire G, Hage FG, Heo J, Iskandrian AE. Regadenoson: a focused update. J Nucl Cardiol 2013;20:284-8.
38. Iskandrian AE, Bateman TM, Belardinelli L et al. Adenosine versus regadenoson comparative evaluation in myocardial perfusion imaging: results of the ADVANCE phase 3 multicenter international trial. J Nucl Cardiol 2007;14:645-58.
39. Cerqueira MD, Nguyen P, Staehr P, Underwood SR, Iskandrian AE. Effects of age, gender, obesity, and diabetes on the efficacy and safety of the selective A2A agonist regadenoson versus adenosine in myocardial perfusion imaging integrated ADVANCE-MPI trial results. JACC Cardiovasc Imaging 2008;1:307-16.
40. Thomas GS, Tammelin BR, Schiffman GL et al. Safety of regadenoson, a selective adenosine A2A agonist, in patients with chronic obstructive pulmonary disease: A randomized, double-blind, placebo-controlled trial (RegCOPD trial). J Nucl Cardiol 2008;15:319-28.
41. Leaker BR, O'Connor B, Hansel TT et al. Safety of regadenoson, an adenosine A2A receptor agonist for myocardial perfusion imaging, in mild asthma and moderate asthma patients: a randomized, double-blind, placebo-controlled trial. J Nucl Cardiol 2008;15:329-36.
42. Naresh NK, Chen X, Roy RJ, Antkowiak PF, Annex BH, Epstein FH. Accelerated dual-contrast first-pass perfusion MRI of the mouse heart: development and application to diet-induced obese mice. Magnetic resonance in medicine 2015;73:1237-45.
43. Smits P, Corstens FH, Aengevaeren WR, Wackers FJ, Thien T. False-negative dipyridamole-thallium-201 myocardial imaging after caffeine infusion. J Nucl Med 1991;32:1538-41.
44. Kubo S, Tadamura E, Toyoda H et al. Effect of caffeine intake on myocardial hyperemic flow induced by adenosine triphosphate and dipyridamole. J Nucl Med 2004;45:730-8.
45. Reyes E, Loong CY, Harbinson M, Donovan J, Anagnostopoulos C, Underwood SR. High-dose adenosine overcomes the attenuation of myocardial perfusion reserve caused by caffeine. J Am Coll Cardiol 2008;52:2008-16.
46. Camici PG, Prasad SK, Rimoldi OE. Stunning, hibernation, and assessment of myocardial viability. Circulation 2008;117:103-14.
47. Geleijnse ML, Elhendy A, Fioretti PM, Roelandt JR. Dobutamine stress myocardial perfusion imaging. J Am Coll Cardiol 2000;36:2017-27.
48. Picano E, Mathias W, Jr., Pingitore A, Bigi R, Previtali M. Safety and tolerability of dobutamine-atropine stress echocardiography: a prospective, multicentre study. Echo Dobutamine International Cooperative Study Group. Lancet 1994;344:1190-2.
49. Cheng TO. First selective coronary arteriogram. Circulation 2003;107:E42-2; author reply E42-2.
50. Ludmann P. BCIS Audit Returns 2014. 2014.
51. Reddy BK, Brewster PS, Walsh T, Burket MW, Thomas WJ, Cooper CJ. Randomized comparison of rapid ambulation using radial, 4 French femoral access, or femoral access with AngioSeal closure. Catheter Cardiovasc Interv 2004;62:143-9.
52. Nallamothu BK, Spertus JA, Lansky AJ et al. Comparison of clinical interpretation with visual assessment and quantitative coronary angiography in patients undergoing percutaneous coronary intervention in contemporary practice: the Assessing Angiography (A2) project. Circulation 2013;127:1793-800.

53. Hermiller JB, Cusma JT, Spero LA, Fortin DF, Harding MB, Bashore TM. Quantitative and qualitative coronary angiographic analysis: review of methods, utility, and limitations. Cathet Cardiovasc Diagn 1992;25:110-31.
54. Bruschke AV, Proudfit WL, Sones FM, Jr. Progress study of 590 consecutive nonsurgical cases of coronary disease followed 5-9 years. II. Ventriculographic and other correlations. Circulation 1973;47:1154-63.
55. Bruschke AV, Proudfit WL, Sones FM, Jr. Progress study of 590 consecutive nonsurgical cases of coronary disease followed 5-9 years. I. Arterographic correlations. Circulation 1973;47:1147-53.
56. Yusuf S, Zucker D, Peduzzi P et al. Effect of coronary artery bypass graft surgery on survival: overview of 10-year results from randomised trials by the Coronary Artery Bypass Graft Surgery Trialists Collaboration. Lancet 1994;344:563-70.
57. Califf RM, Phillips HR, 3rd, Hindman MC et al. Prognostic value of a coronary artery jeopardy score. J Am Coll Cardiol 1985;5:1055-63.
58. Morton GD, De Silva K, Ishida M et al. Validation of the BCIS-1 myocardial jeopardy score using cardiac magnetic resonance perfusion imaging. Clin Physiol Funct Imaging 2013;33:101-8.
59. Seven-year outcome in the Bypass Angioplasty Revascularization Investigation (BARI) by treatment and diabetic status. J Am Coll Cardiol 2000;35:1122-9.
60. Pijls NH, van Son JA, Kirkeeide RL, De Bruyne B, Gould KL. Experimental basis of determining maximum coronary, myocardial, and collateral blood flow by pressure measurements for assessing functional stenosis severity before and after percutaneous transluminal coronary angioplasty. Circulation 1993;87:1354-67.
61. De Bruyne B, Baudhuin T, Melin JA et al. Coronary flow reserve calculated from pressure measurements in humans. Validation with positron emission tomography. Circulation 1994;89:1013-22.
62. van de Hoef TP, Meuwissen M, Escaned J et al. Fractional flow reserve as a surrogate for inducible myocardial ischaemia. Nat Rev Cardiol 2013;10:439-52.
63. Tonino PA, De Bruyne B, Pijls NH et al. Fractional flow reserve versus angiography for guiding percutaneous coronary intervention. N Engl J Med 2009;360:213-24.
64. Pijls NH, Klauss V, Siebert U et al. Coronary pressure measurement after stenting predicts adverse events at follow-up: a multicenter registry. Circulation 2002;105:2950-4.
65. Pijls NH, van Schaardenburgh P, Manoharan G et al. Percutaneous coronary intervention of functionally nonsignificant stenosis: 5-year follow-up of the DEFER Study. J Am Coll Cardiol 2007;49:2105-11.
66. Pijls NH, Fearon WF, Tonino PA et al. Fractional flow reserve versus angiography for guiding percutaneous coronary intervention in patients with multivessel coronary artery disease: 2-year follow-up of the FAME (Fractional Flow Reserve Versus Angiography for Multivessel Evaluation) study. J Am Coll Cardiol 2010;56:177-84.
67. De Bruyne B, Pijls NH, Kalesan B et al. Fractional flow reserve-guided PCI versus medical therapy in stable coronary disease. N Engl J Med 2012;367:991-1001.
68. Tani S, Watanabe I, Kobari C et al. Mismatch between results of myocardial fractional flow reserve (FFR) measurements and myocardial perfusion SPECT for identification of the severity of ischemia: pitfall of FFR in patients with prior myocardial infarction. Jpn Heart J 2004;45:867-72.

69. De Bruyne B, Pijls NH, Bartunek J et al. Fractional flow reserve in patients with prior myocardial infarction. Circulation 2001;104:157-62.
70. De Silva K, Foster P, Guilcher A et al. Coronary wave energy: a novel predictor of functional recovery after myocardial infarction. Circ Cardiovasc Interv 2013;6:166-75.
71. Meuwissen M, Chamuleau SA, Siebes M et al. Role of variability in microvascular resistance on fractional flow reserve and coronary blood flow velocity reserve in intermediate coronary lesions. Circulation 2001;103:184-7.
72. Kern MJ, Lerman A, Bech JW et al. Physiological assessment of coronary artery disease in the cardiac catheterization laboratory: a scientific statement from the American Heart Association Committee on Diagnostic and Interventional Cardiac Catheterization, Council on Clinical Cardiology. Circulation 2006;114:1321-41.
73. Davies JE, Whinnett ZI, Francis DP et al. Evidence of a dominant backward-propagating "suction" wave responsible for diastolic coronary filling in humans, attenuated in left ventricular hypertrophy. Circulation 2006;113:1768-78.
74. Sen S, Escaned J, Malik IS et al. Development and validation of a new adenosine-independent index of stenosis severity from coronary wave-intensity analysis: results of the ADVISE (ADenosine Vasodilator Independent Stenosis Evaluation) study. J Am Coll Cardiol 2012;59:1392-402.
75. Sen S, Asrress KN, Nijjer S et al. Diagnostic classification of the instantaneous wave-free ratio is equivalent to fractional flow reserve and is not improved with adenosine administration. Results of CLARIFY (Classification Accuracy of Pressure-Only Ratios Against Indices Using Flow Study). J Am Coll Cardiol 2013;61:1409-20.
76. Berry C, van 't Veer M, Witt N et al. VERIFY (VERification of Instantaneous Wave-Free Ratio and Fractional Flow Reserve for the Assessment of Coronary Artery Stenosis Severity in EverydaY Practice): a multicenter study in consecutive patients. J Am Coll Cardiol 2013;61:1421-7.
77. Jeremias A, Maehara A, Genereux P et al. Multicenter core laboratory comparison of the instantaneous wave-free ratio and resting Pd/Pa with fractional flow reserve: the RESOLVE study. J Am Coll Cardiol 2014;63:1253-61.
78. Nijjer SS, Sen S, Petraco R, Mayet J, Francis DP, Davies JE. The Instantaneous wave-Free Ratio (iFR) pullback: a novel innovation using baseline physiology to optimise coronary angioplasty in tandem lesions. Cardiovasc Revasc Med 2015;16:167-71.
79. McNeer JF, Margolis JR, Lee KL et al. The role of the exercise test in the evaluation of patients for ischemic heart disease. Circulation 1978;57:64-70.
80. Mark DB, Shaw L, Harrell FE, Jr. et al. Prognostic value of a treadmill exercise score in outpatients with suspected coronary artery disease. N Engl J Med 1991;325:849-53.
81. Gianrossi R, Detrano R, Mulvihill D et al. Exercise-induced ST depression in the diagnosis of coronary artery disease. A meta-analysis. Circulation 1989;80:87-98.
82. Kwok Y, Kim C, Grady D, Segal M, Redberg R. Meta-analysis of exercise testing to detect coronary artery disease in women. Am J Cardiol 1999;83:660-6.
83. Underwood SR. NICE and chest pain diagnosis. W(h)ither the exercise ECG? Bmj 2010;340:c2387.
84. Marwick TH. Stress echocardiography. Heart 2003;89:113-8.
85. Beleslin BD, Ostojic M, Djordjevic-Dikic A et al. Integrated evaluation of relation between coronary lesion features and stress echocardiography results: the importance of coronary lesion morphology. J Am Coll Cardiol 1999;33:717-26.

86. Geleijnse ML, Fioretti PM, Roelandt JR. Methodology, feasibility, safety and diagnostic accuracy of dobutamine stress echocardiography. J Am Coll Cardiol 1997;30:595-606.
87. Metz LD, Beattie M, Hom R, Redberg RF, Grady D, Fleischmann KE. The prognostic value of normal exercise myocardial perfusion imaging and exercise echocardiography: a meta-analysis. J Am Coll Cardiol 2007;49:227-37.
88. McCully RB, Roger VL, Mahoney DW et al. Outcome after normal exercise echocardiography and predictors of subsequent cardiac events: follow-up of 1,325 patients. J Am Coll Cardiol 1998;31:144-9.
89. Marwick TH, Case C, Vasey C, Allen S, Short L, Thomas JD. Prediction of mortality by exercise echocardiography: a strategy for combination with the duke treadmill score. Circulation 2001;103:2566-71.
90. Vogel R, Indermuhle A, Reinhardt J et al. The quantification of absolute myocardial perfusion in humans by contrast echocardiography: algorithm and validation. J Am Coll Cardiol 2005;45:754-62.
91. Elhendy A, O'Leary EL, Xie F, McGrain AC, Anderson JR, Porter TR. Comparative accuracy of real-time myocardial contrast perfusion imaging and wall motion analysis during dobutamine stress echocardiography for the diagnosis of coronary artery disease. J Am Coll Cardiol 2004;44:2185-91.
92. de Jong MC, Genders TS, van Geuns RJ, Moelker A, Hunink MG. Diagnostic performance of stress myocardial perfusion imaging for coronary artery disease: a systematic review and meta-analysis. Eur Radiol 2012;22:1881-95.
93. Bhatia VK, Senior R. Contrast echocardiography: evidence for clinical use. J Am Soc Echocardiogr 2008;21:409-16.
94. Dolan MS, Gala SS, Dodla S et al. Safety and efficacy of commercially available ultrasound contrast agents for rest and stress echocardiography a multicenter experience. J Am Coll Cardiol 2009;53:32-8.
95. Tsutsui JM, Elhendy A, Anderson JR, Xie F, McGrain AC, Porter TR. Prognostic value of dobutamine stress myocardial contrast perfusion echocardiography. Circulation 2005;112:1444-50.
96. Mulvagh SL, Rakowski H, Vannan MA et al. American Society of Echocardiography Consensus Statement on the Clinical Applications of Ultrasonic Contrast Agents in Echocardiography. J Am Soc Echocardiogr 2008;21:1179-201; quiz 1281.
97. Abusaid GH, Ahmad M. Real time three-dimensional stress echocardiography advantages and limitations. Echocardiography 2012;29:200-6.
98. Cullom SJ, Case JA, Bateman TM. Electrocardiographically gated myocardial perfusion SPECT: technical principles and quality control considerations. J Nucl Cardiol 1998;5:418-25.
99. Baggish AL, Boucher CA. Radiopharmaceutical agents for myocardial perfusion imaging. Circulation 2008;118:1668-74.
100. Zaret BL, Rigo P, Wackers FJ et al. Myocardial perfusion imaging with 99mTc tetrofosmin. Comparison to 201Tl imaging and coronary angiography in a phase III multicenter trial. Tetrofosmin International Trial Study Group. Circulation 1995;91:313-9.
101. Kapur A, Latus KA, Davies G et al. A comparison of three radionuclide myocardial perfusion tracers in clinical practice: the ROBUST study. Eur J Nucl Med Mol Imaging 2002;29:1608-16.
102. Germano G, Kavanagh PB, Berman DS. An automatic approach to the analysis, quantitation and review of perfusion and function from myocardial perfusion SPECT images. Int J Card Imaging 1997;13:337-46.

103. Hachamovitch R, Berman DS, Shaw LJ et al. Incremental prognostic value of myocardial perfusion single photon emission computed tomography for the prediction of cardiac death: differential stratification for risk of cardiac death and myocardial infarction. Circulation 1998;97:535-43.
104. Cerqueira MD, Weissman NJ, Dilsizian V et al. Standardized myocardial segmentation and nomenclature for tomographic imaging of the heart. A statement for healthcare professionals from the Cardiac Imaging Committee of the Council on Clinical Cardiology of the American Heart Association. Circulation 2002;105:539-42.
105. Johansson L, Lomsky M, Marving J, Ohlsson M, Svensson SE, Edenbrandt L. Diagnostic evaluation of three cardiac software packages using a consecutive group of patients. EJNMMI Res 2011;1:22.
106. Brindis RG, Douglas PS, Hendel RC et al. ACCF/ASNC appropriateness criteria for single-photon emission computed tomography myocardial perfusion imaging (SPECT MPI): a report of the American College of Cardiology Foundation Quality Strategic Directions Committee Appropriateness Criteria Working Group and the American Society of Nuclear Cardiology endorsed by the American Heart Association. J Am Coll Cardiol 2005;46:1587-605.
107. Klocke FJ, Baird MG, Lorell BH et al. ACC/AHA/ASNC guidelines for the clinical use of cardiac radionuclide imaging--executive summary: a report of the American College of Cardiology/American Heart Association Task Force on Practice Guidelines (ACC/AHA/ASNC Committee to Revise the 1995 Guidelines for the Clinical Use of Cardiac Radionuclide Imaging). J Am Coll Cardiol 2003;42:1318-33.
108. Iskander S, Iskandrian AE. Risk assessment using single-photon emission computed tomographic technetium-99m sestamibi imaging. J Am Coll Cardiol 1998;32:57-62.
109. Navare SM, Mather JF, Shaw LJ, Fowler MS, Heller GV. Comparison of risk stratification with pharmacologic and exercise stress myocardial perfusion imaging: a meta-analysis. J Nucl Cardiol 2004;11:551-61.
110. Shaw LJ, Iskandrian AE. Prognostic value of gated myocardial perfusion SPECT. J Nucl Cardiol 2004;11:171-85.
111. Hakeem A, Bhatti S, Dillie KS et al. Predictive value of myocardial perfusion single-photon emission computed tomography and the impact of renal function on cardiac death. Circulation 2008;118:2540-9.
112. Hachamovitch R, Hayes SW, Friedman JD, Cohen I, Berman DS. Comparison of the short-term survival benefit associated with revascularization compared with medical therapy in patients with no prior coronary artery disease undergoing stress myocardial perfusion single photon emission computed tomography. Circulation 2003;107:2900-7.
113. Hachamovitch R, Rozanski A, Hayes SW et al. Predicting therapeutic benefit from myocardial revascularization procedures: are measurements of both resting left ventricular ejection fraction and stress-induced myocardial ischemia necessary? J Nucl Cardiol 2006;13:768-78.
114. Shaw LJ, Berman DS, Maron DJ et al. Optimal medical therapy with or without percutaneous coronary intervention to reduce ischemic burden: results from the Clinical Outcomes Utilizing Revascularization and Aggressive Drug Evaluation (COURAGE) trial nuclear substudy. Circulation 2008;117:1283-91.
115. Hachamovitch R, Rozanski A, Shaw LJ et al. Impact of ischaemia and scar on the therapeutic benefit derived from myocardial revascularization vs. medical

therapy among patients undergoing stress-rest myocardial perfusion scintigraphy. Eur Heart J 2011;32:1012-24.
116. Slomka PJ, Pan T, Berman DS, Germano G. Advances in SPECT and PET Hardware. Prog Cardiovasc Dis 2015;57:566-78.
117. Slomka PJ, Patton JA, Berman DS, Germano G. Advances in technical aspects of myocardial perfusion SPECT imaging. J Nucl Cardiol 2009;16:255-76.
118. Piccinelli M, Garcia EV. Advances in software for faster procedure and lower radiotracer dose myocardial perfusion imaging. Prog Cardiovasc Dis 2015;57:579-87.
119. Shaw LJ, Hachamovitch R, Berman DS et al. The economic consequences of available diagnostic and prognostic strategies for the evaluation of stable angina patients: an observational assessment of the value of precatheterization ischemia. Economics of Noninvasive Diagnosis (END) Multicenter Study Group. J Am Coll Cardiol 1999;33:661-9.
120. Underwood SR, Godman B, Salyani S, Ogle JR, Ell PJ. Economics of myocardial perfusion imaging in Europe--the EMPIRE Study. Eur Heart J 1999;20:157-66.
121. Berman DS, Kang X, Slomka PJ et al. Underestimation of extent of ischemia by gated SPECT myocardial perfusion imaging in patients with left main coronary artery disease. J Nucl Cardiol 2007;14:521-8.
122. DePuey EG, 3rd. How to detect and avoid myocardial perfusion SPECT artifacts. J Nucl Med 1994;35:699-702.
123. Hendel RC, Corbett JR, Cullom SJ, DePuey EG, Garcia EV, Bateman TM. The value and practice of attenuation correction for myocardial perfusion SPECT imaging: a joint position statement from the American Society of Nuclear Cardiology and the Society of Nuclear Medicine. J Nucl Cardiol 2002;9:135-43.
124. Parker MW, Iskandar A, Limone B et al. Diagnostic accuracy of cardiac positron emission tomography versus single photon emission computed tomography for coronary artery disease: a bivariate meta-analysis. Circ Cardiovasc Imaging 2012;5:700-7.
125. Nandalur KR, Dwamena BA, Choudhri AF, Nandalur SR, Reddy P, Carlos RC. Diagnostic performance of positron emission tomography in the detection of coronary artery disease: a meta-analysis. Acad Radiol 2008;15:444-51.
126. Morton G, Chiribiri A, Ishida M et al. Quantification of absolute myocardial perfusion in patients with coronary artery disease: comparison between cardiovascular magnetic resonance and positron emission tomography. J Am Coll Cardiol 2012;60:1546-55.
127. Marwick TH, Shan K, Patel S, Go RT, Lauer MS. Incremental value of rubidium-82 positron emission tomography for prognostic assessment of known or suspected coronary artery disease. Am J Cardiol 1997;80:865-70.
128. Yoshinaga K, Chow BJ, Williams K et al. What is the prognostic value of myocardial perfusion imaging using rubidium-82 positron emission tomography? J Am Coll Cardiol 2006;48:1029-39.
129. Kuhle WG, Porenta G, Huang SC et al. Quantification of regional myocardial blood flow using 13N-ammonia and reoriented dynamic positron emission tomographic imaging. Circulation 1992;86:1004-17.
130. Ridgway JP. Cardiovascular magnetic resonance physics for clinicians: part I. J Cardiovasc Magn Reson 2010;12:71.
131. Biglands JD, Radjenovic A, Ridgway JP. Cardiovascular magnetic resonance physics for clinicians: Part II. J Cardiovasc Magn Reson 2012;14:66.

132. Pennell DJ. Cardiovascular magnetic resonance: twenty-first century solutions in cardiology. Clin Med 2003;3:273-8.
133. Charoenpanichkit C, Hundley WG. The 20 year evolution of dobutamine stress cardiovascular magnetic resonance. J Cardiovasc Magn Reson 2010;12:59.
134. Nandalur KR, Dwamena BA, Choudhri AF, Nandalur MR, Carlos RC. Diagnostic performance of stress cardiac magnetic resonance imaging in the detection of coronary artery disease: a meta-analysis. J Am Coll Cardiol 2007;50:1343-53.
135. Nagel E, Lehmkuhl HB, Bocksch W et al. Noninvasive diagnosis of ischemia-induced wall motion abnormalities with the use of high-dose dobutamine stress MRI: comparison with dobutamine stress echocardiography. Circulation 1999;99:763-70.
136. Hundley WG, Hamilton CA, Thomas MS et al. Utility of fast cine magnetic resonance imaging and display for the detection of myocardial ischemia in patients not well suited for second harmonic stress echocardiography. Circulation 1999;100:1697-702.
137. Mordi I, Stanton T, Carrick D et al. Comprehensive dobutamine stress CMR versus echocardiography in LBBB and suspected coronary artery disease. JACC Cardiovasc Imaging 2014;7:490-8.
138. Baer FM, Voth E, Schneider CA, Theissen P, Schicha H, Sechtem U. Comparison of low-dose dobutamine-gradient-echo magnetic resonance imaging and positron emission tomography with [18F]fluorodeoxyglucose in patients with chronic coronary artery disease. A functional and morphological approach to the detection of residual myocardial viability. Circulation 1995;91:1006-15.
139. Baer FM, Theissen P, Schneider CA et al. Dobutamine magnetic resonance imaging predicts contractile recovery of chronically dysfunctional myocardium after successful revascularization. J Am Coll Cardiol 1998;31:1040-8.
140. Giusca S, Kelle S, Nagel E et al. Ischemic burden and clinical outcome: is one 'culprit' ischemic segment by dobutamine stress magnetic resonance predictive? PLoS One 2014;9:e115182.
141. Hundley WG, Morgan TM, Neagle CM, Hamilton CA, Rerkpattanapipat P, Link KM. Magnetic resonance imaging determination of cardiac prognosis. Circulation 2002;106:2328-33.
142. Kelle S, Chiribiri A, Vierecke J et al. Long-term prognostic value of dobutamine stress CMR. JACC Cardiovasc Imaging 2011;4:161-72.
143. Gebker R, Jahnke C, Manka R et al. Additional value of myocardial perfusion imaging during dobutamine stress magnetic resonance for the assessment of coronary artery disease. Circ Cardiovasc Imaging 2008;1:122-30.
144. Gebker R, Mirelis JG, Jahnke C et al. Influence of left ventricular hypertrophy and geometry on diagnostic accuracy of wall motion and perfusion magnetic resonance during dobutamine stress. Circ Cardiovasc Imaging 2010;3:507-14.
145. Wahl A, Paetsch I, Gollesch A et al. Safety and feasibility of high-dose dobutamine-atropine stress cardiovascular magnetic resonance for diagnosis of myocardial ischaemia: experience in 1000 consecutive cases. Eur Heart J 2004;25:1230-6.
146. Kuijpers D, Janssen CH, van Dijkman PR, Oudkerk M. Dobutamine stress MRI. Part I. Safety and feasibility of dobutamine cardiovascular magnetic resonance in patients suspected of myocardial ischemia. Eur Radiol 2004;14:1823-8.
147. Rodgers GP, Ayanian JZ, Balady G et al. American College of Cardiology/American Heart Association Clinical Competence Statement on Stress Testing. A Report of the American College of Cardiology/American Heart Association/American

College of Physicians-American Society of Internal Medicine Task Force on Clinical Competence. Circulation 2000;102:1726-38.
148. Garot J, D Oh-I. Dobutamine stress CMR: can we predict outcome? JACC Cardiovasc Imaging 2011;4:173-5.
149. Wu E, Judd RM, Vargas JD, Klocke FJ, Bonow RO, Kim RJ. Visualisation of presence, location, and transmural extent of healed Q-wave and non-Q-wave myocardial infarction. Lancet 2001;357:21-8.
150. Kim RJ, Fieno DS, Parrish TB et al. Relationship of MRI delayed contrast enhancement to irreversible injury, infarct age, and contractile function. Circulation 1999;100:1992-2002.
151. Kwong RY, Chan AK, Brown KA et al. Impact of unrecognized myocardial scar detected by cardiac magnetic resonance imaging on event-free survival in patients presenting with signs or symptoms of coronary artery disease. Circulation 2006;113:2733-43.
152. Gulati A, Jabbour A, Ismail TF et al. Association of fibrosis with mortality and sudden cardiac death in patients with nonischemic dilated cardiomyopathy. Jama 2013;309:896-908.
153. Weinmann HJ, Brasch RC, Press WR, Wesbey GE. Characteristics of gadolinium-DTPA complex: a potential NMR contrast agent. AJR Am J Roentgenol 1984;142:619-24.
154. Salerno M, Beller GA. Noninvasive assessment of myocardial perfusion. Circ Cardiovasc Imaging 2009;2:412-24.
155. Ricciardi MJ, Wu E, Davidson CJ et al. Visualization of discrete microinfarction after percutaneous coronary intervention associated with mild creatine kinase-MB elevation. Circulation 2001;103:2780-3.
156. Wagner A, Mahrholdt H, Holly TA et al. Contrast-enhanced MRI and routine single photon emission computed tomography (SPECT) perfusion imaging for detection of subendocardial myocardial infarcts: an imaging study. Lancet 2003;361:374-9.
157. Kim RJ, Wu E, Rafael A et al. The use of contrast-enhanced magnetic resonance imaging to identify reversible myocardial dysfunction. N Engl J Med 2000;343:1445-53.
158. Wellnhofer E, Olariu A, Klein C et al. Magnetic resonance low-dose dobutamine test is superior to SCAR quantification for the prediction of functional recovery. Circulation 2004;109:2172-4.
159. Greenwood JP, Maredia N, Younger JF et al. Cardiovascular magnetic resonance and single-photon emission computed tomography for diagnosis of coronary heart disease (CE-MARC): a prospective trial. Lancet 2012;379:453-60.
160. Schwitter J, Wacker CM, van Rossum AC et al. MR-IMPACT: comparison of perfusion-cardiac magnetic resonance with single-photon emission computed tomography for the detection of coronary artery disease in a multicentre, multivendor, randomized trial. Eur Heart J 2008;29:480-9.
161. Schwitter J, Wacker CM, Wilke N et al. MR-IMPACT II: Magnetic Resonance Imaging for Myocardial Perfusion Assessment in Coronary artery disease Trial: perfusion-cardiac magnetic resonance vs. single-photon emission computed tomography for the detection of coronary artery disease: a comparative multicentre, multivendor trial. Eur Heart J 2013;34:775-81.
162. Arnold JR, Karamitsos TD, Bhamra-Ariza P et al. Myocardial oxygenation in coronary artery disease: insights from blood oxygen level-dependent magnetic resonance imaging at 3 tesla. J Am Coll Cardiol 2012;59:1954-64.

163. Zun Z, Varadarajan P, Pai RG, Wong EC, Nayak KS. Arterial spin labeled CMR detects clinically relevant increase in myocardial blood flow with vasodilation. JACC Cardiovasc Imaging 2011;4:1253-61.
164. Wolff SD, Schwitter J, Coulden R et al. Myocardial first-pass perfusion magnetic resonance imaging: a multicenter dose-ranging study. Circulation 2004;110:732-7.
165. Nagel E, Klein C, Paetsch I et al. Magnetic resonance perfusion measurements for the noninvasive detection of coronary artery disease. Circulation 2003;108:432-7.
166. Ishida M, Ichihara T, Nagata M et al. Quantification of myocardial blood flow using model based analysis of first-pass perfusion MRI: extraction fraction of Gd-DTPA varies with myocardial blood flow in human myocardium. Magnetic resonance in medicine 2011;66:1391-9.
167. Jerosch-Herold M, Wilke N, Stillman AE. Magnetic resonance quantification of the myocardial perfusion reserve with a Fermi function model for constrained deconvolution. Med Phys 1998;25:73-84.
168. Paetsch I, Foll D, Langreck H et al. Myocardial perfusion imaging using OMNISCAN: a dose finding study for visual assessment of stress-induced regional perfusion abnormalities. J Cardiovasc Magn Reson 2004;6:803-9.
169. Jerosch-Herold M. Quantification of myocardial perfusion by cardiovascular magnetic resonance. J Cardiovasc Magn Reson 2010;12:57.
170. Utz W, Niendorf T, Wassmuth R, Messroghli D, Dietz R, Schulz-Menger J. Contrast-dose relation in first-pass myocardial MR perfusion imaging. J Magn Reson Imaging 2007;25:1131-5.
171. Christian TF, Rettmann DW, Aletras AH et al. Absolute myocardial perfusion in canines measured by using dual-bolus first-pass MR imaging. Radiology 2004;232:677-84.
172. Christian TF, Aletras AH, Arai AE. Estimation of absolute myocardial blood flow during first-pass MR perfusion imaging using a dual-bolus injection technique: comparison to single-bolus injection method. J Magn Reson Imaging 2008;27:1271-7.
173. Utz W, Greiser A, Niendorf T, Dietz R, Schulz-Menger J. Single- or dual-bolus approach for the assessment of myocardial perfusion reserve in quantitative MR perfusion imaging. Magnetic resonance in medicine 2008;59:1373-7.
174. Gatehouse PD, Elkington AG, Ablitt NA, Yang GZ, Pennell DJ, Firmin DN. Accurate assessment of the arterial input function during high-dose myocardial perfusion cardiovascular magnetic resonance. J Magn Reson Imaging 2004;20:39-45.
175. Lee DC, Johnson NP. Quantification of absolute myocardial blood flow by magnetic resonance perfusion imaging. JACC Cardiovasc Imaging 2009;2:761-70.
176. Patel AR, Antkowiak PF, Nandalur KR et al. Assessment of advanced coronary artery disease: advantages of quantitative cardiac magnetic resonance perfusion analysis. J Am Coll Cardiol 2010;56:561-9.
177. Knowles BR, Batchelor PG, Parish V et al. Pharmacokinetic modeling of delayed gadolinium enhancement in the myocardium. Magnetic resonance in medicine 2008;60:1524-30.
178. Mordini FE, Haddad T, Hsu LY et al. Diagnostic accuracy of stress perfusion CMR in comparison with quantitative coronary angiography: fully quantitative, semiquantitative, and qualitative assessment. JACC Cardiovasc Imaging 2014;7:14-22.
179. Kellman P, Arai AE. Imaging sequences for first pass perfusion --a review. J Cardiovasc Magn Reson 2007;9:525-37.

180. Judd RM, Reeder SB, Atalar E, McVeigh ER, Zerhouni EA. A magnetization-driven gradient echo pulse sequence for the study of myocardial perfusion. Magnetic resonance in medicine 1995;34:276-82.
181. Gerber BL, Raman SV, Nayak K et al. Myocardial first-pass perfusion cardiovascular magnetic resonance: history, theory, and current state of the art. J Cardiovasc Magn Reson 2008;10:18.
182. Kim D, Cernicanu A, Axel L. B(0) and B(1)-insensitive uniform T(1)-weighting for quantitative, first-pass myocardial perfusion magnetic resonance imaging. Magnetic resonance in medicine 2005;54:1423-9.
183. Atkinson DJ, Burstein D, Edelman RR. First-pass cardiac perfusion: evaluation with ultrafast MR imaging. Radiology 1990;174:757-62.
184. Wieben O, Francois C, Reeder SB. Cardiac MRI of ischemic heart disease at 3 T: potential and challenges. Eur J Radiol 2008;65:15-28.
185. Oshinski JN, Delfino JG, Sharma P, Gharib AM, Pettigrew RI. Cardiovascular magnetic resonance at 3.0 T: current state of the art. J Cardiovasc Magn Reson 2010;12:55.
186. Elkington AG, Gatehouse PD, Cannell TM et al. Comparison of hybrid echo-planar imaging and FLASH myocardial perfusion cardiovascular MR imaging. Radiology 2005;235:237-43.
187. Ding S, Wolff SD, Epstein FH. Improved coverage in dynamic contrast-enhanced cardiac MRI using interleaved gradient-echo EPI. Magnetic resonance in medicine 1998;39:514-9.
188. Ferreira PF, Gatehouse PD, Firmin DN. Myocardial first-pass perfusion imaging with hybrid-EPI: frequency-offsets and potential artefacts. J Cardiovasc Magn Reson 2012;14:44.
189. Wang Y, Moin K, Akinboboye O, Reichek N. Myocardial first pass perfusion: steady-state free precession versus spoiled gradient echo and segmented echo planar imaging. Magnetic resonance in medicine 2005;54:1123-9.
190. Hunold P, Maderwald S, Eggebrecht H, Vogt FM, Barkhausen J. Steady-state free precession sequences in myocardial first-pass perfusion MR imaging: comparison with TurboFLASH imaging. Eur Radiol 2004;14:409-16.
191. Weber S, Kronfeld A, Kunz RP et al. Comparison of three accelerated pulse sequences for semiquantitative myocardial perfusion imaging using sensitivity encoding incorporating temporal filtering (TSENSE). J Magn Reson Imaging 2007;26:569-79.
192. Fenchel M, Helber U, Simonetti OP et al. Multislice first-pass myocardial perfusion imaging: Comparison of saturation recovery (SR)-TrueFISP-two-dimensional (2D) and SR-TurboFLASH-2D pulse sequences. J Magn Reson Imaging 2004;19:555-63.
193. Lyne JC, Gatehouse PD, Assomull RG et al. Direct comparison of myocardial perfusion cardiovascular magnetic resonance sequences with parallel acquisition. J Magn Reson Imaging 2007;26:1444-51.
194. Barkhausen J, Hunold P, Jochims M, Debatin JF. Imaging of myocardial perfusion with magnetic resonance. J Magn Reson Imaging 2004;19:750-7.
195. Storey P, Chen Q, Li W, Edelman RR, Prasad PV. Band artifacts due to bulk motion. Magnetic resonance in medicine 2002;48:1028-36.
196. Ferreira PF, Gatehouse PD, Mohiaddin RH, Firmin DN. Cardiovascular magnetic resonance artefacts. J Cardiovasc Magn Reson 2013;15:41.

197. Di Bella EV, Parker DL, Sinusas AJ. On the dark rim artifact in dynamic contrast-enhanced MRI myocardial perfusion studies. Magnetic resonance in medicine 2005;54:1295-9.
198. Arena L, Morehouse HT, Safir J. MR imaging artifacts that simulate disease: how to recognize and eliminate them. Radiographics 1995;15:1373-94.
199. Motwani M, Maredia N, Fairbairn TA et al. High-resolution versus standard-resolution cardiovascular MR myocardial perfusion imaging for the detection of coronary artery disease. Circ Cardiovasc Imaging 2012;5:306-13.
200. Felmlee JP, Ehman RL. Spatial presaturation: a method for suppressing flow artifacts and improving depiction of vascular anatomy in MR imaging. Radiology 1987;164:559-64.
201. Plein S, Kozerke S, Suerder D et al. High spatial resolution myocardial perfusion cardiac magnetic resonance for the detection of coronary artery disease. Eur Heart J 2008;29:2148-55.
202. Kozerke S, Plein S. Accelerated CMR using zonal, parallel and prior knowledge driven imaging methods. J Cardiovasc Magn Reson 2008;10:29.
203. Vitanis V, Manka R, Giese D et al. High resolution three-dimensional cardiac perfusion imaging using compartment-based k-t principal component analysis. Magnetic resonance in medicine 2011;65:575-87.
204. Dill T. Contraindications to magnetic resonance imaging: non-invasive imaging. Heart 2008;94:943-8.
205. Hamon M, Fau G, Nee G, Ehtisham J, Morello R. Meta-analysis of the diagnostic performance of stress perfusion cardiovascular magnetic resonance for detection of coronary artery disease. J Cardiovasc Magn Reson 2010;12:29.
206. Jaarsma C, Leiner T, Bekkers SC et al. Diagnostic performance of noninvasive myocardial perfusion imaging using single-photon emission computed tomography, cardiac magnetic resonance, and positron emission tomography imaging for the detection of obstructive coronary artery disease: a meta-analysis. J Am Coll Cardiol 2012;59:1719-28.
207. Rieber J, Huber A, Erhard I et al. Cardiac magnetic resonance perfusion imaging for the functional assessment of coronary artery disease: a comparison with coronary angiography and fractional flow reserve. Eur Heart J 2006;27:1465-71.
208. Costa MA, Shoemaker S, Futamatsu H et al. Quantitative magnetic resonance perfusion imaging detects anatomic and physiologic coronary artery disease as measured by coronary angiography and fractional flow reserve. J Am Coll Cardiol 2007;50:514-22.
209. Watkins S, McGeoch R, Lyne J et al. Validation of magnetic resonance myocardial perfusion imaging with fractional flow reserve for the detection of significant coronary heart disease. Circulation 2009;120:2207-13.
210. Hussain ST, Paul M, Plein S et al. Design and rationale of the MR-INFORM study: stress perfusion cardiovascular magnetic resonance imaging to guide the management of patients with stable coronary artery disease. J Cardiovasc Magn Reson 2012;14:65.
211. Jahnke C, Nagel E, Gebker R et al. Prognostic value of cardiac magnetic resonance stress tests: adenosine stress perfusion and dobutamine stress wall motion imaging. Circulation 2007;115:1769-76.
212. Buckert D, Dewes P, Walcher T, Rottbauer W, Bernhardt P. Intermediate-term prognostic value of reversible perfusion deficit diagnosed by adenosine CMR: a prospective follow-up study in a consecutive patient population. JACC Cardiovasc Imaging 2013;6:56-63.

213. Ingkanisorn WP, Kwong RY, Bohme NS et al. Prognosis of negative adenosine stress magnetic resonance in patients presenting to an emergency department with chest pain. J Am Coll Cardiol 2006;47:1427-32.
214. Lipinski MJ, McVey CM, Berger JS, Kramer CM, Salerno M. Prognostic value of stress cardiac magnetic resonance imaging in patients with known or suspected coronary artery disease: a systematic review and meta-analysis. J Am Coll Cardiol 2013;62:826-38.
215. Steel K, Broderick R, Gandla V et al. Complementary prognostic values of stress myocardial perfusion and late gadolinium enhancement imaging by cardiac magnetic resonance in patients with known or suspected coronary artery disease. Circulation 2009;120:1390-400.
216. Bruder O, Schneider S, Nothnagel D et al. EuroCMR (European Cardiovascular Magnetic Resonance) registry: results of the German pilot phase. J Am Coll Cardiol 2009;54:1457-66.
217. Fenchel M, Kramer U, Nael K, Miller S. Cardiac magnetic resonance imaging at 3.0 T. Top Magn Reson Imaging 2007;18:95-104.
218. Gutberlet M, Noeske R, Schwinge K, Freyhardt P, Felix R, Niendorf T. Comprehensive cardiac magnetic resonance imaging at 3.0 Tesla: feasibility and implications for clinical applications. Invest Radiol 2006;41:154-67.
219. Meyer C, Strach K, Thomas D et al. High-resolution myocardial stress perfusion at 3 T in patients with suspected coronary artery disease. Eur Radiol 2008;18:226-33.
220. Klumpp BD, Seeger A, Doesch C et al. High resolution myocardial magnetic resonance stress perfusion imaging at 3 T using a 1 M contrast agent. Eur Radiol 2010;20:533-41.
221. Cheng AS, Pegg TJ, Karamitsos TD et al. Cardiovascular magnetic resonance perfusion imaging at 3-tesla for the detection of coronary artery disease: a comparison with 1.5-tesla. J Am Coll Cardiol 2007;49:2440-9.
222. Deshpande VS, Shea SM, Li D. Artifact reduction in true-FISP imaging of the coronary arteries by adjusting imaging frequency. Magnetic resonance in medicine 2003;49:803-9.
223. Atalay MK, Poncelet BP, Kantor HL, Brady TJ, Weisskoff RM. Cardiac susceptibility artifacts arising from the heart-lung interface. Magnetic resonance in medicine 2001;45:341-5.
224. Hu X, Norris DG. Advances in high-field magnetic resonance imaging. Annu Rev Biomed Eng 2004;6:157-84.
225. Mueller A, Kouwenhoven M, Naehle CP et al. Dual-source radiofrequency transmission with patient-adaptive local radiofrequency shimming for 3.0-T cardiac MR imaging: initial experience. Radiology 2012;263:77-85.
226. Strach K, Clauberg R, Muller A et al. Feasibility of high-dose dobutamine stress SSFP Cine MRI at 3 Tesla with patient adaptive local RF Shimming using dual-source RF transmission: initial results. Rofo 2013;185:34-9.
227. Schar M, Vonken EJ, Stuber M. Simultaneous B(0)- and B(1)+-map acquisition for fast localized shim, frequency, and RF power determination in the heart at 3 T. Magnetic resonance in medicine 2010;63:419-26.
228. Buehrer M, Pruessmann KP, Boesiger P, Kozerke S. Array compression for MRI with large coil arrays. Magnetic resonance in medicine 2007;57:1131-9.
229. Schmitt M, Potthast A, Sosnovik DE et al. A 128-channel receive-only cardiac coil for highly accelerated cardiac MRI at 3 Tesla. Magnetic resonance in medicine 2008;59:1431-9.

230. Pruessmann KP, Weiger M, Scheidegger MB, Boesiger P. SENSE: sensitivity encoding for fast MRI. Magnetic resonance in medicine 1999;42:952-62.
231. Goldfarb JW. The SENSE ghost: field-of-view restrictions for SENSE imaging. J Magn Reson Imaging 2004;20:1046-51.
232. Griswold MA, Jakob PM, Heidemann RM et al. Generalized autocalibrating partially parallel acquisitions (GRAPPA). Magnetic resonance in medicine 2002;47:1202-10.
233. Madore B, Glover GH, Pelc NJ. Unaliasing by fourier-encoding the overlaps using the temporal dimension (UNFOLD), applied to cardiac imaging and fMRI. Magnetic resonance in medicine 1999;42:813-28.
234. Tsao J, Kozerke S. MRI temporal acceleration techniques. J Magn Reson Imaging 2012;36:543-60.
235. Kozerke S, Tsao J. Reduced data acquisition methods in cardiac imaging. Top Magn Reson Imaging 2004;15:161-8.
236. Pedersen H, Kozerke S, Ringgaard S, Nehrke K, Kim WY. k-t PCA: temporally constrained k-t BLAST reconstruction using principal component analysis. Magnetic resonance in medicine 2009;62:706-16.
237. Ge L, Kino A, Griswold M, Mistretta C, Carr JC, Li D. Myocardial perfusion MRI with sliding-window conjugate-gradient HYPR. Magnetic resonance in medicine 2009;62:835-9.
238. Ma H, Yang J, Liu J et al. Myocardial perfusion magnetic resonance imaging using sliding-window conjugate-gradient highly constrained back-projection reconstruction for detection of coronary artery disease. Am J Cardiol 2012;109:1137-41.
239. Salerno M, Sica CT, Kramer CM, Meyer CH. Optimization of spiral-based pulse sequences for first-pass myocardial perfusion imaging. Magnetic resonance in medicine 2011;65:1602-10.
240. Chen L, Adluru G, Schabel MC, McGann CJ, Dibella EV. Myocardial perfusion MRI with an undersampled 3D stack-of-stars sequence. Med Phys 2012;39:5204-11.
241. Shin T, Nayak KS, Santos JM, Nishimura DG, Hu BS, McConnell MV. Three-dimensional first-pass myocardial perfusion MRI using a stack-of-spirals acquisition. Magnetic resonance in medicine 2013;69:839-44.
242. Plein S, Radjenovic A, Ridgway JP et al. Coronary artery disease: myocardial perfusion MR imaging with sensitivity encoding versus conventional angiography. Radiology 2005;235:423-30.
243. Plein S, Schwitter J, Suerder D, Greenwood JP, Boesiger P, Kozerke S. k-Space and time sensitivity encoding-accelerated myocardial perfusion MR imaging at 3.0 T: comparison with 1.5 T. Radiology 2008;249:493-500.
244. Manka R, Vitanis V, Boesiger P, Flammer AJ, Plein S, Kozerke S. Clinical feasibility of accelerated, high spatial resolution myocardial perfusion imaging. JACC Cardiovasc Imaging 2010;3:710-7.
245. Lockie T, Ishida M, Perera D et al. High-resolution magnetic resonance myocardial perfusion imaging at 3.0-Tesla to detect hemodynamically significant coronary stenoses as determined by fractional flow reserve. J Am Coll Cardiol 2011;57:70-5.
246. Morton G, Ishida M, Schuster A et al. Perfusion cardiovascular magnetic resonance: Comparison of an advanced, high-resolution and a standard sequence. J Cardiovasc Magn Reson 2012;14:34.

247. Kramer CM, Barkhausen J, Flamm SD, Kim RJ, Nagel E. Standardized cardiovascular magnetic resonance (CMR) protocols 2013 update. J Cardiovasc Magn Reson 2013;15:91.
248. Wijns W, Kolh P, Danchin N et al. Guidelines on myocardial revascularization. Eur Heart J 2010;31:2501-55.
249. Motwani M, Jogiya R, Kozerke S, Greenwood JP, Plein S. Advanced cardiovascular magnetic resonance myocardial perfusion imaging: high-spatial resolution versus 3-dimensional whole-heart coverage. Circ Cardiovasc Imaging 2013;6:339-48.
250. Takase B, Nagata M, Kihara T et al. Whole-heart dipyridamole stress first-pass myocardial perfusion MRI for the detection of coronary artery disease. Jpn Heart J 2004;45:475-86.
251. Shin T, Hu HH, Pohost GM, Nayak KS. Three dimensional first-pass myocardial perfusion imaging at 3T: feasibility study. J Cardiovasc Magn Reson 2008;10:57.
252. Shin T, Pohost GM, Nayak KS. Systolic 3D first-pass myocardial perfusion MRI: Comparison with diastolic imaging in healthy subjects. Magnetic resonance in medicine 2010;63:858-64.
253. Manka R, Jahnke C, Kozerke S et al. Dynamic 3-dimensional stress cardiac magnetic resonance perfusion imaging: detection of coronary artery disease and volumetry of myocardial hypoenhancement before and after coronary stenting. J Am Coll Cardiol 2011;57:437-44.
254. Petersen SE, Jerosch-Herold M, Hudsmith LE et al. Evidence for microvascular dysfunction in hypertrophic cardiomyopathy: new insights from multiparametric magnetic resonance imaging. Circulation 2007;115:2418-25.
255. Quyyumi AA, Panza JA, Diodati JG, Lakatos E, Epstein SE. Circadian variation in ischemic threshold. A mechanism underlying the circadian variation in ischemic events. Circulation 1992;86:22-8.
256. Muhling OM, Dickson ME, Zenovich A et al. Quantitative magnetic resonance first-pass perfusion analysis: inter- and intraobserver agreement. J Cardiovasc Magn Reson 2001;3:247-56.
257. Elkington AG, Gatehouse PD, Ablitt NA, Yang GZ, Firmin DN, Pennell DJ. Interstudy reproducibility of quantitative perfusion cardiovascular magnetic resonance. J Cardiovasc Magn Reson 2005;7:815-22.
258. Chih S, Macdonald PS, Feneley MP, Law M, Graham RM, McCrohon JA. Reproducibility of adenosine stress cardiovascular magnetic resonance in multi-vessel symptomatic coronary artery disease. J Cardiovasc Magn Reson 2010;12:42.
259. Geisterfer-Lowrance AA, Christe M, Conner DA et al. A mouse model of familial hypertrophic cardiomyopathy. Science 1996;272:731-4.
260. Schwitter J, Nanz D, Kneifel S et al. Assessment of myocardial perfusion in coronary artery disease by magnetic resonance: a comparison with positron emission tomography and coronary angiography. Circulation 2001;103:2230-5.
261. Laine H, Raitakari OT, Niinikoski H et al. Early impairment of coronary flow reserve in young men with borderline hypertension. J Am Coll Cardiol 1998;32:147-53.
262. Pop-Busui R, Kirkwood I, Schmid H et al. Sympathetic dysfunction in type 1 diabetes: association with impaired myocardial blood flow reserve and diastolic dysfunction. J Am Coll Cardiol 2004;44:2368-74.
263. Ortiz PA, Garvin JL. Cardiovascular and renal control in NOS-deficient mouse models. Am J Physiol Regul Integr Comp Physiol 2003;284:R628-38.

264. Prinzen FW, Bassingthwaighte JB. Blood flow distributions by microsphere deposition methods. Cardiovasc Res 2000;45:13-21.
265. Kass DA, Hare JM, Georgakopoulos D. Murine cardiac function: a cautionary tail. Circ Res 1998;82:519-22.
266. Hirai T, Nohara R, Hosokawa R et al. Evaluation of myocardial infarct size in rat heart by pinhole SPECT. J Nucl Cardiol 2000;7:107-11.
267. Raher MJ, Thibault H, Poh KK et al. In vivo characterization of murine myocardial perfusion with myocardial contrast echocardiography: validation and application in nitric oxide synthase 3 deficient mice. Circulation 2007;116:1250-7.
268. Vandsburger MH, Janiczek RL, Xu Y et al. Improved arterial spin labeling after myocardial infarction in mice using cardiac and respiratory gated look-locker imaging with fuzzy C-means clustering. Magnetic resonance in medicine 2010;63:648-57.
269. Kober F, Iltis I, Cozzone PJ, Bernard M. Myocardial blood flow mapping in mice using high-resolution spin labeling magnetic resonance imaging: influence of ketamine/xylazine and isoflurane anesthesia. Magnetic resonance in medicine 2005;53:601-6.
270. Herold V, Morchel P, Faber C, Rommel E, Haase A, Jakob PM. In vivo quantitative three-dimensional motion mapping of the murine myocardium with PC-MRI at 17.6 T. Magnetic resonance in medicine 2006;55:1058-64.
271. Gilson WD, Kraitchman DL. Cardiac magnetic resonance imaging in small rodents using clinical 1.5 T and 3.0 T scanners. Methods 2007;43:35-45.
272. Makowski M, Jansen C, Webb I et al. First-pass contrast-enhanced myocardial perfusion MRI in mice on a 3-T clinical MR scanner. Magnetic resonance in medicine 2010;64:1592-8.
273. Roth DM, Swaney JS, Dalton ND, Gilpin EA, Ross J, Jr. Impact of anesthesia on cardiac function during echocardiography in mice. American journal of physiology Heart and circulatory physiology 2002;282:H2134-40.
274. de Kemp RA, Epstein FH, Catana C, Tsui BM, Ritman EL. Small-animal molecular imaging methods. J Nucl Med 2010;51 Suppl 1:18S-32S.
275. van Nierop BJ, Coolen BF, Dijk WJ et al. Quantitative first-pass perfusion MRI of the mouse myocardium. Magnetic resonance in medicine 2013;69:1735-44.
276. Van Oosterhout MF, Willigers HM, Reneman RS, Prinzen FW. Fluorescent microspheres to measure organ perfusion: validation of a simplified sample processing technique. Am J Physiol 1995;269:H725-33.
277. Serrat MA. Measuring bone blood supply in mice using fluorescent microspheres. Nat Protoc 2009;4:1779-58.
278. Gussakovsky E, Kuzio B, Yang Y, Kupriyanov V. Fluorescence imaging to quantify the fluorescent microspheres in cardiac tissue. J Biophotonics 2011;4:277-87.
279. Chen GH, Tang J, Leng S. Prior image constrained compressed sensing (PICCS): a method to accurately reconstruct dynamic CT images from highly undersampled projection data sets. Med Phys 2008;35:660-3.
280. Mistretta CA. Undersampled radial MR acquisition and highly constrained back projection (HYPR) reconstruction: potential medical imaging applications in the post-Nyquist era. J Magn Reson Imaging 2009;29:501-16.
281. Jogiya R, Kozerke S, Morton G et al. Validation of dynamic 3-dimensional whole heart magnetic resonance myocardial perfusion imaging against fractional flow reserve for the detection of significant coronary artery disease. J Am Coll Cardiol 2012;60:756-65.

282. Jogiya R, Morton G, De Silva K et al. Ischemic burden by 3-dimensional myocardial perfusion cardiovascular magnetic resonance: comparison with myocardial perfusion scintigraphy. Circ Cardiovasc Imaging 2014;7:647-54.
283. Jogiya R, Schuster A, Zaman A et al. Three-dimensional balanced steady state free precession myocardial perfusion cardiovascular magnetic resonance at 3T using dual-source parallel RF transmission: initial experience. J Cardiovasc Magn Reson 2014;16:90.
284. Manning WJ, Atkinson DJ, Grossman W, Paulin S, Edelman RR. First-pass nuclear magnetic resonance imaging studies using gadolinium-DTPA in patients with coronary artery disease. J Am Coll Cardiol 1991;18:959-65.
285. DiBella EV, Chen L, Schabel MC, Adluru G, McGann CJ. Myocardial perfusion acquisition without magnetization preparation or gating. Magn Reson Med 2012;67:609-13.
286. Manka R, Paetsch I, Kozerke S et al. Whole-heart dynamic three-dimensional magnetic resonance perfusion imaging for the detection of coronary artery disease defined by fractional flow reserve: determination of volumetric myocardial ischaemic burden and coronary lesion location. Eur Heart J 2012;33:2016-24.
287. Giri S, Xue H, Maiseyeu A et al. Steady-state first-pass perfusion (SSFPP): a new approach to 3D first-pass myocardial perfusion imaging. Magn Reson Med 2014;71:133-44.
288. Motwani M, Kidambi A, Sourbron S et al. Quantitative three-dimensional cardiovascular magnetic resonance myocardial perfusion imaging in systole and diastole. J Cardiovasc Magn Reson 2014;16:19.
289. Schmidt JF, Wissmann L, Manka R, Kozerke S. Iterative k-t principal component analysis with nonrigid motion correction for dynamic three-dimensional cardiac perfusion imaging. Magn Reson Med 2014;72:68-79.
290. Akcakaya M, Basha TA, Pflugi S et al. Localized spatio-temporal constraints for accelerated CMR perfusion. Magn Reson Med 2014;72:629-39.
291. Wang H, Bangerter NK, Park DJ et al. Comparison of centric and reverse-centric trajectories for highly accelerated three-dimensional saturation recovery cardiac perfusion imaging. Magn Reson Med 2015;74:1070-6.
292. Manka R, Wissmann L, Gebker R et al. Multicenter evaluation of dynamic three-dimensional magnetic resonance myocardial perfusion imaging for the detection of coronary artery disease defined by fractional flow reserve. Circ Cardiovasc Imaging 2015;8.
293. McDiarmid AK, Ripley DP, Mohee K et al. Three-dimensional whole-heart vs. two-dimensional high-resolution perfusion-CMR: a pilot study comparing myocardial ischaemic burden. Eur Heart J Cardiovasc Imaging 2015.
294. Manka R, Kuhn FP, Kuest SM, Gaemperli O, Kozerke S, Kaufmann PA. Hybrid cardiac magnetic resonance/computed tomographic imaging: first fusion of three-dimensional magnetic resonance perfusion and low-dose coronary computed tomographic angiography. Eur Heart J 2011;32:2625.
295. Gotschy A, Wissmann L, Goolaub DS et al. First fusion and combined evaluation of 3D-CMR perfusion with 3D-MR coronary angiography. Int J Cardiol 2016;202:62-3.
296. Ahlander BM, Maret E, Brudin L, Starck SA, Engvall J. An echo-planar imaging sequence is superior to a steady-state free precession sequence for visual as well as quantitative assessment of cardiac magnetic resonance stress perfusion. Clin Physiol Funct Imaging 2015.

297. Windecker S, Kolh P, Alfonso F et al. 2014 ESC/EACTS Guidelines on myocardial revascularization: The Task Force on Myocardial Revascularization of the European Society of Cardiology (ESC) and the European Association for Cardio-Thoracic Surgery (EACTS)Developed with the special contribution of the European Association of Percutaneous Cardiovascular Interventions (EAPCI). Eur Heart J 2014;35:2541-619.
298. Jahnke C, Kozerke S, Schnackenburg B, Marx N, Paetsch I. Three-dimensional contrast-enhanced and non-contrast-enhanced cardiac magnetic resonance imaging for the assessment of myocardial ischemic reactions: the practice of looking deeply into the myocardium. J Nucl Cardiol 2011;18:937-51.
299. Jogiya R, Makowski M, Phinikaridou A et al. Hyperemic stress myocardial perfusion cardiovascular magnetic resonance in mice at 3 Tesla: initial experience and validation against microspheres. J Cardiovasc Magn Reson 2013;15:62.
300. Trabold F, Pons S, Hagege AA et al. Cardiovascular phenotypes of kinin B2 receptor- and tissue kallikrein-deficient mice. Hypertension 2002;40:90-5.
301. Coolen BF, Moonen RP, Paulis LE, Geelen T, Nicolay K, Strijkers GJ. Mouse myocardial first-pass perfusion MR imaging. Magn Reson Med 2010;64:1658-63.
302. van Nierop BJ, Coolen BF, Bax NA et al. Myocardial perfusion MRI shows impaired perfusion of the mouse hypertrophic left ventricle. Int J Cardiovasc Imaging 2014;30:619-28.
303. Naresh NK, Chen X, Moran E, Tian Y, French BA, Epstein FH. Repeatability and variability of myocardial perfusion imaging techniques in mice: Comparison of arterial spin labeling and first-pass contrast-enhanced MRI. Magn Reson Med 2015.
304. Maredia N, Radjenovic A, Kozerke S, Larghat A, Greenwood JP, Plein S. Effect of improving spatial or temporal resolution on image quality and quantitative perfusion assessment with k-t SENSE acceleration in first-pass CMR myocardial perfusion imaging. Magn Reson Med 2010;64:1616-24.
305. Chiribiri A, Hautvast GL, Lockie T et al. Assessment of coronary artery stenosis severity and location: quantitative analysis of transmural perfusion gradients by high-resolution MRI versus FFR. JACC Cardiovasc Imaging 2013;6:600-9.
306. Thiele H, Plein S, Ridgway JP et al. Effects of missing dynamic images on myocardial perfusion reserve index calculation: comparison between an every heartbeat and an alternate heartbeat acquisition. J Cardiovasc Magn Reson 2003;5:343-52.
307. Morton G, Jogiya R, Plein S, Schuster A, Chiribiri A, Nagel E. Quantitative cardiovascular magnetic resonance perfusion imaging: inter-study reproducibility. Eur Heart J Cardiovasc Imaging 2012;13:954-60.
308. Larghat AM, Maredia N, Biglands J et al. Reproducibility of first-pass cardiovascular magnetic resonance myocardial perfusion. J Magn Reson Imaging 2013;37:865-74.
309. Goykhman P, Mehta PK, Agarwal M et al. Reproducibility of myocardial perfusion reserve - variations in measurements from post processing using commercially available software. Cardiovasc Diagn Ther 2012;2:268-77.
310. Santelli C, Schaeffter T, Kozerke S. Radial k-t SPIRiT: autocalibrated parallel imaging for generalized phase-contrast MRI. Magn Reson Med 2014;72:1233-45.

# Appendix A

## Multi-center Evaluation of Dynamic Three-dimensional Magnetic Resonance Myocardial Perfusion Imaging for the Detection of Coronary Artery Disease Defined by Fractional Flow Reserve

Robert Manka[1,2], Lukas Wissmann[1], Rolf Gebker[3], Roy Jogiya[4], Manish Motwani[5], Michael Frick[6], Sebastian Reinartz[6], Bernhard Schnackenburg[3], Markus Niemann[2], Alexander Gotschy[2], Christiane Kuhl[6], Eike Nagel[4], Eckart Fleck[3], Nikolaus Marx[6], Thomas F. Luescher[2], Sven Plein[5], Sebastian Kozerke[1],

1. University and ETH Zurich, Zurich, Switzerland
2. University Heart Center, University Hospital Zurich, Zurich, Switzerland
3. German Heart Institute, Berlin, Germany
4. King's College London, London, United Kingdom
5. University of Leeds, Leeds, United Kingdom
6. University Hospital RWTH Aachen, Germany

Short title
Multi-center Evaluation of 3D MR Myocardial Perfusion Imaging

Correspondence Sebastian Kozerke, PhD
Institute for Biomedical Engineering
University and ETH Zurich
Gloriastrasse 35
8092 Zurich
Switzerland
Tel. +41 44 632 35 49
Fax. +41 44 632 11 93
E-mail: kozerke@biomed.ee.ethz.ch

**Abstract**

**Background** – First-pass myocardial perfusion cardiovascular magnetic resonance (CMR) imaging yields high diagnostic accuracy for the detection of coronary artery disease (CAD). However, standard 2D multi-slice CMR perfusion techniques provide only limited cardiac coverage and hence considerable assumptions are required to assess myocardial ischemic burden. The aim of this prospective study was to assess the diagnostic performance of 3D myocardial perfusion CMR to detect functionally relevant CAD with FFR as a reference standard in a multi-center setting.

**Methods and Results** – A total of 155 patients with suspected CAD listed for coronary angiography with FFR were prospectively enrolled from 5 European centers. 3D perfusion CMR was acquired on 3T MR systems from a single vendor under adenosine stress and at rest. All CMR perfusion analyses were performed in a central laboratory and blinded to all clinical data. 150 patients were successfully examined (mean age 62.9+/-10 years, 45 female). The prevalence of CAD defined by FFR (<0.8) was 56.7% (85 of 150 patients). The sensitivity and specificity of 3D perfusion CMR were 84.7% and 90.8% relative to the FFR reference. Comparison to QCA (≥50%) yielded a prevalence of 65.3%, sensitivity and specificity of 76.5% and 94.2%, respectively.

**Conclusions** – In this multi-center study 3D myocardial perfusion CMR proved highly diagnostic for the detection of significant CAD as defined by FFR.

**Keywords –** myocardial perfusion, cardiovascular magnetic resonance, three-dimensional perfusion imaging, myocardial ischemic burden, fractional flow reserve, multi-center study

## Introduction

Myocardial perfusion imaging with cardiovascular magnetic resonance (CMR) yields high diagnostic accuracy for the detection of coronary artery disease (CAD)[1-8] and its prognostic value has also been documented[9-13]. Standard two-dimensional (2D) multi-slice perfusion CMR techniques have been compared with single photon emission computed tomography (SPECT) in multi-center and single center trials[2, 5, 7, 14, 15] confirming the high diagnostic accuracy of CMR in prospective patient cohorts. Excellent diagnostic performance has been documented relative to hemodynamic measurements using fractional flow reserve (FFR) at 1.5T in a single center setting[16]. A potential limitation of standard 2D techniques, however, relates to the limited spatial coverage, which requires geometrical assumptions for the quantification of ischemic tissue volume to guide therapy as recommended by the recent European guidelines on myocardial revascularization[17]. Compared with methods that cover the whole heart, the acquisition of a limited number of slice may also affect the diagnostic performance as has been indicated previously by comparing 3D versus simulated 3-slice 2D perfusion imaging[18].

In order to address the limited, non-contiguous coverage of 2D multi-slice myocardial perfusion CMR techniques, three-dimensional (3D) methods have been developed based on recent advances in CMR scan acceleration methodology[19, 20]. Whole-heart coverage is achieved by employing data undersampling strategies in conjunction with appropriate image reconstruction techniques[21] such as (*k*-*t*) imaging including sensitivity encoding (SENSE)[19, 20, 22-24] or principal component analysis (PCA)[25]. The diagnostic accuracy of 3D perfusion CMR has recently been validated in single-center studies against both quantitative coronary angiography (QCA)[18] and FFR[26] in patients with known or suspected CAD. Estimates of myocardial ischemic burden from 3D perfusion CMR have

also been shown to strongly correlate with those from SPECT[27]. In addition, the high inter-study reproducibility of 3D myocardial perfusion CMR at 1.5 Tesla has been shown in two different centers [28].

The objective of the current study was to prospectively evaluate the diagnostic performance of dynamic whole-heart 3D myocardial perfusion CMR at 3.0 Tesla for the detection of significant CAD as defined by FFR in a multi-center setting.

## Methods

### Study Population

The present prospective study was conducted at five European centers (University Hospital Zurich, Switzerland; University Hospital RWTH Aachen, Germany; German Heart Institute Berlin, Germany; King's College London, United Kingdom; University of Leeds, United Kingdom). The study was approved by the local ethics review boards and patients were prospectively enrolled upon written informed consent. Patients scheduled for diagnostic coronary angiography for the evaluation of suspected CAD were consecutively recruited between November 2011 and August 2013. Patients were instructed to refrain from caffeine-containing substances 24 hours prior to the examination. Exclusion criteria were standard contraindications for CMR imaging (e.g. incompatible metallic implants and claustrophobia) and adenosine infusion (e.g. high grade atrio-ventricular block and asthma).

### Cardiovascular Magnetic Resonance Protocol

CMR imaging was performed with the patient in the supine position using 3.0 Tesla MR systems (Philips Healthcare, Best, The Netherlands). Depending on the actual MR scanner version, either 6-element cardiac or 28-element torso coil arrays were used for signal reception and cardiac synchronization was performed using a vector-ECG.

After the acquisition of standard cine scans for the assessment of left ventricular function, 3D myocardial perfusion CMR imaging was planned in short-axis geometry with full left-ventricular coverage. Adenosine was administered intravenously at a dose of 140µg/kg/min under continuous monitoring of heart rate and blood pressure. After at least three minutes of adenosine infusion stress first-pass perfusion imaging (i.v.

bolus application of 0.075mmol/kg b.w. of a gadolinium-based contrast agent, Gadovist, Bayer Healthcare, Berlin, Germany; injection rate 4.0ml/s followed by 20ml saline flush) was performed. After a 15-minute waiting period for equilibration of the contrast agent within the myocardium, the identical 3D myocardial perfusion CMR scan was repeated at rest. Dynamic perfusion data were acquired in every heartbeat over 30 cardiac cycles with a 3D saturation prepared spoiled turbo gradient echo sequence (TR/TE/flip angle 1.8ms/0.7ms/15°, saturation pre-pulse delay 150ms, acquisition timed to end-systole, 75% partial Fourier sampling in two directions including an elliptical k-space shutter, 10x k-t acquisition with 49 training profiles resulting in a net acceleration of 7x and an acquisition window per heartbeat of 200ms, *k-t* principal component analysis reconstruction of 16 contiguous slices of 5mm thickness, acquired voxel size 2.3x2.3mm$^2$)[20]. Perfusion imaging was performed during a single inspiration breathhold. Shallow expiration was permitted in case the inspiration breathhold could not be sustained during the scan. Using this approach, data acquisition in all patients suitable for CMR exams was possible.

Following a further 15-minute waiting period late gadolinium enhancement (LGE) imaging (0.15 mmol/kg b.w. cumulative dose) was performed in the identical short-axis geometry with a 3D inversion prepared spoiled gradient-echo sequence (TR/TE/flip angle: 3.6 ms/1.8 ms/15°, voxel size 1.6x1.6x10 mm$^3$). The inversion recovery pre-pulse delay was determined using a Look-Locker sequence and adjusted accordingly.

Example whole-heart 3D myocardial perfusion CMR images acquired during adenosine stress and at rest are presented in Figure 1.

**Visual Assessment of Perfusion Scans**

CMR images were analyzed visually in a central data analysis lab by reviewers blinded to clinical and angiographic patient data using a dedicated workstation (ExtendedWorkSpace, Philips Healthcare, Best, The Netherlands).

Overall image quality of stress and rest perfusions scans was graded on a scale between 1 and 4 (1= non-diagnostic, 2= poor, 3= good, 4= excellent). From all acquired image slices the subset of short-axis slices with clearly identifiable left-ventricular cavity enhancement during contrast agent passage and with >75% circumferential left-ventricular myocardium present were identified. The selected short-axis slices were divided into 6 equally distributed circumferential segments each and evaluated visually. Perfusion defects on the stress perfusion images seen in any segment (≥1 segment) with ≥25% transmurality persisting for ≥3 consecutive dynamics, which were not visible in the rest perfusion scan and showed no enhancement in the LGE scan, were marked to be pathologic and the overall study was considered as abnormal.

**Assessment of Myocardial Ischemic Burden**

Myocardial ischemic burden (MIB) was estimated based on the quantification of the tissue volume exhibiting myocardial hypo-enhancement using dedicated software (GTVolume, GyroTools LLC, Zurich, Switzerland). For determination of myocardial hypo-enhancement the dynamic frame of the stress perfusion scan showing the maximum extent of regional hypo-enhancement during peak signal enhancement of remote myocardium was selected [19,20]. In the presence of extensive ischemia-related hypo-enhancement (e.g. high grade triple vessel disease) remote myocardium either represented an entire myocardial segment or its subepicardial layer. The left ventricular

endo- and epicardial borders were manually identified in all slices to determine myocardial volume. Quantification of hypo-enhanced tissue volume was performed automatically using threshold-based segmentation with a signal intensity threshold >2x standard deviation (SD) below the signal of remote myocardium. Segmentation of myocardial hypo-enhancement during stress is illustrated in Figure 2 for the patient data shown in Figure 1.

Total volumes of left ventricular myocardium and hypo-enhanced myocardium were calculated using the disk summation method. Myocardial ischemic burden (MIB) was defined by the volume of hypo-enhancement normalized to total left ventricular myocardial volume and is quoted in percentage. In case of concurrent presence of myocardial scar as identified on LGE images, the amount of scar tissue volume was calculated based on segmentation of hyper-intense tissue. Subsequently, the scar tissue volume was subtracted from the volume of hypo-enhancement prior to MIB calculation.

**Fractional Flow Reserve and Quantitative Coronary Angiography Measurements**

Fractional flow reserve (FFR) was measured using standard methods[28] with a 0.014-inch coronary pressure sensor–tip wire (Volcano Therapeutics, San Diego, California or Pressure-Wire Certus, St. Jude Medical Systems AB, Uppsala, Sweden) in vessels visually assessed by the angiographers as having ≥50% and ≤80% diameter stenosis in two orthogonal views with ≥2mm luminal diameter. For the purpose of the study and in accordance to guidelines, stenoses in vessels with less than 2mm luminal diameter were considered non-significant[29]. Coronary stenosis with an FFR value <0.8 were classified as hemodynamically relevant. Total/subtotal occlusion or high-grade stenosis (>80% diameter stenosis) did not undergo pressure wire assessment and were considered hemodynamically significant.

Coronary angiography was performed by routine techniques. At least two orthogonal views of every major coronary vessel and its side branches were acquired. Quantitative coronary angiography (QCA) was performed off-line by an independent core laboratory being blinded to the results of CMR imaging.

**Statistical Analysis**

Data analysis was performed using SPSS for Windows 17.0.0 (SPSS Inc., Chicago, Illinois, USA). Data were evaluated on a patient basis to determine sensitivity, specificity, negative and positive predictive values with corresponding 95%-confidence intervals [95%-CI] according to standard definitions. Continuous variables are expressed as mean±standard deviation (SD); categorical variables are expressed as proportions. The paired Student's t-test was used to assess the statistical significance of continuous variables between rest and stress. All tests were two-tailed; $P<0.05$ was considered significant. Receiver-operator characteristic curve (ROC) analysis was used to determine the diagnostic accuracy (area under curve [AUC]) and optimal cut-off value of MIB to detect significant CAD defined by fractional flow reserve <0.8.

## Results

### Patient Characteristics

The characteristics of the patient cohort are listed in Table 1. Of the 155 recruited patients, 2 studies were lost due to data storage failure, 1 study was incomplete because of patient claustrophobia, 1 study had to be terminated due to a bronchospasm during adenosine infusion and 1 study was incomplete because of an unknown ferromagnetic splint in the chest wall. Accordingly, a total of 150 patients (n=30 from Zurich, n=30 from Aachen, n=32 from Berlin, n=31 from London and n=27 from Leeds; n=105 (70%) male; mean age 62.9±10.0 years, range 33-83 years) formed the final population for analysis. Table 2 lists the hemodynamic data recorded during the CMR examination.

### Diagnostic Performance

The prevalence of CAD as defined by FFR <0.8 was 56.7% (85 of 150 patients) and the sensitivity of 3D perfusion CMR was 84.7% (95% CI: 75.3 to 91.6) with a specificity of 90.8% (95% CI: 81.0 to 96.5) and diagnostic accuracy of 87.3% (95% CI: 81.1 to 91.7). Positive and negative predictive values were 92.3% (95% CI: 84.0 to 97.1) and 81.9 (95% CI: 71.1 to 90.0), respectively. The prevalence of CAD as defined by QCA≥50% was 65.3% (98 of 150 patients). Analysis of 3D CMR perfusion data with QCA as the reference standard yielded a sensitivity of 76.5% (95% CI: 66.9 to 84.5), specificity of 94.2% (95% CI: 84.0 to 98.7), and diagnostic accuracy of 82.6% (95% CI: 75.8 to 87.9). The positive predictive value was 96.2% (95% CI: 89.2 to 99.2) and the negative predictive value was 68.1% (95% CI: 56.0 to 78.55).

**Myocardial Ischemic Burden**

The mean MIB in all patients was 10.1±12.2% (range, 0 to 51.7%). The mean MIB in patients grouped by FFR status is given in Figure 3.

The diagnostic accuracy (AUC) of MIB to detect significant CAD as defined by FFR was 0.91; and the optimal MIB cut-off value was 4.1%, which resulted in a sensitivity and specificity of 84.7% (95% CI 75.3-91.6) and 92.3% (95% CI 82.9 to 97.3), respectively (Figure 4).

**Image Quality**

The 3D CMR stress and rest perfusion scans of all 150 patients were of diagnostic image quality (image quality score ≥2). The mean visual scores of 3D stress and rest CMR perfusion scans were 3.57 ± 0.58 and 3.65 ± 0.51, respectively.

## Discussion

The present multi-center study has assessed the diagnostic performance of whole-heart 3D myocardial perfusion CMR for the detection of significant CAD as determined by FFR and QCA. The main findings of the study are: (1) 3D myocardial perfusion CMR at 3.0 Tesla is a robust technique for the detection of CAD in a European multi-center, single-vendor setting; (2) the diagnostic accuracy of 3D myocardial perfusion CMR to detect functionally significant CAD is high and confirms previous data on 2D multi-slice and 3D whole-heart myocardial perfusion CMR using FFR as the reference standard[16, 26, 28, 31]; and (3) the myocardial ischemic burden derived from 3D whole-heart myocardial perfusion CMR provides an accurate diagnostic tool for the detection of flow-limiting CAD.

Relative to previous single-center (3T CMR) and dual-center (1.5T CMR) 3D CMR perfusion studies using FFR as a reference, our results compare well for sensitivity and specificity (85% vs. 91%[26] vs. 90%[28] and 91% vs. 90%[26] vs. 82%[28]) demonstrating robustness of the method also in a European multi-center setting. The added benefit of 3D myocardial perfusion CMR over 2D three-slice imaging for assessing MIB has recently been indicated[27]. Furthermore, the high inter-study, intra- and inter-reader reproducibility has been confirmed[18, 28]. While the present multi-center study was conducted using 3.0T CMR systems, the protocol is readily applicable to 1.5T machines as demonstrated previously[28]. Application of the method on MR systems from different vendors is possible upon modification of the pulse sequence and image reconstruction software. To this end, the image reconstruction code is provided upon request.

While previous single-center validation of three-slice 2D approaches using 1.5T CMR systems yielded similarly high sensitivity and specificity relative to FFR[18], the assessment of ischemic tissue volume was not possible given the limited coverage of 2D

methods. As demonstrated previously, the diagnostic performance of 3D perfusion imaging compares favorably against simulated 3-slice data extracted from the 3D volume[18, 26].

According to current guidelines, the decision to perform coronary revascularization procedures should be based on an objective documentation of myocardial ischemia preferably together with its anatomical localization and amount[17].

Based on current and previous studies, 3D myocardial perfusion CMR may prove a valuable alternative to methods using ionizing radiation to monitor and guide treatment. CMR also allows imaging of at least the proximal coronary anatomy and fusion of 3D CMR perfusion with coronary CMR or low-dose coronary computed tomography angiography (CCTA) offering promise for future comprehensive non-invasive assessment of CAD[33].

The amount of myocardial ischemia is a key factor to guide treatment decisions, i.e. revascularization is recommended in case myocardial ischemic burden exceeds 10%[30] of total left-ventricular myocardium. However, these cut-off values were derived from nuclear studies[34, 35] and, although never directly compared, may not apply to 2D perfusion CMR in view of its limited cardiac coverage. Three-dimensional myocardial perfusion CMR and SPECT agree well with the 10% threshold[27], highlighting another potential benefit of 3D whole-heart versus 2D multi-slice myocardial perfusion CMR.

Today, the invasive assessment of the functional significance of coronary lesions is the basis of therapeutic decision-making[36, 37], even though FFR measurements are invasive, time-consuming and associated with radiation exposure rendering the method less attractive for monitoring patients. To this end and based on the evidence presented here and elsewhere 3D myocardial perfusion CMR may be considered a non-invasive alternative to stratify patients according to guidelines.

## Study Limitations

An important limitation of the study design is that only patients who were already scheduled for a coronary angiogram were recruited in the study. This fact reflects the current practice of referral by external physicians. In line with current guidelines and in order to minimize complications of FFR measurements, hemodynamic assessments were only performed in vessels with luminal stenosis of 50% to 80% at angiography. In addition, the assessment of MIB was given as percentage ischemic myocardium reflecting only relative myocardial perfusion distribution at one particular time point during the dynamic first-pass of the contrast agent. Accordingly, MIB is not a direct measure of quantitative myocardial blood flow. It is furthermore acknowledged that all CMR centers involved in our study are specialized in CMR imaging and it remains to be demonstrated how the technique performs at sites with less experience and expertise.

## Conclusion

This multi-center study has demonstrated the robustness and accuracy of 3D myocardial perfusion CMR to detect functionally significant coronary artery disease as measured by FFR.

## Funding sources

The authors acknowledge support from the Swiss National Science Foundation, grant #CR3213_132671/1, Bayer Healthcare and Philips Healthcare.

## Disclosures

TFL has received consulting honoraria from Philips Healthcare.

References

1. Cheng AS, Pegg TJ, Karamitsos TD, Searle N, Jerosch-Herold M, Choudhury RP, Banning AP, Neubauer S, Robson MD, Selvanayagam JB. Cardiovascular magnetic resonance perfusion imaging at 3-tesla for the detection of coronary artery disease: A comparison with 1.5-tesla. J Am Coll Cardiol. 2007;49:2440-2449

2. Greenwood JP, Maredia N, Younger JF, Brown JM, Nixon J, Everett CC, Bijsterveld P, Ridgway JP, Radjenovic A, Dickinson CJ, Ball SG, Plein S. Cardiovascular magnetic resonance and single-photon emission computed tomography for diagnosis of coronary heart disease (ce-marc): A prospective trial. Lancet. 2012 Feb 4;379(9814):453-60.

3. Nagel E, Klein C, Paetsch I, Hettwer S, Schnackenburg B, Wegscheider K, Fleck E. Magnetic resonance perfusion measurements for the noninvasive detection of coronary artery disease. Circulation. 2003;108:432-437

4. Paetsch I, Jahnke C, Wahl A, Gebker R, Neuss M, Fleck E, Nagel E. Comparison of dobutamine stress magnetic resonance, adenosine stress magnetic resonance, and adenosine stress magnetic resonance perfusion. Circulation. 2004;110:835-842

5. Schwitter J, Wacker CM, van Rossum AC, Lombardi M, Al-Saadi N, Ahlstrom H, Dill T, Larsson HB, Flamm SD, Marquardt M, Johansson L. Mr-impact: Comparison of perfusion-cardiac magnetic resonance with single-photon emission computed tomography for the detection of coronary artery disease in a multicentre, multivendor, randomized trial. Eur Heart J. 2008;29:480-489

6. Manka R, Vitanis V, Boesiger P, Flammer AJ, Plein S, Kozerke S. Clinical feasibility of accelerated, high spatial resolution myocardial perfusion imaging. JACC Cardiovasc Imaging. 2010;3:710-717

7. Greenwood JP, Motwani M, Maredia N, Brown JM, Everett CC, Nixon J, Bijsterveld P, Dickinson CJ, Ball SG, Plein S. Comparison of cardiovascular magnetic resonance and

single-photon emission computed tomography in women with suspected coronary artery disease from the clinical evaluation of magnetic resonance imaging in coronary heart disease (ce-marc) trial. Circulation. 2014;129:1129-1138

8. Jaarsma C, Leiner T, Bekkers SC, Crijns HJ, Wildberger JE, Nagel E, Nelemans PJ, Schalla S. Diagnostic performance of noninvasive myocardial perfusion imaging using single-photon emission computed tomography, cardiac magnetic resonance, and positron emission tomography imaging for the detection of obstructive coronary artery disease: A meta-analysis. J Am Coll Cardiol. 2012;59:1719-1728

9. Jahnke C, Nagel E, Gebker R, Kokocinski T, Kelle S, Manka R, Fleck E, Paetsch I. Prognostic value of cardiac magnetic resonance stress tests: Adenosine stress perfusion and dobutamine stress wall motion imaging. Circulation. 2007;115:1769-1776

10. Coelho-Filho OR, Seabra LF, Mongeon FP, Abdullah SM, Francis SA, Blankstein R, Di Carli MF, Jerosch-Herold M, Kwong RY. Stress myocardial perfusion imaging by cmr provides strong prognostic value to cardiac events regardless of patient's sex. JACC Cardiovasc Imaging. 2011;4:850-861

11. Jahnke C, Furundzija V, Gebker R, Manka R, Frick M, Schnackenburg B, Marx N, Paetsch I. Gender-based prognostic value of pharmacological cardiac magnetic resonance stress testing: Head-to-head comparison of adenosine perfusion and dobutamine wall motion imaging. Int J Cardiovasc Imaging. 2012;28:1087-1098

12. Shah R, Heydari B, Coelho-Filho O, Murthy VL, Abbasi S, Feng JH, Pencina M, Neilan TG, Meadows JL, Francis S, Blankstein R, Steigner M, di Carli M, Jerosch-Herold M, Kwong RY. Stress cardiac magnetic resonance imaging provides effective cardiac risk reclassification in patients with known or suspected stable coronary artery disease. Circulation. 2013;128:605-614

13. Steel K, Broderick R, Gandla V, Larose E, Resnic F, Jerosch-Herold M, Brown KA, Kwong RY. Complementary prognostic values of stress myocardial perfusion and late gadolinium enhancement imaging by cardiac magnetic resonance in patients with known or suspected coronary artery disease. Circulation. 2009;120:1390-1400

14. Schwitter J, Wacker CM, Wilke N, Al-Saadi N, Sauer E, Huettle K, Schonberg SO, Debl K, Strohm O, Ahlstrom H, Dill T, Hoebel N, Simor T. Superior diagnostic performance of perfusion-cardiovascular magnetic resonance versus spect to detect coronary artery disease: The secondary endpoints of the multicenter multivendor mr-impact ii (magnetic resonance imaging for myocardial perfusion assessment in coronary artery disease trial). Journal of cardiovascular magnetic resonance : official journal of the Society for Cardiovascular Magnetic Resonance. 2012;14:61

15. Schwitter J, Wacker CM, Wilke N, Al-Saadi N, Sauer E, Huettle K, Schonberg SO, Luchner A, Strohm O, Ahlstrom H, Dill T, Hoebel N, Simor T. Mr-impact ii: Magnetic resonance imaging for myocardial perfusion assessment in coronary artery disease trial: Perfusion-cardiac magnetic resonance vs. Single-photon emission computed tomography for the detection of coronary artery disease: A comparative multicentre, multivendor trial. Eur Heart J. 2013;34:775-781

16. Watkins S, McGeoch R, Lyne J, Steedman T, Good R, McLaughlin MJ, Cunningham T, Bezlyak V, Ford I, Dargie HJ, Oldroyd KG. Validation of magnetic resonance myocardial perfusion imaging with fractional flow reserve for the detection of significant coronary heart disease. Circulation. 2009;120:2207-221

17. Windecker S, Kolh P, Alfonso F, Collet JP, Cremer J, Falk V, Filippatos G, Hamm C, Head SJ, Juni P, Kappetein AP, Kastrati A, Knuuti J, Landmesser U, Laufer G, Neumann FJ, Richter DJ, Schauerte P, Sousa Uva M, Stefanini GG, Taggart DP, Torracca L, Valgimigli M, Wijns W, Witkowski A. 2014 esc/eacts guidelines on myocardial revascularization: The

task force on myocardial revascularization of the european society of cardiology (esc) and the european association for cardio-thoracic surgery (eacts)developed with the special contribution of the european association of percutaneous cardiovascular interventions (eapci). Eur Heart J. 2014

18. Manka R, Jahnke C, Kozerke S, Vitanis V, Crelier G, Gebker R, Schnackenburg B, Boesiger P, Fleck E, Paetsch I. Dynamic 3-dimensional stress cardiac magnetic resonance perfusion imaging: Detection of coronary artery disease and volumetry of myocardial hypoenhancement before and after coronary stenting. J Am Coll Cardiol. 2011;57:437-444

19. Shin T, Hu HH, Pohost GM, Nayak KS. Three dimensional first-pass myocardial perfusion imaging at 3t: Feasibility study. Journal of cardiovascular magnetic resonance : official journal of the Society for Cardiovascular Magnetic Resonance. 2008;10:57

20. Vitanis V, Manka R, Giese D, Pedersen H, Plein S, Boesiger P, Kozerke S. High resolution three-dimensional cardiac perfusion imaging using compartment-based k-t principal component analysis. Magn Reson Med. 2011;65:575-587

21. Kozerke S, Plein S. Accelerated cmr using zonal, parallel and prior knowledge driven imaging methods. Journal of cardiovascular magnetic resonance : official journal of the Society for Cardiovascular Magnetic Resonance. 2008;10:29

22. Plein S, Ryf S, Schwitter J, Radjenovic A, Boesiger P, Kozerke S. Dynamic contrast-enhanced myocardial perfusion mri accelerated with k-t sense. Magn Reson Med. 2007;58:777-785

23. Tsao J, Boesiger P, Pruessmann KP. K-t blast and k-t sense: Dynamic mri with high frame rate exploiting spatiotemporal correlations. Magn Reson Med. 2003;50:1031-1042

24. Gebker R, Jahnke C, Manka R, Frick M, Hucko T, Kozerke S, Schnackenburg B, Fleck E, Paetsch I. High spatial resolution myocardial perfusion imaging during high dose dobutamine/atropine stress magnetic resonance using k-t sense. International journal of cardiology. 2012;158:411-416

25. Pedersen H, Kozerke S, Ringgaard S, Nehrke K, Kim WY. K-t pca: Temporally constrained k-t blast reconstruction using principal component analysis. Magn Reson Med. 2009;62:706-716

26. Jogiya R, Kozerke S, Morton G, De Silva K, Redwood S, Perera D, Nagel E, Plein S. Validation of dynamic 3-dimensional whole heart magnetic resonance myocardial perfusion imaging against fractional flow reserve for the detection of significant coronary artery disease. J Am Coll Cardiol. 2012;60:756-765

27. Jogiya R, Morton G, De Silva K, Reyes E, Hachamovitch R, Kozerke S, Nagel E, Underwood R, Plein S. Ischemic burden by three-dimensional myocardial perfusion cardiovascular magnetic resonance: Comparison with myocardial perfusion scintigraphy. Circ Cardiovasc Imaging. 2014 Jul;7(4):647-54.

28. Manka R, Paetsch I, Kozerke S, Moccetti M, Hoffmann R, Schroeder J, Reith S, Schnackenburg B, Gaemperli O, Wissmann L, Wyss CA, Kaufmann PA, Corti R, Boesiger P, Marx N, Luscher TF, Jahnke C. Whole-heart dynamic three-dimensional magnetic resonance perfusion imaging for the detection of coronary artery disease defined by fractional flow reserve: Determination of volumetric myocardial ischaemic burden and coronary lesion location. Eur Heart J. 2012;33:2016-2024

29. Pijls NH, De Bruyne B, Peels K, Van Der Voort PH, Bonnier HJ, Bartunek JKJJ, Koolen JJ. Measurement of fractional flow reserve to assess the functional severity of coronary-artery stenoses. N Engl J Med. 1996;334:1703-1708

30. Wijns W, Kolh P, Danchin N, Di Mario C, Falk V, Folliguet T, Garg S, Huber K, James S, Knuuti J, Lopez-Sendon J, Marco J, Menicanti L, Ostojic M, Piepoli MF, Pirlet C, Pomar JL, Reifart N, Ribichini FL, Schalij MJ, Sergeant P, Serruys PW, Silber S, Sousa Uva M, Taggart D, Vahanian A, Auricchio A, Bax J, Ceconi C, Dean V, Filippatos G, Funck-Brentano C, Hobbs R, Kearney P, McDonagh T, Popescu BA, Reiner Z, Sechtem U, Sirnes PA, Tendera M, Vardas PE, Widimsky P, Alfieri O, Dunning J, Elia S, Kappetein P, Lockowandt U, Sarris G, Vouhe P, von Segesser L, Agewall S, Aladashvili A, Alexopoulos D, Antunes MJ, Atalar E, Brutel de la Riviere A, Doganov A, Eha J, Fajadet J, Ferreira R, Garot J, Halcox J, Hasin Y, Janssens S, Kervinen K, Laufer G, Legrand V, Nashef SA, Neumann FJ, Niemela K, Nihoyannopoulos P, Noc M, Piek JJ, Pirk J, Rozenman Y, Sabate M, Starc R, Thielmann M, Wheatley DJ, Windecker S, Zembala M. Guidelines on myocardial revascularization: The task force on myocardial revascularization of the european society of cardiology (esc) and the european association for cardio-thoracic surgery (eacts). Eur Heart J. 2010;31:2501-2555

31. Lockie T, Ishida M, Perera D, Chiribiri A, De Silva K, Kozerke S, Marber M, Nagel E, Rezavi R, Redwood S, Plein S. High-resolution magnetic resonance myocardial perfusion imaging at 3.0-tesla to detect hemodynamically significant coronary stenoses as determined by fractional flow reserve. J Am Coll Cardiol. 2011;57:70-75

32. Rieber J, Huber A, Erhard I, Mueller S, Schweyer M, Koenig A, Schiele TM, Theisen K, Siebert U, Schoenberg SO, Reiser M, Klauss V. Cardiac magnetic resonance perfusion imaging for the functional assessment of coronary artery disease: A comparison with coronary angiography and fractional flow reserve. Eur Heart J. 2006;27:1465-1471

33. Manka R, Kuhn FP, Kuest SM, Gaemperli O, Kozerke S, Kaufmann PA. Hybrid cardiac magnetic resonance/computed tomographic imaging: First fusion of three-

dimensional magnetic resonance perfusion and low-dose coronary computed tomographic angiography. Eur Heart J. 2011;32:2625

34. Hachamovitch R, Hayes SW, Friedman JD, Cohen I, Berman DS. Comparison of the short-term survival benefit associated with revascularization compared with medical therapy in patients with no prior coronary artery disease undergoing stress myocardial perfusion single photon emission computed tomography. Circulation. 2003;107:2900-2907

35. Shaw LJ, Berman DS, Maron DJ, Mancini GB, Hayes SW, Hartigan PM, Weintraub WS, O'Rourke RA, Dada M, Spertus JA, Chaitman BR, Friedman J, Slomka P, Heller GV, Germano G, Gosselin G, Berger P, Kostuk WJ, Schwartz RG, Knudtson M, Veledar E, Bates ER, McCallister B, Teo KK, Boden WE. Optimal medical therapy with or without percutaneous coronary intervention to reduce ischemic burden: Results from the clinical outcomes utilizing revascularization and aggressive drug evaluation (courage) trial nuclear substudy. Circulation. 2008;117:1283-1291

36. Pijls NH, Fearon WF, Tonino PA, Siebert U, Ikeno F, Bornschein B, van't Veer M, Klauss V, Manoharan G, Engstrom T, Oldroyd KG, Ver Lee PN, MacCarthy PA, De Bruyne B. Fractional flow reserve versus angiography for guiding percutaneous coronary intervention in patients with multivessel coronary artery disease: 2-year follow-up of the fame (fractional flow reserve versus angiography for multivessel evaluation) study. J Am Coll Cardiol. 2010;56:177-184

37. Tonino PA, Fearon WF, De Bruyne B, Oldroyd KG, Leesar MA, Ver Lee PN, Maccarthy PA, Van't Veer M, Pijls NH. Angiographic versus functional severity of coronary artery stenoses in the fame study fractional flow reserve versus angiography in multivessel evaluation. J Am Coll Cardiol. 2010;55:2816-2821

**Table 1**

**Patient demographics and clinical data.**

| Parameter | n = 150 |
|---|---|
| Male, n (%) | 105 (70) |
| Age (years) | 62.9 ± 10.0 |
| Age Range | 33 – 83 |
| BMI (kg/m$^2$) | 27.8 ± 4.3 |
| Cardiovascular risk factors, n (%) | |
| Arterial hypertension | 109 (73) |
| Diabetes mellitus | 27 (18) |
| Hyperlipidemia | 100 (67) |
| Smoking | 73 (49) |
| Family history of CAD | 55 (37) |
| Medication, n (%) | |
| β - Blocker | 76 (51) |
| ACE – Inhibitor | 71 (47) |
| Statin | 91 (61) |
| Nitrats | 14 (9) |
| Diuretics | 33 (22) |
| ARBs | 24 (16) |
| Ca-Antagonist | 27 (18) |
| Aspirin | 112 (75) |
| Coronary artery disease, n (%) | |
| Single-vessel disease | 41 (27) |
| Multi-vessel disease | 57 (38) |
| Left ventricular function | |
| LVEF (%) | 62.1 ± 7.2 |
| LVEDV (mL) | 132 ± 36 |
| LVESV (mL) | 51 ± 22 |

Data are presented as n (%) or mean ± SD. BMI, body mass index; CAD, coronary artery disease; LVEF, left ventricular ejection fraction; LVEDV, left ventricular end-diastolic volume; LVESV, left ventricular end-systolic volume.

**Table 2**

**Hemodynamic parameters.**

| Parameter | n = 150 |
|---|---|
| Heart rate (b.p.m.) | |
| At rest | 65.5 ± 12.5 |
| Adenosine stress | 83.2 ± 15.4* |
| Systolic blood pressure (mmHg) | |
| At rest | 129 ± 21 |
| Adenosine stress | 127 ± 21 |
| Diastolic blood pressure (mmHg) | |
| At rest | 73 ± 10 |
| Adenosine stress | 71 ± 10$^{+}$ |

Data are presented as mean ± SD. *P < 0.0001 and $^{+}$P < 0.05 for rest vs. stress (paired Student's t-test)

## Figure Legends

Figure 1. Example whole-heart 3D CMR perfusion data acquired during adenosine stress and at rest. A perfusion defect is seen in the anterior and anteroseptal segments extending from base to apex (a,b). Invasive X-ray angiography confirms a relevant stenosis of the ostial left anterior descending artery with an FFR value of 0.53 (c,d). The circumflex and right coronary artery had no stenosis (e).

Figure 2. Segmentation of myocardial hypo-enhancement during stress for the patient data shown in Figure 1. The volume of myocardial hypo-enhancement normalized to the left-ventricular volume is 37%.

Figure 3. Myocardial ischemic burden (MIB) of the study population given as mean values and corresponding 95% confidence intervals as function haemodynamic stenosis significance as defined by fractional flow reserve (FFR). Differences between groups are statistically significant (P = 0.0001).

Figure 4. Receiver-operator characteristic (ROC) analysis to determine the cut-off value of myocardial ischaemic burden predictive of the presence or absence of significant coronary artery disease as defined by fractional flow reserve. A cut-off value of myocardial ischaemic burden > 4.1% was found to be most significant.

Figure 1

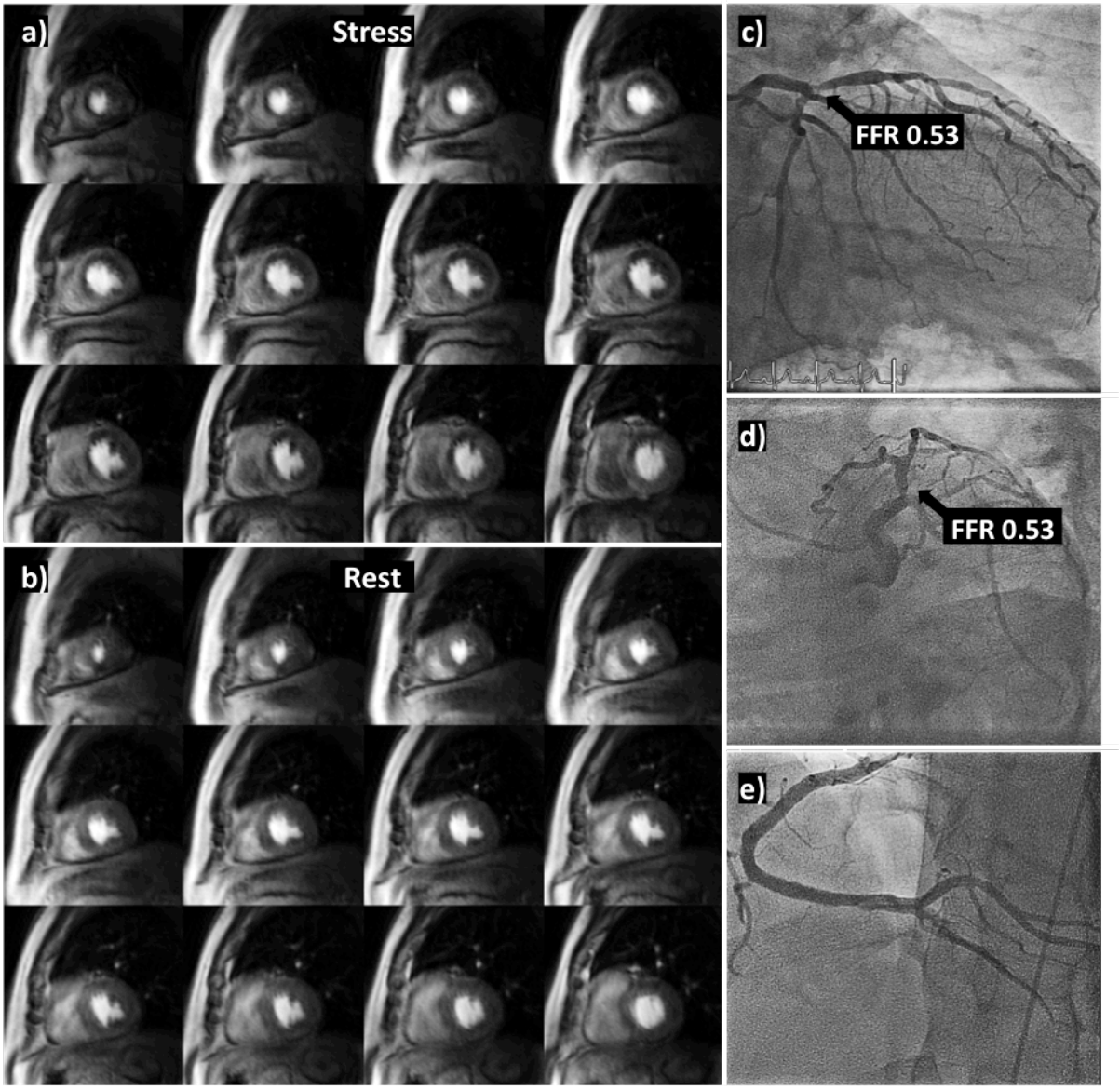


*Figure 1. Example whole-heart 3D CMR perfusion data acquired during adenosine stress and at rest. A perfusion defect is seen in the anterior and anteroseptal segments extending from base to apex (a,b). Invasive X-ray angiography confirms a relevant stenosis of the ostial left anterior descending artery with an FFR value of 0.53 (c,d). The circumflex and right coronary artery had no stenosis (e).*

Figure 2

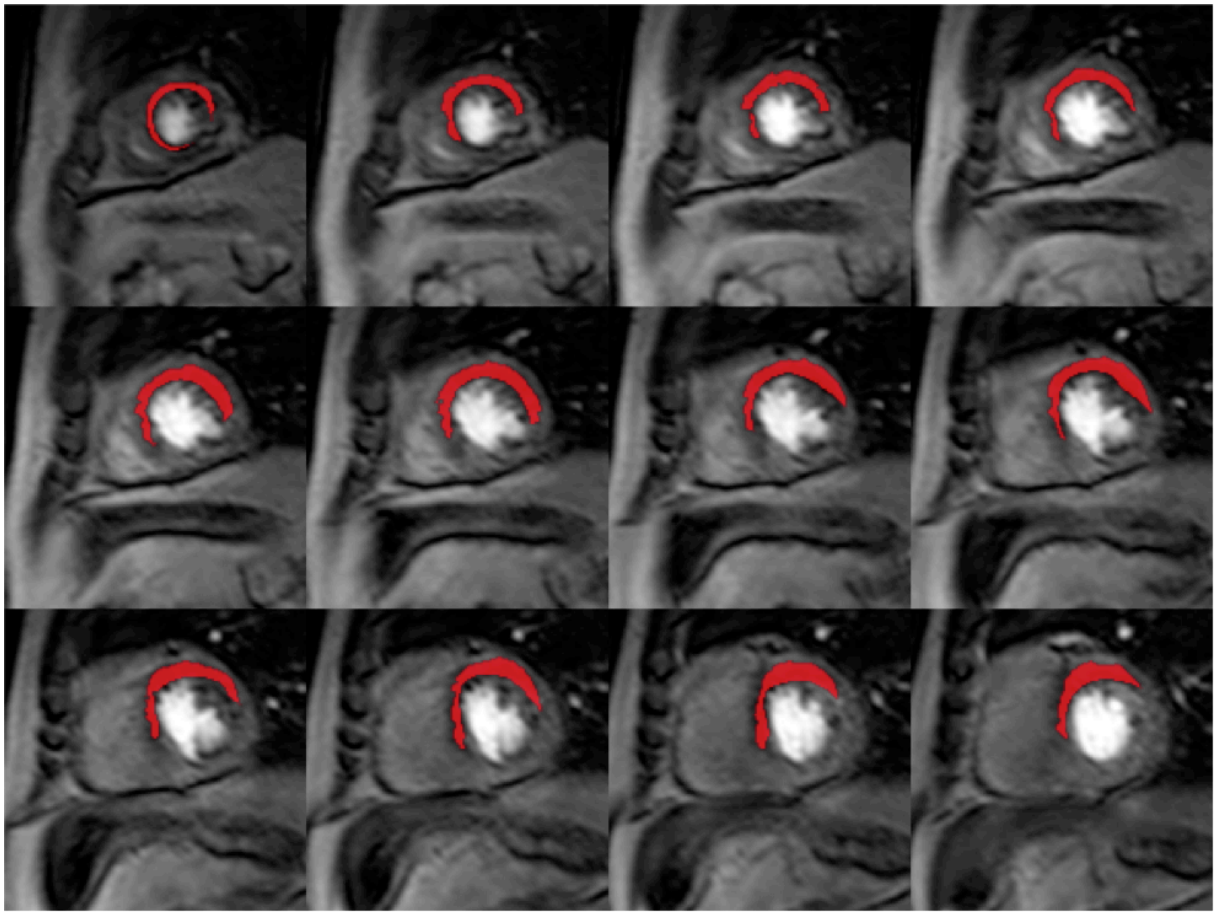

*Figure 2. Segmentation of myocardial hypo-enhancement during stress for the patient data shown in Figure 1. The volume of myocardial hypo-enhancement normalized to the left-ventricular volume is 37%.*

Figure 3

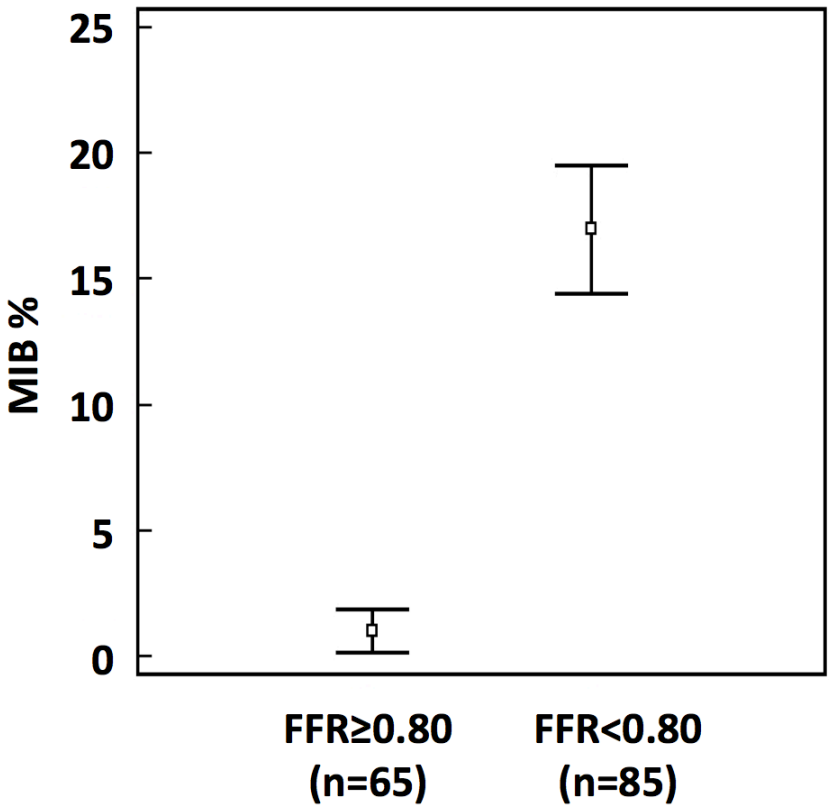


*Figure 3. Myocardial ischemic burden (MIB) of the study population given as mean values and corresponding 95% confidence intervals as function haemodynamic stenosis significance as defined by fractional flow reserve (FFR). Differences between groups are statistically significant (P = 0.0001).*

Figure 4

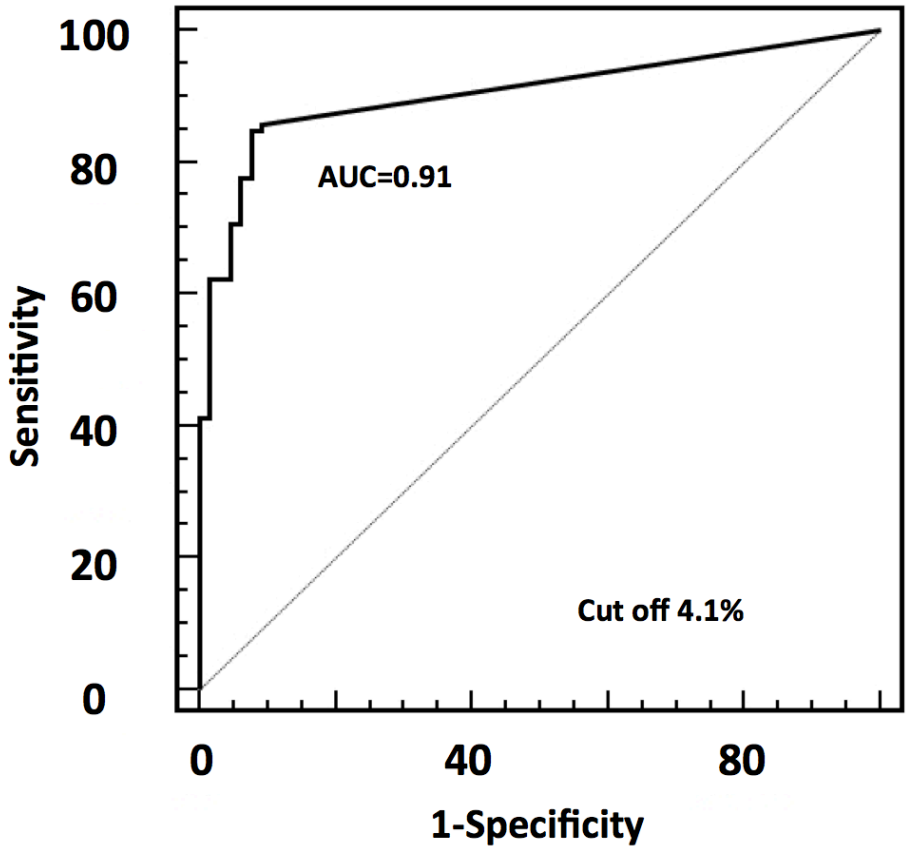


*Figure 4. Receiver-operator characteristic (ROC) analysis to determine the cut-off value of myocardial ischaemic burden predictive of the presence or absence of significant coronary artery disease as defined by fractional flow reserve. A cut-off value of myocardial ischaemic burden > 4.1% was found to be most significant.*

## Appendix B

# Quantitative Cardiovascular Magnetic Resonance Perfusion Imaging: Inter-study Reproducibility

Geraint Morton, Roy Jogiya, Sven Plein, Andreas Schuster, Amedeo Chiribiri, Eike Nagel.

King's College London British Heart Foundation (BHF) Centre of Excellence; National Institute of Health Research (NIHR) Biomedical Research Centre at Guy's and St. Thomas' NHS Foundation Trust; Wellcome Trust and Engineering and Physical Sciences Research Council (EPSRC) Medical Engineering Centre; Division of Imaging Sciences and Biomedical Engineering; The Rayne Institute, St. Thomas´ Hospital, London, United Kingdom

Address for correspondence: Geraint Morton, King's College London - Division of Imaging Sciences, The Rayne Institute, 4th Floor Lambeth Wing, St. Thomas' Hospital; London SE1 7EH, Phone: +44 20 7188 5441; Fax: +44 20 7188 5442
geraintmorton@gmail.com

## Abstract

### Aims

The aims of the study were to evaluate the inter-study reproducibility of quantitative Cardiovascular Magnetic Resonance (CMR) myocardial perfusion imaging and to assess whether perfusion is affected by diurnal variation. Data on these are limited despite being crucially important for performing serial examinations in both clinical practice and in trials.

### Methods and Results

16 healthy volunteers underwent high-resolution 3T perfusion imaging 3 times during a single day to evaluate inter-study reproducibility and for the effects of diurnal variation.

Absolute perfusion was determined in each coronary artery territory and globally by Fermi constrained deconvolution of myocardial signal intensity curves. Left ventricular volumes and function were also calculated.

11 full datasets were suitable for quantitative perfusion analysis. Global rest and stress perfusion and myocardial perfusion reserve (MPR) were 0.6±0.1ml/min/g, 2.5±0.5ml/min/g and 4.3±0.9 respectively for the first scan and were 0.5±0.2ml/min/g, 2.1±0.5ml/min/g and 4.2±1.2 for the second (p=0.1, 0.19 and 0.37 respectively). Inter-study reproducibility was moderate. The coefficient of variation (CV) was 16.0%, 26.8% and 23.9% for global rest and stress perfusion and MPR respectively. Corresponding territorial CV were 27.5%, 35.2% and 33.5%. The reproducibility of left ventricular volumes and function was excellent (CV 4%, 7.7% and 4.6% for end-diastolic volume,

end-systolic volume and ejection fraction respectively). There were no significant diurnal variations in perfusion or LV volumes and function ($p \geq 0.05$ for all).

Conclusions

The inter-study reproducibility of quantitative myocardial perfusion is reasonable and best for global rest perfusion. No significant diurnal variation in perfusion was observed.

Keywords

Cardiovascular magnetic resonance, myocardial perfusion, inter-study reproducibility, diurnal variation

## Introduction

Evaluation of myocardial perfusion is a key function of non-invasive cardiac imaging and is important for diagnosis, prognosis and management [1]. Cardiovascular magnetic resonance (CMR) perfusion imaging has emerged relatively recently as a clinically useful tool [2]. The myocardium is repeatedly imaged during the first-pass of a contrast agent. Abnormal perfusion results in slower arrival of less contrast agent in affected regions of myocardium. Typically these areas are identified visually as darker regions of myocardium. However, identification of abnormalities by this approach is limited by a requirement for the presence of normally perfused myocardium for comparison. Quantification of myocardial perfusion overcomes this limitation. Moreover quantification of perfusion should allow more robust calculation of ischaemic burden and more precise characterisation of changes in perfusion due to physiological variation, disease and therapeutic interventions. PET studies have demonstrated that quantification may be superior to visual analysis of myocardial perfusion [3].

CMR myocardial signal intensity curve analysis allows absolute quantification of myocardial perfusion and has been validated against microspheres [4], coronary sinus flow [5] and PET [6]. One of the main advantages of CMR over other imaging modalities is that the absence of ionising radiation makes it ideal for repeated studies. However, in order for quantitative CMR perfusion imaging to be a useful tool for repeated studies, inter-study reproducibility must be acceptable. Data on the reproducibility of myocardial perfusion imaging are limited. PET studies have reported reasonably good inter-study reproducibility in volunteers [7]. However the inter-study reproducibility of fully quantitative CMR has only previously been reported in terms of myocardial perfusion reserve (MPR) [8] or with long intervals between studies [9]. Furthermore,

cardiovascular function is affected by diurnal variation and changes in heart rate, blood pressure and ischaemic threshold during the course of the day are well recognised [10]. Previous studies have not assessed whether myocardial perfusion is also affected by diurnal variation despite the fact that this is important in determining whether serial measurements need to be performed under the same conditions.

The objectives of this study were therefore to evaluate the inter-study reproducibility of hyperaemic and rest myocardial perfusion and MPR and also whether these are affected by diurnal variations.

## Methods

### *Population*

16 healthy volunteers were recruited by via University email and underwent 3 stress and rest perfusion scans on the same day. Exclusion criteria were: known cardiac, respiratory or renal disease or a contraindication to MRI. The local ethics committee approved the study and all participants gave written informed consent.

### *Data acquisition*

CMR imaging was performed on a 3 Tesla clinical MRI scanner (Achieva, Philips Medical Systems, Best, The Netherlands), using a 32-channel phased array receiver cardiac coil. Participants were given clear written and verbal instructions to abstain from all foods and beverages containing caffeine or other adenosine antagonists, and also from smoking, for 24 hours prior to any imaging until all imaging was completed. They were also instructed to fast from midnight on the day of the scans. Those who did not were excluded. Participants then underwent 3 CMR examinations as close as possible to 09:00

(scan 1), 09:30 (scan 2) and 14:00 (scan 3). Between scan 2 and 3 participants left the department and ate and drank freely apart from the restrictions on adenosine antagonists described above. Scan 1 and 2 were used to evaluate perfusion inter-study reproducibility under the same conditions. Scan 3 was used to evaluate whether diurnal variations in perfusion could be detected, due to circadian rhythms, changes in subject hydration or any other cause.

Each CMR scan lasted approximately 30-minutes and followed the same protocol as follows:

- survey, coil reference scan and planning to define imaging planes
- 4-chamber cine
- 2-chamber cine
- test perfusion
- stress perfusion
- short axis stack to cover entire left ventricle (LV)
- 3-chamber cine
- rest perfusion

Cine images were acquired using a standard balanced steady state free precession (SSFP) sequence. Perfusion imaging was performed with a high-resolution *k-t* turbo gradient echo sequence with shortest echo time (range 0.85-0.99ms), shortest repetition time (range 2.45-2.75ms), 20° flip angle; 90° prepulse, 120ms prepulse delay and acquired resolution of 1.3 x 1.3 x 10mm. Perfusion imaging was planned from the systolic phase of the 4 and 2-chamber cines. Three equally spaced short axis slices at basal, mid and apical left ventricular levels were acquired every heartbeat [11]. Imaging geometry, voxel size and field of view from the first stress perfusion scan were kept

constant for each subsequent perfusion sequence. In order to account for higher heart rates at stress, if required, the voxel size was increased stepwise, to maintain imaging at every heartbeat. (This was required in 3 subjects; 2 were imaged at 1.6 x 1.6 x 10mm and 1 at 1.9 x 1.9 x 10mm). Hyperaemia was induced with adenosine administered at 140mcg/kg/min for 4.5 minutes. Perfusion imaging commenced 3 minutes into the infusion and continued for 1.5 minutes. A dual bolus of weight adjusted of gadolinium contrast agent (Gadobutrol/Gadovist, Schering, Germany) was injected at 4ml/s by a power injector (Spectris Solaris® EP, MEDRAD, INC., USA) as previously described [12]. The dual bolus method was designed to overcome signal saturation effects in the LV whilst maintaining adequate myocardial contrast to noise thus permitting estimation of myocardial perfusion. For this study the dual bolus consisted of equal volumes of 0.0045mmol/kg followed by 0.045mmol/kg of contrast agent, each flushed with 25ml of normal saline and separated by a 25 second pause. During the 90 seconds of perfusion image acquisition participants performed a short breath hold during injection of the first (dilute) bolus and to breath hold for as long as possible during the main bolus of contrast agent. Both breath holds were performed at end-expiration and volunteers breathed gently during the pause between injections.

Data analysis

*Myocardial Perfusion*

Quantitative analysis was performed by a blinded observer using dedicated prototype software (ViewForum, Philips Healthcare, Best, The Netherlands). The mid myocardial slice was used for further analysis. The data were analysed visually initially and any studies affected by severe artefact during the first pass of the main bolus of contrast agent, such that reliable signal intensity curves would not be produced, were excluded. Myocardial border detection was automated and manually corrected where required.

Global myocardial perfusion and perfusion in each of the 3 myocardial territories according to a standard definition [13] were determined using the previously validated Fermi deconvolution method [4]. Cases where deconvolution was not possible were also excluded. MPR was defined as the ratio of stress to rest perfusion.

*Left ventricular volumes and function*

Images were analysed in a random order by a blinded experienced observer using CMR42 (Circle, Calgary, Canada). The mitral valve plane and apex were identified from the 4-chamber view in end-diastole and end-systole. The LV endocardial border was automatically defined in the corresponding end-systolic and end-diastolic short axis slices and was manually corrected where required. Papillary muscles were excluded.

*Statistical analysis*

Statistical analysis was performed using Microsoft Excel and IBM SPSS Statistics version 19. For inter-study reproducibility a coefficient of variation (CV), and Bland Altman plots were calculated. CV was defined as the standard deviation of the intra-subject differences between scans 1 and 2 divided by the mean of the relevant parameter, in keeping with previous studies of inter-study reproducibility [14]. Analyses were all performed on a per observation basis.

The Shapiro-Wilk test determined that the data were normally distributed. Mean values from scans 1, 2 and 3 were compared with ANOVA with repeated measures. Post hoc tests using the Bonferroni correction were used for pairwise comparisons. Continuous data are presented as mean ± standard deviation. Significance was determined as $p<0.05$.

Results

16 volunteers were included. 5 were later excluded and 11 full datasets included in the final analysis. Reasons for exclusion were: 1 subject withdrawal, 1 failure of scanner gradients prior to test completion, in 3 subjects 1 or more perfusion scans were unsuitable for quantitative analysis due to artefact. Of those excluded due to artefact one volunteer failed to hear the breath-hold commands during two perfusion sequences due to intermittent headphone failure and one volunteer failed to breath hold adequately during the rest perfusion sequence of exam 2. The third volunteer was excluded as during the rest perfusion scan from exam 2 there was no increase in myocardial signal intensity and deconvolution was not possible.

Participants included in the final analysis were 27±5 years old and five were male. Body mass index was 28.0±7.4 (median 26.2). They were all non-smokers with no significant medical problems and were not taking any medications.

*Perfusion imaging*

There were ≥10 minutes between all perfusion scans. During scans 1 and 2 the interval between CA injections was 13.9±2.8 minutes and during scan 3 it was 16±3.7 minutes. The interval between scans 2 and 3 was 236.9±29.3 minutes.

A representative stress perfusion study with territorial segmentation is shown in figure 1. Myocardial perfusion and haemodynamics for all 3 studies, and the significance of associated differences, are shown in table 1. Stress heart rate and rate pressure product (RPP) were significantly higher in scan 1. There was a trend for rest and stress perfusion to be lower in scan 2 than in scan 1 although this did not meet statistical significance. No significant diurnal variation in perfusion could be detected.

The mean differences between perfusion in scan 1 and 2 with associated CV are shown in table 2. These demonstrate moderate inter-study reproducibility. Global perfusion is more reproducible than territorial perfusion and rest perfusion more reproducible than stress perfusion. Bland Altman plots for territorial rest and stress perfusion and MPR are shown in figure 2. Mean differences and CV between scans 1 and 3 are also shown in table 2b in the appendix.

*Left ventricular volumes and function*

LV mean volumes and ejection fractions, mean differences between scan 1 and 2 and associated CV are shown in table 3. There were no significant changes in LV volumes or function between scans. Inter-study reproducibility was excellent with low CV for all parameters.

## Discussion

This study demonstrates that fully quantitative CMR perfusion analysis has moderate inter-study reproducibility in normal hearts. Global perfusion is more reproducible than territorial and rest more reproducible than stress. Furthermore, with current techniques, diurnal variations in perfusion are not detectable.

*The value of inter-study reproducibility*

CMR does not use ionising radiation and there are no known long-term adverse sequelae as a result of repeated imaging. Consequently CMR is an ideal modality for serial examinations. Many diseases affecting myocardial perfusion are chronic and patients require serial examinations. This may be in order to monitor disease progression or to determine the timing or efficacy of therapeutic interventions. This is applicable to

patients with coronary artery disease but also to other patient groups, for example, PET studies have demonstrated that quantitative perfusion can provide additional information about the coronary microcirculation [15]. Quantitative perfusion therefore also has a potential role in the characterisation and management of patients with microvascular disease, such as those with hypertension, diabetes and angina with normal epicardial coronary arteries. In addition to routine clinical practice serial examinations and surrogate end-points are required for clinical trials. Quantitative perfusion could potentially detect changes in perfusion, which cannot be detected by non-quantitative analysis. Furthermore, inter-study reproducibility is related to the number of subjects required for studies to detect significant results. Improved reproducibility means fewer subjects and studies that are easier and less expensive to complete. It is, therefore, crucially important to know the inter-study reproducibility to understand the potential role for CMR imaging in these clinical and research settings.

*Inter-study reproducibility of quantitative perfusion imaging*

The degree of variability between measurements, and hence the magnitude of the CV, which is acceptable will vary depending on what is clinically relevant. It is therefore important to interpret these findings in the context of the magnitude of changes that need to be detected. For example, studies in patients with coronary artery disease [16, 17] have shown that stress perfusion differs by approximately 100% or more between coronary territories subtended by normal arteries and severely diseased arteries. Therefore, based on the reproducibility findings reported here, it would be expected that stress perfusion imaging could reliably detect changes of this magnitude and reproducibility could therefore be described as reasonable. Conversely, large studies

would be required to detect smaller changes in perfusion, such as those that may be expected as a result of drug therapy.

To date there are very limited data on the inter-study reproducibility of quantitative CMR perfusion. A previous study analysed the inter-study reproducibility of quantitative CMR perfusion [8] in a combined cohort of volunteers and patients with coronary artery disease. They performed two perfusion studies at a mean interval of 13±18 days, and also quantified perfusion from a single a midventricular slice, acquired at high-resolution, using Fermi deconvolution. However, in contrast to our study, they did not report absolute perfusion values. They reported a CV for global MPR of 21% and CVs for regional perfusion of 26-35%. These values are very similar to the corresponding global and territorial values in our study (23.9% and 27.5-35.2% respectively). They also found absolute quantification to be more reproducible than semi-quantitative analysis. Important differences between the study by Elkington et al. and ours include the fact that our study was performed at 3T using a *k-t* accelerated perfusion technique whereas the former was performed at 1.5T using a non selective saturation recovery FLASH sequence. It is therefore noteworthy that these differences do not appear to result in superior reproducibility.

A sub-study of the Multi-Ethnic Study of Atherosclerosis [9] evaluated inter-study reproducibility of quantitative CMR perfusion. This study also demonstrated reasonable reproducibility and, in agreement with our study, they also found global and rest perfusion to be the most reproducible. However the interval between the 2 examinations was very long (mean 334 days) as reproducibility assessment was not the primary aim of the main study.

Semi-quantitative analysis of CMR perfusion has also been found to have moderate to good reproducibility in another study of a mixed cohort of normal volunteers and patients with coronary artery disease. [8, 18] The reproducibility of a semi-quantitative index of MPR derived from normalised upslope analysis was also comparable to ours. However although of a similar magnitude, they reported consistently lower CV than we found for fully quantitative MPR. Furthermore there was also less of a difference between global (17.6%) and territorial (17.6-20.7%) CV.

Data on the inter-study reproducibility of quantitative PET myocardial perfusion are also limited. One recent study performed serial 82-Rubidium PET perfusion imaging in volunteers without cardiac disease at a median interval of 22 days [7]. This study reported repeatability coefficients (1.96 x standard deviation of differences divided by mean) in 56 true normal subjects of 35%, 34% and 38% for global rest and stress perfusion and MPR respectively. The equivalent repeatability coefficients for this study are 32%, 53% and 47% suggesting that CMR may be less reproducible than PET at present. However, it is noteworthy that in this PET study reproducibility was significantly worse in subjects who were retrospectively classified as not normal on the basis extensive clinical, biochemical and ECG screening. This is by far the largest PET study of inter-study reproducibility. Previous studies have been similar to ours involving relatively small cohorts of normal subjects [19-23]. Follow-up perfusion studies were performed either immediately, as in our study, or after a short interval. These studies reported similar reproducibility to the 82-Rb study described above and some also found that reproducibility was best for global and rest perfusion [19, 20].

In this study we found that there was a significant reduction in stress RPP between studies 1 and 2 despite using the same adenosine protocol. Furthermore there was a trend towards reduced territorial stress and rest perfusion although this did not reach significance (p=0.05 for both). Inter-individual variation in the response to adenosine is well reported [24] and significant reductions in heart rate response are seen when adenosine infusion is repeated after caffeine intake [25]. However, in this study it may be that familiarisation with the protocol meant that subjects were less anxious during the second administration of adenosine. This change in RPP could explain the trend towards reduced stress perfusion between scans 1 and 2 but does not account for the trend towards reduced rest perfusion. Quantitative CMR perfusion relies on myocardial signal intensity analysis. The half-life of the contrast agent used in this study is approximately 90-minutes whereas the interval between perfusion imaging between scans 1 and 2 was much shorter. Consequently the baseline myocardial signal continues to increases after each dose of contrast agent. The signal intensity in a region of interest at the start of each perfusion scan was subtracted for baseline correction of each signal curve. However this correction may result in an under-estimation of perfusion in subsequent studies. This finding has implications for quantitative analysis of serial perfusion studies repeated at a short interval. For example, both in clinical practice and in studies it is common to perform both stress and rest perfusion during the same examination. Moreover both stress and rest perfusion are clearly required for calculation of MPR. It is therefore important that this observation is evaluated further in future studies.

A number of different CMR techniques and perfusion sequences are used for clinical and research perfusion imaging. For this study we used our standard clinical perfusion sequence, which includes three slices at basal, mid and apical left ventricular levels, in

order to establish reproducibility with a sequence in routine clinical use. Since this study only included normal volunteers we do not expect that important differences in perfusion between slices exist and therefore selected segments to represent all three coronary territories from the mid-slice for analysis. However, since the mid slice is acquired in mid systole, signal from the blood pool is less likely to be included and this could potentially affect reproducibility. Nonetheless we would anticipate any such effect to be small and large sample sizes would therefore be necessary to investigate whether there are systematic differences between slices.

Moreover to date it remains unknown how much the lack of standardization of quantitative perfusion CMR techniques might affect reproducibility. Many factors such as magnetic field strength, imaging sequence, contrast agent, post processing methods and inter-observer reproducibility might influence inter-study reproducibility. We deliberately kept all other factors constant to specifically evaluate inter-study reproducibility and for diurnal variation. We believe further studies are required to assess the influence of these other factors further. However despite these potential limitations our findings were very similar to those reported previously as discussed above.

Myocardial perfusion values reported here are lower than some studies have previously reported [26] and may therefore represent an underestimate. However, they are very similar to values previously reported for healthy volunteers in previous $^{13}$N-ammonia PET studies [22, 27]. Discrepancies in normal perfusion ranges seen in studies may arise due to small sample sizes. Alternatively they may arise as a result of differences in study populations, scanners, tracers or contrast agents, methods of sampling arterial input

function or myocardial regions of interest, or mathematical perfusion models [28, 29]. Since MPR is a ratio of stress to rest perfusion this corrects for many of these differences and the MPR values found in this study are in keeping with previous literature.

Diurnal variations in cardiovascular functions are known to occur, for example in heart rate and blood pressure [30]. Despite designing the study to try and maximise diurnal variation between scan 1 and 3 we could not detect any significant changes in LV volumes or function or myocardial perfusion. However small differences in perfusion are unlikely to have been detectable using current methods. This suggests that diurnal variations in perfusion are not important for study design or clinical practice at present. It is also noteworthy that we only measured perfusion at two different times of day and if we had examined participants at more time points, particularly during the night, it may have been possible to detect diurnal variation. However most perfusion CMR imaging takes place during working hours, in keeping with the times used here, and therefore the findings are of practical relevance. Finally this study confirms the excellent inter-study reproducibility of CMR LV volumes and function described in previous studies [31].

Limitations

The main limitations of the study are the small sample size and inclusion of healthy volunteers rather than patients. However there are no previously reported quantitative CMR perfusion studies reporting absolute perfusion values from multiple examinations performed within a short space of time. Furthermore the equivalent PET literature consists of a modest number of studies most which have small sample sizes and involve normal volunteers.

The *k-t* accelerated sequence is susceptible to respiratory artefacts which can be problematic for quantification. Three subjects were excluded as a result of the unsuitability of 1 or more of the perfusion scans for quantitative analysis. However this relatively high exclusion rate also reflects the fact that 3 stress and 3 rest scans were required for each subject whereas usually fewer scans would be required for clinical care or studies.

## Conclusions

Quantitative CMR myocardial perfusion analysis is a promising technique with the potential to provide user-independent results, which are more robust than qualitative methods. Inter-study reproducibility is reasonable using current methods. Global perfusion is more reproducible than territorial perfusion and rest perfusion more reproducible than stress. No significant diurnal variation could be detected in myocardial perfusion. On-going refinement of quantitative post-processing methods should result in further improvements in inter-study reproducibility in the future.

Acknowledgments

This work was supported by a European Union Grant (Grant number 224495 to GM, EN) the British Heart Foundation (RE/08/003 and FS/10/029/28253 to AS, EN) and the Biomedical Research Centre (BRC-CTF 196).

References

1. Morton G, Schuster A, Perera D, Nagel E. Cardiac magnetic resonance imaging to guide complex revascularization in stable coronary artery disease. Eur Heart J 2010:1-8.

2. Nandalur KR, Dwamena BA, Choudhri AF, Nandalur MR, Carlos RC. Diagnostic performance of stress cardiac magnetic resonance imaging in the detection of coronary artery disease: a meta-analysis. Journal of the American College of Cardiology 2007;50(14):1343-53.

3. Knuuti J, Kajander S, Mäki M, Ukkonen H. Quantification of myocardial blood flow will reform the detection of CAD. J Nucl Cardiol 2009;16(4):497-506.

4. Christian TF, Rettmann DW, Aletras AH, Liao SL, Taylor JL, Balaban RS, Arai AE. Absolute myocardial perfusion in canines measured by using dual-bolus first-pass MR imaging. Radiology 2004;232(3):677-84.

5. Ichihara T, Ishida M, Kitagawa K, Ichikawa Y, Natsume T, Yamaki N, Maeda H, Takeda K, Sakuma H. Quantitative analysis of first-pass contrast-enhanced myocardial perfusion MRI using a patlak plot method and blood saturation correction. Magn. Reson. Med. 2009;62(2):373-383.

6. Fritz-Hansen T, Hove JD, Kofoed KF, Kelbaek H, Larsson HBW. Quantification of MRI measured myocardial perfusion reserve in healthy humans: a comparison with positron emission tomography. Journal of magnetic resonance imaging : JMRI 2008;27(4):818-24.

7. Sdringola S, Johnson NP, Kirkeeide RL, Cid E, Gould KL. Impact of unexpected factors on quantitative myocardial perfusion and coronary flow reserve in young, asymptomatic volunteers. JACC Cardiovasc Imaging 2011;4(4):402-12.

8. Elkington A, Gatehouse P, Ablitt N, Yang G-Z, Firmin D, Pennell D. Interstudy Reproducibility of Quantitative Perfusion Cardiovascular Magnetic Resonance. J. of Cardiovascular Magnetic Resonance 2005;7(5):815-822.

9. Jerosch-Herold M, Vazquez G, Wang L, Jacobs DR, Folsom AR. Variability of myocardial blood flow measurements by magnetic resonance imaging in the multi-ethnic study of atherosclerosis. Investigative radiology 2008;43(3):155-61.

10. Fox KM, Mulcahy DA. Circadian rhythms in cardiovascular function. Postgraduate medical journal 1991;67 Suppl 3:S33-6.

11. Messroghli DR, Bainbridge GJ, Alfakih K, Jones TR, Plein S, Ridgway JP, Sivananthan MU. Assessment of regional left ventricular function: accuracy and reproducibility of positioning standard short-axis sections in cardiac MR imaging. Radiology 2005;235(1):229-36.

12. Ishida M, Schuster A, Morton G, Chiribiri A, Hussain S, Paul M, Merkle N, Steen H, Lossnitzer D, Schnackenburg B, Alfakih K, Plein S, Nagel E. Development of a universal dual-bolus injection scheme for the quantitative assessment of myocardial perfusion cardiovascular magnetic resonance. Journal of cardiovascular magnetic resonance : official journal of the Society for Cardiovascular Magnetic Resonance 2011;13:28.

13. Cerqueira MD, Weissman NJ, Dilsizian V, Jacobs AK, Kaul S, Laskey WK, Pennell DJ, Rumberger JA, Ryan T, Verani MS, Imaging AHAWGoMSaRfC. Standardized myocardial segmentation and nomenclature for tomographic imaging of the heart: a statement for healthcare professionals from the Cardiac Imaging Committee of the Council on Clinical Cardiology of the American Heart Association. Circulation 2002;105(4):539-42.

14. Grothues F, Smith GC, Moon JCC, Bellenger NG, Collins P, Klein HU, Pennell DJ. Comparison of interstudy reproducibility of cardiovascular magnetic resonance with

two-dimensional echocardiography in normal subjects and in patients with heart failure or left ventricular hypertrophy. Am J Cardiol 2002;90(1):29-34.

15. Camici PG, Crea F. Coronary microvascular dysfunction. N Engl J Med 2007;356(8):830-40.

16. Uren NG, Melin JA, De Bruyne B, Wijns W, Baudhuin T, Camici PG. Relation between myocardial blood flow and the severity of coronary-artery stenosis. N Engl J Med 1994;330(25):1782-8.

17. Di Carli M, Czernin J, Hoh CK, Gerbaudo VH, Brunken RC, Huang SC, Phelps ME, Schelbert HR. Relation among stenosis severity, myocardial blood flow, and flow reserve in patients with coronary artery disease. Circulation 1995;91(7):1944-51.

18. Chih S, Macdonald PS, Feneley MP, Law M, Graham RM, McCrohon JA. Reproducibility of adenosine stress cardiovascular magnetic resonance in multi-vessel symptomatic coronary artery disease. Journal of cardiovascular magnetic resonance : official journal of the Society for Cardiovascular Magnetic Resonance 2010;12:42.

19. Kaufmann PA, Gnecchi-Ruscone T, Yap JT, Rimoldi O, Camici PG. Assessment of the reproducibility of baseline and hyperemic myocardial blood flow measurements with 15O-labeled water and PET. J Nucl Med 1999;40(11):1848-56.

20. Wyss CA, Koepfli P, Mikolajczyk K, Burger C, von Schulthess GK, Kaufmann PA. Bicycle exercise stress in PET for assessment of coronary flow reserve: repeatability and comparison with adenosine stress. Journal of Nuclear Medicine 2003;44(2):146-54.

21. Manabe O, Yoshinaga K, Katoh C, Naya M, deKemp RA, Tamaki N. Repeatability of rest and hyperemic myocardial blood flow measurements with 82Rb dynamic PET. Journal of Nuclear Medicine 2009;50(1):68-71.

22. Nagamachi S, Czernin J, Kim AS, Sun KT, Böttcher M, Phelps ME, Schelbert HR. Reproducibility of measurements of regional resting and hyperemic myocardial blood flow assessed with PET. Journal of Nuclear Medicine 1996;37(10):1626-31.

23. El Fakhri G, Kardan A, Sitek A, Dorbala S, Abi-Hatem N, Lahoud Y, Fischman A, Coughlan M, Yasuda T, Di Carli MF. Reproducibility and Accuracy of Quantitative Myocardial Blood Flow Assessment with 82Rb PET: Comparison with 13N-Ammonia PET. Journal of Nuclear Medicine 2009;50(7):1062-1071.

24. Wilson RF, Wyche K, Christensen BV, Zimmer S, Laxson DD. Effects of adenosine on human coronary arterial circulation. Circulation 1990;82(5):1595-606.

25. Reyes E, Loong CY, Harbinson M, Donovan J, Anagnostopoulos C, Underwood SR. High-dose adenosine overcomes the attenuation of myocardial perfusion reserve caused by caffeine. Journal of the American College of Cardiology 2008;52(24):2008-16.

26. Muehling O, Jerosch?Herold M, Panse P, Zenovich A, Wilson B, Wilson R, Wilke N. Regional Heterogeneity of Myocardial Perfusion in Healthy Human Myocardium: Assessment with Magnetic Resonance Perfusion Imaging #. Journal of cardiovascular magnetic resonance : official journal of the Society for Cardiovascular Magnetic Resonance 2004;6(2):499-507.

27. Muzik O, Duvernoy C, Beanlands RS, Sawada S, Dayanikli F, Wolfe ER, Schwaiger M. Assessment of diagnostic performance of quantitative flow measurements in normal subjects and patients with angiographically documented coronary artery disease by means of nitrogen-13 ammonia and positron emission tomography. Journal of the American College of Cardiology 1998;31(3):534-40.

28. Ishida M, Morton G, Schuster A, Nagel E, Chiribiri A. Quantitative Assessment of Myocardial Perfusion MRI. curr cardiovasc imaging rep 2010;3(2):65-73.

29. Schwaiger M, Muzik O. Assessment of myocardial perfusion by positron emission tomography. The American Journal of Cardiology 1991;67(14):35D-43D.

30. Pickering TG, Harshfield GA, Kleinert HD, Blank S, Laragh JH. Blood pressure during normal daily activities, sleep, and exercise. Comparison of values in normal and hypertensive subjects. JAMA : the journal of the American Medical Association 1982;247(7):992-6.

31. Bellenger N, Davies L, Francis J, Coats A, Pennell D. Reduction in Sample Size for Studies of Remodeling in Heart Failure by the Use of Cardiovascular Magnetic Resonance. J. of Cardiovascular Magnetic Resonance 2000;2(4):271-278.

Appendix

Table 2b: Inter-study reproducibility between scans 1 and 3.

| | | Territorial | Global |
|---|---|---|---|
| Stress perfusion (ml/min/g) | Mean Difference±SD | 0.28±0.82 | 0.28±0.69 |
| | Coefficient of Variation | 34.9% | 29.0% |
| Rest perfusion (ml/min/g) | Mean Difference±SD | 0.04±0.17 | 0.04±0.11 |
| | Coefficient of Variation | 29.6% | 19.0% |
| MPR | Mean Difference±SD | 0.19±1.54 | 0.23±1.04 |
| | Coefficient of Variation | 36.3% | 25.2% |

Table 1: Myocardial perfusion and haemodynamics for the subjects during each of the three scans.

| | Scan 1 | Scan 2 | Scan 3 | p |
|---|---|---|---|---|
| Perfusion-Territorial (ml/min/g) | | | | |
| Stress | | | | |
| Mean | 2.5±0.8 | 2.1±0.6 | 2.2±0.8 | 0.05 |
| *LAD* | *2.5±0.9* | *2.2±0.6* | *2.2±0.8* | |
| *Circumflex* | *2.2±0.7* | *2.0±0.7* | *2.0±0.6* | |
| *RCA* | *2.7±0.8* | *2.1±0.7* | *2.4±0.9* | |
| Rest | | | | |
| Mean | 0.6±0.2 | 0.5±0.1 | 0.5±0.2 | 0.05 |
| *LAD* | *0.6±0.1* | *0.5±0.1* | *0.6±0.1* | |
| *Circumflex* | *0.5±0.1* | *0.5±0.1* | *0.5±0.1* | |
| *RCA* | *0.7±0.2* | *0.6±0.2* | *0.6±0.2* | |
| Perfusion-global (ml/min/g) | | | | |
| Stress | 2.5±0.5 | 2.1±0.5 | 2.2±0.7 | 0.19 |
| Rest | 0.6±0.1 | 0.5±0.2 | 0.5±0.2 | 0.1 |
| MPR | | | | |
| Territorial | 4.3±1.3 | 4.3±1.4 | 4.1±1.1 | 0.34 |
| Global | 4.3±0.9 | 4.2±1.2 | 4.0±0.6 | 0.37 |
| Heart rate (bpm) | | | | |
| Stress | 111±14 | 105±16 | 106±17 | 0.03 |
| Rest | 74±10 | 73±9 | 73±14 | 0.92 |
| SBP (mmHg) | | | | |
| Stress | 121±16 | 120±14 | 122±16 | 0.54 |
| Rest | 119±21 | 119±16 | 120±23 | 0.92 |
| RPP (HR.SBP) | | | | |
| Stress | 13550±2747 | 12696±2592 | 13009±2758 | 0.046 |
| Rest | 8919±2639 | 8764±1698 | 8789±2377 | 0.90 |
| DBP | | | | |
| Stress | 73±7 | 70±11 | 70±8 | 0.24 |
| Rest | 69±9 | 66±6 | 64±9 | 0.06 |

Data are mean ± standard deviation. Small differences in the average values are due to rounding.

MPR=myocardial perfusion reserve; SBP=systolic blood pressure;

RPP=rate pressure product; DBP=diastolic blood pressure

Table 2: Inter-study reproducibility of perfusion imaging

| | | Territorial | Global |
|---|---|---|---|
| Stress perfusion (ml/min/g) | Mean Difference±SD | 0.35±0.81 | 0.36±0.62 |
| | Coefficient of Variation | 35.2% | 26.8% |
| Rest perfusion (ml/min/g) | Mean Difference±SD | 0.07±0.16 | 0.07±0.09 |
| | Coefficient of Variation | 27.5% | 16.0% |
| MPR | Mean Difference±SD | 0.07±1.43 | 0.07±1.03 |
| | Coefficient of Variation | 33.5% | 23.9% |

Table 3: Mean values, intra-subject differences and inter-study reproducibility for LV volumes and function.

| | Scan | | | | Mean | |
|---|---|---|---|---|---|---|
| | 1 | 2 | 3 | p | difference ± SD | CV* |
| LVEDV | 161.7±33.3ml | 162.5±37.0ml | 161.2±39.7ml | 0.76 | -2.1±6.7 | 4.0% |
| LVESV | 67.5±17.3ml | 68.9±20.0ml | 64.9±18.3ml | 0.28 | -1.9±5.5 | 7.7% |
| LVEF | 58.5±3.2% | 58.0±4.3% | 59.6±4.5% | 0.86 | 0.55±2.7 | 4.6% |

*CV=coefficient of variation based on scans 1 and 2.

SD=standard deviation, LVEDV=left ventricular end-diastolic volume; LVESV= left ventricular end-systolic volume; LVEF=left ventricular ejection fraction.

Figure legends

Figure 1: Stress perfusion image with territorial segmentation.

Still image, from a representative study, showing a single frame from the first pass of the main bolus of contrast agent. The standard coronary artery territories used for the study are demonstrated. LAD-left anterior descending artery; RCA-right coronary artery.

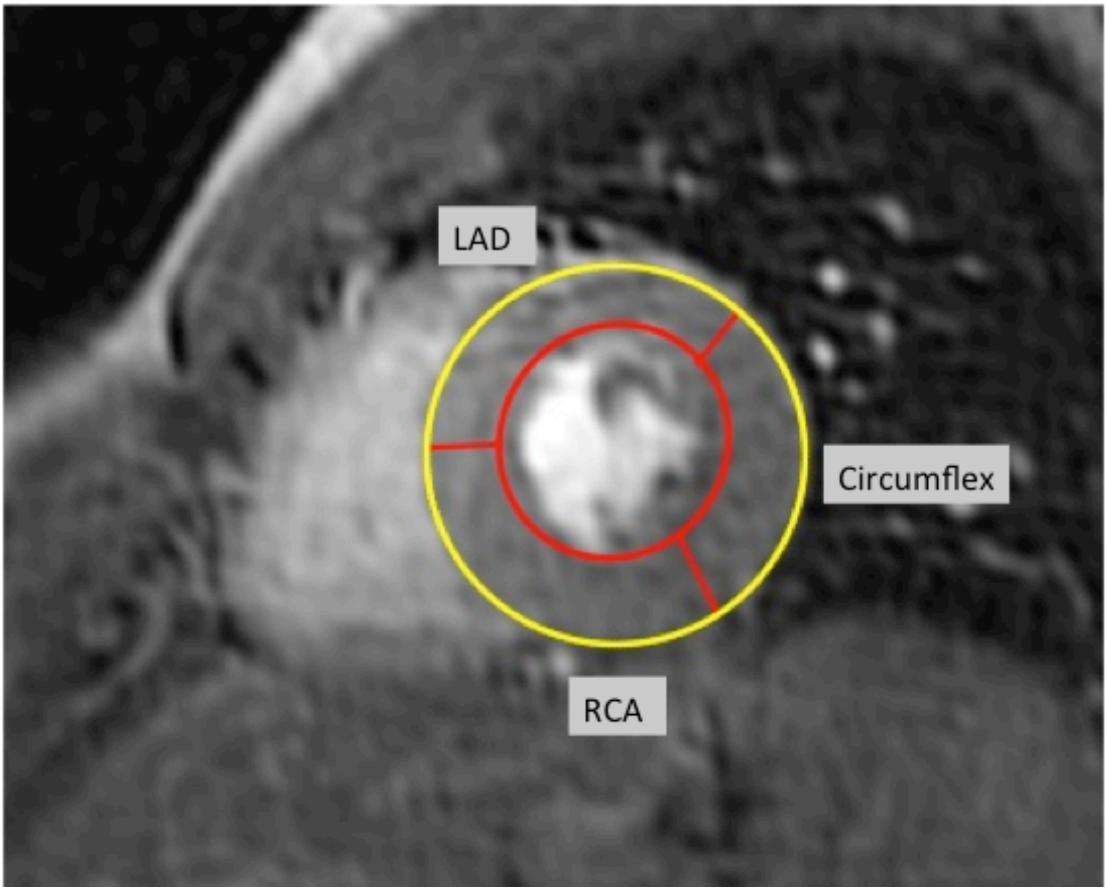

Figure 2: Inter-study reproducibility of quantitative CMR perfusion imaging.

Bland Altman plots showing the inter-study agreement between territorial stress and rest perfusion and myocardial perfusion reserve (MPR) between scans 1 and 2. The mean difference and limits of agreement (1.96 standard deviations) are shown.

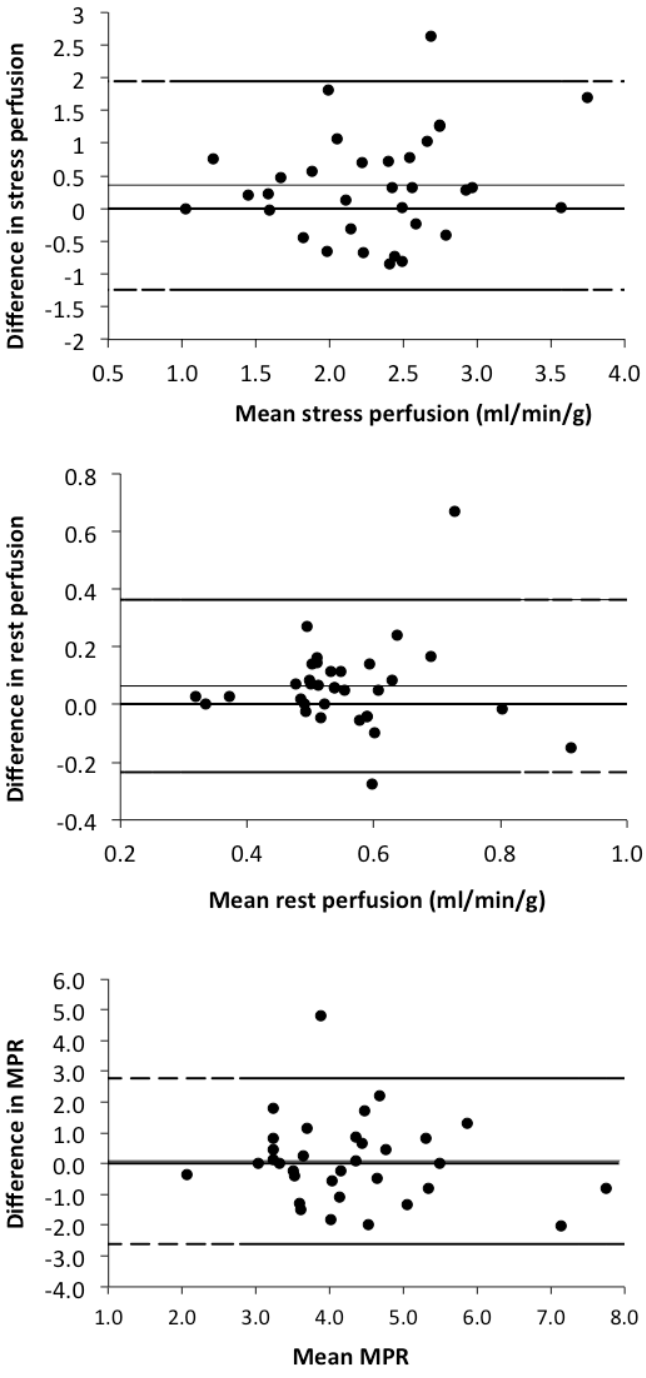

# Appendix C

# Advanced Cardiovascular Magnetic Resonance Myocardial Perfusion Imaging – High Spatial Resolution versus 3-Dimensional Whole-heart Coverage

## INTRODUCTION

Myocardial perfusion imaging with cardiovascular magnetic resonance (CMR) has now been established as a highly accurate method for the detection of coronary artery disease (CAD)(1–4). The recent CE-MARC study found it to have a higher overall diagnostic accuracy compared to single-photon emission computed tomography (SPECT)(1). Over the past 5 years, advanced acceleration techniques have been applied to perfusion CMR and the speed-up afforded by such acceleration has been invested into either higher in-plane spatial resolution or 3-dimensional (3D) whole-heart coverage. Several authors have demonstrated the feasibility and accuracy of high-resolution perfusion CMR (5–9). Benefits of high-resolution acquisition include a reduction in dark-rim artefact, better detection of subendocardial ischemia and potentially better integration with late-gadolinium enhancement imaging (5,9,10). Furthermore, in a recent comparative study, the high-resolution technique had a greater overall diagnostic accuracy compared to standard-resolution(9).

Other authors have reported on the feasibility and accuracy of investing acceleration into 3D coverage instead (11–13)(14). The latter overcomes the long-standing limitation of perfusion CMR to only 3-4 slices during each heart beat and therefore allows the true myocardial ischemic burden to be assessed (13). Furthermore, 3D perfusion CMR acquires all slices at the same point in the cardiac cycle which is another potential advantage - particularly as significant differences between systolic and diastolic myocardial blood flow estimates have been determined with CMR (15).

The comparative advantages and disadvantages of the alternative uses of acceleration, as well as their likely clinical roles, remain undefined. This article briefly reviews the

principles behind advanced acceleration in perfusion CMR and offers discussion as to its optimal application into either high spatial-resolution or 3D whole-heart coverage.

## ADVANCED ACCELERATION METHODS

The most advanced methods used to speed-up data acquisition in perfusion CMR are 'prior-knowledge' techniques(16,17). These are based on the observation that dynamic data sets exhibit considerable correlation in space and time. In perfusion CMR, for example, large regions of the image such as the chest wall are relatively static and neighbouring time frames of the heart are very similar.

Several advanced techniques for acceleration are therefore based on the under-sampling of spatial and temporal domains in order to capitalise on this image redundancy(16,17). Most prominent among these techniques are two closely related methods, *k-t* broad linear speed up technique (*k-t* BLAST) and *k-t* sensitivity encoding (*k-t* SENSE); as well as the recently proposed highly constrained back-projection reconstruction (HYPR) (16,18,19). With these techniques, it is possible to accelerate image acquisition up to a factor of 10 times (20). This speed-up can be utilized to increase signal-to-noise ratio (SNR), improve spatial resolution (high-resolution perfusion CMR) or shorten acquisition time per slice facilitating greater spatial coverage (3D perfusion CMR) (10)(17).

### *k-t* techniques

In *k-t* BLAST and *k-t* SENSE, under-sampling is applied along *k*-space and time whilst a low spatial resolution image ('training data') is obtained in a separate scan or in an interleaved fashion during the acquisition (20). A non-aliased, full image series is then

reconstructed using prior-knowledge derived from the training data. Both "*k-t* techniques" are very similar, but *k-t* SENSE is technically a hybrid method as it additionally employs receiver coil sensitivity information to facilitate image reconstruction.

*k-t* techniques add complexity to the acquisition of perfusion CMR and one particular problem is the sensitivity to respiration motion and cardiac arrhythmias. This vulnerability relates to the periodicity assumed in the reconstruction. However, previous studies have shown that in compliant patients, respiratory artefacts tend to only occur after myocardial contrast passage at the end of a breath-hold - and therefore rarely interfere with interpretation(5,9,10). A recent refinement, known as *k-t* principal component analysis (*k-t* PCA), has been shown to be more robust to respiratory motion and improve temporal fidelity because image reconstruction is constrained using temporal basis functions derived from the low-resolution training data acquired in every heartbeat(21).

**Highly constrained back-projection reconstruction**

HYPR is a recently developed, promising method of advanced acceleration, that can reduce acquisition windows, increase spatial coverage and improve spatial resolution as well as SNR - without a trade-off between these parameters (19)(22). This surprising feat is possible as full rather than partial *k*-space data is sampled and hence the reconstructed images have high spatial resolution and SNR. In order to achieve this with sufficient speed, *k*-space data is acquired in acutely undersampled radial projections at different time points before being combined into a complete dataset. Once combined, the full *k*-space data is used to reconstruct a high-resolution, high SNR composite image which is used to normalise the series of low resolution images reconstructed at each

time point. The result is higher spatial coverage, higher spatial resolution and higher SNR than conventional protocols without significant penalty(19)(22). One recent single-centre study, using a variant known as sliding-window conjugate-gradient HYPR (6 contiguous slices, 1.6mm in plane spatial resolution) demonstrated clinical feasibility and a high diagnostic accuracy in 50 patients with suspected CAD – but this technique still requires further evaluation and validation in multiple centers(22).

**HIGH-RESOLUTION PERFUSION CMR**

The first feasibility study of high-resolution perfusion CMR used 5-fold *k-t* SENSE to achieve an in-plane spatial resolution of 1.5mm in a group of 10 volunteers(20). Image quality was similar to that from a standard-resolution sequence (in-plane spatial resolution of 2.6mm) but there was a significant reduction in the severity of dark-rim artefact (mean thickness: 1.7 vs. 2.4mm; $p<0.01$). Images acquired at high-resolution also displayed an increased SNR compared to standard-resolution when corrected for pixel size. In three of the volunteers, higher *k-t* SENSE acceleration factors of 8 and 10 were successfully demonstrated, without compromise in image quality or signal intensity characteristics.

The reduction of dark-rim artefact with high-resolution acquisition was confirmed in another volunteer study (n=10) by Maredia et al. In this study, mean artefact thickness was 3.4mm with standard-resolution, compared to only 1.1mm with a *k-t* SENSE high-resolution acquisition ($p<0.001$). Dark-rim artefacts are a common finding in conventional perfusion CMR and are thought to be caused by magnetic susceptibility effects, Gibbs ringing and cardiac motion during acquisition (23). As these artefacts are directly proportional to voxel size, the use of high-resolution perfusion CMR is a significant advantage. (Figure 1)

After the initial volunteer studies, the clinical feasibility and high diagnostic accuracy of high-resolution perfusion CMR have been demonstrated in several patient studies (5–7,10) (Table 1). In the first of these, Plein et al used an identical sequence to their previous volunteer study (1.5-T, 5-fold *k-t* SENSE, in-plane resolution 1.4mm) in 51 patients with known or suspected CAD. (5). High-resolution acquisition was found to have a high diagnostic accuracy (area under the curve [AUC] = 0.85), high image quality and additionally allowed the transmural extent of ischemia to be assessed. Notably, the diagnostic accuracy in single-vessel disease and multi-vessel disease was similar (AUC: 0.87 vs. 0.82 respectively) suggesting that sufficient spatial resolution to resolve a transmural ischemic gradient can overcome one of the major limitations of perfusion imaging in multi-vessel disease i.e. its dependence on a reference area of normal perfusion (Figure 2). Other benefits of high-resolution acquisition noted in the study were better integration with cine and LGE data; and minimal dark-rim artefact. A subsequent study demonstrated the clinical feasibility of high-resolution perfusion CMR at 3.0-T and confirmed the expected improvement in image quality and SNR compared to 1.5-T (Table 1)(6).

Manka et al followed with an extension of the *k-t* SENSE technique at 3.0-T to achieve 8-fold acceleration and an in-plane spatial resolution of 1.1mm which was then evaluated in 20 patients with suspected CAD. The combined benefits of higher field strength and greater acceleration led to an incremental improvement in spatial resolution and an even greater AUC of 0.94 (95% CI: 0.74-0.99) (7).

Most recently, in the only study to offer a direct comparison, high-resolution perfusion CMR (8-fold *k-t* BLAST, in-plane spatial resolution 1.6mm) was found to have a significantly greater overall diagnostic accuracy compared to standard-resolution in 100 patients with suspected CAD (AUC 0.93 vs. 0.83; $p < 0.001$) – and this was attributed to

better detection of subendocardial ischemia (Figure 2) (9). As the endocardial layer is the most vulnerable, the ability to detect subendocardial ischemia is a clear advantage in the earlier detection of CAD(24).

Whereas the previous studies have all used quantitative coronary angiography (QCA) as their reference standard, Lockie et al used fractional flow reserve (FFR), and showed high-resolution perfusion CMR (5-fold *k-t* BLAST, in-plane resolution 1.2 mm) had a high diagnostic accuracy (AUC=0.92) for the detection of hemodynamically significant lesions (FFR<0.75) (8). To have a non-invasive method that so closely correlates with FFR is highly attractive; and more widespread use could have a significant impact on clinical pathways - especially in patients with anatomically complex and multi-vessel disease (25). The MR-INFORM study which is currently underway will compare the clinical outcome in patients with stable angina managed with FFR-guided treatment to those guided by high-resolution perfusion CMR (26).

**THREE-DIMENSIONAL PERFUSION CMR**

Until recently, cardiac coverage with perfusion CMR has been limited to 3-4 non-contiguous slices through the left ventricle (LV). However, nuclear studies have demonstrated that the extent of hypoperfusion and overall ischemic burden is a strong marker of prognostic outcomes (27,28). Therefore, despite the high diagnostic accuracy of conventional 2-dimenional perfusion CMR, the lack of complete myocardial coverage remains a significant limitation.

Recent advances in hardware, particularly at 3.0-T, and spatio-temporal undersampling techniques have made faster dynamic imaging with CMR possible(16,18,29). Such acceleration has provided the opportunity for 3D acquisition during perfusion imaging i.e. full LV coverage, whilst preserving adequate temporal and spatial resolution(2). This

remains a promising area of active development and recent studies have shown 3D perfusion CMR to be clinically feasible, highly accurate and to have a potential role in the assessment and follow-up of ischemic burden (11–14).

In the first clinical study of 3D perfusion CMR, Manka et al evaluated 146 patients with suspected CAD using 6-fold *k-t* SENSE acceleration to achieve 16-slice coverage and an in-plane spatial resolution of 2.3mm(12). Image quality was consistently high and the overall sensitivity, specificity, and diagnostic accuracy to detect significant CAD (QCA≥50%) were 92%, 74% and 83% respectively. Although the diagnostic accuracy was very high, it was comparable to that seen in other studies with conventional 2D perfusion CMR(1). However, the study noted that the main advantage of 3D perfusion CMR was its ability to quantify myocardial ischemic burden (expressed as a percentage of LV myocardial hypo-enhancement to total LV myocardium) without geometric assumptions (Figure 3). In 48 patients that had a repeat scan after PCI, there was a relative reduction in myocardial ischemic burden of 79 ± 25%, and this highlighted the potential role of 3D perfusion CMR to serially monitor the response to anti-ischemic therapies(12). In addition, the quantification of ischemic burden using myocardial hypo-enhancement volumetry (with a signal intensity threshold of 2 standard deviations below remote myocardium) was found to be highly reproducible on intra-reader and inter-reader assessment.

Although the previous study used QCA ≥50% as the reference standard for CAD, two recent studies (one at 1.5-T and one at 3.0-T) have validated 3D perfusion CMR against FFR with high diagnostic accuracy(13,14). In the study by Manka et al, 3D perfusion CMR at 1.5-T was found to have a sensitivity, specificity and diagnostic accuracy of 90%, 82% and 87% respectively(13). At 3.0-T, the study by Jogiya et al found similar figures of 91%, 90% and 91% respectively(14). Both of these studies further verified the

feasibility and reproducibility of ischemic burden quantification using volumetry of myocardial hypo-enhancement. Additionally, Manka et al also found that the quantified myocardial ischemic burden had a high diagnostic accuracy (AUC=0.90) for identifying FFR-defined CAD - with an optimal cut-off value of >4.4%.

Although FFR is the reference standard for determining the hemodynamic significance of a coronary stenosis, it does not provide any information about the magnitude of consequent ischemia. This deficiency highlights a potential role for 3D perfusion CMR - and in both of the validation studies against FFR, it demonstrated a higher ischemic burden with proximal lesions compared to distal lesions(13,14). Furthermore, Jogiya et al, found a strong correlation ($r = 0.82$; 95% CI: 0.70 to 0.89; $p<0.0001$) between the myocardial ischemic burden on 3D perfusion CMR and the Duke Jeopardy score - which is a validated invasive assessment of ischemic burden based on lesion severity and location(14,30,31).

## DISCUSSION

Whether the benefits of high spatial resolution such as detection of subendocardial ischemia and reduction of dark-rim artefact outweigh the potential benefits of whole-heart coverage is difficult to answer. However, what is certain is that these techniques cannot be separated on the merits of diagnostic accuracy alone - as both are highly accurate and both have been validated against FFR. The answer will most likely lie in the individual patients, the indication for stress imaging and the local expertise. For example, in a patient with a de-novo suspicion of CAD, one could make a case for either technique and indeed conventional perfusion CMR would be more than adequate. However, in a patient who has already undergone angiography and found to have diffuse multi-vessel disease with possible PCI targets, then perhaps high-resolution acquisition might be

favourable on account of its ability to detect subendocardial ischemia and potentially diminish the effects of balanced ischemia (Figure 2). In another patient with a history of several myocardial infarctions and suspected peri-infarct ischemia, a 3D perfusion scan would allow each slice of scar-sensitive late-gadolinium gadolinium enhancement (LGE) imaging to be compared with a corresponding perfusion slice - rather than just three representative slices. This approach would allow improved delineation and quantification of peri-infarct ischemia rather than an assumption based on three sparse slices. Figures 4-7, show 3 examples of patients undergoing both acquisitions and the relative merits of both techniques are discussed in each case.

**CONCLUSION**

The application of advanced acceleration techniques in perfusion CMR has led to two highly accurate alternative strategies. It is impossible to definitively state whether high-resolution or 3D whole-heart coverage is the optimal approach as both techniques have unique advantages over the other. However, where expertise in both exist, this choice gives us the opportunity to tailor the type of perfusion sequence used to an individual patient in order to best answer the clinical question being posed. Finally, promising developments such as HYPR offer the tantalising prospect of both high-resolution and whole-heart coverage - and these methods are currently undergoing further evaluation.

**REFERENCES –**


1. Greenwood JP, Maredia N, Younger JF, Brown JM, Nixon J, Everett CC, Bijsterveld P, Ridgway JP, Radjenovic A, Dickinson CJ, Ball SG, Plein S. Cardiovascular magnetic resonance and single-photon emission computed tomography for diagnosis of coronary heart disease (CE-MARC): a prospective trial. *The Lancet*. 2012; 379:453-460.

2. Schwitter J, Wacker CM, van Rossum AC, Lombardi M, Al-Saadi N, Ahlstrom H, Dill T, Larsson HBW, Flamm SD, Marquardt M, Johansson L. MR-IMPACT: comparison of perfusion-cardiac magnetic resonance with single-photon emission computed tomography for the detection of coronary artery disease in a multicentre, multivendor, randomized trial. *Eur. Heart J.* 2008; 29:480-9.

3. Schwitter J, Wacker CM, Wilke N, Al-Saadi N, Sauer E, Huettle K, Schönberg SO, Luchner A, Strohm O, Ahlstrom H, Dill T, Hoebel N, Simor T. MR-IMPACT II: Magnetic Resonance Imaging for Myocardial Perfusion Assessment in Coronary artery disease Trial: perfusion-cardiac magnetic resonance vs. single-photon emission computed tomography for the detection of coronary artery disease:a comparative m. *Eur. Heart J.* 2012;:doi:10.1093/eurheartj/ehs022.

4. Hamon M, Fau G, Née G, Ehtisham J, Morello R, Hamon M. Meta-analysis of the diagnostic performance of stress perfusion cardiovascular magnetic resonance for detection of coronary artery disease. *J Cardiovasc Magn Reson*. 2010; 12:29.

5. Plein S, Kozerke S, Suerder D, Luescher TF, Greenwood JP, Boesiger P, Schwitter J. High spatial resolution myocardial perfusion cardiac magnetic resonance for the detection of coronary artery disease. *Eur. Heart J.* 2008; 29:2148-55.

6. Plein S, Schwitter J, Suerder D, Greenwood JP, Boesiger P, Kozerke S. k-Space and Time Sensitivity Encoding–accelerated Myocardial Perfusion MR Imaging at 3.0 T: Comparison with 1.5 T1. *Radiology*. 2008; 249:493.

7. Manka R, Vitanis V, Boesiger P, Flammer AJ, Plein S, Kozerke S. Clinical feasibility of accelerated, high spatial resolution myocardial perfusion imaging. *JACC. Cardiovascular imaging*. 2010; 3:710-7.

8. Lockie T, Ishida M, Perera D, Chiribiri A, De Silva K, Kozerke S, Marber M, Nagel E, Rezavi R, Redwood S, Plein S. High-resolution magnetic resonance myocardial perfusion imaging at 3.0-Tesla to detect hemodynamically significant coronary stenoses as determined by fractional flow reserve. *J. Am. Coll. Cardiol.* 2010; 57:70-5.

9. Motwani M, Maredia N, Fairbairn T a., Kozerke S, Radjenovic A, Greenwood JP, Plein S. High-Resolution Versus Standard-Resolution Cardiovascular Magnetic Resonance Myocardial Perfusion Imaging for the Detection of Coronary Artery Disease. *Circulation: Cardiovascular Imaging*. 2012; 5:306-13.

10. Maredia N, Radjenovic A, Kozerke S, Larghat A, Greenwood JP, Plein S. Effect of improving spatial or temporal resolution on image quality and quantitative perfusion assessment with k-t SENSE acceleration in first-pass CMR myocardial perfusion imaging. *Magn Reson Med*. 2010; 64:1616-24.

11. Shin T, Hu HH, Pohost GM, Nayak KS. Three dimensional first-pass myocardial perfusion imaging at 3T: feasibility study. *J Cardiovasc Magn Reson*. 2008; 10:57.

12. Manka R, Jahnke C, Kozerke S, Vitanis V, Crelier G, Gebker R, Schnackenburg B, Boesiger P, Fleck E, Paetsch I. Dynamic 3-dimensional stress cardiac magnetic resonance perfusion imaging: detection of coronary artery disease and volumetry of myocardial hypoenhancement before and after coronary stenting. *J. Am. Coll. Cardiol.* 2011; 57:437-44.

13. Manka R, Paetsch I, Kozerke S, Moccetti M, Hoffmann R, Schroeder J, Reith S, Schnackenburg B, Gaemperli O, Wissmann L, Wyss C a, Kaufmann P a, Corti R, Boesiger P, Marx N, Lüscher TF, Jahnke C. Whole-heart dynamic three-dimensional magnetic resonance perfusion imaging for the detection of coronary artery disease defined by fractional flow reserve: determination of volumetric myocardial ischaemic burden and coronary lesion location. *Eur. Heart J.* 2012;

14. Jogiya R, Kozerke S, Morton G, De Silva K, Redwood S, Perera D, Nagel E, Plein S. Validation of Dynamic 3-Dimensional Whole Heart Magnetic Resonance Myocardial Perfusion Imaging Against Fractional Flow Reserve for the Detection of Significant Coronary Artery Disease. *J. Am. Coll. Cardiol.* 2012; xx:1-10.

15. Motwani M, Fairbairn TA, Larghat A, Mather AN, Biglands JD. Systolic Versus Diastolic Acquisition in Myocardial Perfusion MR Imaging. *Radiology*. 2012; 262:816-23.

16. Kozerke S, Plein S. Journal of Cardiovascular Magnetic Accelerated CMR using zonal , parallel and prior knowledge driven imaging methods. *Journal of Cardiovascular Magnetic Resonance*. 2008; 18:1-18.

17. Motwani M, Lockie T, Greenwood JP, Plein S. Accelerated, high spatial resolution cardiovascular magnetic resonance myocardial perfusion imaging. *J Nucl Cardiol*. 2011;

18. Tsao J, Boesiger P, Pruessmann KP. k-t BLAST and k-t SENSE: dynamic MRI with high frame rate exploiting spatiotemporal correlations. *Magn Reson Med*. 2003; 50:1031-42.

19. Ge L, Kino A, Griswold M, Mistretta C, Carr JC, Li D. Myocardial perfusion MRI with sliding-window conjugate-gradient HYPR. *Magnetic Resonance in Medicine*. 2009; 62:835–839.

20. Plein S, Ryf S, Schwitter J, Radjenovic A, Boesiger P, Kozerke S. Dynamic contrast-enhanced myocardial perfusion MRI accelerated with k-t sense. *Magn Reson Med*. 2007; 58:777-85.

21. Pedersen H, Kozerke S, Ringgaard S, Nehrke K, Kim WY. k t PCA: Temporally constrained k t BLAST reconstruction using principal component analysis. *Magnetic Resonance in Medicine*. 2009; 62:706-716.

22. Ma H, Yang J, Liu J, Ge L, An J, Tang Q, Li H, Zhang Y, Chen D, Wang Y, Liu J, Liang Z, Lin K, Jin L, Bi X, Li K, Li D. Myocardial perfusion magnetic resonance imaging using sliding-

window conjugate-gradient highly constrained back-projection reconstruction for detection of coronary artery disease. *Am. J. Cardiol.* 2012; 109:1137-41.

23. Di Bella EVR, Parker DL, Sinusas a J. On the dark rim artifact in dynamic contrast-enhanced MRI myocardial perfusion studies. *Magn Reson Med*. 2005; 54:1295-9.

24. Bache RJ, Schwartz JS. Effect of perfusion pressure distal to a coronary stenosis on transmural myocardial blood flow. *Circulation*. 1982; 65:928.

25. Tonino P a. L, Fearon WF, De Bruyne B, Oldroyd KG, Leesar M a., Ver Lee PN, MacCarthy P a., van't Veer M, Pijls NHJ. Angiographic Versus Functional Severity of Coronary Artery Stenoses in the FAME StudyFractional Flow Reserve Versus Angiography in Multivessel Evaluation. *J. Am. Coll. Cardiol.* 2010; 55:2816-2821.

26. MR INFORM - MR Perfusion Imaging to Guide Management of Patients With Stable Coronary Artery Disease - Full Text View - ClinicalTrials.gov [Internet]. [cited 2011 May 18];Available from: http://clinicaltrials.gov/ct2/show/NCT01236807

27. Brown KA, Boucher CA, Okada RD, Guiney TE, Newell JB, Strauss HW, Pohost GM. Prognostic value of exercise thallium-201 imaging in patients presenting for evaluation of chest pain. *J. Am. Coll. Cardiol.* 1983; 1:994-1001.

28. Hachamovitch R, Berman DS, Shaw LJ, Kiat H, Cohen I, Cabico JA, Friedman J, Diamond GA. Incremental prognostic value of myocardial perfusion single photon emission computed tomography for the prediction of cardiac death: differential stratification for risk of cardiac death and myocardial infarction. *Circulation*. 1998; 97:535.

29. Willinek W, Gieseke J, Kukuk G. Dual-source parallel radiofrequency excitation body MR imaging compared with standard MR imaging at 3.0 T: initial clinical experience 1. *Radiology*. 2010; 256.

30. Califf RM, Phillips HR, Hindman MC, Mark DB, Lee KL, Behar VS, Johnson RA, Pryor DB, Rosati RA, Wagner GS. Prognostic value of a coronary artery jeopardy score. *J. Am. Coll. Cardiol.* 1985; 5:1055-1063.

31. Liao L, Kong DF, Shaw LK, Sketch MH, Milano CA, Lee KL, Mark DB. A new anatomic score for prognosis after cardiac catheterization in patients with previous bypass surgery. *J. Am. Coll. Cardiol.* 2005; 46:1684-1692.

**TABLE 1**

| | | | | | | | |
|---|---|---|---|---|---|---|---|
| *Ma 2012* | 50 | 3.0-T | SW-CG-HYPR | 1.6 mm | 6 slices (WH) | QCA ≥50% | 0.90† |
| | | | | **n** | | **Standard** | |
| **High-Resolution** | | | | | | | |
| *Plein 2008* | 51 | 1.5-T | 5 x *k-t*-SENSE | 1.4 mm | 4 slices (NC) | QCA>50 % | 0.85* |
| *Plein 2008* | 33 | 1.5-T | 5 x *k-t* SENSE | 1.5 mm | 4 slices (NC) | QCA>50 % | 0.80* |
| *Plein 2008* | 33 | 3.0-T | 5 x *k-t* SENSE | 1.3 mm | 4 slices (NC) | QCA>50 % | 0.89* |
| *Manka 2010* | 20 | 3.0-T | 8 x *k-t* SENSE | 1.1 mm | 3 slices (NC) | QCA>50 % | 0.94* |
| *Motwani 2012* | 100 | 1.5-T | 8 x k-t BLAST | 1.6 mm | 3 slices (NC) | QCA ≥50% | 0.93* |
| *Lockie 2011* | 42 | 3.0-T | 5 x *k-t* BLAST | 1.2 mm | 3 slices (NC) | FFR<0.75 | 0.92* |
| **3-D** | | | | | | | |
| *Manka 2011* | 146 | 3.0-T | 6 x *k-t* SENSE | 2.3 mm | 16 slices (WH) | QCA ≥50% | 0.83† |
| *Manka 2012* | 120 | 1.5-T | 10 x *k-t* PCA | 2.0 mm | 16 slices (WH) | FFR<0.75 | 0.87† |
| *Jogiya 2012* | 53 | 3.0-T | 10 x *k-t* PCA | 2.3 mm | 12 slices (WH) | FFR<0.75 | 0.91† |
| **HYPR** | | | | | | | |

* In these studies, diagnostic accuracy was calculated by receiver-operating characteristic analysis and expressed as area under the curve. †In these studies, diagnostic accuracy was expressed as the proportion of correctly classified subjects (true positives + true negatives) among all subjects. 3-D = 3-dimensional; HYPR = highly constrained back-projection reconstruction; T= Tesla; SENSE = sensitivity encoding; BLAST = broad linear speed-up technique; PCA = principal component analysis; SW-CG-HYPR= sliding-window conjugate-gradient HYPR; NC = non-contiguous; WH= whole-heart; QCA = quantitative coronary angiography

**FIGURE LEGENDS**

**Figure 1 – Dark-Rim Artefact**

A 60-year-old man with suspected angina underwent stress perfusion CMR at 1.5-T with both standard-resolution (2.5mm in-plane) and high-resolution (1.5 mm in-plane) acquisition. High-resolution acquisition was facilitated by 8-fold *k-t* BLAST acceleration. There were no significant stress-induced perfusion defects seen with either acquisition (mid-ventricular slices shown) but there was significant dark-rim artefact on the standard-resolution images (arrows). Subsequent X-ray angiography confirmed normal coronary arteries. CMR = cardiovascular magnetic resonance; BLAST = broad linear speed-up technique

**Figure 2 – High-resolution Perfusion CMR in Multi-vessel Disease**

A 48-year-old lady with suspected angina underwent stress perfusion CMR at 1.5-T using a high-resolution (1.4 mm in-plane) technique facilitated by 5x *k-t*-BLAST. Stress-induced perfusion defects were seen in all three territories (arrows, A, B) and are clearly demarcated as subendocardial. Subsequent X-ray angiography revealed significant three-vessel disease (arrows, C, D). This case highlights the ability of high-resolution acquisition to overcome the potential effects of balanced ischemia in multi-vessel disease by detecting transmural perfusion gradients and subendocardial ischemia. CMR = cardiovascular magnetic resonance; BLAST = broad linear speed-up technique.

**Figure 3 – Myocardial Ischemic Burden Quantification with 3D Perfusion CMR**

Panel (A) shows consecutive slices of a 3D perfusion CMR scan during adenosine stress in a patient with significant stenoses in the proximal right coronary artery and distal left anterior descending coronary artery. Panel (B) shows identical images illustrating

volumetry of myocardial hypo-enhancement using a signal intensity threshold of 2 standard deviations below remote myocardium (segmented red areas). The volume of myocardial hypo-enhancement was 30.4% of total myocardium. 3D = 3-dimensional; CMR = cardiovascular magnetic resonance

**Figure 4 – Case Example 1**

A 62 year-old man with a history of previous bypass surgery 10 years ago, re-presented with increasing angina. The top panel dimensional shows 3D perfusion CMR at stress (2.5mm in-plane resolution, 12 slices); the middle panel shows LGE imaging (1.5mm in-plane resolution) and the bottom panel shows high-resolution stress perfusion CMR (1.1mm in-plane resolution, 3 slices) - all performed on the same patient at 3.0-T. Both 3D perfusion and high-resolution techniques show inferior perfusion defects from base to apex. The benefit of whole-heart coverage with the 3D technique is demonstrated in this case, as hypoperfusion is seen to extend beyond the scar into the apical cap (top panel, arrows) which is not covered by the three-slice high-resolution technique. On the other hand, the perfusion defects and their transmural extent are better delineated with the high-resolution technique particularly at the mid-ventricular level. By virtue of their similar in-plane spatial resolution, it is easier to correlate LGE images with high-resolution perfusion CMR on a per slice basis, compared to the 3D technique. CMR = cardiovascular magnetic resonance; 3D = 3-Dimensional; LGE = late-gadolinium enhancement.

**Figure 5 – Case Example 2**

A 45 year-old man with previous PCI to the LAD re-presented with significant angina. The top panel dimensional shows 3D perfusion CMR (12 slices) at stress; the middle panel shows LGE imaging and the bottom panel shows high-resolution (1.1mm in-plane)

stress perfusion CMR - all performed at 3.0-T. 3D perfusion CMR shows stress-induced hypo-perfusion throughout the anterior wall from base to apex – i.e. well beyond the area of scar seen in the mid-anterior wall on LGE imaging. This example shows the benefit of whole-heart coverage with the 3D acquisition, as the 3-slice high-resolution techniques did not demonstrate any significant ischemia beyond the established scar in the mid-ventricle. X-ray angiography confirmed a sub-total occlusion of a large diagonal branch, accounting for the anterior ischemia (black arrow). CMR = cardiovascular magnetic resonance; 3D = 3-Dimensional; LGE = late-gadolinium enhancement; VLA = vertical long axis.

**Figure 6 – Case Example 3**

A 57 year-old man presented with worsening angina after a myocardial infarction 6 months ago. The top panel dimensional shows stress 3D perfusion CMR (12 slices); the middle panel shows LGE imaging; and the bottom panel shows high-resolution (1.1mm in-plane) stress perfusion CMR - all performed at 3.0-T. Both 3D perfusion and high-resolution perfusion techniques show an inferior perfusion defect from base to apex consistent with the infarction seen on LGE imaging. However, the perfusion defects are better delineated at high-resolution and a small amount of peri-infarct ischemia can be seen in each of the 3 slices (arrows) beyond the established scar on corresponding LGE images. With 3D acquisition, the lower spatial resolution (2.5mm in-plane) means that the borders of the perfusion defect within each slice are less distinct and are more difficult to distinguish from dark-rim artefact in the mid to apical anteroseptal regions (endocardial border opposite dashed lines). CMR = cardiovascular magnetic resonance; 3D = 3-Dimensional; LGE = late-gadolinium enhancement; VLA = vertical long axis.

**Figure 7 – Case Example 4**

The top panel dimensional shows stress 3D perfusion CMR (12 slices); the middle panel shows LGE imaging; and the bottom panel shows high-resolution (1.1mm in-plane) stress perfusion CMR - all performed at 3.0T. The 3D technique demonstrated significant stress-induced hypoperfusion in the inferior wall from base to apex and extending into the basal inferolateral segments; but there was also significant dark-rim artefact in the septum (endocardial border opposite dashed lines). X-ray angiography confirmed total occlusion of the mid left circumflex artery (arrow). Due to the sparsity of coverage, the 3-slice high-resolution technique only detected a significant perfusion defect at the mid-ventricular level and therefore significantly underestimated the ischemic burden in this case, compared to the 3D technique. Additionally, interpretation of the apical high-resolution slice is difficult as it is significantly more diastolic than the other slices, which is a disadvantage of all 2-dimensional acquisitions which employ a single-shot technique. By comparison, with 3D perfusion CMR all slices are acquired at the same point in the cardiac cycle which makes it easier to determine the extent of perfusion defects across different myocardial sections. CMR = cardiovascular magnetic resonance; 3D = 3-Dimensional; LGE = late-gadolinium enhancement; VLA = vertical long axis.

**Figure 1**

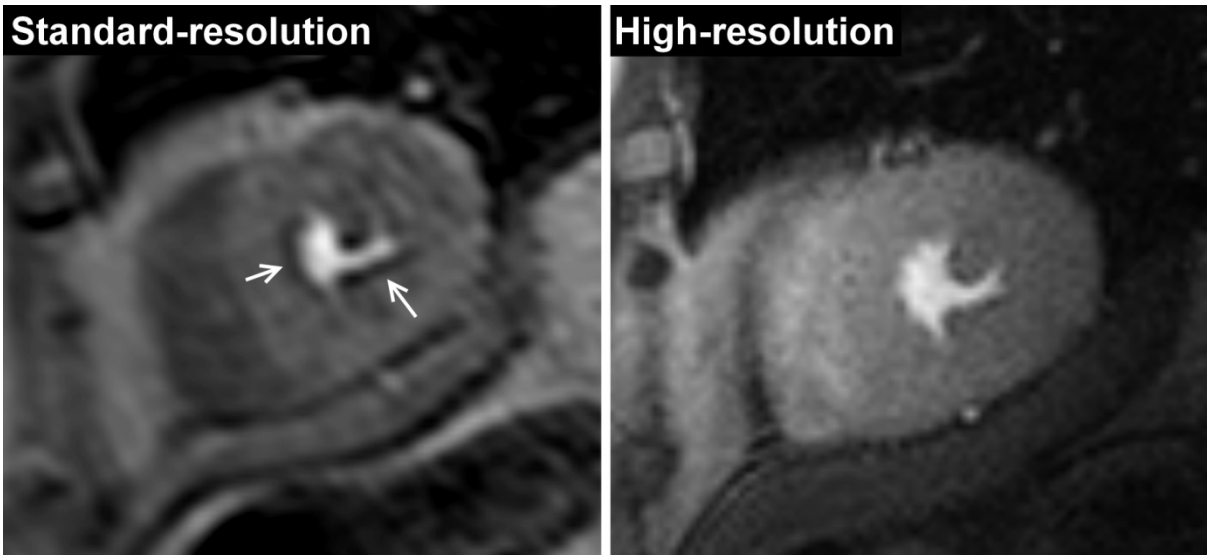

**Figure 2**

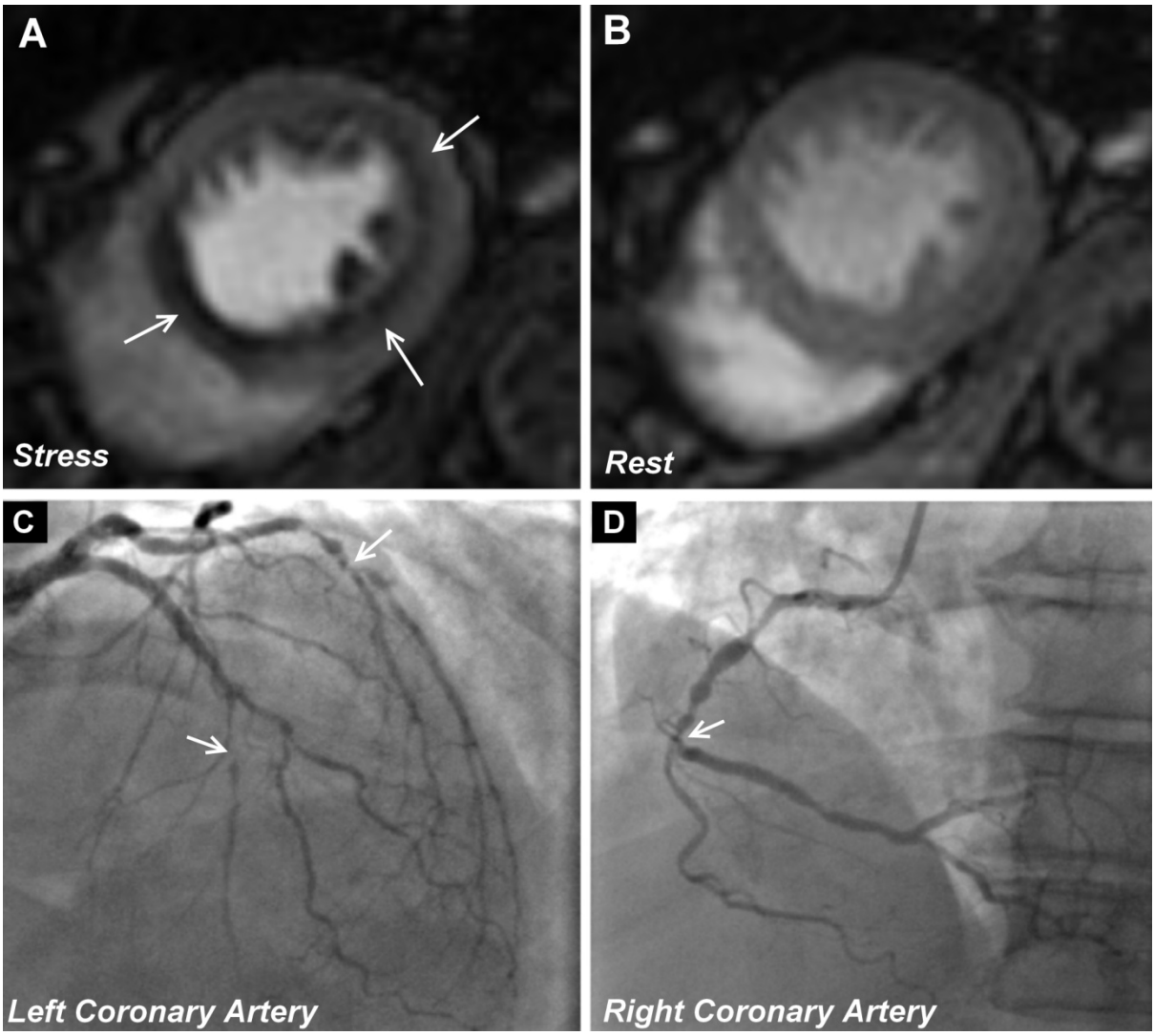
A
Stress
B
Rest
C
Left Coronary Artery
D
Right Coronary Artery

**Figure 3**

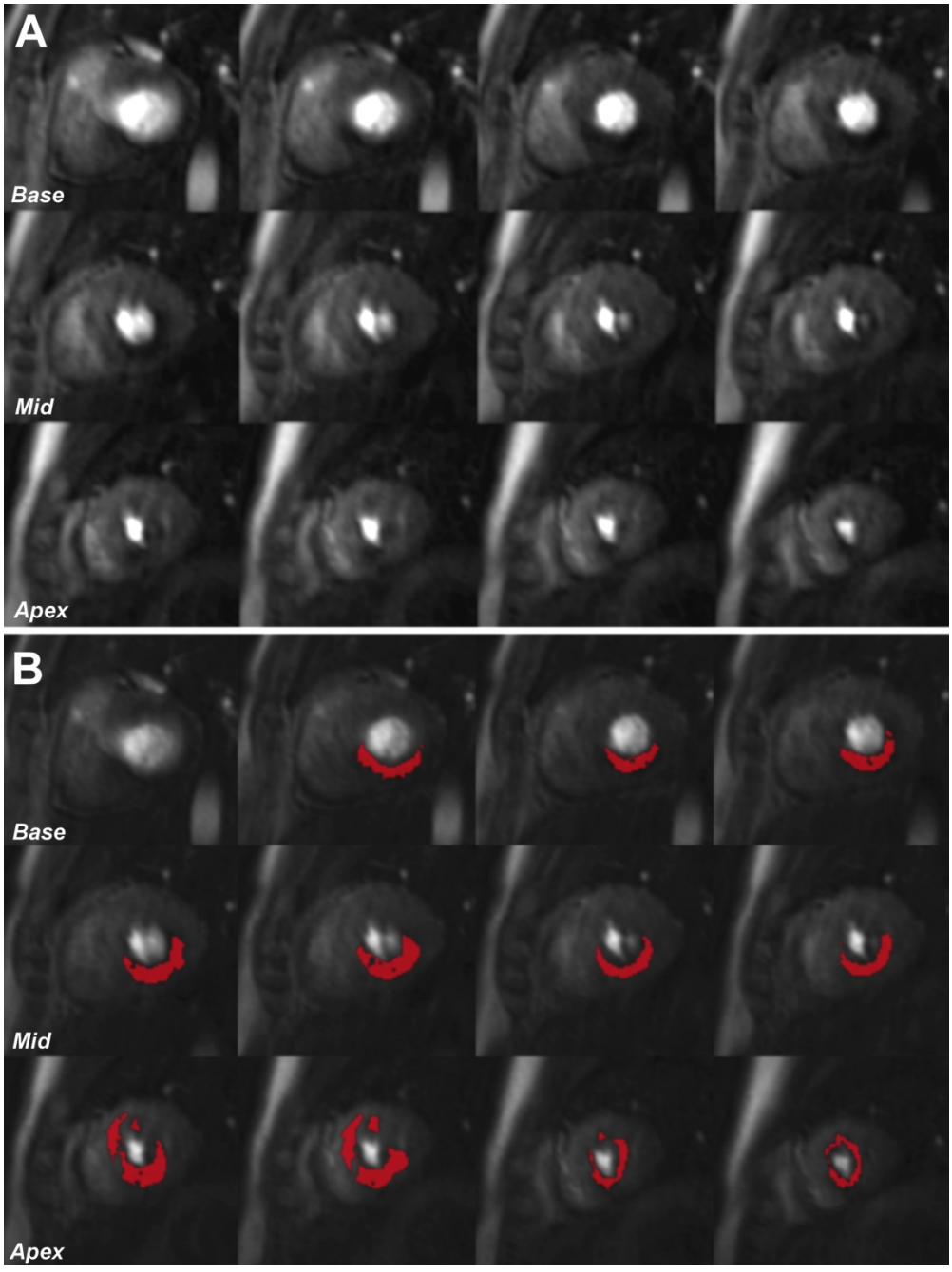

**Figure 4 – Case 1**

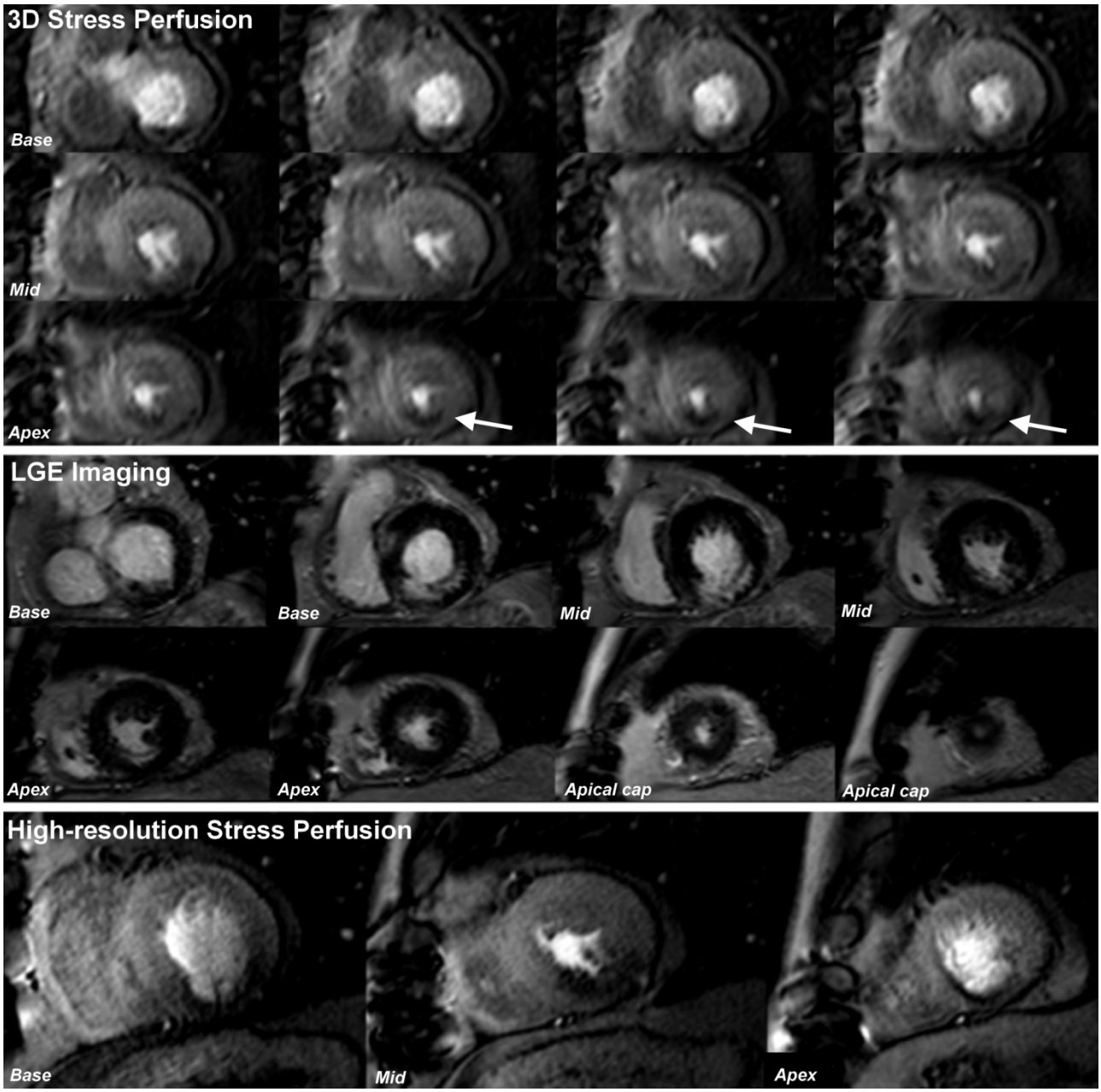

**Figure 5 – Case 2**

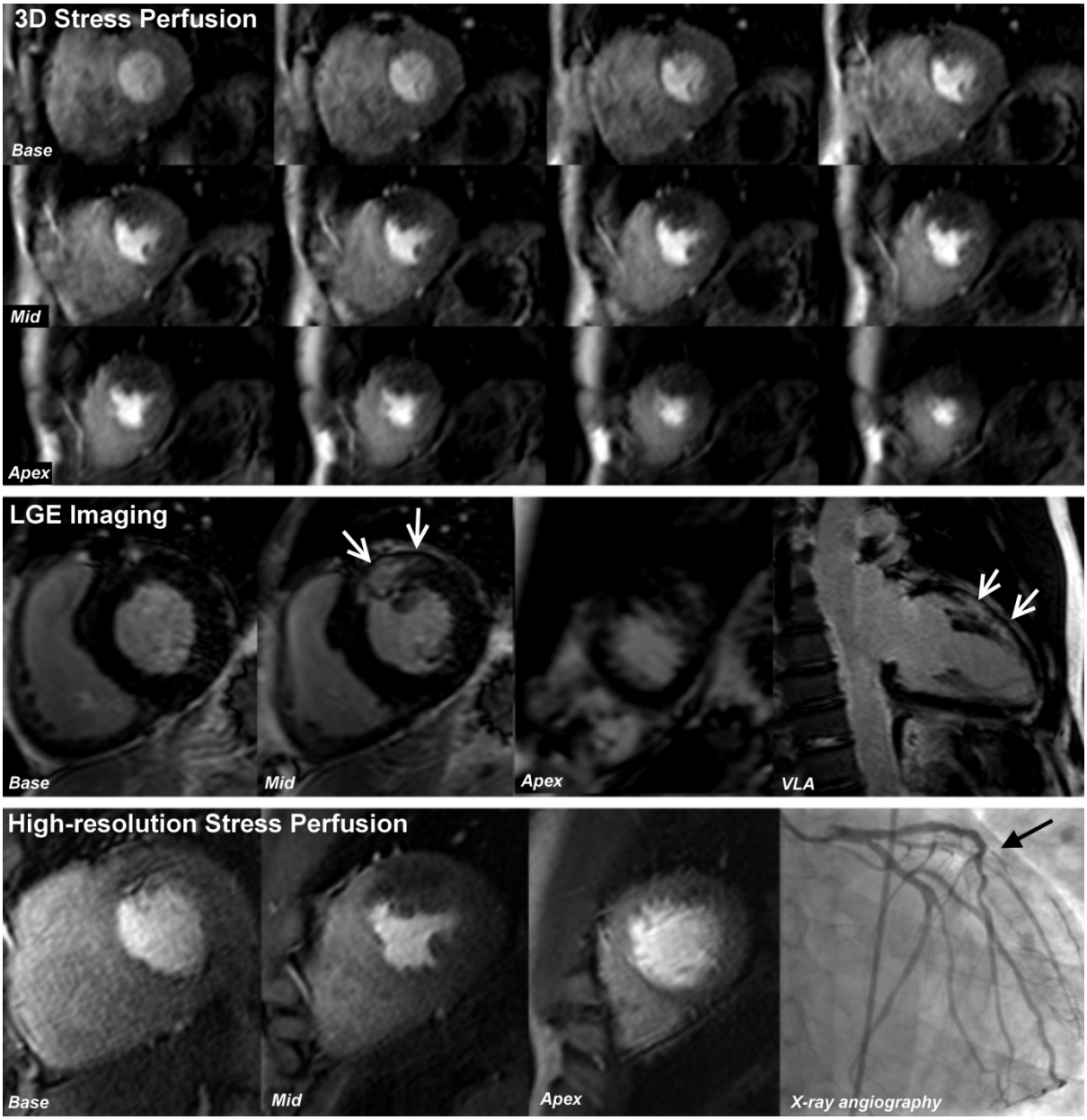

**Figure 6 – Case 3**

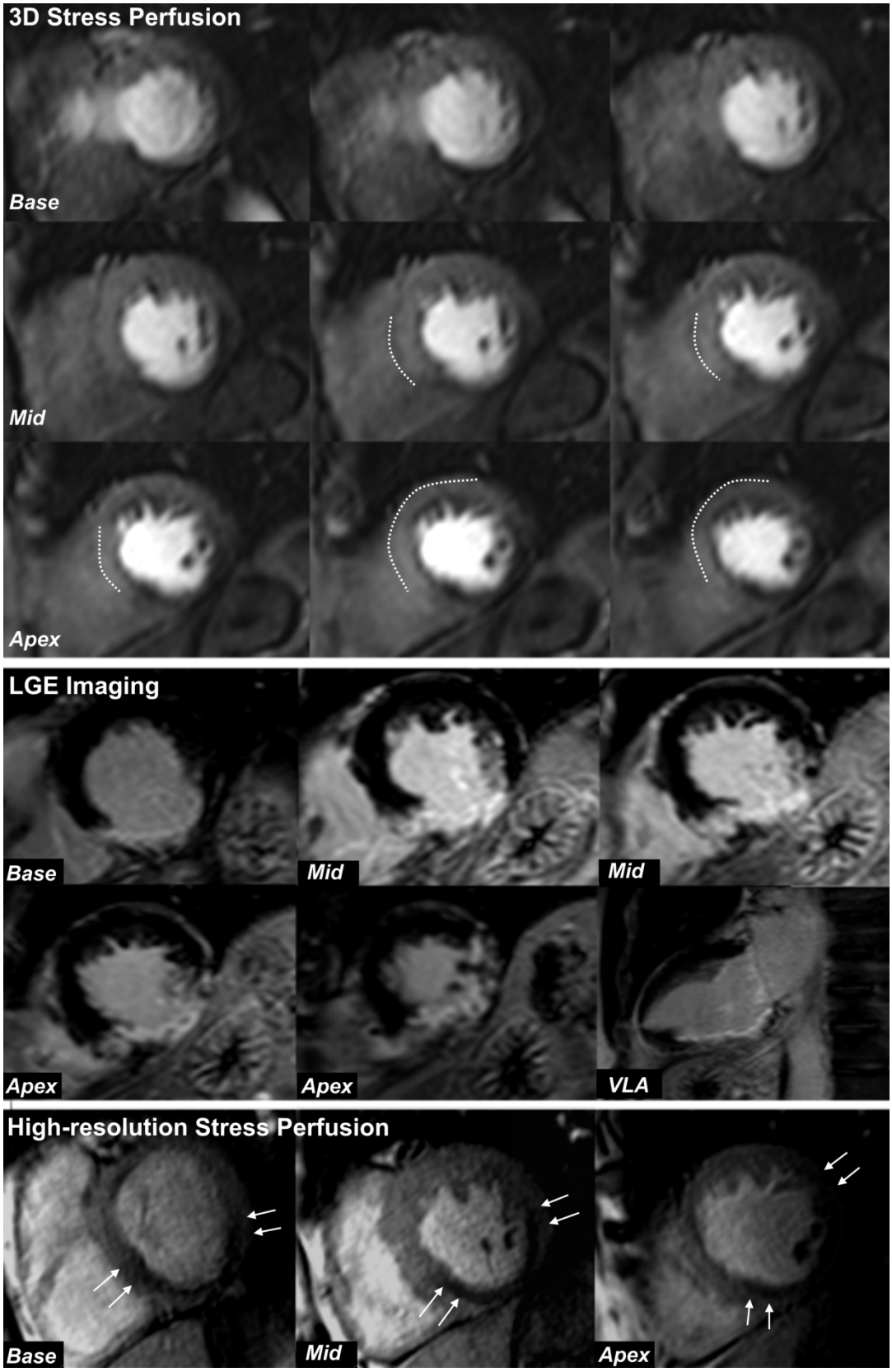

Figure 7 – Case 4